Adrián Posado Fernández
Mestre em Biomedicina

In the Siege of Alzheimer´s Castle: Contribution to Immunotherapy

Dissertação para obtenção do Grau de Doutor em Biologia

Orientador	Doutor Alcino Orfeu de Leão e Flores, CEO, STAB VIDA Lda
Co-orientador	Doutor Luís Jaime Mota, Prof. Auxiliar, FCT NOVA
	Doutora Cláudia Guimas Almeida, Group Leader, CEDOC NMS

Júri:

Presidente	Prof. Doutor Paulo Limão-Vieira, Prof Catedrático, FCT NOVA
Arguentes	Prof. Doutora Isabel Dos Santos Cardoso, Investigadora Principal, I3S, Universidade do Porto
	Prof. Doutor Miguel Medina Padilla, Deputy Scientific Director at CIBERNED
Vogais	Prof. Doutor José Luís Capelo Martínez, Prof. Associado com Agregação, FCT NOVA
	Doutor Alcino Orfeu de Leão e Flores, CEO, STAB VIDA Lda

FACULDADE DE CIÊNCIAS E TECNOLOGIA
UNIVERSIDADE NOVA DE LISBOA

Setembro 2018

A mis padres, a mi hermana y a mi abuela Luzdivina.

Acknowledgements

Desde mucho antes de acceder a la universidad mi interés por los seres vivos que me rodeaban y mi curiosidad sobre cómo funcionaban aquellos maravillosos y misteriosos "mecanismos" ya parecía evidente. Durante mi etapa en el I.E.S. "Los Sauces", mi interés por materias relacionadas con Biología se volvió a ver reflejado y, como era previsible, y a pesar de algunos intentos por reencaminar mi carrera universitaria hacia un campo más "prometedor", mi tozudez me llevó a entrar en la entonces Licenciatura en Biología en la Universidad de León.

De León me llevo muchos de los recuerdos, amistades y enseñanzas más importantes de mis 30 años, entre los que destaca la definición de esa pasión por la Biología en forma de un Máster en Biomedicina y la firme intención de orientar mi futuro hacia la investigación biológica. Entonces, tras de casi dos años tras terminar el Máster, hace algo más de cuatro años, y después de algunos malos golpes anímicos y profesionales, se me fue dada la que posiblemente sea la mayor oportunidad profesional de cuantas he tenido en mi vida.

En Lisboa (o Caparica, para ser más exactos), se me ofreció la oportunidad de desarrollar un doctorado bajo el paraguas del proyecto EXTRABRAIN, financiado por las prestigiosas Marie Sklodowska Curie Actions. En una pequeña empresa (STAB VIDA Lda) y gracias a diferentes y productivas colaboraciones fui capaz de introducirme en el campo de la Neurobiología y de la inmunoterapia. Y nada más y nada menos, que con el objetivo de abordar algo tan complejo, ambicioso y emocionante como el tratamiento de la enfermedad del Alzheimer, cuyo golpe ya ha sufrido en repetidas ocasiones mi propia familia.

Y hoy, 4 años después del inicio de este proyecto, y tras geniales, buenos y malos momentos, me hace inmensamente feliz poder mostrar al mundo académico el conjunto de trabajos que he conseguido llevar a cabo en este tiempo.

Ahora, dado que todo el camino que me ha traído hasta aquí, no puedo dejar de agradecer a un buen número de personas el haberme acompañado en este trayecto.

Em primeiro lugar quero agradecer ao Doutor Orfeu Flores pela sua orientação e confiança, e por esta maravilhosa oportunidade que me tem permitido fazer, de uma paixão, uma carreira profissional digna. Também aos meus outros dois orientadores desta tese, ao Doutor Jaime Mota e a Doutora Cláudia Almeida pela atenção e ajuda no desenvolvimento desta tese.

Aos meus colegas de trabalho e universidade, obrigado. Obrigado pela ajuda, por serem companheiros de laboratório, professores de português, guias turísticos, agentes imobiliários, conselheiros e, sobre tudo, bons amigos: Pinto, Paulinho, Eduardo, Gonçalo, Rui, Penedo, Carlos, Nuno, Lidia, Juan Luis, Magda, Filipa, Lili, Fábio, Ana, Vitaliy, Carla, Daniela, Sofia, Nanci, e mais alguns de quem me possa estar a esquecer.

Durante estes 4 anos, para além do trabalho de bancada e computador, também tenho tido a oportunidade de percorrer e desfrutar de uma boa parte do mundo em companhia de alguns dos melhores companheiros de viagem, com menção especial ao Pinto e Paulo, entre outros. Espero que essa paixão não decaia!

I would also like to express my gratitude to the members of the EXTRABRAIN consortium and to the professors in whose groups I performed several and vital experiments for the development of this thesis, Dr. Eurico J. Cabrita, Dr. José Luís Capelo Martínez (BIOSCOPE), Dr. Jochen Herms and Dr. Francisco Wandosell, with special emphasis to Dr. Lara Ordóñez, who has always been an inestimable help and to Cláudia Afonso for her help with the NMR epitope mapping.

And of course, I also had the opportunity to make amazing friends and workmates within the EXTRABRAIN consortium while traveling along some of the best laboratories in Europe, Alberto, Benham, Maura, Elena, Bárbara, Alex, James, Matteo, Gabriela and Ahmad, with whom I strongly wish to keep and feed our friendship, and even collaborate in future!

Tampoco me puedo olvidar de toda la gente que me ha acompañado desde la universidad, empezando por Chus, Billy & Ñues, continuando con mi querida Lolaila, Alario, Esty y demás séquito, magníficos alicates de la Europa (Prosi, Jimmy…) y terminando con el resto de mis honorables compañeros de Licenciatura y Máster, Diego, Melón, Santi & Cía, además de mis queridos y añorados Yiyo y Brandán.

Y por último, a mi familia, mis padres y mi hermana Laura, gracias por vuestro apoyo, tanto emocional, como material, por vuestra educación y, sobre todo, por vuestra paciencia infinita. Vuestro apoyo y vuestra guía es lo que me ha traído hasta aquí, ¡lo que no está nada mal! Muchas gracias de todo corazón.

A todos vosotros, infinitas gracias.

To all of you, huge thanks.

Abstract

The accumulation of amyloid-beta (Aβ) and intracellular neurofibrillary tangles (tau) in the brain are the two major neuropathological hallmarks of Alzheimer's Disease (AD). Active and passive immunotherapies have been tested for limiting cerebral Aβ deposition and/or accelerate its clearance. In such way, with our focus on AD diagnosis and therapy, we have created and characterized a bunch of antibodies targeting Aβ and tau.

The STAB-Mab was developed in 2011 with theranostic purposes, and now has been biochemically characterized and tested in pre-clinical trials, demonstrating significant biochemical and cognitive improvements in mice AD models. The use of a number of analytical techniques, form WB to NMR, allowed us to confirm a widespread epitope centered within the first half of the Aβ peptide. This interaction allows STAB-Mab to bind several aggregated species, besides monomers and APP and to inhibit the stabilization of β-strand motifs, which could be the reason of the promising pre-clinical results.

The two minibodies derived from the STAB-Mab were designed for being significantly smaller and more versatile, however, their functionality was seriously affected, having a significantly lower affinity and being unable to stop AD pathology in mice AD models.

On the other hand, within another European Project addressing tau pathology, we have developed a series of hybridomas producing monoclonal antibodies specifically targeting tau wearing certain post-transcriptional modifications. The most promising specific antibodies targeting acetylated and phosphorylated tau were delivered to the partners to be tested with biological and clinical samples.

Keywords: Alzheimer´s, Aβ, APP, tau, antibody, immunotherapy, theranostic

Resumo

A acumulação de beta amilóide (Aβ) e nós neurofibrilares intracelulares (tau) no cérebro são duas das principais características neuropatológicas da doença de Alzheimer (AD). Imunoterapias ativa e passiva tem sido duas das estratégias mais testadas para limitar a deposição cerebral e/ou acelerar a eliminação destas duas proteínas. Assim, com o foco no diagnóstico e terapia de AD, temos criado vários anticorpos dirigidos contra Aβ e tau.

O STAB-Mab foi desenvolvido em 2011 com fins diagnósticos e terapêuticos, e é agora caracterizado e testado em ensaios pré-clínicos, mostrando melhorias significativas em modelos cognitivos e bioquímicas de modelos animais de AD. O uso de um número de técnicas de análise, desde WB ao RMN, tem permitido confirmar um amplo epitopo e centrado na metade N-terminal do péptido do Aβ. Esta interação deverá permitir ao STAB-Mab reconhecer várias espécies agregadas de Aβ, para além de monómeros e APP e, simultaneamente, inibir a estabilização de estruturas β-strand, o que pode ser a razão para os promissórios resultados pré-clínicos observados.

Dois Minibodies derivados do STAB-Mab foram concebidos para ser significativamente menor e versátil, no entanto, a sua funcionalidade parece ter sido gravemente afetada, com uma afinidade significativamente menor e incapazes de retraçar a patologia em modelos animais de AD.

Além disso, em outro projeto europeu, que aborda a patologia da tau, tem sido desenvolvida uma série de hibridomas a produzir anticorpos monoclonais específicos para tau com certas modificações pós-transcricionais. Os anticorpos específicos mais promissores a reconhecer dois fragmentos da proteína tau, um acetilado e outro fosforilado em diferentes resíduos foram entregues aos parceiros do projeto para serem testados com amostras biológicas e clinicas.

Palavras chave: Alzheimer, Aβ, APP, tau, anticorpo, imunoterapia, diagnostico

Index

Figures index

Tables index

Abbreviations

5-HT$_6$	5-hydroxytryptamine receptor 6
a7nAChR	A7 Nicotinic Acetylcholine Receptor
Aβ	Amyloid Beta
ABCA7	Tp-Binding Cassette (Abc) Transporter A7
AcD	Acidic Domain
acTAU	Acetylated tau peptide
AD	Alzheimer´s Disease
ADDL	Aβ-Derived Diffusible Ligands
ADP	Adenosine Diphosphate
AEP	Asparagine Endopeptidase
AICD	Amyloid Precursor Protein Intracellular Cytoplasmic/C-Terminal Domain
AGD	Agyrophilic Grain Disease
Akt1	Serine-Threonine Protein Kinase 1
ALS	Autophagy-Lysosome System
AMPA	Alpha-Amino-3-Hydroxyl-5-Methyl-4-Isoxazolepropionate
AMPAR	Alpha-Amino-3-Hydroxyl-5-Methyl-4-Isoxazolepropionate Receptor
APP	Amyloid Precusor Protein
APH-1	Anterior Pharynx-defective 1
ApoE	Apolipoprotein E
ApoE2	Apolipoprotein E2
ApoE3	Apolipoprotein E3
ApoE4	Apolipoprotein E4
Arc	Activity-Regulated Cytoskeleton-Associated Protein
Arf6	Adp-Ribosylation Factor
ARH	Autosomal Recessive Hypercholesterolemia Protein
ARIA-E	Amyloid-Related Imaging Abnormalities With Brain Edema
ASC	Adaptor Protein Apoptosis-Associated Speck-Like Protein Containing A Card (Asc)
ASPDs	Amylospheroids
BACE1	Beta-secretase 1
BACE2	Beta-secretase 2
BBB	Blood-Brain Barrier
BDNF	Brain-Derived Neurotrophic Factor
BIN1	Bridging Integrator 1
BRI2	Brichos Domain-Containing 2
BSA	Bovine Serum Albumin
CaMKII	Calmodulin Kinase Ii
CaSR	Calcium-Sensing Receptor
CBD	Corticobasal Degeneration
CD2AP	Cd2-Associated Protein
CDK5	Cyclin Dependent Kinase 5
CDR	Complementary-Determining Regions
CFA	Complete Freund´S Adjuvant
CHO	Chinese Hamster Ovary Cell Line
CHT	High-Affinity Choline Transporter
CLU	Clusterin
CNS	Central Nervous System
COL1	Collagen Type 1
CPEB	Cytoplasmic Polyadenylation Element-Binding Protein

CR1	Complement Component (3b/4b) Receptor 1
CRBN	Protein Cerebron
CREB	Camp-Regulatory Element Binding Protein.
CSF	Cerebrospinal Fluid
CTFα	C-terminal Fragment α
CTFβ	C-terminal Fragment β
Ctrl	Control
CuBD	Copper-Binding Domain
DAB1	Disabled Homologue 1
DI	Discrimination Index
DISC1	Protein Disrupted In Schizophrenia 1
DMEM	Dulbecco´s
DNA	Deoxyribonucleic acid
DMSO	Dimethyl Sulfoxide
DPPC	Dipalmitoyl-Sn-Glycero-3-Phosphocholine
DTT	Dithiothreitol
EDC	1-Ethyl-3-(3-Dimethylaminopropyl)Carbodiimide
eFAD	Early Onset Familial Alzheimer´s Disease
ELISA	Enzyme-Linked Immunosorbent Assay
EMA	European Medicines Agency
EPHA1	Ephrin Type-A Receptor 1
ER	Endoplasmic Reticulum
ERK2	Extracellular Signal-Regulated Kinase 2
eSAD	Early Onset Sporadic Alzheimer´s Disease
eTau	N-Terminally Fragmented Forms Of Tau
FBLN1	Fibulin 1
FBS	Fetal bovine serum
FcGRT	FcRn Receptor
FDA	Us Food And Drug Administration
FKBP12	Fk506 Binding Protein 12
FLOT1	Flotilin 1
FOs	Fibrillar Oligomers
FPRL1/2	Formyl Peptide Receptor-Like 1
FTDP-17	Fronto-Temporal Dementia With Parkinsonism-17
GABABR	Gaba Type B Receptor
GERAD	Genetic And Environmental Risk For Alzheimer's Disease Consortium
GFAP	Glial Fibrillary Acidic Protein
GFLD	Factor-Like Domain Growth
GMP	Good Manual Practises
GPC1	Glypican 1
GRB2	Growth Factor Receptor-Bound Protein 2
GSK-3	Glycogen Synthase Kinase-3
GSK-3β	Glycogen Synthase Kinase-3β
GWAS	Genome-Wide Association Studies
HAT	hypoxanthine-aminopterin-thymidine medium
HBD	Heparin-Binding Domain
HD	Huntington Disease
HEPES	4-(2-hydroxyethyl)-1-piperazineethanesulfonic acid
HFIP	1,1,1,3,3,3- Hexafluoro-2-Propanol
HHV	Human Herpesvirus
HSC70	Heat Shock Cognate 70

HSP	Heat Shock Protein
HSQC	Heteronuclear Single Quantum Correlation
HT	Hypoxanthine Thymidine supplement
IDE	Insulin-Degrading Enzyme
IFA	Incomplete Freund´S Adjuvant
IFAD	Late-Onset Familial Alzheimer´s Disease
IFN-γ	Interferon-γ
Ig	Immunoglobulin
IGF-1	Insulin-Like Growth Factor-1
IGF-1R	Insulin-Like Growth Factor-1 Receptor
IL-1	Interleukin 1
IL-6	Interleukin 6
ISAD	Late-Onset Sporadic Alzheimer´s Disease
ISF	Interstitial Fluid
IVIg	Intravenous Immunoglobulins
JIP	Jun N-Terminal Kinase-Interacting Protein
JNK	C-Jun N-Terminal Kinase
KLH	Keyhole Limpet Hemocyanin
KO	Knock Out
LDLR	Low Density Lipoprotein Receptor
LINGO1	Leucine-Rich Repeat And Ig Domain-Containing Nogo Receptor-Interacting Protein 1
Lip	Liposome
LRP1	LDLR-Related Protein 1
LRP2	LDLR-Related Protein 2
LTD	Long-Term Depression
LTP	Long-Term Potential
mAb	Monoclonal Antibody
MALDI	Matrix-Assisted Laser Desorption/Ionization
MALDI-TOF	Matrix-Assisted Laser Desorption/Ionization-Time-Of-Flight
MAPK1	Mitogen-Activated Protein Kinase 1
MAP1	Microtubule-Associated Protein 1
MAP2	Microtubule-Associated Protein 2
MAPT	Microtubule-Associated Protein Tau
MCI	Mild Cognitive Impairment
MED12	Mediator Complex Subunit 12
MEM	Minimum Essential Medium
mGluR5	Metabotropic Glutamate Receptor 5
MNPs	Magnetic Nanoparticles
MRI	Magnetic Resonance Imaging
MVBs	Multivesicular Bodies
MW	Molecular Weight
nCTF	C-terminal Fragment n
NFATc4	Nuclear Factor Of Activated T-Cells;
NFTs	Neuro Fibrillary Tangles
NGF	Nerve Growth Factor
NHS	N-Hydroxysuccinimide
NiReg	Neuroimmune Regulatory Proteins Activity
NMDA	N-Methyl-D-Aspartate
NMDAR	N-Methyl-D-Aspartate Receptor
NMR	Nuclear Magnetic Resonance
NO	Nitric Oxide

NOGOR	Nogo-66 Receptor
NOR	Novel Object Recognition
NPs	Nanoparticles
NTN1	Netrin 1
OLFM1	Olfactomedin 1
P75NTR	P75 Neurotrophin Receptor
P75NTR	Low Affinity Neurotrophin Receptor P75
pAb	Polyclonal Antibody
PACA	Poly (Alkyl Cyanoacrylate)
PAT1	Protein Interacting With App Tail 1
PBS	Phosphate Buffered Saline
PET	Positron Emission Tomography
PEG	Polyethilene Glycol
PFA	Paraformaldehyde
PFs	Protofibrils
PFOs	Prefibrillar Oligomers
pGlu-Aβ	Pyro-Glutamated Forms Of Aβ
PHFs	Paired Helical Filaments
PI3K/AKT	Serine/Threonine Kinases
PICALM	Phosphatidylinositol Binding Clathrin Assembly Protein
PiD	Pick Disease
PIN1	Peptidyl-Prolyl Cis–Trans Isomerase Nima-Interacting 1
PKA	Protein Kinase A
PP1	Protein Phosphatase 1
PrPc	Cellular Prion Protein
PSA	Puromycin-Sensitive Aminopeptidase
PSD95	Post-Synaptic Density Protein 95
PSEN1	Presenilin 1
PSEN2	Presenilin 2
PSP	Progressive Supranuclear Palsy
pTAU	Phosphorylated tau Peptide
rab4	Ras-Related Protein 4
RabGTPases	Ras-Related Protein-associated GTPases
RAGE	Scavenger Receptor For Advanced Glycation End Products
RELN	Reelin
RFU	Relative Fluorescence Units
RNA	Ribonucleic Acid
sAPP	Soluble APP
sAPPβ	Soluble APP β fragment
sAPP α	Soluble APP α fragment
SDS	Sodium Dodecyl Sulfate
SHC	Src Homology 2 Domain-Containing-Transforming Protein 1
SLN	Solid Lipid Nps
SNX	Sortin Nexin
SORL1	Sortilin-Related Receptor
SORT1	Sortilin 1
SP	Signalpeptide
SPON1	F-Spondin
STUB1	Stip1 Homology And Ubox-Containing Protein 1
SYT1	Synaptotagmin 1
SYP	Synaptophysin

TAG1	Transient Axonal Glycoprotein
TEM	Transmission Electron Microscopy
TFA	Trifluoroacetic Acid
TFE	Trifluoroethanol
TFCP2	Transcription Factor Cp2
TG	Transgenic
TGF-β	Transforming-Growth Factor-β
TGN	Trans-Golgi Network
ThT	Thioflavin T
TMD	Transmembrane Domain
TNF-α	Tumor Necrosis Factor A
TRKA	Tyrosine Kinase Receptor A
UPS	Ubiquitin-Proteasome System
VAMP2	Vesicle-Associated Membrane Protein 2
VLDLR	Very Low-Density Lipoprotein Receptor
VPS	Vacuolar Protein Sorting-Associated Protein
VSMCs	Vascular Smooth Muscle Cells
WB	Western Blot
WT	Wild Type

1. State of the Art

1.1. Disease description

1.1.1.History

Back in 1906 South-West German Psychiatrists meeting in Tubingen (Germany), Alois Alzheimer, a psychiatrist and neuroanatomist, described a strange and severe disease found in a 50-year-old woman called Auguste Deter. He reported the woman had suffered a progressive disorder consisting in paranoia, sleep alteration, memory disturbance, aggression, confusion and finally death 5 years later after her admission. The disease pathology presented defined plaques and neurofibrillary tangles that were identified in post-mortem brain histology examinations of this case and other patient´s cases described by Alzheimer in 1909 and 1911. Rapidly, “Alzheimer´s disease” was included in the 3th edition of Psychiatrie in 1910 and, later on, Alzheimer gained the chair of psychiatry in Breslau before his death in 1915 [1].

More recently, in 1984, a meeting gathering some prominent scientist took place in Scotland to discuss the pressing problem of a severe disease affecting goats and sheep, scrapie disease. This illness jumped from animal to animal without leaving vestige of any virus or microorganism and the only trace it left behind was insoluble plaques formed by numerous aggregated protein clumps. On the first dinner of that meeting a neurologist called Colin Masters and a protein sequencing expert Konrad Beyreuther talked about the similarities between scrapie and a human disease that also presented plaques in the brain. It was called Alzheimer´s disease (AD). Masters and Beyreuther started to collaborate in this field, unleashing the smallest stable protein present in AD samples, a ≈40 amino acids peptide that they called A4. This peptide was later known as amyloid beta (Aβ). Their collaboration was probably the most important stimulus to modern AD research and launched one of the most important study lines, the amyloid hypothesis [33].

1.1.2.AD Numbers

According to 2015 World Alzheimer Report [2], AD is one of the most widespread diseases among heart disease, cancer and stroke, affecting 46.8 million people worldwide nowadays. Projection of the AD cases in the future predicts that there will be around 74.7 million in 2030 and 131.5 million in 2050 (Figure 1.1). That means that the number will almost double every 20 years, estimations 12-13% higher than those made for the World Alzheimer Report 2009. On the other hand, new AD incidence estimations are 30% higher than the ones calculated in 2010, reaching 9.9 million cases per year. These new cases are regionally distributed as 4.9 million (49% of the total) in Asia, 2.5 million (25%) in Europe, 1.7 million (18%) in the Americas, and 0.8 million (8%) in Africa [2].

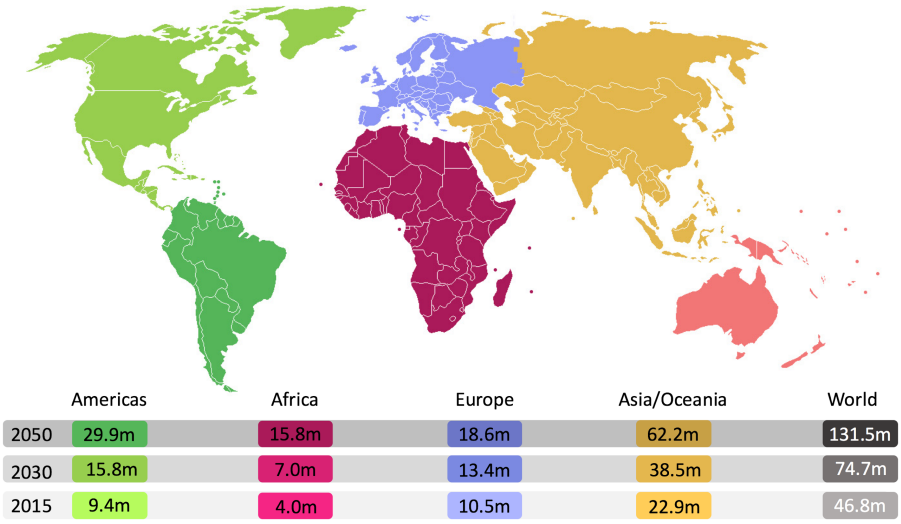

Figure 1.1. Number of cases registered and described in the 2015 World Alzheimer Report. Cases are distributed by regions and worldwide. The estimations for years 2030 and 2050 were calculated from the evolution of the cases between the World Alzheimer Reports of 2010 and 2015 [2, 557].

Global costs are also dramatically increasing year by year, reaching US$ 818 billion in 2016, drawing a projection in the future of a 35% increase per year, passing the US$ trillion in 2018. For instance, this is affecting all health systems around the world, taking huge amounts of human and material resources and money [556].

1.1.3.A short description of AD

During the last years, AD has been described as a neurodegenerative disorder that causes dementia, depriving people of their memory, functionality and dignity. It is an important neurodegenerative disease that affects the central nervous system and physiologically characterized by the presence of increased extracellular Aβ deposits (neuritic plaques) and intracellular tau protein neurofibrillary tangles. But also deposits of α-synuclein (Lewy bodies) and TDP43 are frequently found in AD patient's brains among cerebrovascular lesions. Some identified early symptoms of AD are short-term memory loss, difficulty in daily life tasks developing and social life deterioration [33].

However, that disease description based on clinical symptoms such as memory loss and cognitive decline has been recently reformulated in order to be focused on the biological basis and changes that lead to the development of AD [487]. The committee designated by the National Institute on Aging and the Alzheimer´s Association (NIA-AA) agreed that only biomarkers that are specific for hallmark AD proteinopathies (i.e., Aβ and pathologic tau) should be considered as potential biomarker definitions of the disease. In this regard, Aβ (A), pathologic tau (T) and neurodegenerative/neuronal injury biomarkers (N) and cognitive symptoms (C) were taken as the reference parameters for the new clinical definition and staging. A and T indicate specific neuropathological changes that define Alzheimer's disease, whereas (N) and (C) are not specific to Alzheimer's disease and are therefore placed in parentheses. According to these new guidelines, the biomarker profiles would be associated to a disease category as is shown in Table 1.1:

Table 1.1. New proposed descriptive nomenclature: Syndromal cognitive staging combined with biomarkers (adapted from ref 487).

	Cognitive stage (C)		
AT(N) Profile	**Cognitive Unimpaired**	**Mild Cognitive Impairment**	**Dementia**
A-T-(N)-	normal AD biomarkers, cognitively unimpaired	normal AD biomarkers with MCI	normal AD biomarkers with MCI
un	Preclinical Alzheimer's pathologic change	Preclinical Alzheimer's pathologic change	Preclinical Alzheimer's pathologic change
A+T+(N)-	Preclinical Alzheimer's disease	Preclinical Alzheimer's disease	Preclinical Alzheimer's disease
A+T+(N)+			
A+T-(N)+	Alzheimer's and concomitant suspected non Alzheimer's pathologic change, cognitively unimpaired	Alzheimer's and concomitant suspected non Alzheimer's pathologic change, cognitively unimpaired	Alzheimer's and concomitant suspected non Alzheimer's pathologic change, cognitively unimpaired
A-T+(N)-	non-Alzheimer's pathologic change, cognitively unimpaired	non-Alzheimer's pathologic change, cognitively unimpaired	non-Alzheimer's pathologic change, cognitively unimpaired
A-T-(N)+	non-Alzheimer's pathologic change with MCI	non-Alzheimer's pathologic change with MCI	non-Alzheimer's pathologic change with MCI
A-T+(N)+	non-Alzheimer's pathologic change with dementia	non-Alzheimer's pathologic change with dementia	non-Alzheimer's pathologic change with dementia

1.1.4.Anatomic Brain Changes During AD

Anatomically, AD affects different brain areas depending on the pathology progression. In AD progression, the hippocampus and its connected structures are the first areas affected. This affects the formation of new memories or learning new information. The hippocampus is needed for formation and retrieval of memories, although retrieving long term memories may depend less on it.

Amygdala may be the next area affected after the hippocampus. Due to it, a person with AD will often recall emotional aspects even if they do not recall the factual content. As AD pathology spreads through the brain, additional areas such the cortex are affected, suffering important cell loss becoming thinner and shrinking. This is when also older memories are lost.

The left hemisphere is one of the areas affected after amygdala and cortex, and which damage is linked to problems with semantic memory and language. Also the visual system in the temporal lobes is affected, making recognizing familiar faces and objects harder. However, due to the pathways for vision and hearing are separate, AD patients may still know who that person is if they hear them speak. At the right parietal lobe, pathology spreading might cause problems with judging distances in three dimensions.

As the damage expands to the frontal lobes, decision-making, planning or organizing functions would be affected. A complex task composed by a sequence of steps, might become much harder.

However, in contrast to these losses, some abilities could be retained, particularly those acquired long ago. Learned relying on procedural memories are mostly stored deep within the brain, allowing these skills to be retained the longest.

1.1.5.Tau Braak Stages

Also the changes in tau neurofibrillary metabolism and morphology occurring during AD pathology development permit to differentiate several stages. These stages definition has been extensively used for AD diagnosis during the last years. The distribution pattern allows to identify six stages, that could be summarized into more general three steps. This recognizable pattern and its stages are the so-called “Braak Stages”, and are summarized here [490]:

Table 1.2. Summary of the main Braak stages with the physiological and anatomical changes in the brain observed at each stage.

Braak Stage	Stage description
Stage I.	- First lesions in the transentorhinhal region are detectable. - The projection cells in this region are the first in accumulate detectable hyperphosphorylated tau.
Stage II	- Lesions spread from transentorhinal to entorhinal region, particularly to its superficial cellular layer. - AT8-positive* areas start to appear in hippocampal CA1 and CA2 regions. - First neuritic plaques (NPs) became detectable in CA1.
Stage III	- Lesions detected in stages I and II become more severe. - The disease progression encroaches through the fusiform and lingual giry of the neocortex. - All the external layers in entorhinal area show a number of AT8-positive* neurites, as in CA1 and CA2 hippocampal areas. Moreover, CA3 and CA4 start to present a number of AT8-positive* mossy cells. - Few NPs start to develop in the neocortex II to IV layers.
Stage IV	- Lesions progress widely into neocortical associated areas. Areas affected in Stage III present even worse symptoms. - CA1 and CA2 present dense AT8 immunoreactivity, as it present large numbers of mossy cells in CA3 and CA4 areas. - The pathology invades the mature neocortex, accompanied with the develop of neuritic plexuses in the middle temporal convolution while the occipital neocortex remains unaffected or presenting few AT8-positive pyramidal cells and NPs in the Broadmann area 19.
Stage V	- Neocortical disease progression spread through frontal, superolateral and occipital directions, reaching the peristriate region. - Lesions extend through first temporal convolution and association areas of the frontal, parietal and occipital neocortex. - Primary visual field (striate area) also starts to show punctual AT8-positive* areas.
Stage VI	- The pathology extends to the secondary and primary neocortex areas and reaches the striate area in the occipital lobe. - In the final stage of the disease progression almost all the neocortex present severe lesions, in addition to all the areas affected in the previous stages.

*AT8 is a monoclonal antibody that specifically binds hyperphosphorylated tau protein. It is widely used in clinic.

1.1.6.Types

Although AD mainly affects people older than 65 years-old (50% of the people older than 85 face the risk of suffering the disease), it is not necessarily an age-related disease. In fact, we can classify different types of AD in function of its origin and the age of onset. By these criteria we can dissect AD into four categories: early onset familial AD (eFAD), late onset familial AD (lFAD), early onset sporadic AD (eSAD) and late onset sporadic AD (lSAD) [436, 68, 369].

However, we should consider AD as a continuum, a combination of several factors and different grades across these elements. Although there is not clear consensus, an AD diagnosis in the thirties, forties and fifties is considered early onset AD and from 75 years old and ahead, late onset AD. Formal diagnostic tests set the differentiation line in 65 years old.

By this way, eFAD is characterized by a very early presentation of the symptoms, caused by genetic factors related to APP and its processing that will be detailed in next section. Literature estimates that this AD form conforms the 2 to 5% of all AD cases, although is quite difficult to assess due to complex diagnosis of the disease. eSAD is another class of patients which present the symptoms in an early stage (before 65 years-old) but without any confirmed correlation with any genetic factor. On the other hand, among patients presenting the first symptoms after the age of 65, we can differentiate between confirmed genetic cause (lFAD) and others without a genetic correlation (lSAD) [368, 369].

We still do not understand completely the contribution of genetics and environment to AD, but it must be considered as a drawing spectrum following the premise that the later the onset of AD, the more environment and aging factors are supposed to influence and dominate over genetic predisposition and, on the other hand, the earlier the age of onset, the more probable AD will be driven by genetic factors [436].

1.1.7.Risk factors

Despite there is not a complete consensus about the pathophysiology of AD [3], in 2011 the National Institute of Neurological and Communicative Disorders and Stroke and the Alzheimer Disease and Related Disorders Association (NINCDS-ADRDA) updated the criteria set developed in 1984 to allow clinicians and researchers to maintain certain diagnosis coherence based in the most recent technological advances and scientific data related to the genetic understanding of the disease or newly found biomarkers [11, 12]. From these studies, there have been found evidences of a number of different factors that seem to contribute, to a greater or lesser extent to AD incidence.

1.1.7.1. Genetic factors

AD is a genetically complex disease, showing a heritability between 54 and 79%. The AD form denominated eFAD is the result of some autosomal-dominant genetic mutations in chromosomes 1, 14 and 21, responsible for amyloid precursor protein (APP), presenilin 2 (PSEN2) and presenilin 1 (PSEN1) coding respectively. Among these three, PSEN1 mutation seems to be the most frequent in eFAD patients (Table 1.3) [65, 66, 67, 364].

These high penetrant mutations, are essentially autosomal inherited and lead to increased Aβ(1-42) peptide production and aggregation rates and to early onset of AD, usually starting during the fourth or fifth decade of patient´s life. APP mutations are present in less than 1% of all AD patients. All APP missense mutations affect the protein processing and/or aggregation due to being positioned in or near the Aβ-coding exons (16 and 17) (see AD Mutation Database, http://www.molgen.vib-ua.be/ADMutations/). Another APP gene mutation found related with AD involves a microduplication in the APP locus in chromosome 21 [369].

Nowadays there have been identified more than 180 mutations related with AD in PSEN1 gene meanwhile only 14 mutations have been identified in PSEN2 gene. The vast majority of mutations in PSEN genes are single-nucleotide substitutions, but there also been identified some small deletions and insertions. Mutations in PSEN genes alter the γ-secretase proteolytic cleavage of APP, leading to an increased Aβ(1-42)/ Aβ(1-40) ratio, which suggest a partial loss-of-function instead of a gain-of-function [68]. Mutations in these genes represent a low percentage of total AD cases, but their discovery lead to an essential understanding of the role of Aβ in the pathogenesis of AD. In consonance with these findings, Aβ hypothesis point to that

neurodegenerative processes present in AD pathology are a consequence of the imbalance between Aβ production and clearance, suggesting that other genes related to these pathways could also be risk factors [369].

Regarding the so-called common variants typically related to late-onset AD, ApoE seems to be the strongest factor, which Apoε4 variant, even without been considered a deterministic mutation, is a classic risk factor supposed to be related with an important increase of the probability to develop AD and the earlier apparition of the disease. Multiple allelism (ε2, ε3, and ε4) has been described, where ε3 is considered a neutral allele, ε4 the high-risk allele, and ε2 a protective allele. It has been also found that allele ε4 could influence the disease onset in a dose-dependent way [69]. However, the percentages of cases supposedly related to ε4 allele is about 20% (Table 1.3) [70].

Table 1.3. Main gene variants associated with AD (adapted from ref. 369).

Gene	Main alteration	Presumed mechanism
Amyloid precursor protein (APP)	Mutation	Autosomal dominant, mostly early onset
Presenilin 1 (PSEN1)	Mutation	Autosomal dominant, mostly early onset
Presenilin 2 (PSEN2)	Mutation	Autosomal dominant, mostly early onset
Apolipoprotein-E (APOE)	Common variant	Familial and sporadic, late onset
Sortilin-related receptor (LDLR class)	Common variant	Familial and sporadic, late onset
Clusterin (CLU)	Common variant	Sporadic, late onset
Phosphatidylinositol binding clathrin assembly protein (PICALM)	Common variant	Sporadic, late onset
Complement component (3b/4b) receptor 1 (CR1)	Common variant	Sporadic, late onset
Bridging integrator 1 (BIN1)	Common variant	Sporadic, late onset
ABCA7	Common variant	Sporadic, late onset

Moreover, several Genome-Wide Association Studies (GWAS) performed by the Genetic and Environmental Risk for Alzheimer's disease Consortium (GERAD) in the last years have identified several novel variants in clusterin (CLU), phosphatidylinositol binding clathrin assembly protein (PICALM), complement component (3b/4b) receptor 1 (CR1), bridging integrator 1 (BIN1), the TP-binding cassette (ABC) transporter A7 (ABCA7), CD2-associated protein (CD2AP), CD33 receptor and Ephrin type-A receptor 1 (EPHA1) genes associated to the development of the disease and other underlying pathologic mechanisms [71, 72, 73, 363, 364, 366, 367, 368]. Some of these genetic variants have been confirmed in other non-Hispanic and Hispanic populations [74, 75, 76], while others have not (Table 1.3) [367, 124].

1.1.7.2. Non-genetic factors

Regarding to AD-related non-genetic risk factors, cerebrovascular disease including infarcts, cerebral haemorrhage or vasculopathies seem to be some of the most solid factors, but also hypertension, diabetes, obesity, smoking and dyslipidemia all seemed to be related to the disease development [369].

It has been found that presence of cerebrovascular disease or stroke accidents could increase two-fold the incidence of new-onset dementias [48], may be due to destruction of brain parenchyma, thalamic strokes, atrophy [49, 50] and an increased levels of p25 gene expression; a deregulator of the cyclin dependent kinase 5 (CDK5) activity, ultimately leading to the accumulation of hyperphosphorylated forms of the microtubule-associated protein tau; and β-secretase (BACE1), which could lead to a higher Aβ production and deposition [51, 52].

Some cross-sectional and longitudinal studies have pointed to a significant relation between high blood pressure during mid-age and the incidence of dementia in the late-ages [53, 54, 55].

However, trials using anti-hypertensive drugs in AD have reported non-conclusive results [56, 57].

Type II diabetes has also been associated with about two-fold increase in AD incidence [58, 59, 558]. It is hypothesized that the hyperinsulinemia could interfere with Aβ clearance through competition for the insulin-degrading enzyme (IDE) [58,60]. Moreover, adiponectin, resistin, leptin, interleukin 6 (IL-6) or tumor necrosis factor α (TNF-α) expression seem to be correlated with hyperinsulinemia and insulin resistance, factors directly and indirectly related with AD development [61, 62].

Some of these complications are derived from diet and other habits, like smoking, contributing to imbalance oxidative metabolism, cholesterol levels, increasing vascular risk and increasing cell death [13, 14, 15, 16, 17].

Another non-genetic risk proposed by some researchers in the last years is the infection of the central nervous system (CNS) by fungi or viruses. Some works published since 2014 found fungal proteins, RNA and DNA in AD patient´s brains, pointing to fungal infection as one of the causes of, at least, some types of AD [501]. One more work published in 2018 described the presence of viral RNA and DNA in AD patients from different cohorts, finding pathogenic regulation of molecular, clinical, and neuropathological networks by two strains of human herpesvirus (HHV-6A and HHV-7) [559]. However, whether these findings represent a causal and significant contribution, or reflect the presence of opportunistic passengers during neurodegeneration, is still something unclear and difficult to resolve.

1.1.7.3. Protective factors

On the other hand, some types of activities or habits could be related with a decrease in AD incidence and severity, called “protective factors”. A higher education, physical activities or an increased leisure activity are supposed to provide an “extra” cognitive reserve, increased lipid metabolism, neuronal plasticity and brain vascularization, and general mental stimulation [37, 38, 44, 45, 47]. Diet seems to also play an important role, with special mention to Mediterranean diet and omega-3 fatty acids, with could be related to higher levels of antioxidant and anti-inflammatory brain factors [41, 42, 43]. Although those factors seemed to work as a protection against the disease development, there is still a lot of controversy between results from different populations and methods and must be taken into account with reserve [369].

1.1.8.Pathophysiological description

Aggregation and misfolding of certain proteins seem to be in the origin of diseases like AD and Parkinson. Pathologic signals are derived from the conversion of starting monomeric and soluble species into aggregated, organized, insoluble fibrillary species. This process is controlled and could be affected by a number of mechanisms and parameters in the complexity of the cellular environment. Multiple hypothesis have been risen on the basis of the multiple factors responsible for the disorder such as amyloid hypothesis, tau hypothesis, cholinergic hypothesis, inflammation hypothesis and, as previously assessed, fungal or viral infections [4, 501, 559].

Most recent and important research works on the field point to amyloid and tau hypothesis as major players in the disease origin and progression, but, how, when and where AD leading Aβ(1-42) starts to gain pathological role in the disease progression? Or maybe is some form of tau the triggering cause for the Aβ pathology-related molecular processes? Several works leaded by Braak and colleagues have pointed that the apparent very early appearance and spread of intraneuronal hyperphosphorylated tau forms from the brainstem to the superior cerebral cortex areas is not accompanied nor preceded by Aβ(1-42) extracellular deposits [147]. However, the lack of a known link between tau mutations and AD weakens the hypothesis of being tau the only and primary origin of the disease. On the other hand, there are a number of published works supporting that Aβ(1-42) oligomers in fact could induce tau hyperphosphorylation, neurofibrillary tangles (NFTs) formation, and synaptic pathology even in the absence of visible senile plaques. In fact, the easily visualized fibrillary and insoluble Aβ(1-42) deposits are not the main toxic elements [152, 308].

Nevertheless, the difficult visualization and control of soluble Aβ(1-42) oligomer species and other tau species make complicated to follow the pathology and could induce to errors [148, 149, 150,

151]. A schematic representation of a theoretical model considering all these main suspects and their evolution along the disease progression is presented in Figure 1.2.

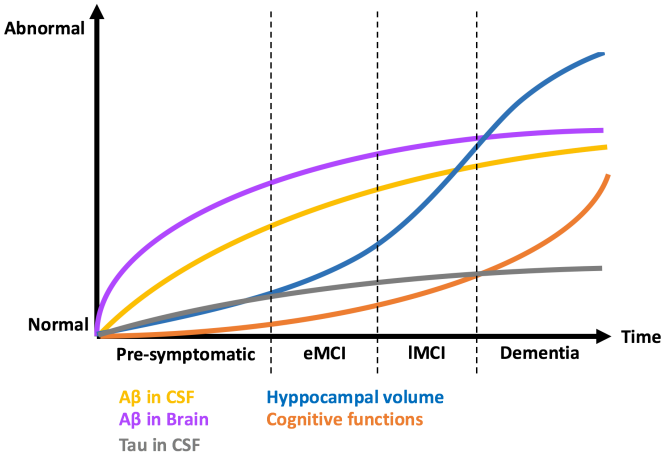

Figure 1.2. Arbitrary graphic showing the evolution of different biomarkers and cognitive decline during the development of AD. Cerebrospinal fluid (CSF) Aβ(1-42) and imaging of aggregated Aβ(1-42) in the brain show a fast accumulation in both compartments during the first pre-symptomatic stages of the disease, preceding cognitive and functional decline. Tau seems to have a more stable and gradual accumulation in CSF along the disease development, stabilizing in the late stages. On the other hand, is has been observed that hippocampal shrinking is more accentuated along the previous phase to dementia, being correlated by an important decline in cognitive functions (adapted from ref 437).

1.1.8.1. Aβ hypothesis

Under normal healthy conditions, Aβ seems to work as a synaptic activity regulator [153] and even to play an important role in memory formation and consolidation [154]. In these physiological conditions Aβ(1-42) monomers are degraded by several proteases such as IDE, neprilysin, or deriving those monomers into the circulation, outside brain [150, 151]. But when the organism ages, neurons become fragile and prone to develop other disorders that decreases the Aβ(1-42) degrading and clearing capacity to the vascular compartment, leading to the accumulation of these species and aggregation forming extracellular toxic oligomers, fibrils and plaques. Here we present a comprehensive compendium of the last and most important findings on this mechanistic hypothesis:

1.1.8.1.1. APP

The first player in this process is APP, a type I single-pass transmembrane protein encoded by a unique gene placed in GRCh38.p7, chromosome 21 with a large extracellular domain formed by E1 and E2 subdomains linked by the acidic domain (AcD), a transmembrane region and a shorter cytoplasmic tail (Figure 1.3). It is synthesized in the endoplasmic reticulum (ER) and transported to the cell membrane via the secretory pathway. As transiting through Golgi apparatus, APP can suffer several post-transcriptional modifications such as phosphorylation, glycosylation and sulfation. APP is later delivered to the plasma membrane. [159, 160, 161].

Three major isoforms derived from alternative splicing have been described: APP695 APP751 and APP770. APP family physiological functions are very extensive and diverse, from neuroprotection, cell adhesion, synaptogenesis, synapsis stability and plasticity, gene regulation, subcellular trafficking or necroptosis, being able to work as cell surface receptor-like proteins or as ligands and to form cis and trans dimers, but it is probable that there still exist more unknown functions and interacting ligands (Figure 1.3) [10, 162, 163, 164, 165, 166].

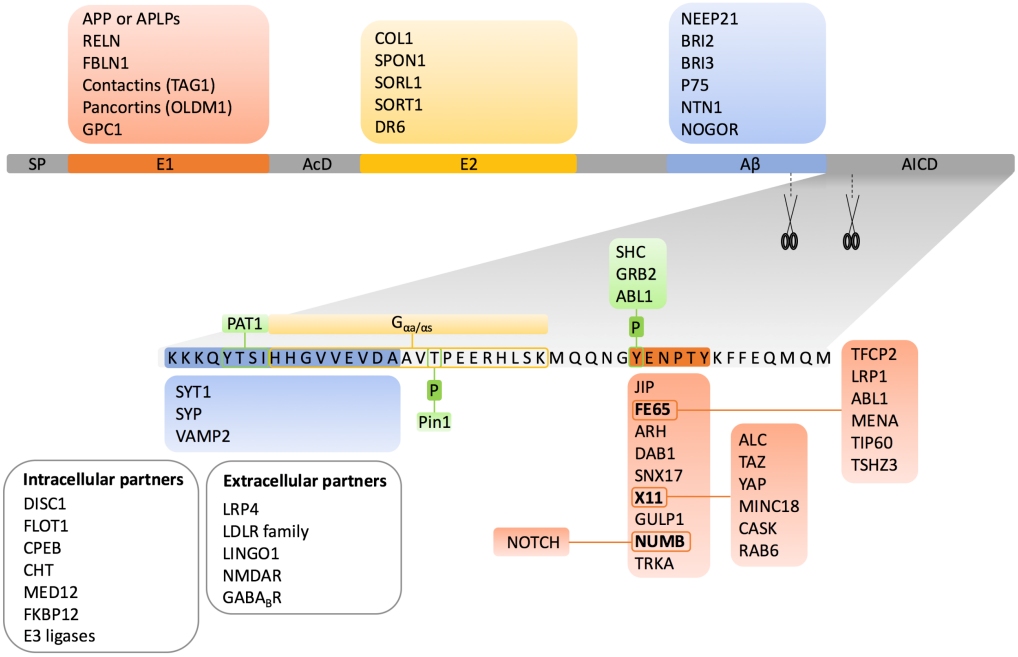

Figure 1.3. Schematic representation of APP and molecular interacting partners. Some of the APP molecular partners have their interacting domains already mapped (in the figure, in the same color of the interacting sequence). There are also some proteins that require adaptors for interacting with APP (shown in bold and subsequent panels). Also some members of the low density lipoproteins receptor´s (LDLR) family are known to interact with APP both with its extracellular and intracellular domain (adapted from ref 10).

Although there is no spatial structure solved of the whole APP molecule, there is available information from X-ray crystal structure studies for the independently folded E1 (4PWQ, 3KTM) [441,442] and E2 (3NYJ) [440] extracellular subdomains. Some studies have shown that APP can form intracellular dimers, but the mechanisms implicated remain controversial. It has been observed that three regions of APP, including the conserved domain E2, which is believed to have trophic functions as well, are involved in APP dimerization [440, 10]. E1 subdomain is composed by the growth factor-like domain (GFLD), which contains the first heparin-binding domain (HBD), and the copper-binding domain (CuBD). In the most common APP isoform APP695, the AcD is most likely to be unfolded and highly flexible, directly linking E1 to E2. There also are NMR solved structures of the cytoplasmic tail [444] and C-terminal fragment-β (CTFβ) [443], including the transmembrane domain (TMD). The TMD is a flexibly curved α-helix, target of γ-secretase. It also seems to be a suitable binding site for cholesterol, pointing to a mechanistic way to how cholesterol promotes amyloidogenesis. It also contains several membrane-buried GXXXG motifs which have demonstrated to have an important role in oligomerization besides to play a key role in cholesterol binding (Figure 1.4) [10].

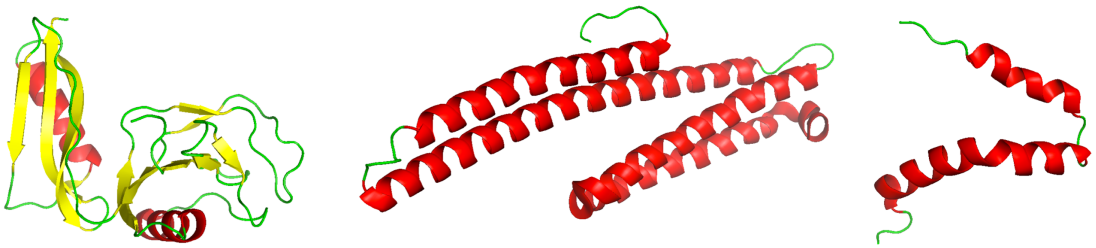

Figure 1.4. Solved structures of APP: E1(left, PDB ID: 4PWQ), E2 (center, PDB ID: 3NYJ) and CTFβ (right, PDB ID: 2LP1) domains solved by X-ray diffraction and NMR. Solved E1 structure is conformed by the growth factor like and the copper binding domains. E2 domain, proposed as a contributor to APP dimerization, is conformed by several well conserved α helices that interact with homologous structures by residues in position 369 and 433. The CTFβ solved structures show an extracellular amino terminus conformed by a surface-embedded N-helix connected to the TMD by a short loop.

1.1.8.1.1.1. APP trafficking

APP trafficking implies a complex network composed by several protein interactions. Starting with the internalization of the protein from the membrane in specialized clathrin-mediated endocytic pathway, process that requires previous clustering of APP via cholesterol and flotillins (REF). At the same time, BACE1 is also internalized via ADP-ribosylation factor 6 (ARF6) pathway, meeting APP at the early endosomes. In early endosomes, the pH is the ideal for APP β-secretase cleavage, generating the β-cleaved soluble ectodomain and the β-CTF fragment. The β-CTF fragment is further cleaved by γ-secretase at early and late endosomes. The APP intracellular domain (AICD) might be sorted to the nucleus for gene regulation functions [166] while Aβ would be transported to the multivesicular bodies (MVBs), where it can accumulate [169] or be released in exosomes or autophagosomes [18, 371].

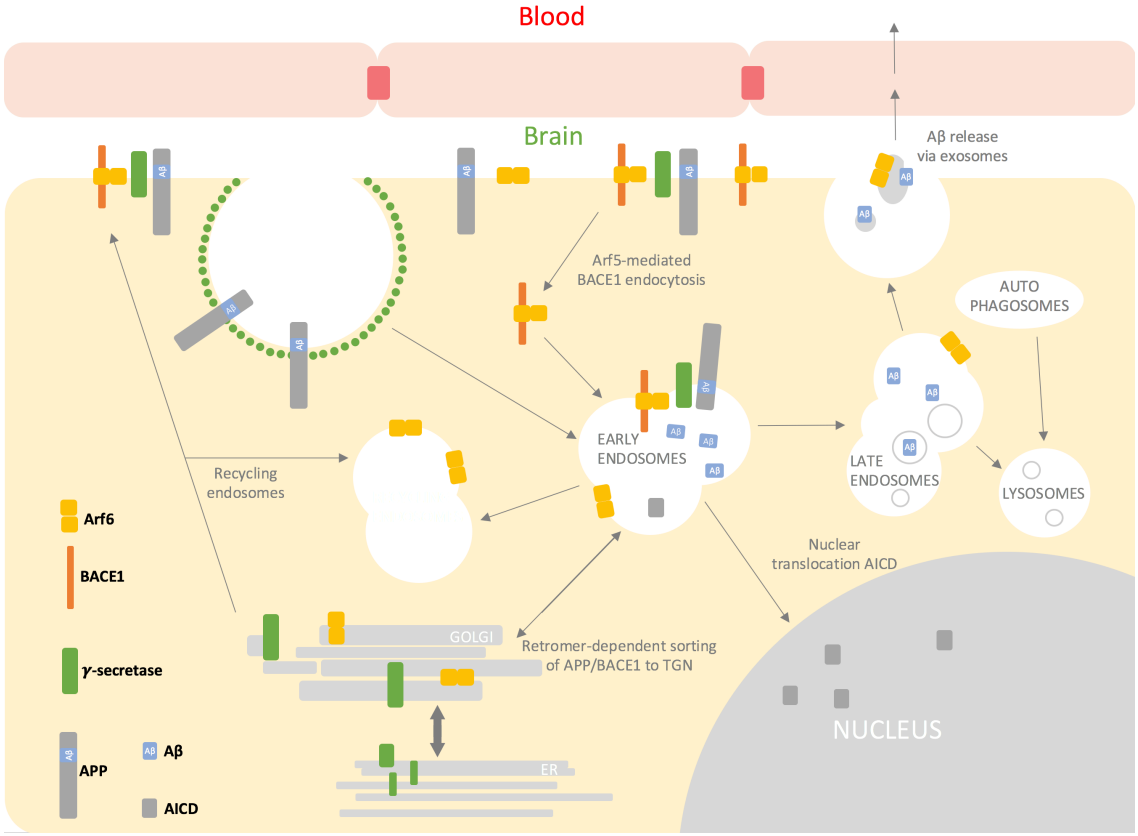

Figure 1.5. Membrane trafficking and processing pathways of APP. APP is internalized, processed and alternatively sorted to trans-Golgi network (TGN), nucleus or membrane retrieved via several pathways. β- and γ-cleavage of APP are produced at the early endosomes and then the products are sorted to the nucleus (AICD), to the lysosomal compartment or released to the extracellular space via exosomes (Aβ) (adapted from ref 18).

APP can also be subject of retrieval to the membrane via ras-related protein 4 (rab4) [94]. However, some protein complexes such as vacuolar protein sorting-associated protein 26 (VPS26), VPS29, VPS35 or sortin nexins (SNX) could bind to the sortilin-related receptors SorLA/SorCS1 and other retrieval receptors and lead APP to the TGN (Figure 1.5) [18].

Furthermore, it has been recently observed that APP sorted into MVBs upon ubiquitinations via CD2AP at early endosomes at the dendrites [372] (Figure 1.5).

1.1.8.1.1.2. APP Processing

In the canonical Aβ cascade hypothesis, APP is cleaved by the α-secretase in normal physiological conditions, producing sAPPα fragment and CTFα fragment, which then is cleaved by γ-secretase generating the P3 peptide [18]. Alternatively, APP is processed by β-secretase, which is a membrane-bound aspartyl protease, producing sAPPβ and CTFβ fragments [111]. There exist two known major forms of the enzyme, BACE1 and BACE2 [112, 113]. Although the

major responsible for the Aβ production, BACE1, is mainly expressed in brain, is also found at lower levels in other organs [111]. On the other hand, its homologous form, BACE2, is more commonly expressed in peripheral tissues rather than in brain [113]. However, some studies have shown that, although BACE1 exerts the major β-secretase activity in brain, some residual activity might be accountable to BACE2 [135] and even compete for the same substrates. BACE1 has been targeted by a number of pre-clinical and clinical trials [143], however, no successful treatments have been found to the date [307].

The γ-secretase complex, comprising PSEN1, PSEN-2, APH-1 and nicastrin subunits, is a membrane-embedded protease that controls a number of important cellular functions through substrate cleavage [91, 228, 292]. The γ-secretase cuts CTFβ in several transmembrane cleavage sites, liberating shorter and less harmful Aβ species. However, an inefficient cleaving of the fragment results in the generation of longer and more susceptible to aggregate Aβ species, ultimately leading to pathology spreading [19, 20, 21, 292] (Figure 1.6).

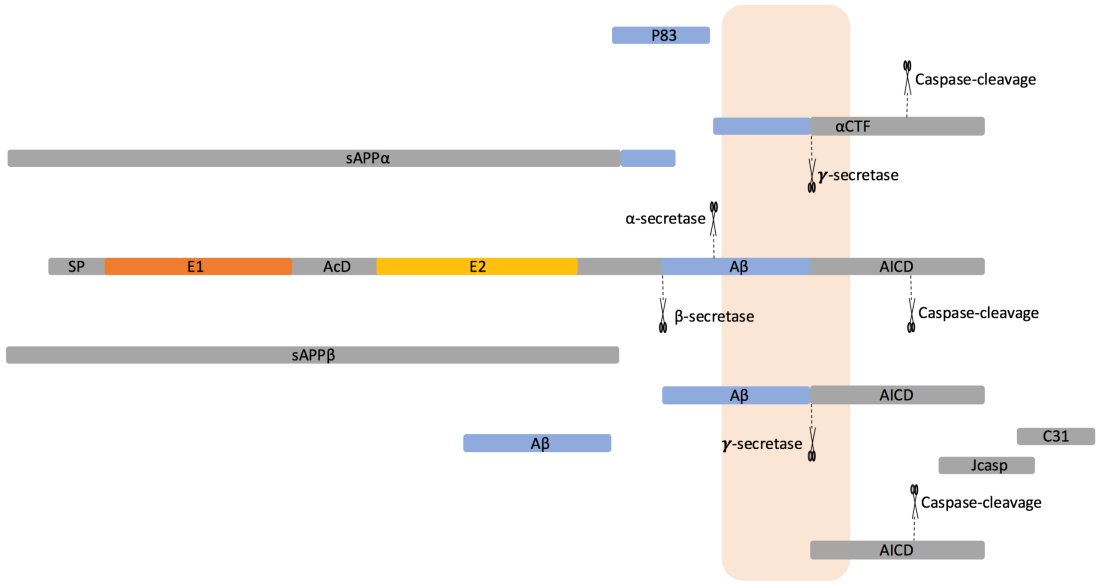

Figure 1.6. APP processing related to the canonical Aβ cascade hypothesis. APP canonical cleavage is produced by four secretases, α-secretase, β-secretase, γ-secretase and caspase, generating several products with different metabolic functions and pathologic roles. So Aβ would be generated by cleavage of β- and γ-secretases, being a disequilibrium of the α-secretase activity the main reason of Aβ accumulation in the cell.

However, recent studies have enlightened that APP metabolism is much more complex than it was thought, implying more enzymes, interactions between them and generating other Aβ species that could be as important as Aβ(1-42) peptide for the AD development [560].

Δ-secretase

Δ-secretase, or asparagine endopeptidase (AEP), has been linked to AD due to it is able to cleave tau, but it was recently shown that it can also process APP in two extracytoplasmatic sites, generating several products among which, one of them, the sAPP1-373, was found to be toxic for primary cultures of neurons [22].

n-secretase

Recent works have proposed n-secretase metalloproteinase as responsible for producing longer Aβ fragments related with AD pathology [23, 24]. This enzyme can cleave APP between N504 and M505 residues, producing a soluble 80-95 kDa fragment and a new nCTF that then can be processed by α and β-secretases. Those fragments have been shown to be five-fold more toxic than Aβ, causing synaptic dysfunction and inhibiting long-term potentiation (LTP) in hippocampal neurons. [24].

Mephryin β

Mephryin β is a zinc metalloproteinase with common cleavage sites and proposed as a competitor of β-secretase [25]. It has been shown its product, Aβ2-40 has higher aggregation index compared to Aβ(1-40), which also links this species to oligomeric assemblies' production [26].

Cathepsin B

APP protease cleavage by Cathepsin B has also been proposed as the origin of the production of N-terminally truncated pyro-glutamated forms of Aβ (pGlu-Aβ) with own increased aggregation proclivity [27]. However, the direct relation between the activity of Cathepsin B and the production of pGlu-Aβ remains unclear [560].

All these characters may play significant roles in AD pathology, which undoubtedly makes essential to study all those activities and fragments in detail besides the already relatively well known metabolic products of the canonical proteolytic pathways.

1.1.8.1.2. Aβ functions and structures

Aβ encompasses a group of peptides ranging from 37 to 49 residues, resulting from the proteolytic cleavage of APP and is related to several disorders, from Alzheimer disease, to type II diabetes or other systemic conditions [33, 39, 46, 95, 563, 60].

There exist three main regions within the Aβ peptide, distinguishable in terms of hydrophobicity character of the residues, that determine the interactions between the residues from the same peptide and with other molecules. Such interactions may facilitate the secondary and tertiary structures and the formation of more or less organized aggregates. Meanwhile the N-terminal region (1-14) is mainly polar and water-soluble and use to lack of any organized structure [526], the central region, from Asp13 to His23, and the C-terminal region, embracing residues Ala30 to Ala42 are a highly apolar zones, with a remarkable hydrophobicity and with tendency to form secondary and tertiary structures [87, 101] (Figure 1.7).

Aβ monomers are very prone to aggregation in different assemblies, including oligomers, protofibrils and amyloid fibrils, making the prediction of its behavior and structure under normal and pathological conditions extremely challenging [23, 39, 99, 87]. Although the most abundant form of Aβ is the (1-40) peptide (80-90%), the (1-42) (5-10%) is believed to be one of the most harmful species, particularly its oligomeric aggregates are believed to be the most dangerous [39, 46, 95, 96]. In consequence, mechanisms by which Aβ aggregates and form several aggregation species, such as fibrils or plaques have been extensively explored [80, 81, 82, 83, 84, 85, 86].

However, there still are several unresolved key points related to the molecular mechanisms by Aβ forms *in vivo* neurotoxic oligomeric and fibril species and the molecular basis behind the different normal function and neurotoxic properties between them [87, 88, 89, 90]. To overcome these issues and elucidate the structural and kinetic characteristics of Aβ aggregation is decisive for developing future therapeutic strategies against AD. In anyways, it seems that conformation changes from soluble α-helices to β-sheets in the peptide are critical for toxicity and for aggregation (Figure 1.7).

The three-dimensional solution structure of different fragments of Aβ have been studied mainly through NMR and molecular modelling. The structural models proposed are highly dependent on the type of fragment and the experimental conditions, but there are evidences of the formation of alpha-helical conformers that can transition more or less rapidly into β-sheets [32, 525]. The transition of alpha-helical conformers into β-sheets seems to play a key role in determining the state of protein aggregation [102, 525].

The two residue difference in Aβ(1-40) and Aβ(1-42) leads to great differences in their biophysical behavior. In aqueous in sodium dodecyl sulfate (SDS) micelles the solution structure of Aβ(1-40) peptide reveals that the C-terminus of the peptide has a preference to adopt an α-helix conformation between residues 15 and 36 with a hinge between residues 25-27, while the peptide is unstructured between residues 1 and 14, which, as previously exposed, are mainly polar and likely solvated by water [526, 561]. Although in high percentages of apolar solvents the tertiary structure is similar for both peptides, with two helical regions linked by a β-strand centered in residues 13-26, when increasing the water content to 90%, the Aβ(1-42) peptide predominantly forms secondary β-strand structures [524, 525, 21]. Residues 25-35, placed in the hinge region

could be key for the structural changes from α- to the more toxic-related β-structures [87, 101]. The N- and C-termini of the peptides lack of a stable structure, however, interactions with the hydrophobic helix in the central region determine relatively defined structures in the extremes. This facilitates the formation and stabilization of the hairpin structure. In addition, salt-bridges between Lys28 and Asp23 and Ala42 seem to be involved in the hairpin bend stabilization in Aβ self-assembly [562, 538]. Also in C-terminus region, interaction between F19 and G38 residues seems to facilitate another hairpin conformation [26] (Figure 1.7).

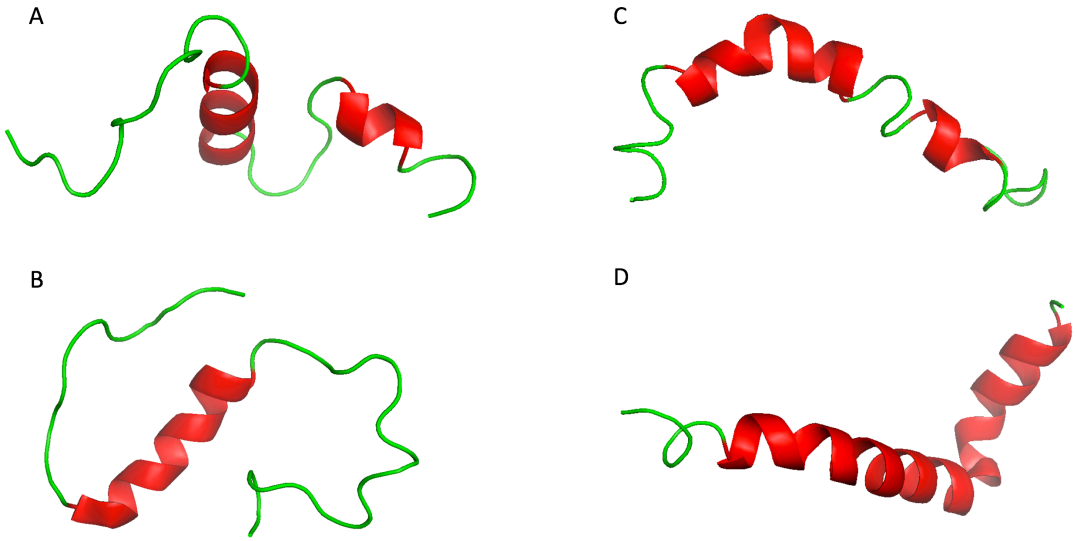

Figure 1.7. Different three-dimensional NMR-solved structures of Aβ submitted at the Protein Data Bank. A. PDB ID 1AML: Aβ(1-40) structure in 40% TFA in water published by Sticht et al. (1995) adopting two helix englobing residues G15-A23 and I31-M35 [561]. B. Aβ(1-40) structure in aqueous environment (PDB ID: 2LFM) submitted by Vivekanandan et al. (2011) forming a more compact structure and a helix between residues H13-D23 [526]. C. PDB ID 1Z0Q: Aβ(1-42) structure in aqueous environment/HFIP solved by Tomaselli et al. (2006) in HFIP/H2O 30:70 (v/v) showing that the only secondary structures that were lost on the path from a very apolar to an essentially polar environment were the β-turn around residues 25–26 and, partially, the short C-terminal helix [525] D. Aβ(1-42) structure in apolar environment (PDB ID: 1IYT) published by Crescenzi et al. (2002) forming two α-helices in residues S8-G25 and K28-G38 linked by a β-turn. α-helices are colored in red and disorganized regions in green [524].

The abundant kinetic data obtained and analyzed until now for Aβ(1-42) [131], Aβ(1-40) [132] aggregation phenomena reveal important variations in the main mechanisms implicated in the initiation and proliferation of amyloid aggregated species. Two mechanisms have been proposed that seem to be related with the formation of oligomers and the more organized fibrils. In one of the simplest nucleated polymerization mechanisms found, through a thermodynamically unfavorable process, monomers start to aggregate and form nuclei; then, from these nuclei, fibrils grow with the addition of monomers. These nuclei could be considered the smallest structures that can lead to fibril elongation [128].

Sometimes, some monomers with a well-defined structure are also considered as nuclei due to their high aggregation capacity [129, 130]. On the other hand, it has been observed that monomers can rapidly organize into misfolded aggregates without the proper structural characteristics to form organized fibrils [127]. However, this starting structure can be reorganized to generate nuclei, on which more disorganized oligomers eventually gain the required conformation that leads to fibril elongation [33, 127, 361] (Figure 1.8).

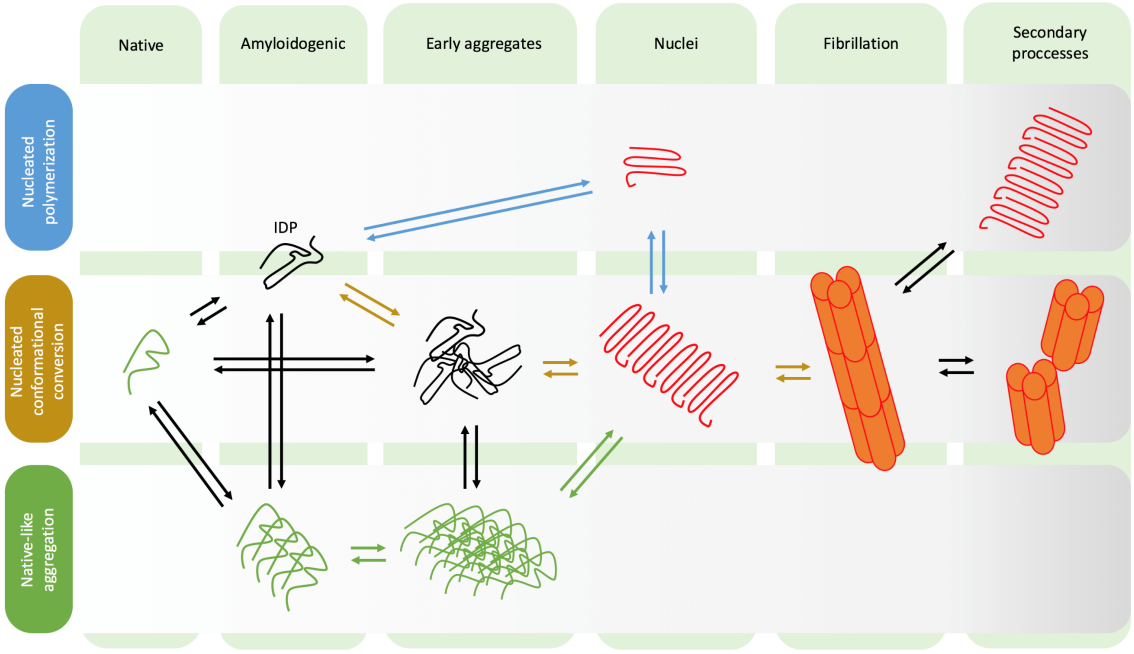

Figure 1.8. Amyloid aggregation pathways. There have been proposed different hypothesis about how amyloidogenic and aggregation mechanisms work. In the figure, vertical cards refer to different aggregation steps, while horizontally there are schematized different aggregation models including nucleated polymerization (brown arrows), nucleated conformational conversion (blue arrows), and native-like aggregation (green arrows). The secondary processes indicated on the right are referring to secondary nucleation (top) and fibril fragmentation (bottom) (adapted from ref 361).

It has also been observed that, the average content of β-sheet structure use to increase with molecular weight, suggesting that an increase in size stabilizes their β-sheet structure. In these oligomers, such β-sheet structure has been shown to involve both antiparallel [98, 105] and parallel and out-of-register strands [100], while in mature fibrils, the β-strands are positioned in a parallel and in-register manner [114, 115, 116, 117, 118].

Among these oligomer populations identified, there are a wide range of aggregated species, such as globulomers, amylospheroids (ASPDs), paranuclei, pentamers, Aβ*56, SDS-stable dimers/trimers, protofibrils (PFs), annular protofibrils (APFs), amyloid-derived diffusible ligands (ADDLs), prefibrillar and fibrillar oligomers (PFOs and FOs), and spherical amyloid intermediates [87, 92, 95, 96, 97, 98, 99, 100, 101, 102, 103, 104].

NMR analysis of several *in vitro* generated Aβ(1-40) fibrils [120, 121, 123] revealed two major models. In both cases, the β-strands are stacked forming a β-sheet, projecting along the axis of the protofilaments with all strands arranged in a parallel, in-register and generating a number of contacts between chains. The major differences between the two models remain in the number of β-sheets forming the primary structure along the protofilament axis, two in the first model and three in the second one, and in the diameter size, among other other intermolecular chain contacts [361].

Fibrillar and protofilamentar structures of N-truncated Aβ(1-42) have revealed similar in-register β-sheet core structures, with flexible N-terminal segments and a number of contacts between chains and different molecules. Again, polymorphisms are present, with fibrils showing 2 or 3 β-strand motifs linked by short coils and with different diameters [118, 538, 122, 117] (Figure 1.9). Some of amyloid fibrils formed in non-pathological conditions could have metabolic and regulatory functions in living systems [77, 78, 79].

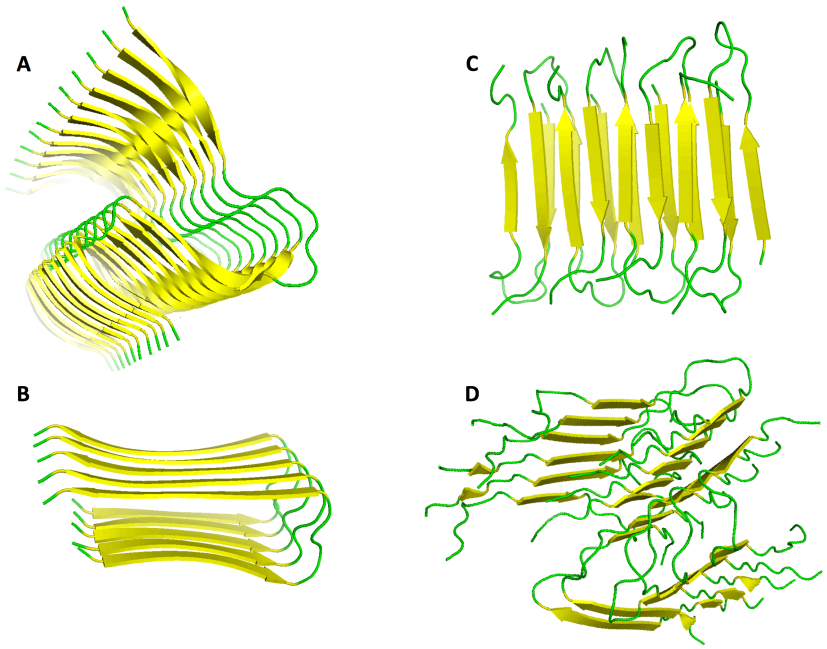

Figure 1.9. Some Aβ fibrillar structures solved. A. Fibril structure (PDB ID: 2MXU) solved by Xiao *et al.* (2015) by NMR in polar ambient formed by Aβ(1-42) peptides showing three β-strand motifs (residues 12–18, 24–33 and 36–40) connected by short coil or turn regions [538]. B. Fibril structure (PDB ID: 2BEG) solved by Luhrs *et al.* (2005) where residues 18-42 form a β-strand-turn-β-strand motif that contains two intermolecular, parallel, in-register β-sheets [118]. C. Lu *et al.* (2012) solved a fibril structure (PDB ID: 2LNQ) formed by the Asp23-to-Asn mutant of Aβ(1-40) (D23N-Aβ(1-40)), which is associated with early onset neurodegeneration, finding that D23N-Aβ(1-40) fibrils can contain not only parallel but also antiparallel β-sheets [123]. D. Structural Model for a Aβ(1-40) fibril (PDB ID: 2LMN) solved by Paravastu *et al*. (2008) showing a two-fold symmetry about the fibril growth axis and containing in-register parallel β-sheets. β-sheets are colored in yellow [120].

Several published works have reported different molecular interactions of Aβ monomers and oligomers in neuronal metabolism (Figure 1.11). Specifically, Aβ(1-42) monomers are known to activate the neuroprotective signaling of insulin-like growth factor-1 receptor (IGF-1R), one of the most potent activators of the serine/threonine kinases PI3K/AKT, stimulating cell growth and proliferation and inhibiting programmed cell death [35, 36]. Aβ produced in early endosomes can be rapidly released to extracellular space in exosomes [176], which can be transported long distances in the brain or trans-synaptically spread from neuron-to-neuron [177, 178], but the mechanisms implicated are still unclear [167] (Figure 1.5).

1.1.8.1.3. Aβ clearance and Blood Brain Barrier (BBB) transport

The BBB is a checkpoint to control entry of blood-derived neurotoxic molecules, cells, and pathogens into the brain and regulate the concentrations of ions, nutrients and energy metabolites in the brain interstitial fluid (ISF) through highly specialized transporters at the brain endothelium [494, 495, 497]. Receptor-mediated transcytosis from the brain across the BBB is crucial for efficient clearance of toxic molecules such as Aβ, which also suffers passive ISF flow to the cerebro spinal fluid (CSF), but in a much smaller amount [498]. On the other hand, tau protein, for which we still do not know any transporter at the BBB, is much slower eliminated from the brain via ISF-CSF passive flow [496]. This case shows the importance of rapid trans-vascular clearance of potentially toxic molecules across the BBB, which is vital for preventing their accumulation in the brain and the affectation of normal neuronal functioning [564].

Brain-derived Aβ is mainly cleared through the BBB principally via low-density lipoprotein receptor-related protein 1 (LRP1)-mediated transcytosis [498, 499] and can cross back into the brain by the receptor for advanced glycation end products (RAGE) [500], as show in more detail in Figure 1.10:

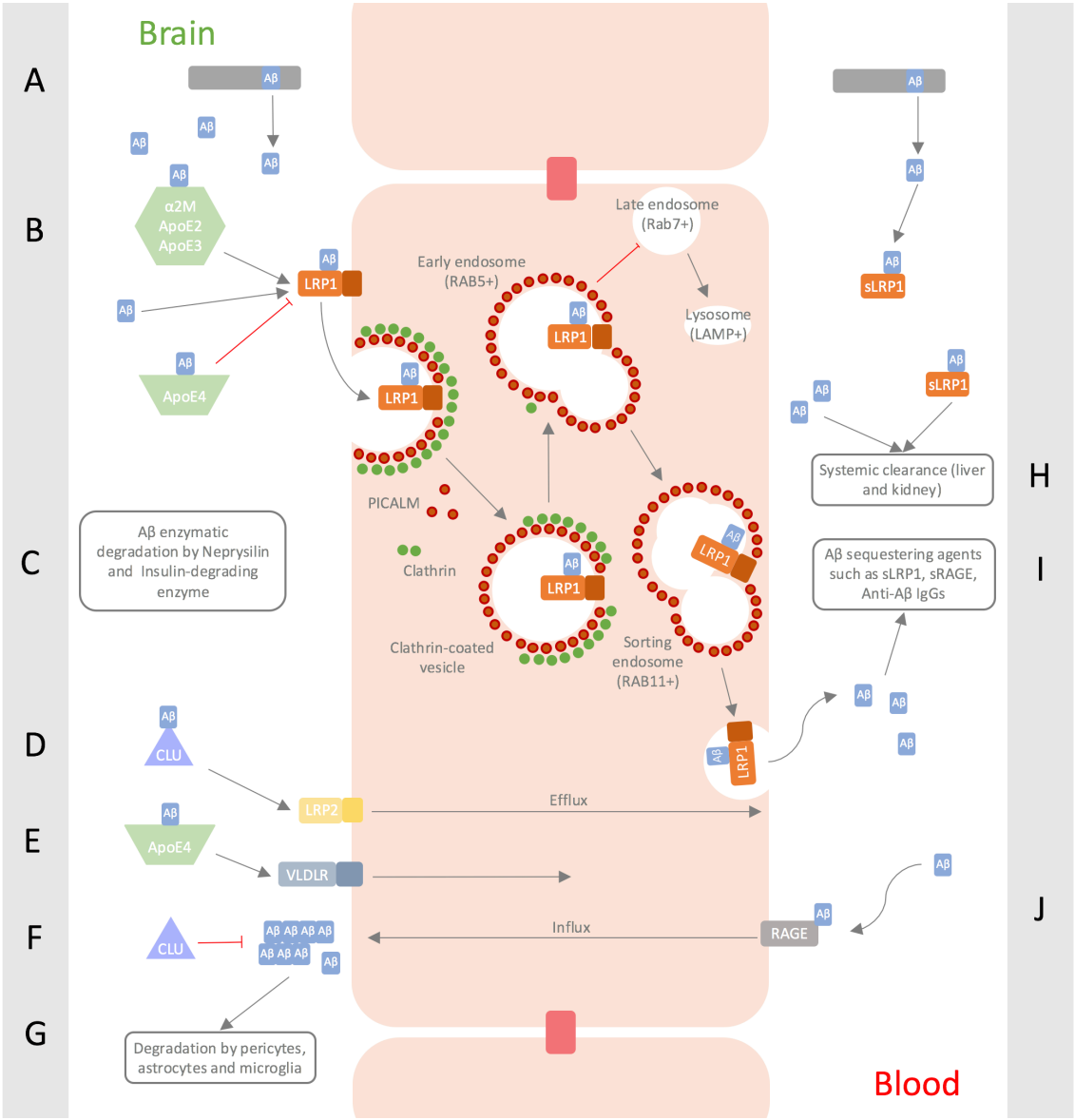

Figure 1.10. Aβ transport across the BBB. (A) Aβ is produced from APP in the brain and in the periphery. (B) Primarily, brain-derived Aβ is cleared through the BBB by the low-density lipoprotein receptor-related protein 1 (LRP1)-mediated transcytosis. LRP1 binds both free Aβ, and Aβ bound to ApoE2, ApoE3, or α2-macroglobulin but not when bound to ApoE4. LRP1 binds Aβ at the brain side of the BBB and triggers a rapid PICALM/clathrin-dependent endocytosis of Aβ-LRP1 complexes. Clathrin rapidly dissociates from the internalized vesicles, but PICALM continues to guide transport of Aβ-LRP1-containing endocytic vesicles for fusion with Rab5-positive early endosomes, and afterwards to Rab11-positive sorting endosomes leading to Aβ exocytosis to the blood compartment. PICALM impedes Aβ to finish in Rab7 late endosomes and lysosomes. (C) Several enzymes in the brain, among neprilysin and IDE, contribute to Aβ enzymatic degradation. (D) Clusterin (CLU) helps in the efflux of Aβ(1-42) across the BBB via LRP2. (E) Aβ conjugated with ApoE4 is not able use fast LRP1-dependent transcytosis, so is cleared through the very low-density lipoprotein receptor (VLDLR) at a substantially slower rate than free Aβ or Aβ bound to ApoE2 or ApoE3. (F) Clusterin function limits Aβ oligomerization and aggregation. (G) Along Aβ clearance across the BBB, several neurovascular cell types (pericytes, astrocytes, microglia, and vascular smooth muscle cells (VSMCs)) and neurons also contribute to Aβ clearance. (I) Aβ sequestering in plasma with agents like soluble LRP1 (sLRP1), soluble RAGE (sRAGE), or antibodies against Aβ may contribute to Aβ clearance from the brain by creating a concentration gradient favoring Aβ efflux, known as a “peripheral sink”. (H) Elimination of circulating Aβ by excretory organs such as liver and kidney leads to its systemic clearance from the body. (J) The receptor for advanced glycation end products (RAGE) is the main effector in the influx of circulating Aβ or Aβ bound to monocytes from blood to the brain across the BBB (adapted from ref 564).

1.1.8.1.4. Aβ-related pathogenesis

However, AD pathology, neurons in vulnerable brain regions seem to accumulate Aβ(1-42) [168], mainly in multivesicular bodies (MVBs) [169]. It is undoubtable that intracellular Aβ(1-42) accumulation is a phenomenon increased with age, that precedes plaque formation and is

correlated with synaptic dysfunction, pointing to an early event in AD pathology [170, 171, 172]. Moreover, other early processes like endosomal dysfunction and an increased expression of Rab GTPases [173], may suggest that deregulation of these metabolic routes contributes to an imbalance in endosomal signalling, recycling and turnover of Aβ peptides. In AD later stages, accompanying dystrophic neurons, has been observed autophagic pathology, probably result of such Aβ reduced clearance and that may contribute to increase even more Aβ products due to γ-secretase activity found in autophagosomes [174, 175].

Regarding aggregated species, recently published works showed that structured oligomers can be more harmful than the ones without a defined structure. Their pathologic potential may depend on their size and solvent-exposition of the most hydrophobic residues. Due to this relationship with pathogenesis, extensive searches have been performed on well-defined oligomers trying to isolate them and determine their structural determinants responsible for their pathogenicity [361, 287, 92, 93, 96, 98, 99, 100, 101, 102, 103, 105, 106, 107, 108, 109, 110]. Nonetheless, it has been proven that this is a very complicated task, due to the elevated heterogeneity, unstable conformations and oligomer populations, which also proves that there are not one single mechanism leading to the formation of the different species, but a number of them (Table 1.4).

Table 1.4. Major soluble Aβ preparations and deleterious effects associated with them (adapted from ref 119)

Species	Structure	Biological effects related
ADDL [89, 30, 133]	3–24-mer Major component, 17 kDa (tetramer) Globular structures 2–5-nm height A11-positive	LTP impairment (500 nM) Tau mis-sorting into dendrites and tau phosphorylation (5 M) Abnormal mitochondrial distribution in neurites caused by impaired tau-dependent axonal transport (800 nM) Cytotoxicity in primary neurons (micromolar concentration) Cognitive impairment in mice
Aβ*56 [95, 134]	12-mer Globulomers 56 kDa A11-positive	NMDAR-dependent synaptotoxicity Memory deficiency in middle-aged mice Tau phosphorylation No cytotoxicity Cognitive impairment in rats (micromolar concentration)
Aβ O [87, 136]	15–20-mer Spherical vesicles 2–5 nm A11-positive	NMDAR-dependent synaptotoxicity Tau phosphorylation Cytotoxicity in human neuronal cultures
Aβ 42 and Aβ 42:40 (3:7) (synthetic oligomers) [137]	β-sheet enriched Transient on-pathway species A11-positive	Impairment of synaptic transmission Tau phosphorylation Cytotoxicity in primary neurons (micromolar concentration) Memory deficiency in mice
Transglutaminase 2-induced oligomers [138]	Apparently no secondary structure Off-pathway A11-positive	LTP impairment Tau phosphorylation No cytotoxicity in primary neurons
Aβ 42CC protofibrils [139]	Intramolecular disulfide bond stabilized antiparallel β-sheet–based structure that does not propagate into fibrils Weak reactivity with A11	Synaptotoxicity Tau phosphorylation Caspase-3 activation in human neuroblastoma cells
Annular protofibrils (APF) [110]	Form pores, 11–14-nm outer diameter; 2.5–4-nm inner diameter Composed of spherical A11-positive Aβ(1-42) oligomers assembled in 6 hexamers, (36-mer), 155 kDa	Hypothesized to cause Ca2+ overload and cytotoxicity
SDS-stable dimers and trimers isolated from wild-type (WT) and FAD hAPP-, PSEN1- and PSEN2-transfected CHO cell culture medium [103, 134, 140, 141]	6-, 8- and 12-kDa assemblies Enriched in N-end (Arg5) truncated species Contain Aβ 40 and Aβ 42	LTP impairment NMDAR and mGluR-dependent LTD facilitation Tau phosphorylation No cytotoxicity Cognitive impairment in mice

SDS-stable brain-derived dimers [29, 144, 145] and synthetic dimers (Aβ (1-40) Ser26Cys)	8–12-kDa assemblies 3–4-nm height No detectable secondary structure	LTP impairment Tau phosphorylation in primary neurons No cytotoxicity to primary neurons but toxic to neurons cultured with microglia
ASPD; synthetic or brain-derived) [108, 146, 11]	10–15-nm spherical assemblies 32–150-mers A11-negative	Synaptic impairment Tau protein kinase 1/ Glycogen Synthase Kinase-3β (GSK-3) activation NMDAR-independent cytotoxicity in neurons The highest toxicity is ascribed to either 32-mer (7.2 nm) or to ASPD >10 nm

*A11 is an oligomer-specific rabbit antibody

It has also been found that extracellular protein oligomers may interact with a number of neuronal and astrocyte receptors among the Frizzled receptor, the metabotropic glutamate receptor 5, insulin receptor, RAGE, NMDA and AMPA receptors, ApoE receptors, formyl peptide receptor-like 1 (FPRL1/2), p75 neurotrophin receptor (p75NTR), cellular prion protein (PrPc), a7 nicotinic ACh receptor (a7nAChR), calcium-sensing receptor (CaSR) and several other cellular elements and receptors [35, 36, 119] (Figure 1.11).

Some more recent works suggest that oligomers could have a major role, increasing oxidative stress, tau hyperphosphorylation and oligodendroglia destruction, resulting in toxic processes that affect to the synapses and neuronal energetic metabolism [3, 4, 9] (Table 1.4). Additionally, oligomers are susceptible of phosphorylation by cell-membrane or extracellular protein kinase A (PKA), which may facilitate their aggregation, reducing proteolytic and glial clearance and increasing their neurotoxicity [155, 157]. Furthermore, when oligomers interact with cell membranes increase their aggregation rate and are able to form pores and calcium ion-permeable channels [157, 158].

Glutamate receptor-dependent cascades are also directly or indirectly affected, leading to LTP impairment and long term depression (LTD) reinforcement [142]. Moreover, abnormal activation of calcineurin and nuclear factor of activated T-cells (NFATc4) lead to dystrophic changes in neurites, and impairment of the induction of AMPAR-based LTP in hippocampus.

Chronic exposure to Aβ oligomers also upregulates the 7-nAChR, causing a hyperactivation which, in consequence, downregulates the extracellular signal-regulated kinase (ERK) and the mitogen-activated protein kinase 1 (MAPK1) cascade leading to LTP dysregulation through decreased phosphorylation of CREB factor. In addition, several protein kinases that mediate pathological phosphorylation of tau and are also required for Aβ synaptotoxicity. Moreover, caspase-3–mediated pathway could have part in the Aβ-mediated LTP impairment upstream of GSK-3β [119, 279, 280, 281, 439] (Figure 1.11).

On the other hand, Aβ(1-42) plaques that appear in late stage of the disease seem to lead to microglia activation. This microglia activation induces production and release of pro-inflammatory cytokines such as interleukin-1 β (IL-1β), tumor necrosis factor-α (TNF-α) or interferon-γ (IFN-γ) [7]. Those liberated cytokines also stimulate neuron and astrocyte Aβ(1-42) production, with turns into a retro-fed process [8].

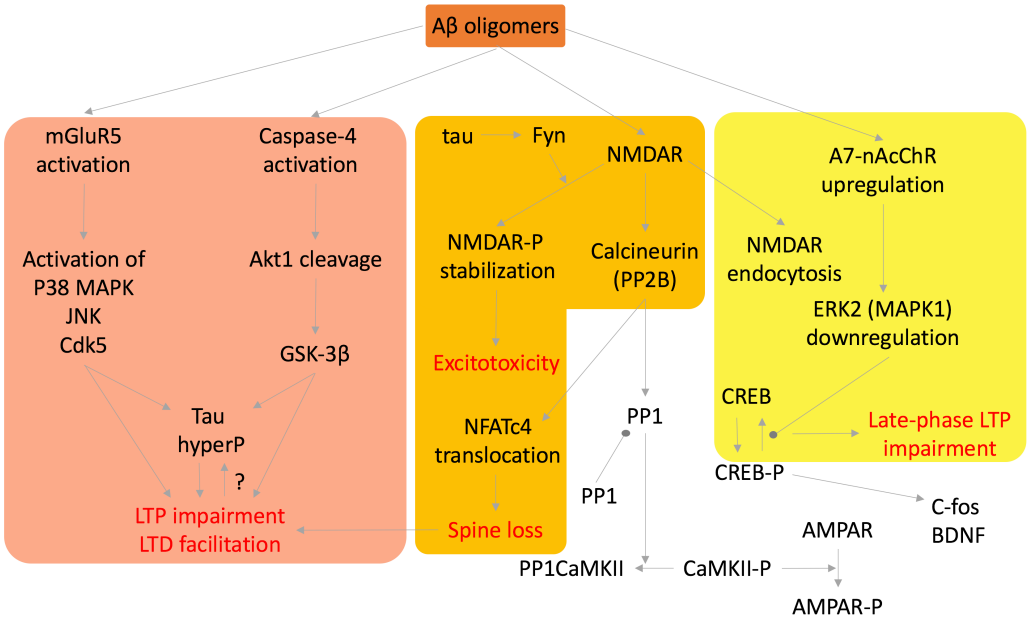

Figure 1.11. Molecular mechanisms of Aβ oligomers toxicity proposed in the literature. The figure describes some pathways involved in several process related with synaptotoxycity. In spite of the extensive research carried out in this field, there is no complete consensus about what mechanism, if any, is the most relevant to AD development (adapted from ref 119).

1.1.8.2. Tau hypothesis

In 1974 a paired helical filament structured protein was isolated from brains of AD patients, but it was not until 1986 that the protein was identified as tau [1]. Human tau is encoded by the microtubule-associated protein tau gene (MAPT gene) comprising 16 exons on chromosome 17q21 [185]. In the brain, tau is principally located in neurons, but it is also detectable in glia [186] and in the extracellular space. It has a capital role in the assembly and stabilization of microtubule cellular system.

In human adult brain there have been identified six tau isoforms, generated by alternative splicing of exon 2 (E2), E3 and E10. The isoforms diverge on the number of 29-residue near-amino-terminal regions, encoded by E2 and E3: isoforms containing 0, 1 or 2 N-terminal inserts are known as 0N, 1N and 2N, respectively. Isoforms can also be classified depending on the number (3 or 4) of carboxy-terminal repeated domains (3R or 4R, respectively; the second repeat is encoded by E10 and is not included in 3R tau) (Figure 1.12). Levels of expression of the MAPT diverse isoforms exhibit regional differences, which may contribute to the differential vulnerability of brain regions to neurodegeneration [187].

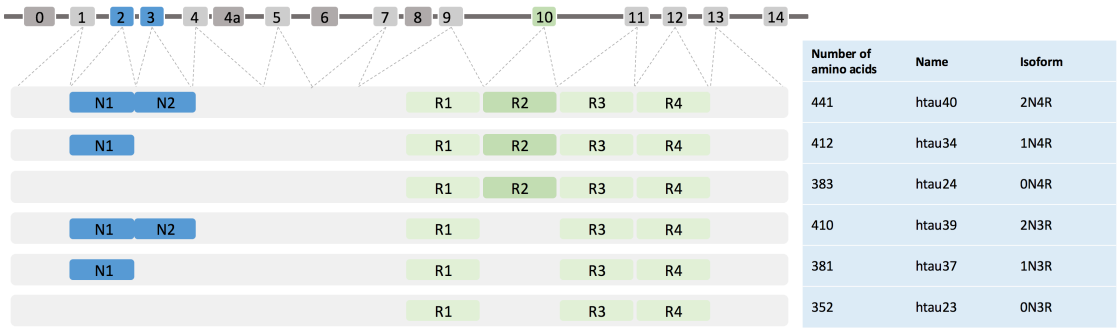

Number of amino acids	Name	Isoform
441	htau40	2N4R
412	htau34	1N4R
383	htau24	0N4R
410	htau39	2N3R
381	htau37	1N3R
352	htau23	0N3R

Figure 1.12. The different tau isoforms derived from alternative splicing of MAPT gene. The human gene contains 16 exons. Exon 1 (E1), E4, E5, E7, E9, E11, E12 and E13 are constitutively expressed, whereas the others are subject to alternative splicing. E0 (the promotor region) and E1 encode the 5' untranslated sequences of MAPT mRNA, meanwhile E14 is part of the 3' untranslated region. The repeated domains are labelled in green and the N-terminal inserts in blue (adapted from ref 179).

Native tau is a strangely hydrophilic protein: its longest isoform (2N4R) contains 80 Ser and Thr residues, 56 negative (Asp and Glu) residues, 58 positive (Lys and Arg) residues and 8 aromatic (5 Tyr and 3 Phe) residues. Tau is predominantly a basic protein although the ~120 N-terminal residues are mainly acidic, and the C-terminal ~40 residues are practically neutral [179].

There can be differentiated two domains in tau protein on the basis of microtubule interaction and the amino acid character: The C-terminal assembly domain responsible for binding to microtubules and for tau aggregation; and the N-terminal projection domain that projects away from microtubules (Figure 1.13).

The protein in native state is unfolded and shows little predisposition to aggregate, but when tau suffers aggregation, forms the so-called paired helical filaments (PHFs). The core of the PHFs is formed by the stacked repeated domain of the protein with the C- and N-terminal domains forming a “fuzzy coat” that surrounds the β-structured core [222]. NFTs formation consists of several steps: dimerization, multimerization, oligomerization and protofibril formation [226, 227, 229, 230, 231] (Figure 1.13).

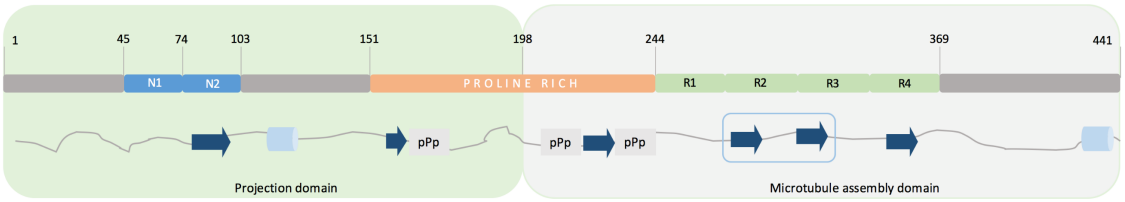

Figure 1.13. Tau secondary structures. Although tau is a predominantly unfolded protein in native form, a few short and transient motifs that can form structures such as α-helices (pale blue cylinders), β-strands (dark blue arrows) and poly-Pro helices (grey boxes). The thin blue rectangle indicates the region comprising two hexapeptide motifs that are responsible for tau aggregation (VQIVYK in R2 and VQIINK in R3). The protein can also be subdivided into two major domains: the assembly domain in the carboxy-terminal (grey shaded); and the projection domain, the amino-terminal section (Green shaded). The middle region of tau (residues 151 to 243) is a Proline-rich domain containing several Thr-Pro or Ser-Pro motifs. Those motifs are targets of proline-directed kinases such as GSK3β, MAPK, CDK5, and JUN N-terminal kinase (JNK) (adapted from ref 179).

Tauopathies can also be classified into three groups depending on the tau isoforms found in the aggregates: 4R tauopathies, 3R tauopathies and 3R+4R tauopathies (for example, AD) [188]. Due to the additional repeated domain R2, 4R tau isoform shows higher affinity for microtubules than 3R tau, and is consequently more efficient in microtubule assembly supporting [189]. On the other hand, the role of the two N-terminal inserts is still unclear, although it is thought that could influence the attachment to the microtubules, regulate the spacing between those and other cell elements [190, 191] or control the subcellular distribution of tau isoforms in neurons [192]. And lastly, some *in vitro* studies have pointed to that the presence of one of these inserts promotes tau aggregation, meanwhile the inclusion of the second insert delays tau aggregation [193] (Figure 1.12).

1.1.8.2.1. Tau functions

Although data about complete physiological functions is still controversial, tau is involved in more processes than only microtubule organization and stabilization.

In axons of adult neurons, tau interacts with microtubules, stabilizing and regulating the dynamics of the reorganization of the cytoskeleton [195, 196]. Tau binds to the complex α-tubulin–β-tubulin heterodimers through residues 224–237, 245–253, 275–284 and 300–317, whereas residues between remain flexible [197]. When associated to microtubules, tau does not turn into a globular structure, but residues 269–284 and 300–310, containing the two following hexapeptide motifs, 275VQIINK280 and 306VQIVYK311 (essential for tau aggregation), can form a local hairpin conformation [197]. This could suggest that tau associated conformation when bound to microtubules impede aggregation.

In addition to microtubule dynamic regulation, tau seems to regulate axonal transport through dynein and kinesin motor proteins mechanism, which transport cargoes towards the cell body and towards the axonal terminus respectively [198]. Tau also seems to be essential for axonal elongation and maturation [199] and moreover, overexpression of tau could promote the

formation of neurites in non-neuronal cells [200]. In dendrites tau may play a role in the regulation of synaptic plasticity, but the mechanisms are still unclear [201]. Moreover, tau also seems to play a part in integrity maintenance of genomic DNA, cytoplasmic RNA and nuclear RNA [202, 203].

And finally, tau may be involved in neurogenesis, neuronal activity regulation, iron export and LTD regulation [204, 205, 206, 207, 208].

1.1.8.2.2. Tau mutations

Although there is not a robust confirmation of any tau mutation that could be related to AD pathology, to the time there are described 80 mutations within the intronic and exonic regions of MAPT. These mutations are linked to other diseases such as fronto-temporal dementia with parkinsonism-17 (FTDP-17), corticobasal degeneration (CBD) and progressive supranuclear palsy (PSP) but not with AD (see Alzforum database).

1.1.8.2.3. Tau post-transcriptional modifications

Researchers know that tau is subject of numerous post-transcriptional modifications that affect to its function, but it is unclear how they affect to the disease development nor which are more important to the neurodegenerative processes.

Phosphorylations. In the early nineties Yasuo Ihara´s group identified several phosphorylated sites in isolated tau from AD brain patients [180]. Along the longest tau isoform (2N4R) of tau there are 85 potential phosphorylation sites (80 Ser or Thr, and 5 Tyr), and most of them are accessible considering its unfolded native structure. They are also mainly clustered in the flanking regions of tau, and among them, 17 Thr-Pro or Ser-Pro motifs have particular interest: these are found to be abnormally hyper-phosphorylated in AD and other tauopathies [211] (Figure 1.14).

The normal physiological phosphorylation pattern of tau variates along the development of the individual, so that, fetal tau (carrying about seven phosphates per molecule) is more highly modified than adult tau (approximately two phosphates per molecule) [209]. In AD, the average of phosphorylated residues in tau is increased to approximately eight phosphates per molecule [210].

Besides pathological or developmental implication, phosphorylations have an essential role in regulating microtubule binding, stabilization and assembly. Whereas phosphorylation of KXGS motifs (specially Ser262), Ser214 or Thr231 could reduce tau affinity to microtubule binding [211, 212], phosphorylations at other Thr-Pro or Ser-Pro motifs placed in the flanking region have a weak influence on tau–microtubule binding (Figure 1.14).

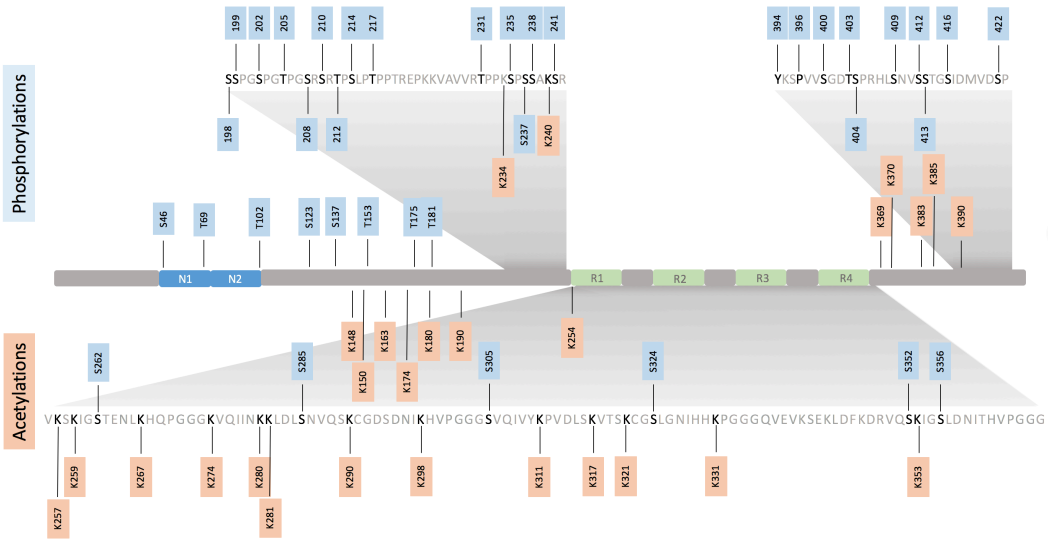

Figure 1.14. Tau protein is subject of several post-transcriptional modifications. Among them, phosphorylations and acetylations in certain residues are two of the best known. Some of them are associated with normal regulation of the protein activity and degradation, but other are related to the development of several neurodegenerative diseases, such AD, due to gain or loss of abnormal functions or otherwise, to aggregation propensity (adapted from ref 565).

The central region of tau (residues 151–243) is a Pro-rich domain containing multiple Thr-Pro and Ser-Pro motifs, which are targets of several proline-directed kinases including GSK3β, CDK5, MAPK and JNK. In or near the repeat domain there are other phosphorylation sites target of several microtubule affinity-regulating kinases (MARKs; also known as PAR1 kinases), cyclic AMP-dependent protein kinase (PKA) and Ca2+- or calmodulin-dependent protein kinase II (CaMKII), among others. In addition, tyrosine kinases such as the SRC family members LCK, SYK and FYN at Tyr18, and the ABL family members ARG and ABL1 at Tyr394 can target on tau [211].

On the other hand, there are several phosphatases such protein phosphatase 1 (PP1), PP2A, PP2B, PP2C and PP5 implicated in the dephosphorylation of tau [211]. Among them, PP2A is the main phosphatase in human brain, accounting for ~70% of tau phosphatase activity, and in fact, its activity was found to be reduced by 20% to 40% in the AD brain [213, 214, 215].

Although phosphorylations are well known post-transcriptional modifications of tau that modulate its functions and pathology, there are other modifications recently characterized, known to have certain functioning or pathologic influence, but still without a proper characterization:

Acetylations. P300 acetyltransferase or CREB-binding protein is able to acetylate several Lys residues in the repeat domain of the flanking region of tau, whereas histone deacetylase 6 (HDAC6) and sirtuin 1 (SIRT1) are the enzymes that can deacetylate respectively these sites. Depending on the acetylated sites, those modifications can inhibit (Lys163, Lys280, Lys281 or Lys369) or facilitate (Lys259, Lys290, Lys321 or Lys353) tau degradation, leading to the protein phosphorylation or aggregation [179, 216, 217]. Pathology-linked acetylations are extensively explained in the section “Tau physiopathology”.

Glycosylation, glycation, deamination, isomerization, nitration, methylation, ubiquitylation, sumoylation and truncation. These are more not very well known post-transcriptional modifications that tau can suffer. These modifications are suspected to modulate several functions of tau such as microtubule binding affinity, phosphorylation, aggregation, degradation, besides being implicated in the development of some diseases such AD and other neurodegenerative diseases [179, 220].

1.1.8.2.4. Tau clearance

Tau levels in neurons can arise due to malfunctions in the protein-degradation systems or because aggregated species block protease´s normal activity. Although the two major degradation systems identified working on tau are the ALS (autophagy-lysosome system) and the UPS (ubiquitin-proteasome system), there also are other proteases able to cleave tau such as calpain, caspases 3, 6 and 9, cathepsins D and L, and PSA [262]. The inefficient cleavage by these systems can lead to neurodegeneration through several mechanisms. (i) The cleavage of tau close to C-terminus could result in the accumulation of amyloidogenic fragments. (ii) The truncation of tau near the N-terminus may lead to an increased production of toxic fragments also related to neurodegeneration. (iii) the ineficient cleavage rate may lead to the accumulation of free tau, facilitating its aggregation. However, the mechanisms underlying these processes remain controversial [249, 250, 251, 252, 253, 254].

Tau degradation through proteasomal pathway. The proteasomal pathway is a major protein-degradation mechanism with an important role in degrading short-lived and misfolded proteins [255]. The 26S proteasome is a multi-catalytic protease composed by three major subunits: one 20S catalytic core and two 19S regulatory caps [256]. The canonical degradation of tau by this mechanism is an ATP and ubiquitin dependent process that implies, initially, the covalent attachment of several ubiquitin molecules to the protein in a three-step cascade, and finally the degradation of the ubiquitinated substrate by the 26S proteasome complex, with the liberation of free and reusable ubiquitin [256].

Tau degradation by the ALS. The other main proteasomal machinery is the autophagy-lysosome system [255]. Depending on the different mechanisms of substrates delivering to lysosomes we can differentiate three types of autophagy: microautophagy, macroautophagy and chaperone-mediated autophagy. In microautophagy, although it has not very well studied, the lysosomal membrane seems to directly engulf part of the cytosol. Macroautophagy is the main pathway for eukaryotic cells to degrade long-lived proteins and organelles. By this way, a small volume of the cytosol is retained into a double membrane vesicle called the autophagosome, which afterwards

fuses with the lysosome. And finally, chaperone-mediated autophagy is a type of selective autophagy targeting soluble cytosolic proteins containing specifically a KFERQ (Lys-Phe-Glu-Arg-Gln) motif [258]. Substrates are recognized by HSC70 and transported to the lysosomal membrane, where are then translocated and degraded [258]. Remarkably, tau contains two KFERQ homology motifs in the repeat domains [257]. As pointed previously, autophagy is involved in the degradation of tau, in both soluble and insoluble forms [257]. Additionally, phosphorylated tau at the KXGS motifs of the repeat domain, impossible to be degraded by the UPS, is degraded by autophagy.

1.1.8.2.5. Tau physiopathology

As previously showed, one of the main hallmarks of several diseases related to tau metabolism such as AD, PSP, CBD, agyrophilic grain disease (AGD), Pick disease (PiD), Huntington disease (HD) and FTDP-17 is the presence of aggregated tau into PHFs and NFTs [194]. Although tau influence in all these diseases is undoubtable, to date, most of aggregation mechanisms and pathways underlying tau-induced neurodegeneration remain elusive or controversial.

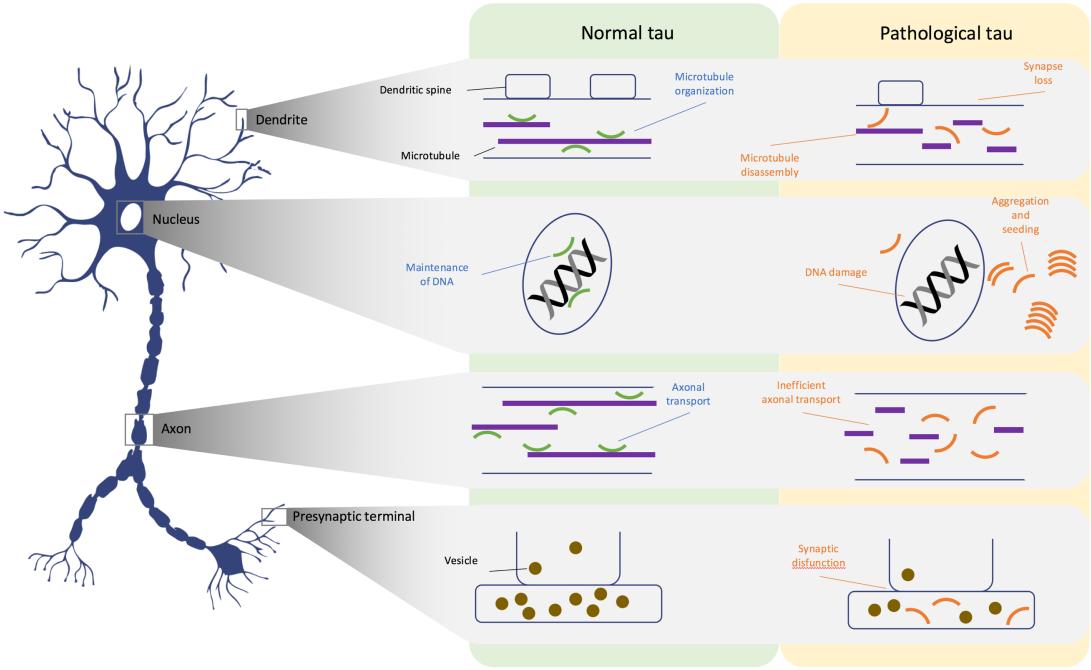

Figure 1.15. Tau has several physiological functions. In normal, healthy neurons, it is commonly distributed in axons stabilizing microtubules and regulating axonal transport. In addition to structural functions, a small amount of tau is also detected in dendrites, where its role is unclear. Tau also locates inside the nucleus, where it seems to play a part in maintaining the integrity of genomic DNA. When tau suffers post-translational modifications that lead to the detachment from microtubules, results in microtubule disassembly. Detached tau can mislocalize into presynaptic terminals and provoke synaptic dysfunction and loss [373]. Besides affecting the presynaptic compartment, tau can enter dendrites and postsynaptic compartments and, in consequence, cause postsynaptic dysfunction, leading to synapse loss there as well [374, 375, 376]. Moreover, pathological tau is unable to enter the nucleus, resulting in DNA damage owing to the loss of the DNA-protective function of tau [377]. Finally, all detached tau tends to aggregate, affecting neuronal general function (adapted from ref 179).

Originally, as aggregated tau in patients with a tauopathy invariably showed hyper-phosphorylation, and as tau hyper-phosphorylation seems to precede aggregation, phosphorylation was assumed to lead to tau aggregation [144]. Although it is known that hyper-phosphorylation or dephosphorylation can affect tau conformation and function, it has been also demonstrated that this modification alone could not induce or eliminate the pathologic role of tau in AD. [181, 182, 183, 184]. Therefore, this information in conjunction with the fact of all tau found to be related to a tauopathy is hyper-phosphorylated, and that it is possible to induce tau aggregation without phosphorylated residues, indicates that other modifications could be involved

in regulating hyper-phosphorylation. It seems reasonable that in pathological conditions, tau may suffer some post-translational modifications that may lead to the detachment from microtubular cell system, resulting in microtubule disassembly in axons and causing interruptions on the cell molecular trafficking. Then, detached tau could mislocalize into presynaptic terminals, causing synaptic dysfunction, reduction in the number of synaptic vesicles in presynaptic and postsynaptic terminals and synapse loss [373, 374, 375, 376]. Another associated problem to the loss of function of tau is the lack of the capability to enter the nucleus and exert its normal DNA-protective functions, which could result in DNA damage [377] (Figure 1.15).

And finally, as previously indicated, tau could aggregate, which leads to an alteration and disruption of normal neuronal function. Additionally, aggregated tau could cross the cell membrane defusing into extracellular space, or pass through tunneling nanotubes and enter other neurons, provoking the dissemination of tau pathology (Figure 1.15).

A post-transcriptional modification that has gained interest as one of the main drivers of tau-mediated neurodegeneration is the reversible acetylation of Lysine residues of tau. Some of them, such as Lys259, Lys290, Lys321 or Lys353 within the KXGS motifs are found to be reduced in AD brains [217]. On the other hand, acetylation of Lys280, which has been related to a number of AD tauopathies [386], and Lys174 are two of the major acetylation sites in tau and seem to delay tau degradation and have been found in PHFs in very early stages of the disease also seem to be increased in AD patient brains [218, 219]. Lys163 have been linked in the same way as Lys280 to microtubule destabilization and tau degradation inhibition [216]. Lys274 and Lys281 are also found to be related to impaired memory in AD, but in this case, affecting to LTP expression [221, 242, 571]. In last times some of these acetylations earned particular interest due to their critical role in neurodegeneration. Lys280, located in the inter-repeat region (275 VQIINKK 280) and Lys281 have demonstrated to be critical for microtubule binding, impairing it and increasing intracellular soluble tau pools susceptible to aggregate into PHFs [259, 260, 261].

In addition to hyperphosphorylation and acetylation, tau truncation has also recently received particular attention. Truncation of tau may promote its aggregation through oligomerization of the repeated domains [232, 233, 234]. Repeat 3 and repeat 2 of 4R tau, containing the β-sheet structure can aggregate forming PHFs [234]. Also tau 151–391 has been found in AD brain extracts [232, 234].

Modification of tau by β-linked N-acetylglucosamine, also known as O-GlcNAcylation, occurs on serine/threonine residues and therefore can also regulate tau phosphorylation. Only six O-GlcNAcylation sites (Thr123, Ser208, Ser238, Ser356, Ser400, and one of Ser409/412/413) have been mapped on the tau protein [236], also found phosphorylated in AD. Remarkably, O-GlcNAcylation rate levels of tau have been found decreased in human AD brains [237], suggesting that decreased O-GlcNAcylation may contribute to tau hyperphosphorylation. Impairment of glucose methabolism in sporadic AD might be the responsible of lower O-GlcNAcylation levels worsening the disease [238].

Ubiquitination was first linked to tau aggregation three decades ago when was identified into NTFs [243]. Interestingly, all reported ubiquitination sites in tau are localized into the microtubule-binding region. It is also known that other modifications in this domain, such as phosphorylation or acetylation, impair tau–microtubule interactions and can facilitate tau aggregation, so we could expect that the ubiquitination of tau in this domain may exert a similar effect [243]. Some recent *in vitro* and *in vivo* experiments have enlighten the way ubiquitination may increase tau aggregation, but some data remain controversial and the causality of this mechanism will require further investigation [244, 245, 246, 247, 248].

On the other hand, although pre-fibrillar soluble oligomeric species are poorly understood, some recent studies have shown that they may play the main pathologic role [224, 225]. In several transgenic mice lines with wild-type or mutant human tau, impaired synaptic function, synapse loss and cognitive deficits occur before or without any presence of NFT, which suggest that soluble tau species, and not NFTs, are the real problem [263, 264, 265]. In AD brains, around 40% of the hyperphosphorylated tau is present as 200,000*g sedimentable oligomers [266, 267].

Opposite to normal tau, which interacts with tubulin and promotes microtubule assembly, hyperphosphorylated tau sequesters normal tau, disrupting the microtubules structures [268, 269]. However, AD brains isolated PHFs have no effect on microtubule assembly *in vitro* [270], suggesting that tau oligomers and not insoluble species represent the cytotoxic face of the hyperphosphorylated protein. So although these insoluble species have been used as diagnostic

markers, they might not be the main pathologic drivers, but actuate as a sink compartment of pathologic forms of tau. The mechanisms underlying this toxic effect are still controversial due to the lack of specific antibodies and the difficulty to isolate those toxic soluble species [225].

Regarding tau degradation pathways linked to tau pathology, some recent studies have shown that the impairment of the protein-degradation systems that results in the accumulation of tau could, in fact, be the main cause of tau aggregation [239, 240, 262].

All these findings point to a complex pathology and a number of elements such as monomeric species, soluble oligomers and insoluble aggregates, among a number of post-transcriptional modifications that may lead to neurodegeneration through several routes and mechanisms.

1.1.8.3. Microglia and inflammation

An important part of the research community has been working on the hypothesis of inflammation as an important target to halt or reverse AD progression. But we still do not know what exact role neuroinflammation plays in the disease. Is it a harmful driver of AD, or maybe it is an insignificant subproduct or consequence of the brain cell damage caused by the disease? Perhaps it is a beneficial activated mechanism for repairing and removing damaged or harmful elements [456].

To understand neuroinflammation, it is mandatory to understand microglia. After neurons, these are the second most common cells in human brain, and belong to the immune system for our CNS. In the absence of pathology, microglia functions as a support for neuronal healthiness through synaptic pruning, promoting normal brain connectivity and development, and through release of neurotrophic factors, contributing for CNS integrity [447].

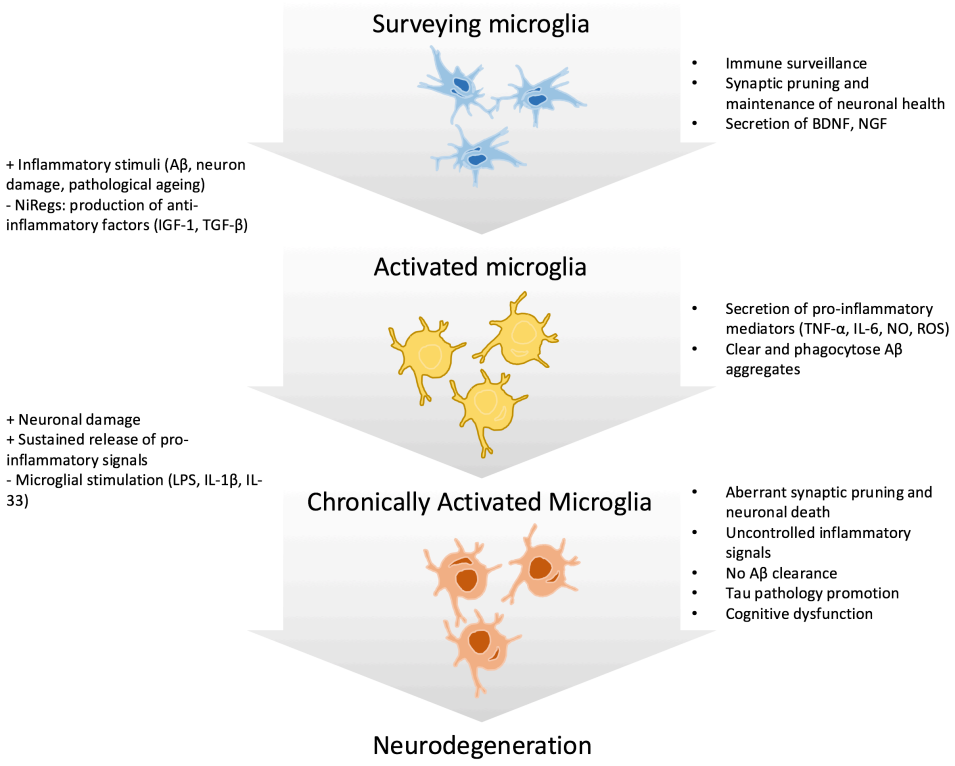

Figure 1.16. Acute and chronic microglial activation in the context of AD. In the surveillance state, microglia "patrols" the brain parenchyma detecting anomalous materials, while simultaneously secreting anti-inflammatory factors and sorting out dormant or damaged synapses maintaining a healthy neuronal state. Disturbances in brain homeostasis, such as Aβ presence, lead to microglia activation and to release pro-inflammatory mediators for recruiting other cells to induce the phagocytose of the detected disturbing body. When the insult is cleared, the inflammatory response is inhibited via Neuroimmune regulatory proteins activity (NiReg), leading to microglia secretion of anti-inflammatory factors for recalling tissue repair and growth. However, in neurodegenerative diseases, the sustained release of pro-inflammatory signals and extended neuronal death drives microglia into a state of chronic activation. Consequently, the loss of the homoeostatic functioning advocates to an accumulation of aggregated proteins, the stripping of synapses and, finally, general neuronal loss (adapted from ref 456 and 447).

Microglia also constantly patrol the brain, seeking for signs of infection or inflammation caused by toxic proteins such as Aβ that could damage neurons. Besides clearing those toxic sources of damage from the brain, microglia further release pro-inflammatory short-live molecules called cytokines that activate other microglia. Those secreted proinflammatory mediators include tumor necrosis factor-α (TNF α), interleukin (IL)-6, nitric oxide (NO) and several reactive oxygen species, among others. All of them hold neurotoxicity properties [448] (Figure 1.16).

Once microglia has been mobilized, neuroimmune regulatory proteins (NiReg) modulate the microglia-mediated immune response to resolve the inflammatory process [449], promoting tissue repair through the secretion of diverse neurotrophic factors, including IGF-1, brain-derived neurotrophic factor (BDNF), transforming-growth factor-β (TGF-β), and nerve growth factor (NGF) [450]. In normal conditions and acute inflammatory events, the pro-inflammatory response resolves and microglia continue their brain vigilance. However, in AD, the amyloid plaques remain as a persistent irritant and the equilibrium between microglial surveillance and activation is disturbed, creating a feedforward loop that results in a chronic neuroinflammatory state, promoting inflammation and tissue atrophy. Healthy brain cells can be caught in the "friendly fire" and the collateral consequences can include injury to healthy cells among increased activity of BACE1 leading to the production of more toxic Aβ [447].

On the other hand, whether microglial activation and inflammatory processes are indeed a cause of or, on the other hand, induced by Aβ accumulation is still controversial. What seems more prudent to assert is that microglia could exert both neuroprotective or neurodegenerative effects in the AD brain depending on the severity and stage of the pathology. Customarily it was believed that microglia activation responded to the presence of Aβ deposits, clearing them via phagocytosis of Aβ fibrils and degrading soluble species [446]. *In vitro* and *in vivo* [445] studies have shown clear evidence that microglia are capable of internalize and degrade Aβ aggregates [451, 452] and demonstrating a beneficial role in early AD [453, 454].

However, other studies point to the neurodegenerative side of microglia activation. It has been recently demonstrated that the adaptor protein apoptosis-associated speck-like protein containing a CARD (ASC) is released from activated microglia and binds to Aβ in the extracellular space promoting its aggregation, directly linking innate immune activation with the pathology progression [455].

1.1.9.AD cascade hypothesis summary

Plentiful data on human and animal models blame Aβ and tau as the primary pathogenesis triggers of AD [488, 489], as well as the observation that the age-related increase of Aβ burden anticipates possible or probable AD development by around 15 years [490].

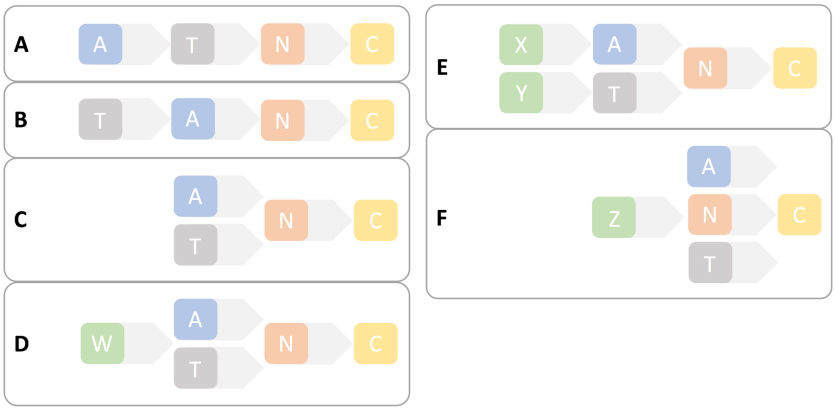

Figure 1.17. Hypothetical mechanistic pathological pathways in AD. Simplified representation of the main possible mechanistic pathways for AD development represented using the new research framework proposed by Clifford *et al.* in ref 487 considering Aβ (A) and tau pathology (T), neurodegeneration (N), and cognitive decline (C). Although the most supported mechanistic hypothesis is the represented in A, others must be, and actually are being considered. The simultaneous effect of A and T in N represented in C is something that has been studied and observed. The rest of the mechanistic models, W, X, Y and Z implies that a fifth or even a sixth element must be the primary trigger of the other A, T and N elements, ultimately leading to C. These new elements (W, X, Y, Z) could be pathogens [501], autoimmune mechanisms [502], or other subjacent vascular or metabolic pathology [13, 48], hypothesis that have been considered and proposed in some research works [501, 559].

Aβ and tau proteinopathies define AD as a singular disease among the many others also related to dementia. To exemplify the main mechanistic hypothesis considered to date, we will represent them as a "chain" of biomarkers using a new recently proposed nomenclature and AD definition proposed [487] (Figure 1.17).

A number of people in the field think of amyloidosis as the main inducer of the spread of pathologic tau, perhaps by promoting pathologic tau strains [491]. In this thought, pathologic tau is intimately linked to neurodegeneration, and neurodegeneration is intimately linked cognitive decline. If it is the case, if the "alternative amyloid cascade hypothesis" were correct, the logical biomarker sequence of AD development would be the one represented in Figure 1.17A [492, 493]. Nonetheless, there exist other biomarker sequences that are indeed possible and might be investigated.

In the hypothesis of T inducing A (Figure 1.17B), individuals with primary tauopathies (namely MAPT mutations producing 3R/4R fibrillar pathological tau that is morphologically identical to tau deposits in AD) would be expected to develop Aβ pathology, but it is not what has been observed until date. In other cases, both A and T could arise spontaneously and independently, or even promoted by a common upstream mechanism (W), leading to N (Figure 1.17C and D). As an example, it is likely that cell senescence [503], or age-related decay of some systems involved in immune control, or debris or toxic proteins clearance mechanisms may conform the upstream cause for both A and T accumulation. Moreover, A and T could be triggered by different and independent upstream mechanisms (X and Y) [504] (Figure 1.17E).

On the other hand, in some cases, an unknown or not-proved upstream element or process (Z) could induce A, T, and N, being A and T side-phenomena that do not make part of the causal pathway of N and C. Z could symbolize a number different possible mechanisms, such as an immune malfunction, uncontrolled inflammatory processes [505], or network failure [506] (Figure 1.17F).

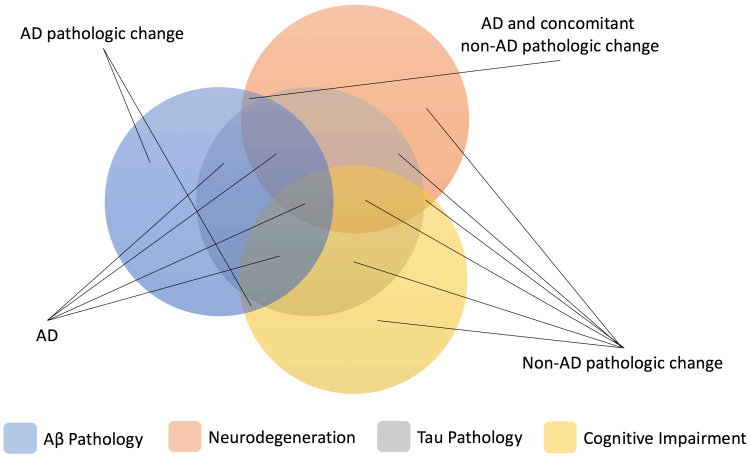

Figure 1.18. Interrelations between the biomarkers in AD. Descriptive nomenclature by a Venn diagram illustrating how AT(N) biomarker grouping and cognitive status may interact for classification of AD pathology. For simplifying, MCI and dementia are combined into a single (cognitively impaired) category and the A-T-(N)- and A+T-(N)+ groups are not represented in the figure. Abbreviations: MCI, mild cognitive impairment. (adapted from ref. 487).

One important consideration above this mechanistic modelling of AD is that the same pathologic mechanism might have different effects in different people. It could happen that the pathway represented in Figure 1.17A is functioning in some individuals, but other individuals might have an additional "player" influencing or even annulling the effect of A on T. However, this hypothesis would need to be delicately addressed, because the simple fact of some individuals can die with A without developing T, N, or C does not necessarily prove the existence of this unknown additional factor [507].

Other hypothesis that emerge using this research framework and must be tested is the hypothetical case where some may lead to A and T but never lead to N and C, making therapeutic interventions targeting A and T useless for preventing N and C. Thus that would be an evidence of neither A nor T are mandatory for the development of AD.

1.2. Therapies

1.2.1. Current approaches

As previously exposed, AD numbers are impressive and growing year by year. Special care cost only in the USA raised to about US$ 818,000 million in 2016 and the predictions point to a 35% increase every year [556].

Although there is still no cure for AD, there are numerous and variated approaches, from small molecules to immunotherapies for trying to stop the apparition and progression of the disease. The only treatments that are currently approved by the US Food and Drug Administration (FDA) for AD are drugs based in cholinesterase inhibitors and NMDA receptors (NMDAR) antagonists, which mitigate the symptoms, but do not stop the disease progression (Table 1.5) [289, 298, 299, 439].

Table 1.5. Therapeutics registered at FDS as clinical trials and drugs approved organized by clinical phase reached and the type of therapeutic approach (adapted from www.alzforum.com databases).

Target type	Dietary Suppl.	Gene/ Stem Cell	Immunotherapy (active)	Immunotherapy (passive)	Other	Procedural Intervention	Small Molecule
Phase 1	0	0	2	6	1	0	8
Phase 1/2	0	0	1	0	0	0	1
Phase 2	3	0	4	4	3	2	34
Phase 2/3	1	0	1	1	1	0	3
Phase 3	1	0	0	4	0	1	14
Phase 4	3	0	0	0	0	0	5
Approved	0	0	0	0	0	0	5
Inactive	2	0	0	2	1	1	13
Discontinued	1	1	2	5	2	0	61
Not regulated	1	0	0	0	0	0	0
Total	12	1	10	22	8	4	144

For the last years, the main focus of research on novel pharmacotherapies was based on the amyloidogenic hypothesis of AD, proposing Aβ peptide as the only responsible for the cognitive impairment and neuronal death. These treatments target, on one hand, the β and γ secretase enzymes for reducing Aβ production and, on the other hand, the clearing mechanisms for dissolution existing Aβ plaques. However, until now these strategies have proven to be modestly effective [439, 569].

In last times, recent studies suggest an alternative strategy centered on Aβ soluble oligomers, which may have a major role in the neuronal damage [283].

Modulation of β-Amyloid transport between the CNS and the peripheral circulation have also been targeted with some potentially therapeutic compounds, such as with peripheral administration of LRP-1. However, the only drugs able to reach clinical stages are some inhibitors and modulators of RAGE, but with discrete results [566, 298] (Figure 1.19).

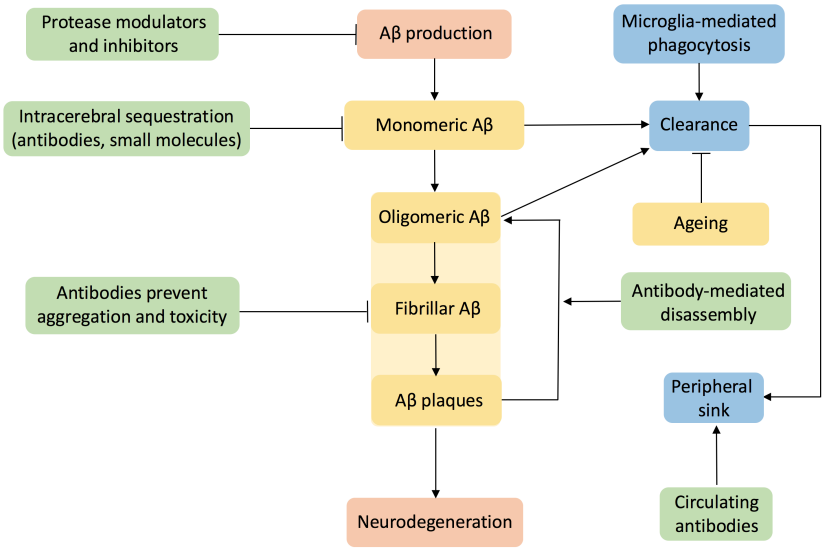

Figure 1.19. Aβ metabolism and pathology offers several potential therapeutic targets (green squares) for directing therapies. The inhibition or modulation of Aβ production may be a good strategy for attacking the problem at its origin. Once the Aβ is present in the brain, it is possible to use antibodies or small molecules to stimulate its clearance or sequestration, reducing neuronal damage and the aggregation in more danger species. Other possibility that has been tested is to use antibodies for disaggregate the pre-formed Aβ aggregates and facilitate the diffusion or clearance of more soluble and smaller species. And finally, the so-called "peripheral sink effect" hypothesis, by which, peripherally administrated antibodies may sequester and stimulate clearance of soluble species in the periphery, creating a gradient that may allow an efflux of Aβ from the brain [271, 281, 286, 293, 312, 330].

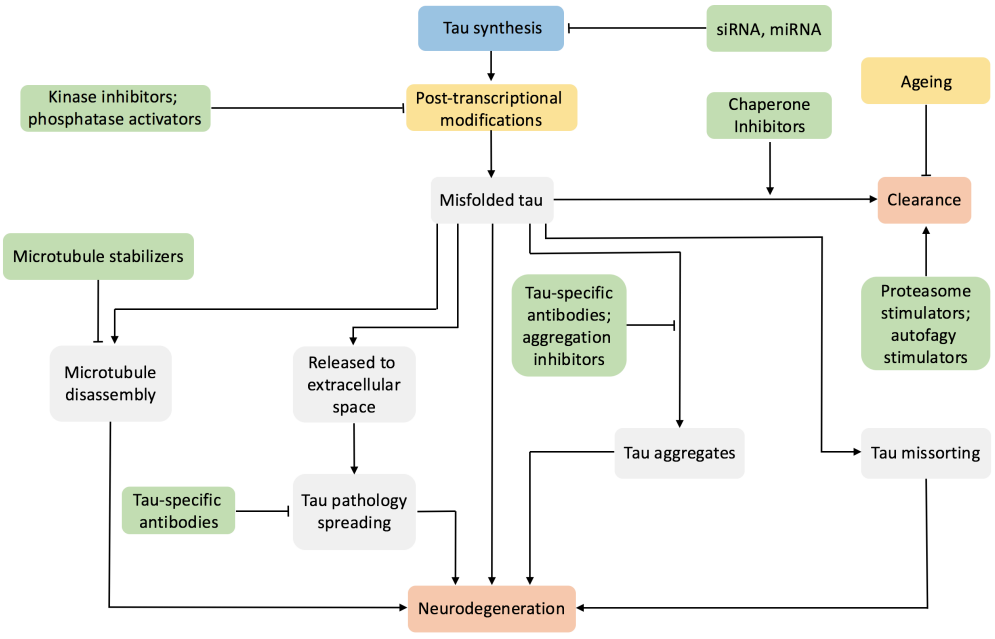

Figure 1.20. Tau pathology and potential therapeutic targets (green squares) based on the different points of the metabolic routes related to normal tau processing and pathologic pathways. SiRNAs and miRNAs can be used for modulating MAPT gene transcription and tau synthesis. Also inhibition of the chaperones heat shock protein 70 (HSP70) and HSP90, among autophagy and proteasome stimulators may facilitate proteasomal degradation instead of refolding, has been proposed as a possible treatment for tauopathies [431]. Obviously, as tau´s main task is to stabilize microtubules, to compensate the loss of function has been one of the targets for testing new tau-directed AD therapies [179]. Tau post-translational modifications, specially phosphorylation, have been extensively studied due to their important role in gain or loss of tau functions. Therefore, suppressing tau hyperphosphorylation by inhibiting kinases or on the contrary stimulating phosphatases, is extensively being investigated as a potential therapeutic approach [432,433]. Tau-based immunotherapy, as for Aβ, is another promising approach, both for targeting aggregated or pathologic tau forms.

Regarding AD tau pathologic hypothesis, treatments have been centered in inhibiting phosphorylation and aggregation by modulating or inhibiting kinases and stimulating phosphatases and using chaperones for interfering aggregation processes [303, 304, 306]. Also microtubule-stabilization drugs have been tested, for trying to compensate the loss of function of pathologic tau [310, 311]. But in last years, immunotherapeutic strategies have gained support for promoting tau aggregates clearance and targeting pathologic forms of tau (Figure 1.20) [298, 299, 301, 302, 305, 309, 312, 439].

Other drugs centered in making targets related to other AD pathologic hypothesis such as cholinergic system [567], inflammation [568], neurotransmitters or 5-HT6 receptors have also been tested in preclinical and clinical trials or are currently accepted by the FDA (Table 1.6).

Table 1.6. Therapeutics registered at FDS as clinical trials and drugs approved organized by clinical phase reached and the type of the target (adapted from www.alzforum.com databases).

Target type	Aβ	Cholesterol	Cholinergic System	Inflammation	Other	Tau	Unknown
Phase 1	5	1	2	2	6	3	2
Phase 1/2	2	0	0	0	0	0	0
Phase 2	13	0	0	5	34	3	5
Phase 2/3	6	0	0	3	2	0	0
Phase 3	10	0	0	3	9	1	1
Phase 4	0	1	0	0	5	0	1
Approved	0	0	4	0	1	0	0
Inactive	4	1	5	2	5	1	3
Discontinued	16	0	18	8	30	4	4
Not regulated	0	0	0	0	1	0	0
Total	56	3	29	23	93	12	16

1.2.2.Immunotherapies

A remarkable application of antibodies is also the one this thesis will put more emphasis, immunotherapy. To use antibodies as therapeutics is one of the most promising clinical approaches in the last years to treat several severe diseases such as cancer or AD.

Until 2017, 72 therapeutic monoclonal antibodies have been approved by the FDA or European Medicines Agency (EMA) (in 2012 were 32). Cancer and autoimmune diseases are the fields where more antibody-based drugs are being used. The mechanisms through therapeutic antibodies exert their activity are diverse and even unknown in some cases, but include from neutralization of substances (toxins [417, 418, 419] or cytokines [420]) to receptors blocking [421], binding to cells, host-immune system activation [422], or a combination of these effects [423].

1.2.2.1. Antibodies

Antibodies, also referred as immunoglobulins are glycoproteins product of an engineering system designed for generating a virtually unlimited collection of complementary molecular surfaces in response to an antigen. Their unlimited structural diversity is needed for an infinite batch of antigenic determinants recognition [435]. Antibodies are produced by B lymphocytes (also known as plasma cells) when an antigen binds a receptor in their surface [434, 278].

Two structurally defined essential roles have been attributed to antibodies. On one hand, antibodies bind to an epitope through the variable regions placed in the two “open arms” of the Y structure. Each arm (Fab) domain contains a binding site, giving to the antibodies a bivalent character, although the interaction of both domains with an antigen is in frequently vital for maintaining the functionality of the antibody. On the other hand, the Fc domain of the structure

confers the antibody the biological effector functions such as natural killer (NK) cell activation, activation of the classical complement pathway, or phagocytosis [278].

The basic structure of antibodies is composed by several small protein domains, formed by two antiparallel β-sheets and belongs to the immunoglobulin (Ig) superfamily. Two identical copies of a heavy (~55 kD) and light (~25 kD) chain are linked together by disulphide and noncovalent bonds, conforming a commonly represented Y-shaped structure weighting around 150 kD (Figure 1.21) [278].

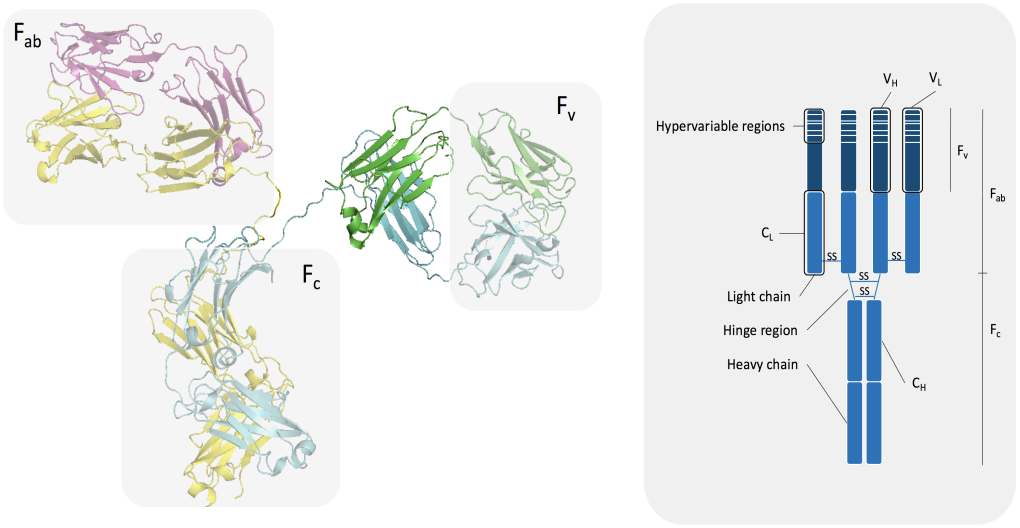

Figure 1.21. Antibodies´ structure. A. Sample structure of an IgG2 immunoglobulin (Mab231) obtained by X-ray diffraction. Heavy chains are colored in yellow and pale blue and light chains in pink and green. Different Fc, Fab and Fv fragments are shaded in grey rectangles. B. Simplified scheme of a typical IgG antibody, formed by four chains (2 light and 2 heavy chains) engaged by disulphide bonds.

Immunoglobulins are composed of two identical polypeptide chains of ~500 amino acids (heavy or H chains) linked by covalent bonds through disulphide bridges to two identical polypeptide chains of about 250 residues (light or L chains). The H and L chains may also be divided into a N-terminal variable (V) portion and a C-terminal constant (C) portion. Each heavy chain contains from four to five Ig domains (VH, CH1, CH2, CH3 ± CH4, depending on the antibody isotype), while each L chain consists of two more domains (VL, CL). The VL and CL domains are disulphide-linked with the VH and CH1 domains, respectively, to form the Fab region of the antibody, which is linked through a hinge region to the Fc domain, formed by noncovalent association of the CH2–3/4 domains from both chains.

The variable domains of molecule (VH and VL), forming the Fv, contain three segments each, which connect the β-strands and are highly variable in length and sequence [278]. These are the so-called complementarity-determining regions (CDRs), and are located in close spatial proximity on the surface of the V domains. These regions determine the conformation of the combining site and, in this way, the CDRs confer specific binding activity to apical regions of the Ig domain to recognize and bind a complementary surface (epitope) on the antigen (Figure 1.21).

1.2.2.1.1. Epitopes

A wide but acceptable definition of epitope could be “a restricted area of a protein that is recognized by a combined site or paratope of an immunoglobulin”. Protein antigenicity relies in these different types of epitopes, which can be differentiated as continuous and discontinuous epitopes, cryptotopes, neotopes, and mimotopes. These epitopes are recognized by the combining sites or paratopes of certain antibodies. Epitopes use to have diffuse boundaries and can be mainly identified only by their ability to be recognized by certain antibodies. However,

cross-reactivity is a common phenomenon due to antibodies are always able to bind a wide range of related epitopes [435].

As previously indicated, epitopes of proteins are used to be classified as continuous or discontinuous (often called conformational) depending on whether the residues included in the epitope are contiguous or not in the peptide chain. The distinction is not clear-cut and difficult to study since discontinuous epitopes frequently contain short segments of some contiguous residues able to bind to antibodies and could be given the status of continuous epitopes when it is not strictly true [435, 272, 275, 276].

The epitope-paratope complementary interaction is formed by a number of physicochemical bonds consisting of electrostatic and polar forces, such as van der Waals or hydrogen bonds found in any other protein interactions.

The mapping of an antibody´s epitope is one of the most important characterization assays to perform, due to it will define the exact interaction with the antigen and the therapeutic effect exerted by the antibody in the case to be used for therapy. Several techniques have been used to map antibodies´ epitopes, from enzyme-linked immunosorbent assays (ELISA) or arrays using several variants and combinations of possible epitopes, to MALDI spectrometry, nuclear magnetic resonance (NMR) or analysis of crystallized antibody-antigen complexes, being these last two some of the most reliable and from which more information can be obtained.

NMR is a powerful tool for obtaining data related to the epitope´s boundaries and the order each residue interacts with antibody´s paratope, obtaining a detailed sequence of affinity for each amino acid. On the other hand, crystallography gives very interesting information regarding the spatial conformation of the interaction and showing how the antibody influences the conformation of the antigen through the interactions with each residue.

However, is must be considered that the structure of an epitope after complexation with a neutralizing antibody could be different to the structure of the peptide unconjugated or even the original structure of the immunogen, thus it is an unreliable guide for identifying the exact epitope structure that was initially recognized by the B-cell receptors during the immunization process [435].

1.2.2.1.2. Avidity, Affinity, Specificity, Discrimination and Cross-Reactivity

There are some more important concepts to understand the mechanisms underlying antibody-antigen interactions.

Affinity (K_A) is defined as the strength of the interaction between an epitope and an antibody's antigen binding site. It is ruled by the same basic thermodynamic principles that govern any reversible biomolecular interaction and is represented by K_A. K_A describes how much antibody-antigen complex exists when an equilibrium is reached. The time taken for this to happen depends on the diffusion rate and is similar for all antibodies. However, high-affinity antibodies will bind a bigger amount of antigen in a shorter period of time than low-affinity antibodies. K_A values vary widely for antibodies from below 10^5 mol^{-1} to above 10^{12} mol^{-1}, and can also be influenced by other external factors such as pH, temperature or buffer composition [411].

$$K_A = \frac{[Ab - Ag]}{[Ab][Ag]}$$

On the other hand, *specificity* measures the degree with the immune system is capable to discriminate between different antigens while cross-reactivity measures the extent to which different antigens appear similar to the immune system. The molecular determinants of specificity and cross-reactivity define the nature of antigenic variation and the selective processes that shape the distribution of variants in populations [411].

Antibody specificity is use to believe to correlate with high affinity, since it is expected that highly specific antibodies should have a better stereochemical complementarity with their antigens than other antibodies with lower affinity. However, there is no crucial link between affinity and specificity, and antibodies with lower affinity may indeed discriminate better between two antigens

than others antibodies of high affinity do [38]. Anyway, it would be more worthwhile to speak of "discrimination potential" than specificity regarding antibodies.

Since proteins shelter many different epitopes, different levels of *cross-reactivity* could be found depending on the epitope related to a particular Mab. In fact, it depends on the aim of the investigator the criterion for deciding whether a particular antibody is specific or not for an intended protein [38]. Antibodies, obviously, are only specific for individual epitopes and never for antigens. It is also important to take into account that antibodies´ potential to discriminate between antigens is optimal only in a restricted range of experimental conditions and that when used at high concentrations could tend to react non-specifically with many other molecules [61, 62]

Regarding the existing and important differences between antigens and immunogens, the following concepts are important: *antigenicity* is the chemical property of proteins that describes the interaction between epitopes and paratopes, the chemical and structural complementarity.

On the other hand, *immunogenicity* is the ability of a protein to trigger an immune response in a host [34], and depends on the biological context and other extrinsic factors influencing the immune system mechanisms. Therefore, when a peptide fragment of a determined protein cross-react antigenically with an antibody raised against the protein, this does not guarantee that it could be able to trigger the production of antibodies that cross-react with the protein [5].

1.2.2.1.3. Types of antibodies

Antibodies can be classified by a number of ways in function of their structure, function, clonality and depending of the species of origin or the artificial modifications made of their structure.

Following a criteria based in structural characteristics, there can be distinguished five primary classes of immunoglobulins are IgG, IgM, IgA, IgD and IgE. Tey are differentiated by the type of heavy chain found in the molecule. IgG molecules have heavy chains known as gamma-chains; IgMs have mu-chains; IgAs have alpha-chains; IgEs have epsilon-chains; and IgDs have delta-chains. Other immunoglobulin classes have been identified in other vertebrates, such as the avian IgYs, the nanobodies found in camelids, which lack of light chains, or monodomain immunoglobulins produced by cartilaginous fishes (Table 1.7) [8, 10].

Table 1.7. Different human Ig classes and subclasses (Isotypes) based on their structure.

Ig class	Subclasses (in human, rat and mouse)	Structure	Properties
IgG	IgG1 IgG2 IgG3 IgG4		- Molecular weight: 150,000 - H-chain type (MW): gamma (53,000) - Serum concentration: 10 to 16 mg/mL - Percent of total immunoglobulin: 75% - Glycosylation (by weight): 3% - Distribution: intra- and extravascular - Function: secondary response
IgM		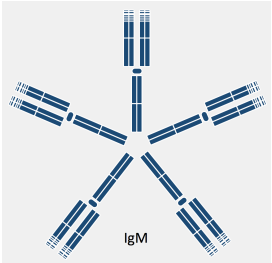	- Molecular weight: 900,000 - H-chain type (MW): mu (65,000) - Serum concentration: 0.5 to 2 mg/mL - Percent of total immunoglobulin: 10% - Glycosylation (by weight): 12% - Distribution: mostly intravascular - Function: primary response

IgA	IgA1  IgA2	- Molecular weight: 320,000 (secretory) - H-chain type (MW): alpha (55,000) - Serum concentration: 1 to 4 mg/mL - Percent of total immunoglobulin: 15% - Glycosylation (by weight): 10% - Distribution: intravascular and secretions - Function: protect mucus membranes
IgD		- Molecular weight: 180,000 - H-chain type (MW): delta (70,000) - Serum concentration: 0 to 0.4 mg/mL - Percent of total immunoglobulin: 0.2% - Glycosylation (by weight): 13% - Distribution: lymphocyte surface - Function: unknown
IgE		- Molecular weight: 200,000 - H-chain type (MW): epsilon (73,000) - Serum concentration: 10 to 400 ng/mL - Percent of total immunoglobulin: 0.002% - Glycosylation (by weight): 12% - Distribution: basophils and mast cells in saliva and nasal secretions - Function: protect against parasites

Regarding clonality, antibodies can be classified into poly- and monoclonal depending on the cells producing them. In a normal biological immunologic response, due to most antigens are highly complex, numerous epitopes into them are recognized by a number of lymphocytes. Then, each activated lymphocyte differentiate into plasma cells, resulting in a polyclonal response [278]. Thus, polyclonal antibodies are produced by several different clones of B cells and recognizes several epitopes of the same antigen (Table 1.8).

Table 1.8. Monoclonal and polyclonal antibodies characteristics and uses and comparison between.

	Advantages	Disadvantages
Monoclonal	- Production of large quantities of identical antibody. - Homogeneity between batches - High specificity - Low of cross reactivity - More accurate results in quantification assays	- Significantly more expensive to produce - More time-consuming for producing and developing the hybridoma - Small changes in the epitope's structure often results in antibody malfunction - Specific storage conditions for the clones - Cell culture and purification trained staff required - Less robust for detecting the protein in a denatured or altered conformation - Poor yield for applications requiring quick capture of the target protein - More sensitive to pH and buffer conditions - More susceptible to binding changes when labelled.

Polyclonal	- Low production costs - Quick production - Easy and cheap to store - Highly stable and tolerant against pH or buffer changes - Higher affinity and more robust detection of the antigen due to multiple epitopes recognition - Higher sensitivity for proteins detection - Optimal as capture antibody for Sandwich ELISA - Quicker binding to antigen - Significantly more robust when detecting proteins wearing slight variations in individual epitopes - Superior detecting native proteins in multiple assay types - Ease for coupling and stability when labelling	- Variability between batches from different animals and different time points - Higher cross reactivity due to multiple epitopes recognition - Affinity purification of the serum is required for minimizing cross reactivity

On the other hand, monoclonal antibodies are produced by a single B cell clone and recognize a unique epitope. Monoclonal antibodies were discovered in sera of multiple myeloma patients and afterwards, in the 70s, Köhler and Milstein developed the technique that allowed to generate monoclonal antibodies against a determined antigen and a desired specificity [278, 354]. In terms of usability, both poly- and monoclonal antibodies have advantages and disadvantages determined by the technique and it requirements (Table 1.8).

1.2.2.1.4. Production

1.2.2.1.4.1. Antigen presentation and immune response

The antigen preparation and presentation is fundamental for antibodies production. It is essential for the immunization the presentation of the antigen to the immune host in the form that elicits the strongest and most specific immune response. Consequently, there is a need to carefully monitor, for example, by mass spectroscopy or other functional assays the quality of the immunogen.

In case of recombinant proteins, post-translational modifications may be critical to the successful isolation of antibodies and needs to be taken into account [340, 341]. For example, abnormal glycosylation could provoke the obscuring of an epitope when produced in E. coli or yeasts, generating antibodies that will not recognize the protein in a mammalian system [342].

Therefore, the quality, integrity, and folding state of an antigen are crucial parameters for successful antibody generation. The antigen characteristics should mimic as closely as possible its condition in the desired application. The use of peptides as immunogens is extended, fast and straightforward. Peptides can be used as substitutes for complete proteins and usually are coupled with a carrier protein, for example, keyhole limpet hemocyanin (KLH) or bovine serum albumin (BSA) in order to elicit a stronger immunoreaction.

1.2.2.1.4.2. Polyclonal antibodies production

Polyclonal antibodies (pAbs) are still widely utilized in research and diagnostics, and there exist more than 100 biotech companies making pAbs around the globe.

To generate pAbs, the host is inoculated with the immunogen, similar to the process of vaccination or for producing mAbs. Once immunogens are infused into the host, the immune response processes lead in proliferation and differentiation of B cells into antibody-secreting plasma cells. Blood serum can be collected and antibodies purified for use. To enhance the antibody response and maximize the antibody titter, adjuvants can be used in combination with the immunogen.

1.2.2.1.4.3. Monoclonal antibodies production

The first technology to obtain monoclonal antibodies (mAbs) was developed by Milstein and Köhler, who in 1975 successfully fused immortal myeloma cell lines with antibody producing B-cells for producing hybridomas. Later, in 1986 the first immunotherapy with monoclonal antibodies was approved for use in humans (Muromonab-CD3) [438]. Muromonab was an unmodified mouse antibody, one of the only four fully murine therapeutic mAbs approved until now for clinical use. There exist several methods for producing, isolating and purify monoclonal antibodies, from hybridoma technology to several *in vitro* display techniques that increase flexibility, speed and the possibility to synthesize chimeric or humanized antibodies.

1.2.2.1.4.3.1. Hybridoma technology

B cells can produce millions of different antibodies. However, each of these B cells can only produce identical antibodies of a certain, predetermined specificity [354]. Kohler and Milstein, who in collaboration with Niels Jerne, were awarded the 1984 Noble prize for physiology and medicine for the development of such technique. The technique was named “hybridoma technology” due to it involves cell hybrids to produce sets of identical monoclonal antibodies against specific antigens. They achieved it by fusing myeloma cells with antibody-producing B cells. By merging the B cell with the myeloma cell, the cell resulting owns the ability to divide rapidly and perpetually, while keeping the capacity of producing antibodies. It can also be selected, allowing to have large numbers of identical antibody producing cells growing in cell culture. The original concept of hybridoma technique has been optimized during the last few years using different new approaches like pearl-chain formation (using electric fields for improving fusion), laser radiation (for guiding the lymphocytes and optimize the fusion), B-cell targeting (for increasing selectivity of the fusions), antigen-biotin and antigen-avidin selection or multitargeting [355].

1.2.2.1.4.3.2. Phage display technology.

The generation of fully human monoclonal antibodies was intimately linked from the beginning to the development of the so-called phage display technology. First described by George Smith in 1985 [357], phage display was initially limited to the selection of peptides. Afterwards, however, it was demonstrated that antibody fragments could be also successfully displayed on phages [358], becoming the most extended alternative for the generation of human antibodies. The technique does not depend on any immune system, being based on genetic engineering of the coating *E. coli* bacteriophage´s proteins and an *in vitro* selection mechanism called “panning” [358, 359]. Phage display of antibody libraries rapidly became a powerful method for both studying the immune response and as a method to rapidly select and evolve human antibodies for therapy. The fist therapeutic monoclonal antibody selected by phage display technique was Adalimumab (Humira), an anti-TNF antibody produced by Cambridge Antibody Technology and marketed by Abbott [360].

1.2.2.1.4.3.3. Other techniques

Besides phage display, several other *in vitro* display techniques such as yeast display, puromycin display, ribosomal display or bacterial display technologies have been developed to match specific needs or to improve the original phage display method [350, 352, 353, 411].

1.2.2.1.4.3.4. Humanization

Because murine antibodies have a shorter therapeutic half-life due to they are recognized by the immune system´s patient as foreign proteins, leading to a human anti-mouse (HAMA) response, they must be humanized. Humanization is a process oriented to modify antibodies sequences to reduce this immunogenicity for the use in human subjects. In the last few decades, since the first approved humanized antibody in 1997 (Daclizumab), a number of new methods have been used to isolate both full antibodies and fragments and to re-engineer those antibodies [570] (Figure 1.22).

These methods englobe well-established techniques including immunization and hybridoma technology, phage display and other more innovative approaches including ribosome display [350, 351], yeast display [353], puromycin display [352], or bacterial display [411]. All these

methodologies follow the same principles: proper antigen presentation, isolation, screening, selection and characterization of the selected binding molecules.

Nowadays there are used two main strategies for the generation of human antibodies: transgenic mice and *in vitro* selection technologies. Transgenic mice are animal containing the human immunoglobulin repertoire instead of the murine one, permitting the generation of human antibodies by hybridoma technology [378, 379, 380]. One of the advantages of this method is the *in vivo* affinity maturation. The limitations are related to toxic and conserved antigens. On the other hand, the popularization of the production of human monoclonal antibodies for research and clinical use was closely related to the development of several *in vitro* selection techniques, specially phage display technology [356].

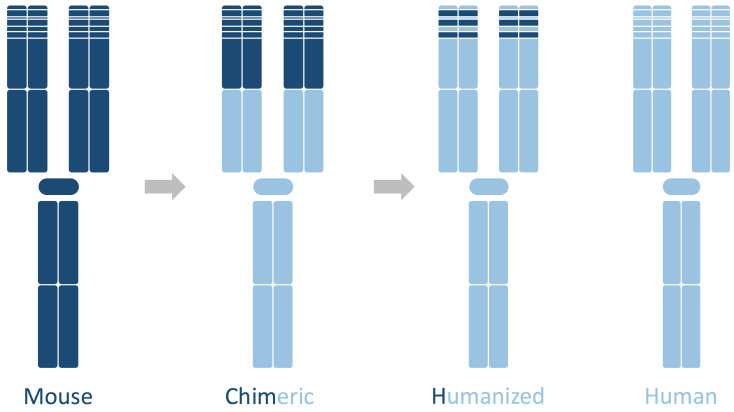

Figure 1.22. Schematic representation of a murine, chimeric, humanized and a human antibody. chimeric antibodies are the result of partial substitution of several fragments of the original antibody by parts from other species. In a more intense way, a humanized antibody is the result of the substitution of the entire sequences of a determined antibody by human sequences, except for the hypervariable regions placed at the CDRs.

1.2.2.1.5. Uses of antibodies

The capability of antibodies to selectively bind specific epitopes has been extensively exploited through the last decades. Several applications have been developed in several work fields, from antigen purification or cells isolations to use antibodies for mediating and modulate physiological effects for research, diagnostic or therapeutic purposes.

Regarding analytic applications, immunoblots, immunostainings and immunoprecipitations are some basic commonly antibodies' uses for identification and location a determined antigen or related molecule in a liquid or solid sample. In this kind of analytic applications, we can gather techniques such as ELISAs, WB, antibody microarrays, X-ray crystallography, FACScan cytometry, immunofluorescence, immunohistochemistry, etc. [383, 384, 385].

As said, antibodies are also useful tools used in purification and sample enrichment. Antibodies covalently linked to a platform such a particle or surface can be used for isolate or enrich antigens washing away other unbound molecules present in the sample of interest. Those platforms can be from fluorophores to magnetic particles, plates or resins [386, 387, 388, 389]

An application used since the mid-1980s, are related to reaction mediation and modulation. These techniques use antibodies (abzymes or catalytic antibodies in this case) as structural elements to facilitate an energetically unfavourable catalytic reaction [390]. Also in this kind of applications, antibodies can be used for blocking, neutralizing or activating cellular pathways in order to study these pathways or generate knock out animal models [391, 392].

1.2.2.1.6. Monoclonal antibodies´ market share

According "The 2017 Market for Research Antibodies: Keys to Success for Commercial Suppliers" report from BioInformatics LLC, it is estimated that monoclonal antibodies for research use hit the US$ 100 billion mark in 2017, with Abcam, Cell Signaling Technology, MilliporeSigma, Santa Cruz Biotechnology and Thermo Fisher Scientific as main characters in this market. Research antibodies are commonly used in basic and clinical research and are commercially

available from hundreds of companies to be used without intellectual property limitations (in most cases).

Regarding scientists who use antibodies, the majority use commercial, pre-made antibodies. In addition to pre-made antibodies, however, scientists still rely on custom antibodies (either from a commercial supplier or made in-house) and antibodies from their colleagues for less common or newly identified gene targets (Figure 1.23).

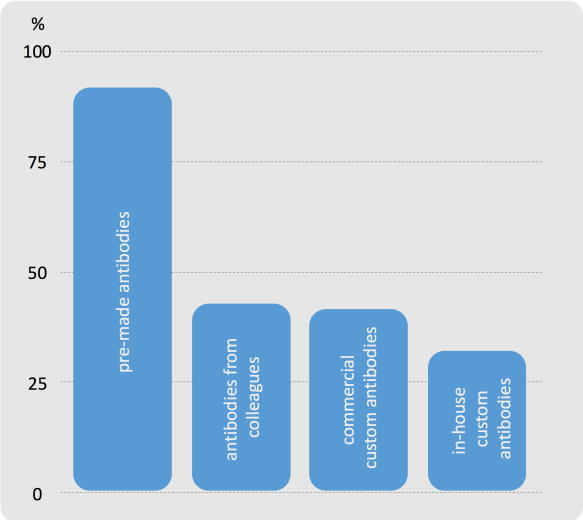

Figure 1.23. Use and market shares of antibodies. Most of the researchers use the typical commercial antibodies (90%), after this main option, other alternatives that seem to be almost equally used are custom antibodies, developed at core facilities or in-lab, or from commercial suppliers, or to use leftover or developed antibodies from other colleagues.

In therapeutic uses, according to a report published recently by Zion Market Research, global monoclonal antibody therapeutics market was valued at approximately US$ 108.01 billion in 2017 and is expected to generate revenue of around US$ 218.97 billion by the end of 2023, an approximate growth of 12.5% between 2017 and 2023. [555].

Immunotherapy

Among all the therapeutic strategies highlighted and used in the last years against AD, immunotherapy is one of the most promising approaches for assessing such a complex disease. These therapies have gained a lot of importance in the last decade, achieving more fails than achievements, but still being one of the most hopeful opportunities to treat AD.

There are two basic approaches in immunotherapy to fight against AD, active and passive immunization. In active immunization, a fragment of amyloid beta or the antigen of interest is inoculated to the subject in order to provoke a response of both antibody and cellular-based immunity. In passive immunization, on the other hand, the intravenous injection of external pre-formed antibodies to the subject has the purpose of target and help the immune system to remove the pathological molecule. Here, depending on the mechanism, antibodies may exert their main effect differently: (i) Microglial phagocytosis: Entering the brain from the bloodstream, antibodies may target aggregates and fibrils, activating microglial phagocytosis via the Fc receptor [475, 476]. However, some studies have showed that Fc mediated phagocytosis is not obligated for clearance of Aβ induced by immunotherapy [477]. (ii) Catalytic disaggregation: In this case, antibodies may also cross the BBB, enter the brain and disrupt the insoluble deposits, neutralizing their toxic effects and/or facilitating the solubilisation of the compounds and their diffusion outside the brain [478, 479, 480]. Nonetheless, it has been shown that, in the case of the Aβ, certain soluble oligomeric species could be the most harmful element, more than insoluble fibrillary deposits. (iii) In the periphery, where they bind to circulating forms of the pathological molecules [471] and restrict translocation to the brain. In addition, the binding of antibody to the molecules may accelerate clearance and degradation by macrophages of the reticuloendothelial system and generate a concentration gradient across the BBB, hypothetically promoting efflux from the brain into the systemic circulation. This phenomenon is known as the “peripheral sink” hypothesis [465, 471, 472, 473, 474].

In 1986, the first antibody, the murine muronomab-CD3 (Orthoclone OKT3®) was approved for therapy [422]. After that, for solving some dosage and reaction problems, the second generation

of therapeutic antibodies were chimeric [424, 425], and later on the antibodies for human clinical tests were humanized [426]. The next important step was in 2002, when the first fully-human antibody, Adalimumab (Humira®), was commercially launched [427]. Although within the last 15 years this field has grown enormously, there are several issues still remaining that are hindering the obtaining of positive results in the clinical trials for treating CNS disorders such AD. Those issues are related to, first, antibodies administrated or generated by the own subject may cross the BBB to exert their major effect. In normal conditions, only about 0.1% of the antibodies present in the circulating tissues cross the BBB. Second, the removal of amyloid of tau deposits from brain once neuronal damage is already produced, has not been so effective as expected, so the key to solve this issue would be to start the treatment in a very early stage of the disease. Third, an even better understanding of the clearance of immune complexes is required to avoid secondary effects and the fatigue of the clearance mechanisms during long treatments [271].

Now, for completing this state-of-the-art review, there will be summarized some of the main clinical and pre-clinical attempts to find an effective immunotherapy for AD, targeting two of the most promising clinical molecular targets, Aβ and tau protein:

1.2.2.2. Aβ-targeted immunotherapy

1.2.2.2.1. Pre-clinical immunotherapeutic trials targeting Amyloid beta

Since Schenk and colleagues reported the beneficial effect of an Aβ immunotherapy in a preclinical study of an Aβ(1-42) active immunization in PDAPP transgenic mice in 1999 [412], numerous attempts have been carried out to try to find positive effects of both active and passive immunization, mainly in mice AD models. Schenk and colleagues reported that immunizing mice prior to the onset of pathology significantly reduced levels of cerebral amyloid and produced high serum antibody titters. Afterwards, two more works demonstrated that Aβ vaccination in CRND8 [413] or APP/PS1 [414] tg mice strongly improved performance in learning and memory tasks. In consequence, many active immunotherapeutic approaches were explored and published during the last decades confirming the Aβ reduction effect of Aβ vaccination in AD-like tg mouse models [415].

On the other hand, passive immunization treatments using Aβ antibodies against the N-terminus, mid-domain, and C-terminus of Aβ have been reportedly tested in AD transgenic mice models. Bard and colleagues published in 2000 a passive immunization report in PDAPP mice using several different monoclonal anti-Aβ antibodies with different IgG isotypes and targeting various Aβ epitopes [416]. It seemed that the anti-Aβ antibodies managed to enter the CNS, bind plaques and induce clearance of pre-existing deposited amyloid. Since then, dozens of preclinical tests have been published showing reductions in Aβ burden and other pathological biomarkers among cognitive improvements. Some of the antibodies tested, like 3D6, m266 or BAM-10 were accepted afterwards to enter to clinical phase trials, being subject of humanization and several modifications for improving their performance in humans.

1.2.2.2.2. Clinical immunotherapeutic trials targeting Aβ

1.2.2.2.2.1. Active immunotherapies

As previously highlighted, active immunotherapies or active vaccination engages the own subject cellular and humoral immune system, among B and T cells, to produce antibodies against the antigen inoculated. An active vaccines consist of an antigen combined with an adjuvant that boost the immunologic response of the subject. On one hand, these active strategies can induce long-term antibodies production in a large population without needing constant administration and reducing costs and, in addition, to lead to a polyclonal antibodies production against multiple and overlapped epitopes, helpful for a broad coverage. However, it also induces T-cell response, increasing the risk of leading to a deleterious immune reaction, being difficult to modulate and shut off [271].

In the mid-nineties, Beka Solomon´s research group proposed that an anti-Aβ molecule could work as a tool to be used to prevent Aβ aggregated forms depositions and even disaggregate pre-formed fibrils [313, 314]. Afterwards, in 1999, Schenk and collaborators at ELAN Pharmaceuticals showed *in vivo* that active immunotherapy against full length Aβ using an adjuvant effectively reduced Aβ plaques burden in AD transgenic mice [315]. Later on, the first active vaccine clinical trial against AD (AN1792), was interrupted in 2002 due to

meningoencephalitis development in 6% of the case studies. It was composed by full length Aβ, a QS-21 (saporin) adjuvant and a plysorbate 80 for stability reasons [316]. Although the study was halted, several new strategies arise from it, such as vaccines based in mimotopes and neoepitopes, Aβ conjugates, or DNA, phage, virus-like particles or viral vectors. Currently, a number of clinical trials are being carried out with second generation Aβ vaccines with the main goals of preventing plaque deposition and enhance Aβ clearance (Table 1.9).

Table 1.9. Summary of the active immunotherapeutic clinical trials performed targeting Aβ (adapted from www.alzforum.com database).

Name	Synonyms	FDA Status	Company	Target	Therapy Type	Approved
ABvac 40		AD (Phase 2)	Araclon Biotech	Amyloid-Related	Immunotherapy (active)	
ACI-24	Pal1-15 acetate salt	AD (Phase 1/2), Down's Syndrome (Phase 1)	AC Immune SA	Amyloid-Related	Immunotherapy (active)	
AN-1792	AIP 001	AD (Discontinued)	Janssen, Pfizer	Amyloid-Related	Immunotherapy (active)	None
Affitope AD02		AD (Phase 2)	AFFiRiS AG	Amyloid-Related	Immunotherapy (active)	
CAD106		AD (Phase 2/3)	Novartis Pharmaceuticals Corporation	Amyloid-Related	Immunotherapy (active)	None
Lu AF20513		AD (Phase 1)	H. Lundbeck, Otsuka Pharmaceutical Co., Ltd.	Amyloid-Related	Immunotherapy (active)	
UB 311		AD (Phase 2)	United Neuroscience	Amyloid-Related	Immunotherapy (active)	
Vanutide cridificar	ACC-001, PF-05236806	AD (Discontinued)	Janssen	Amyloid-Related	Immunotherapy (active)	None

1.2.2.2.2.2. Passive immunotherapies

Passive immunotherapies involve the direct injection of monoclonal antibodies without demanding the own immune system to engage antibody production. Immediate stopping of administration in the case of adverse effects, precise dosing control or the possibility to target specific epitopes without disturbing other similar conformations are some of the benefits of this therapeutic strategy. On the other hand, it requires the production of expensive humanized monoclonal antibodies and frequent injections, making it more complicated for long-term treatment, specially for a large population compared to active immunization. In addition, repeated dosing with antibodies elongated over time could lead to the production of anti-antibodies, which potentially would have a neutralizing effect and/or lead to side effects such as inflammation, cerebrovascular accidents or neuronal hyperactivity [271, 330, 429].

Among the antibodies used until date within this immunotherapeutic approach for treating AD, there can be considered three types of drugs:

1.2.2.2.2.2.1. Humanized antibodies

3D6/Bapineuzumab/AAB-003

Back in the year 2000, Bard and colleagues demonstrated that external systemic administration of a monoclonal antibody against the N-terminal region of Aβ, called 3D6, to transgenic mice resulted in antibody brain entry, Aβ plaque binding and induction of Fc-receptor-mediated microglial phagocytosis of the Aβ deposits [317, 332].

From the crystal structures solved, eleven possible hydrogen bonds were observed between the antibody and Aβ residues including Asp1 (3 bonds), Glu3 (4 bonds) and Arg5 (4 bonds). Moreover, there were identified five water-mediated hydrogen bonds and numerous Van der

Waals contacts made between antibody and the Aβ peptide including nine residues from the light chain and ten residues from the heavy chain [319] (Figure 1.24). All these interactions lead Aβ N-terminal region to form an α-helical conformation similar to what it forms in apolar environments (plaques, membranes). It is believed that this structure is mandatory for the antibody recognize the peptide, so when Aβ N-termini suffer truncation or modifications, such structure is not formed and antibody clinical efficacy is compromised [428].

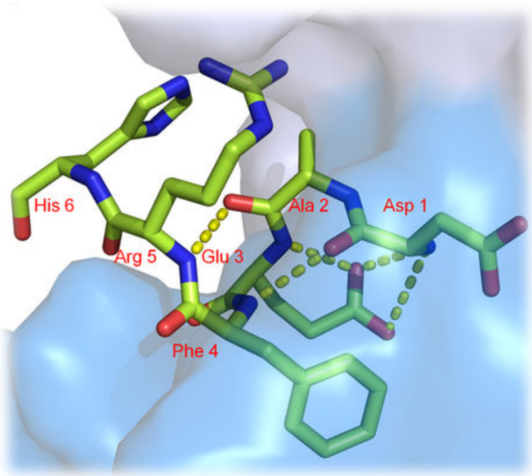

Figure 1.24. The Aβ peptide nested in the groove of the Bapineuzumab´s Fab CDRs. The peptide is shown in green sticks with the Fab light chain in grey and heavy chain in blue. Intra-Aβ hydrogen bonding, shown as dashed lines, stabilizes the helical conformation of the peptide. Image taken from ref. 428.

This murine antibody was the precursor of the humanized N-terminal-specific mAb Bapineuzumab, which was tested in phase I, II and III clinical trials [318, 320]. However, the continuation of new clinical trials was interrupted in 2012.

Solanezumab

In 2001, DeMattos and colleagues tested in transgenic mice an antibody directed to the mid-region Aβ, targeting the central, oligomer-nucleation core in a very similar manner as Crenezumab [324]. The structures show that key interactions between Aβ residues and Solanezumab are mediated by Aβ Lys16, Phe19, Phe20 and Asp23 sidechains, and main-chain elements across the Aβ backbone. Aβ residues 16–18 form an extended coil conformation nested into the CDRs´trench, meanwhile residues C-terminal following the Phe19-Phe20 core, project out of the antibody forming a helical conformation from residue Ala21 to Ser26 (Figure 125).

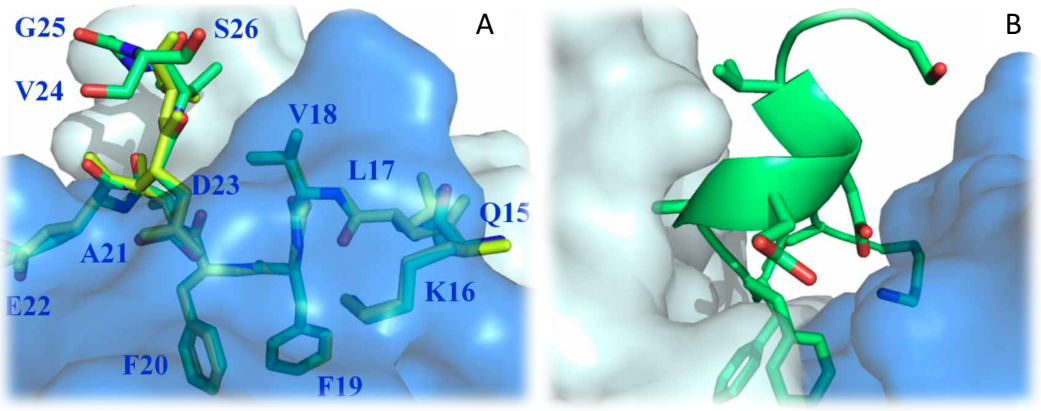

Figure 1.25. Structure of the mid-region (15-26) of the Aβ peptide bound to Solanezumab Fab CDRs. Solanezumab is shown as a transparent surface, light blue (light chain) and darker blue (heavy chain). A. Two models of the peptide in the asymmetric unit of the crystal are shown in green and yellow sticks. B. Helical conformation adopted by C-terminal Aβ residues at the nested Phe19-Phe20 dipeptide. The view was taken 90 degrees' rotation about the Y-axis from that shown in panel A. Images taken from ref. 324. PDB ID: 4XXD.

It preferentially recognized soluble Aβ and reported lowered brain Aβ burden and increased Aβ levels in plasma in mice, suggesting that the antibody could enhance clearance from brain to blood and significant cognitive improvement after only one injection [321, 334]. Solanezumab was the humanized version of m266, property of Eli Lilly & Co. and was already tested in different phase I, II and III clinical trials [322]. Nowadays, there still are two phase III clinical trials ongoing and finishing in 2020 and 2021.

Crenezumab

Genentech's Crenezumab (also known as MABT510A) is a humanized monoclonal antibody recognizing multiple forms of aggregated Aβ, including oligomeric and fibrillar species and amyloid plaques with high affinity, in addition to monomeric Aβ, but with lower affinity.

Crenezumab´s epitope comprises residues 13 to 24 of the Aβ peptide. The complementarity determining regions (CDRs) of Crenezumab show a short H3 loop of 3 residues and a long L1 loop of 16 residues, creating a deep paratope channel where the Aβ peptide is buried. Crenezumab recognizes a consecutive stretch of twelve Aβ(11–25) peptide residues in an extended conformation including His13Aβ–Val24 Aβ residues which adopt a well-defined and nested structure. The flanking residues on the N- and C-termini of the peptide are disordered [430]. This form of interaction makes Crenezumab the only antibody until date that targets the mid-region of Aβ peptide, binding multiple aggregated forms and exerts dissociating effects (Figure 1.26).

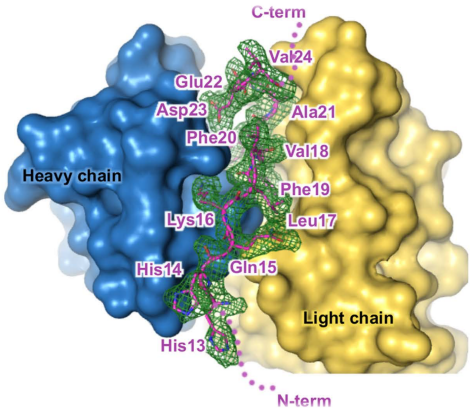

Figure 1.26. The structure of Aβ(11–25) embraced by Crenezumab CDR´s. Fab heavy chain is shown in blue and the light chain in yellow. Aβ peptide is shown in ribbon and sticks. Carbon atoms of Aβ peptide are in magenta. The N- and C-termini of Aβ peptide are disordered in structures as indicated by dots. The Aβ residues are labeled. Green mesh shows the 2Fo-Fc electron density map (contoured at 1xRMSD) corresponding to the Aβ peptide. Image taken from ref. 430.

Interestingly, the characteristics of such antibody binding structure seem to not only impede Aβ aggregation but also promote disaggregation in two ways. First, the antibody occludes part of the Aβ "hydrophobic core" (Leu17Aβ–Ala21), suspect to be responsible for self-association and oligomerization. And second, because the hairpin turn is disrupted.

This humanized antibody uses an IgG4 backbone for a reduced effector function on microglia, trying to stimulate amyloid phagocytosis while limiting release of inflammatory cytokines in order to avoid some side effects such as vasogenic edema. The antibody passed several phase I and II clinical trials and there is a phase III currently ongoing and finishing in 2021 [323]

BAN2401

BAN2401, property of Eisai Co., is a humanized IgG1 monoclonal antibody specifically directed against large, soluble Aβ protofibrils [335]. The objective is to lead to Aβ clearance and/or neutralize its toxicity. This antibody was originally developed at the BioArctic Neuroscience company from the discovery of the "Arctic" mutation in APP gene, which leads to an accumulation of high levels of Aβ protofibrils [325]. Afterwards, BAN2401 was licensed by Eisai, which from 2014 set a collaboration agreement with Biogen Idec for testing this antibody in immunotherapy of AD [336]. BAN2401 was reported to be well-tolerated at all doses in a multicenter phase I trial and in another phase II trial ended in 2018 (Study 201) it reported statistically significant slowing of disease progression at the end of 18 months as compared to a placebo, as presented at the

2018 Alzheimer´s Association International Conference in Chicago the July, 25th. The study will be subject of further investigation.

GSK933776

GSK933776, property of GlaxoSmithKline (GSK), is a humanized mouse IgG1 monoclonal antibody that binds the N-terminus of the Aβ peptide [333]. Its Fc region was engineered for reducing Fc-receptor binding and complement activation; trying to minimize risk of side effects such as ARIA. There were conducted several phase I and phase II trials, however, it was discontinued after failing in the main clinical outcomes in 2014 for treating AD [326, 327].

Ponezumab

Ponezumab (also called PF-04360365) is a passive immunotherapy drug developed by Rinat Neuroscience and now both property of Pfizer. It is a humanized IgG2δA monoclonal antibody that directed against the free C-terminal amino acids 33-40 of the Aβ(1-40) peptide. It forms a complex grasping the highly hydrophobic region (30-AIIGLMVGGVV-40) in an extended coil conformation (Figure 1.27) [328, 328].

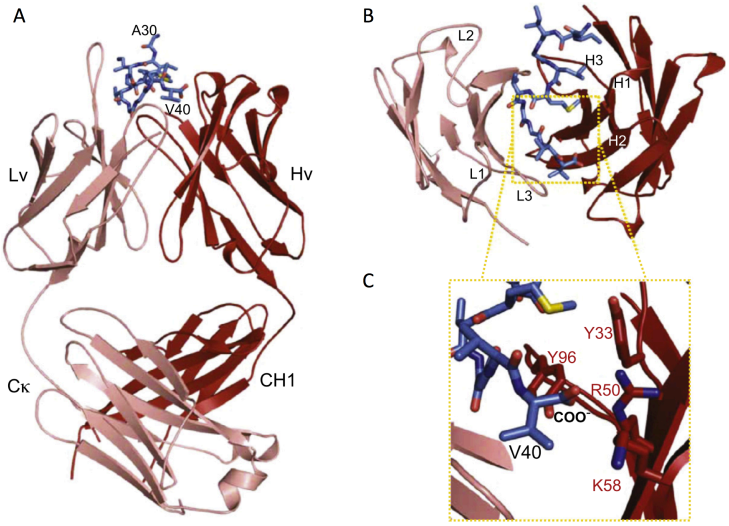

Figure 1.27. Ponezumab complex structure and binding interactions with Aβ peptide. A. General representation of Ponezumab Fab chains (light chain in light brown and heavy chain in red) bound to the last 11 C-terminal residues of Aβ(1-40) peptide (labelled in blue). B. In detail Ponezumab variable domain binding site structure conforms a nest for the Aβ peptide. C. Close-up view of the buried Aβ final Val40 residue´s carboxylic acid´s charge interaction with heavy chains R50, K58, Y33, and Y96. Images taken from ref. 328.

Ponezumab's safety and pharmacokinetics were confirmed in five Phase I trials and in the two phase II trials performed with this antibody for AD therapy concluded in 2011 confirming adequate safety and showed a plasma Aβ(1-40) increase with treatment, suggesting a peripheral sink effect. On the other hand, in a second trial with mild to moderate AD 36 patients, there were not found any changes on brain or CSF Aβ burden. In consequence, Ponezumab development and testing for AD was discontinued.

1.2.2.2.2.2. Autoantibodies

The basis behind this type of fully human monoclonal antibodies relies in healthy donors' immune systems that successfully have resisted AD. The antibodies could be turned into therapeutics by a process called "reverse translational medicine." by selecting human B-cell clones triggered by neo-epitopes present in pathological Aβ aggregates. The screening of libraries of human memory B cells for reactivity against aggregated Aβ led to molecular cloning, sequencing, and recombinant expression. Below, a summary adapted from Alzforum database of the most important clinical trials registered by the FDA based on fully human antibodies (autoantibodies) targeting Aβ:

Gantenerumab

Gantenerumab belongs to the new generation of fully human antibodies used in immunotherapy and is property of Chugai Pharmaceutical Co. and Hoffmann-La Roche [336]. It is an IgG1 isoform antibody designed to bind with subnanomolar affinity to a conformational epitope on Aβ fibrils, and preferentially interacts with aggregated brain Aβ, both parenchymal and vascular. Crystallized Fab fragments of Gantenerumab were incubated with peptide solutions of Aβ(1-11) and Aβ3-11. Minor differences between the two complex structures were observed and Gantenerumab Fab-Aβ complex structures are available at Protein Data Bank (PDB ID 3BKJ), showing a special Aβ binding form of Gantenerumab [324] (Figure 1.28 A).

Bound to the antibody, Aβ(1-11) forms an extended conformation in the trench conformed by CDRs H1, H2, H3, and L3. All amino acids of the Aβ peptide interact with the heavy or light chain, with the exception of Ser8 and Gly9, which seem to form a short turn pointing away from the Fab fragment. The first 4 residues of Aβ(1-11) are mainly interacting with the heavy chain whereas residues 5 to 11 are contacting with both heavy and light chains. The side chain of Phe4 suppose an important anchor point for the peptide, being deeply buried in a hydrophobic complex.

Direct binding of Gantenerumab to synthetic Aβ fibrils was also confirmed by immuno-electron microscopy. As previously showed, high resolution NMR solved Aβ fibrils structure has been determined previously demonstrating that the N-terminal and central portions of Aβ are exposed in close juxtaposition at the surface of the fibril [118].

Based on these models and the dual epitope recognition of Gantenerumab, it was proposed that antibody binding to fibrillar Aβ involves both N-terminal and spatially adjacent central Aβ sequences. According to this prediction, the flexible N-terminal sequence of Aβ would be the initial interaction of Gantenerumab followed by the interaction with the adjacent central Aβ part, conferring increased binding avidity (Figure 1.28 B).

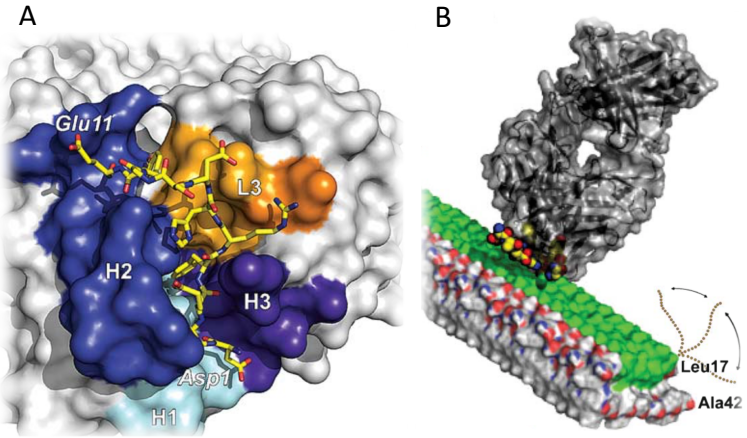

Figure 1.28. Gantenerumab solved structures in complex with Aβ peptide. A. Atomic binding mode of Aβ(1-11) peptide bound to Gantenerumab. The peptide interacts with H1 (shown in cyan), H2 (in blue), H3 (in purple) and L3 (in orange) CDR regions. B. Model of Gantenerumab binding to the Aβ fibril. The initial binding to the flexible free N-terminal part is followed by a second step involving the central Aβ19–26 region (highlighted in green). Images taken from ref. 118.

The intended therapeutic mechanism for this antibody is that it should disassemble and degrade Aβ plaques by recruiting microglia and activating phagocytosis. It has been shown that Gantenerumab induces phagocytosis of human Aβ deposits in AD brain slices co-cultured with human macrophages. Moreover, it is able to neutralize oligomeric Aβ42-mediated inhibitory effects on long-term potentiation in rat brains. In APP/PS-1 transgenic mice preclinical tests, Gantenerumab targeted cerebral Aβ, reduced small plaques load, and prevented new plaque formation. On the other hand, no plasma Aβ alterations were observed [324].

Gantenerumab passed four phase I, one phase II/II and another phase III international clinical trials, and it is involved in a second phase III trial together with Eli Lilly's Solanezumab, that will end by 2023. Moreover, recently, in March 2017, MorphoSys, Roche´s partner in the development of Gantenerumab, announced two new Phase 3 trials for prodromal AD in 2017.

Aducanumab

Also known as BIIB037, Aducanumab is high-affinity and, as Gantenerumab, belongs to the new generation of fully human IgG1 monoclonal antibodies [331]. It was originally isolated by the Neurimmune company in Switzerland, from healthy, aged donors who were cognitively normal.

Aducanumab recognizes aggregated forms of Aβ, and in brain, preferentially binds parenchymal over vascular Aβ [529].

Crystal structure of a recombinant Fab fragment of Aducanumab in complex with Aβ(1-11) peptide confirmed that the antibody recognizes N-terminus of Aβ in an extended coil conformation similar to other antibodies such as 22C11. Although residues from Glu3 to His6 make contact with the antibody, it binds primarily and bury deep in the CDRs groove the Phe4 and His6 of Aβ. In comparison with other anti-N-terminal Aβ antibodies, Aducanumab has an exceptionally compact epitope, which may contribute to its high specificity and avidity for Aβ oligomers and fibrils.

In the preclinical tests, a thirteen-week chronic dosing in old transgenics mice reduced plaques of all sizes while vascular Aβ levels were unaltered and in in summer 2012, Biogen Idec initiated the clinical trials. Main outcomes were fulfilled and Aducanumab is currently being tested in two phase III clinical trials which will end by 2022 and that have already reported significant reductions in brain Aβ in a dose- and time-dependent manner [329].

Conclusions

All these antibodies have different mechanisms of action defined by their epitopes and the way they interact with the antigen. Epitope´s spatial conformation, aggregation kinetics and, therefore, the therapeutic effect are influenced by the antibody binding. It has also been observed that N-terminal antibodies bind primarily aggregates, which could be related to the higher exposure of Aβ's N-terminus in aggregated and plaque-deposited forms [97, 271, 328]. If these mechanisms actually work this way, the atom-by-atom interaction between antibodies and Aβ might influence the outcome of therapeutic trials.

Both mid-region binding Solanezumab and Crenezumab antibodies had common major negative results, but sub-group and post-hoc analyses uncovered some benefits in patients with mild AD. Moreover, both produced low rates of amyloid-related imaging abnormalities with brain edema (ARIA-E). These similarities could be due to Solanezumab did not bind plaques deposited in the brain, it avoids to trigger the microglia-related inflammation. On the other hand, Crenezumab binds aggregated Aβ in addition to monomer, which would suggest that it might triggers more ARIA-E, but whereas Solanezumab is an IgG1 antibody, Crenezumab's IgG4 backbone lower reactivity would provide an explanation for the lower ARIA-E observed in Crenezumab treatments.

Table 1.10. Summary of the general epitope and recognized structures of some of the most important passive immunotherapeutic drugs tested in clinical trials for AD targeting Aβ

Antibody	Epitope	Epitope structure	Conformation recognized				ARIA-E
			Monomers	Oligomers	Protofibrils	Fibrils	
Solanezumab	16-26	Helix-βcoil	Yes				Low
Crenezumab	16-26	Helix-βcoil	Yes	Yes		Yes	Low
Bapineuzumab	1-7	Helix	Yes			Yes	High
Gantenerumab	1-11	Linear		Yes		Yes	Low
Aducanumab	3-6	Linear	No			Yes	High
BAN2401	N-terminal	Conformational			Yes		Low

Furthermore, outcomes from N-terminal antibodies-based trials also share some similarities. Bapineuzumab, Gantenerumab, and Aducanumab all reduced amyloid burden and triggered ARIA-E, reinforcing with the idea that mobilizing plaque-bound Aβ activates microglia. High ARIA-E among lack of cognitive of a Bapineuzumab trial in 2012 failed because of lack of a cognitive benefit in a phase III trial. On the other hand, data from the last clinical trials with Aducanumab confirmed that it nearly eliminated brain amyloid among signs of evident cognitive recover. Which could be the reason for these differences? May it be related to the fact of Aβ adopts extended conformations when bound to Aducanumab and Gantenerumab instead the the helical structures at Bapineuzumab? Moreover, Aducanumab is an autoantibody, isolated from natural Aβ-specific antibodies formed in humans. This could help this antibody to recognize an Aβ conformation that

naturally exists in the human brain and has clinical relevance, while Bapineuzumab and Gantenerumab immunogens were synthetic and phage-displayed peptides, respectively [97, 271, 328, 529] (Table 1.10).

Although we count with a wide published collection of antibody-Aβ structures, it is still unclear if targeting monomeric, oligomeric, or fibrillar forms of Aβ is the adequate strategy for treating AD or which molecular interactions are the ones we must explore. Except for very punctual successes, there are several issues still remaining that are hindering the obtaining of robust positive results in the clinical trials. Those issues are also related to BBB crossing, the difficult early detection of the disease for improving treatment effectiveness and the poorly known clearance of immune complexes mechanisms. [273, 329, 323, 324, 326, 331].

1.2.2.2.2.2.3. IVIg

Another strategy assayed in passive immunization trials are the intravenous immunoglobulins (IVIg) in AD. This approach is based in using pooled antibodies (IVIg) obtained from a donor cohort against the antigen of interest. In a number of autoimmune neurological disorders, IVIg are used as immunosuppressants without major side effects.

However, during the last years, different trials including Octapharma´s phase II [35] and phase III Gammagard trials in mild-moderate AD patients [36] showed no significant slowing of AD progression. After Gammagard clinical results, another attempt for using IVIg for treating AD was started using Gamunex. This is an immunoglobulin preparation used in obstetric to prevent and treat blood conditions related to rhesus factor incompatibility. The primary trial was pretended to finish in December 2017 according to FDA data, but no results have been published until now (Table 1.11).

Table 1.11. Summarized IVIg immunotherapy clinical trials performed until date (adapted from www.alzforum.com)

Name	Synonyms	FDA Status	Company	Target Type	Therapy Type
Gammagard®	Intravenous Immunoglobulin, IVIg	AD (Discontinued)	Baxter Healthcare	Amyloid-Related, Inflammation	Immunotherapy (passive)
Octagram® 10%	Intravenous Immunoglobulin, NewGam	AD (Inactive) Mild Cognitive Impairment	Octapharma	Amyloid-Related, Inflammation	Immunotherapy (passive)
Gamunex	Intravenous Immunoglobulin. Human albumin combined with Flebogamma	AD (Phase 2/3)	Grifols Biologicals Inc.	Amyloid-Related, Inflammation	Immunotherapy (passive)

1.2.2.3. Tau-targeted immunotherapies

As previously exposed, immunotherapy has emerged in the last years as one of the most promising therapeutic strategy for AD, whether targeting Aβ or tau. Both active and passive vaccinations have showed to reduce tau pathology and even improve cognitive and functional performance of transgenic mice in behavioral tests (Table 1.12). The mechanisms of action of the tau-specific antibodies tested in these immunotherapies are still not very clear. When antibodies enter the CNS, in order to reach intraneuronal tau, they may enter neurons via clathrin-mediated endocytosis following binding to low-affinity FcγII or FcγIII receptors on neurons [400] or through other mechanisms [401]. Then, tau-specific antibodies may interact with intracellular tau and inhibit its aggregation. In fact, it has been demonstrated that a cis tau-specific antibody entered neurons through Fcγ receptors and prevent tauopathy development and spread in mice following traumatic brain injury [402]. However, some tau-specific antibodies could elicit their therapeutic effects by interacting with extracellular antigens, even without entering cells, capturing extracellular tau seeds and in that way prevent the seeding and trans-cellular propagation of tau pathology in transgenic mice [403, 404, 405].

1.2.2.3.1. Pre-clinical trials

Pre-clinical immunotherapeutic published studies have put emphasis targeting phosphosphorylated tau in residues S202, T205, S212, S214, S231, S396, S404, S422 and S424, modifications that have been found related to aggregated tau, and in PHF formation. Some of these studies, including both active and passive approaches, are summarized in Table 1.12. Outcomes from these studies have demonstrated that tau immunotherapy can not only reduce tau pathology, but also help to lead to cognitive and functional improvements in mice.

For example, previous active vaccinations targeting pS422 tau reported lower insoluble pS422 tau levels and improvements in cognitive performance in Thy-tau22 transgenic model [391]. In the case of passive immunotherapeutic approaches, after peripheral administrations of an anti-tau/pS422 antibodies in another triple transgenic mouse model, Collin *et al*. (2014) reported reductions of pathologic tau accumulation. Besides, it was observed that the antibody entered neurons, where it was supposed to exert its function at the lysosomes (Table 1.12) [396].

Table 1.12. Active and passive pre-clinical immunotherapeutic assays targeting tau pathology (adapted from ref 399).

Active immunotherapy approach	Outcome	Reference
Tau 379-408 (pS396/pS404)	Tau pathology reduced, cognitive improvements	[387]
Tau 393-408 (pS396/pS404)	Tau pathology reduced	[388]
Tau 395-406 (pS396/pS404)	Tau pathology reduced, functional improvements	[389]
Tau 195-231 (pS202/pT205), Tau 207-220 (pS212/pS214), Tau 224-238 (pS231)	Tau pathology reduced	[390]
Tau (pS422)	Tau pathology reduced	[391]
Tau 395-406 (pS396/pS404)	Tau pathology reduced	[388]
PHF-tau	Tau pathology reduced	[393]
Passive immunotherapy approach		
PHF1	Tau pathology reduced, functional improvements	[392]
PHF1 and MC1	Tau pathology reduced	[394]
DA31, MC31 and PHF1	Tau pathology reduced	[395]
MAb86 (anti-Tau/pS422)	Tau pathology reduced	[396]
Anti-tau	Tau pathology reduced, cognitive improvements	[297]
Anti-tau oligomers	Tau pathology reduced, cognitive improvements, functional improvements	[398]

1.2.2.3.2. Tau clinical trials

Many different approaches for treating tauopathies are currently being explored, but few compounds have already reached clinical development. Among them, two active immunotherapeutic compounds and four passive ones (Table 1.13).

Table 1.13. Summary of the immunotherapeutic clinical trials performed targeting tau pathology (adapted from www.alzforum.com).

Name	Synonyms	FDA Status	Company	Therapy Type
ADDvac-1	Axon peptide 108 conjugated to KLH	AD (Phase 2)	Axon Neuroscience	Immunotherapy (active)
ACI-35		AD (Phase 1)	AC Immune SA Jansen	Immunotherapy (active)
BIIB092	BMS-986168, IPN007	Progressive Supranuclear Palsy (Phase 2), AD (Phase 2)	Biogen, Bristol-Myers Squibb	Immunotherapy (passive)
C2N 8E12	ABBV-8E12	Progressive Supranuclear Palsy (Phase 1), AD (Phase 2)	AbbVie, C2N Diagnostics, LLC	Immunotherapy (passive)
RG7345	RO6926496 (Mab86)	AD (Discontinued)	Roche	Immunotherapy (passive)
RO 7105705	RG 6100	AD (Phase 2)	AC Immune SA, Genentech, Hoffmann-La Roche	Immunotherapy (passive)

1.2.2.3.2.1. Active tau immunotherapy

AADvac-1

The AADvac-1 compound consists in a vaccine composed by a synthetic peptide derived from amino acids 294 to 305 of the tau sequence (KDNIKHVPGGGS). In 2014 there were reported safety outcomes and tau pathology reduction among improvements in sensorimotor function in transgenic rats [409]. Later on, in 2015, there was confirmed that ADDvac-1 was safe, well-tolerated and that the vaccine induced increased antibody productions lead by repeated injections including stable ADAS-cog scores over six months. In March 2016, a phase I trial in mild to moderate AD patients began and will finish in 2019.

ACI-35

ACI-35 is a liposome-based vaccine containing 16 copies of a synthetic tau fragment phosphorylated at residues S396 and S404 anchored to the lipid bilayer. In both wild-type C57BL/6 and P301L mutant tau transgenic mice treatment rapidly generated high titers of polyclonal IgG antibodies specifically directed against phosphorylated tau. ACI-35 also improved increased retention of body weight, delayed onset of a clasping motor phenotype, and extended lifespan. The study also reported negative tests for gliosis, T cell activation, and several inflammatory markers [410]. Similar data in non-human primates were presented at the 2013, which lead to the first human trial, registered in May 2015 and that is ongoing at sites in Finland and the UK.

1.2.2.3.2.2. Passive tau immunotherapy

BIIB092

BIIB092 drug is a humanized IgG4 monoclonal anti-tau antibody originally developed by iPierian company. It targets extracellular, N-terminally fragmented forms of tau (eTau). The antibody

reportedly neutralized toxicity of eTau in mouse models of frontotemporal dementia and confirmed safety parameters for up to eight months after administration of BIIB092. In 2015, a multiple ascending-dose phase I trial in 48 patients with PSP reported results confirmed safety, well-toleration and a dose-dependent accumulation in serum and CSF of the antibody, among reduction of free eTau in CSF. In February 2018 Biogen started a phase 2 trial in AD patients with mild cognitive impairment which will run through 2020.

C2N 8E12

C2N 8E12 is a humanized antibody developed by C2N Diagnostics and AbbVie to treat tauopathies. It binds to aggregated, extracellular forms of pathological tau, so 8E12 mechanism of action requires no uptake into neurons. The mouse version of this antibody reportedly reduced brain neurofibrillary pathology, insoluble tau, microgliosis, brain atrophy, and deficits in the conditioned fear response in P301S tau-transgenic mice [406, 407]. In 2016 it was confirmed safely repeated dosage and, in the same year, it was launched a phase II trial for AD to compare three doses of 8E12 infused over a period of two years to placebo. The trial is intended to be running until October 2020.

RG7345

RG7345 is a humanized monoclonal antibody that targets phospho-tau pS422. In January 2015, Roche started a phase I, single-ascending-dose study treating 48 healthy young men for assessing the safety and pharmacokinetic measures of six different intravenous doses. In October 2015 Roche discontinued the antibody for treatment.

RO 7105705

RO 7105705 is an anti-tau antibody that preferably targets extracellular tau, developed by AC Immune and Genentech. The aim was to explore antibodies with reduced effector function in an effort to limit microglial activation leading to inflammatory responses [554]. RO 7105705 binds the N-terminus of all six isoforms of human tau, both monomeric and oligomeric, regardless of phosphorylation status. After a phase I trial, in 2017, Genentech reported safe single doses up to 16,800 mg. In October 2017 started a phase II study in people with prodromal or probable AD and mild symptoms that would finish in 2022.

For further information, check www.clinicaltrials.gov and www.alzforum.com.

1.2.2.4. Novel immunotherapeutic approaches

Since neurodegenerative diseases attack the CNS, the BBB implies a serious hindrance for the diagnosis and treatment of such diseases. The ability of some nanoparticles (NPs) to cross the BBB provides alternative ways for targeting and drug delivery to the CNS [457]. “Theranosis” (combination of the two greek-origin words “therapy” and “diagnosis”) was proposed few years ago as a term to describe systems that can work as imaging and therapeutic agents simultaneously. Therapy and diagnosis are two major categories in the clinical treatment of disease AD, which as previously sorted, supposes huge economic load to the most developed countries. Several types of nanoparticles are currently being tested for their potential to target AD-related pathologies and for developing more effective and efficient diagnostic and therapeutic systems.

NPs are considered as one of the most promising alternative to traditional approaches due to their multiple advantages and versatility [458]. For example, NPs can be easily loaded one or more type of imaging or therapeutic agents, making them multifunctional nanoplatforms for multipurpose approaches. As NPs can be synthetized with different sizes and functionalization ways, so they can accommodate large amounts of imaging compounds. Moreover, functionalization with molecules making specific target or modifying their physicochemical properties (size, shape, hydrophobicity, surface charge, etc.) can allow NPs to attack specifically certain types of cells or tissues. In fact, it has been observed that multifunctionalized NPs own higher target binding capability and specificity than “simple functionalized” NPs [460].

Functionalization and surface modification of NPs can also significantly reduce the opsonisation probability and improve their peripheral circulation time [461]. Several and diverse types of organic (polymers, proteins, lipids, polysaccharides, etc.) or inorganic (iron, gold, silica, etc.) NPs have been developed until date, and some of them are currently under clinical or preclinical evaluation, or even in the market, for delivery of imaging agents and/or drugs (Table 1.14) [462, 463, 481].

Table 1.14. Different types of NPs used in diagnostics and therapy (adapted from ref. 459)

Type	Advantages	Disadvantages
Organic Nanoparticles		
Polymeric NPs, micelles, biological NPs	- Good loading for lipophilic agents - Homogeneity - Biological synthesis - Biodegradable and biocompatible	- Difficult loading of hydrophilic molecules - Toxicity - Slow biodegradability - Difficult modification and handling
Solid Lipid NP (SLN), Liposomes	- Small uniform size - Easy loading of lipophilic molecules - Easy scale-up of production - FDA approved carriers - Easy surface modification	- High content of surfactants - Possible toxicity/biocompatibility problems - Problem to load hydrophilic molecules - Poor *in vivo* stability - Limited sustained release potential
Dendrimers	- High loading capacity - Controllable and uniform size and chemical composition	- Limited synthetic possibilities - Toxicity issues
Inorganic NPs		
Iron NPs	- Clinically available contrast agent for MRI - Biocompatible - Controllable size, shape and properties	- Poor aqueous stability
Gold NPs	- Optical quenching capability - Controllable size and shape - Easy surface modification - Biocompatible	- Poor aqueous stability
Quantum Dots	- Very good imaging properties - High S/N - In vivo longevity;	- Cytotoxicity - Questionable biocompatibility and clearance
Carbon-based NPs	- Structural rigidity - Mechanical properties - Good electrical properties	- Potential toxicity
Silica NPs	- Biocompatible - High loading capacity	- Mechanical stability

In most cases a prerequisite to address pathologies like AD is the crossing of the BBB, nevertheless, some research approaches have been designed to not need that BBB passing, based on the the so-called “sink effect” theory [466, 459]. However, recently some nanoparticulate systems with high affinity for Aβ peptides have been developed and tested reporting promising *in vivo* results and also demonstrating that the therapeutic efficacy of the immunoliposome-based treatment was superior to free monoclonal antibody administration (part of this thesis) [468, 469, 470].

Other approaches include the controlled disruption or “opening” of the BBB; however, the toxicity related issues can be severe. Also the use of ultrasounds for disrupting the Aβ plaques, facilitating the diffusion out of the brain and the uptake by microglia have been tested *in vivo* and reported memory recovering [467].

2. Objectives

2.1. General objective

As already presented, immunotherapy is one of the most promising therapeutic approaches for some of the most important diseases nowadays. The importance of developing new tools or approaches to address such problems is something quite interesting and attractive, both ethically and economically, meaning a US$ billion-size global market nowadays with a predicted high growing rate.

In this regard, merging the industrial and the scientific interest, we are trying to address the diagnostic and passive immunotherapeutic approach of AD developing and characterizing new antibodies against Aβ and tau protein in a hybrid academic-industrial environment.

2.2. Specific objectives

To develop two new diagnosis and therapy-directed antibodies against post-transcriptionally modified tau protein. The antibodies must specifically bind tau proteins wearing post-transcriptional modifications that have been shown to be related to AD pathology development. One of the antibodies should specifically recognize acetylated tau protein and a second one recognizing phosphorylated tau protein.

To set up a laboratory and the necessary protocols for lab-scale hybridoma culturing and antibody production and purification. The main aim of this objective is to stabilize antibody production for commercial purposes, but also for fulfilling the thesis´ research needs.

To characterize the main biochemical properties and to map the epitope of the previously developed anti-Aβ STAB-Mab, and the derived mini-antibodies (Minibody 1 and Minibody 2), for better understanding of the mechanisms of action behind such antibodies.

To test the therapeutic efficacy of the anti-Aβ STAB-Mab in APP/PS1 transgenic AD mouse model. Diverse immunotherapeutic approaches should be addressed taking advantage of the pre-existing collaborations with STAB-VIDA result of the previous grant from the NAD Project.

To test the therapeutic efficacy of the derived Minibody 2 in APP/PS1 transgenic AD mouse model. The effect of the peritoneal administration of free Minibody 2 should be investigated to unveil if its modifications actually improve its efficacy against AD development.

3. Anti-Aβ Monoclonal Antibodies Production, Characterization and *in vivo* Assays

3.1. Anti-Aβ STAB-Mab production

The STAB-Mab is a full IgG1 murine monoclonal antibody previously generated by hybridoma technology within the Nanoparticles For Therapy And Diagnosis Of Alzheimer Disease (NAD) European FP7 funded project (212043 FP7-NMP) [511]. The NAD project was intended to use NPs specifically engineered for targeting of Aβ, for the diagnosis and therapy of AD by: (i) seeking an interaction with the different pools and forms of Aβ (monomers, oligomers, plaques). The interaction with soluble extracellular Aβ could inhibit its oligomerization, thus preventing amyloidogenesis and plaque formation. The interaction with aggregates, plaques included, could achieve their disaggregation *in vitro* and reduce toxicity *in vitro*. (ii) functionalization of NPs to cross the BBB. (iii) functionalization with MRI and PET contrast agents of NPs crossing the BBB and carrying Aβ ligands. (iv) seeking an interaction with Aβ circulating in the blood. NPs could interact with Aβ in the bloodstream, withdrawing the peptide from the brain through the "sink effect".

The STAB-Mab object of part of this thesis was raised against Aβ, one of the main proteins that accumulates related to AD. The Previous published works to this thesis already confirmed sub-nanomolar affinities for this antibody and its capability for recognizing different types of aggregated species in a variety of samples and using several techniques [511]. Nanoliposomes functionalized with STAB-Mab were also shown to inhibit Aβ aggregation and reduce cytotoxicity in *in vitro* cultures [513, 539]. Moreover, two chimeric Minibodies were synthesized using the STAB-Mab Fabs and partial human FCS in order to try to reduce its molecular weight, reduce immunogenic reaction in humans and increase the BBB transport trough FcRn receptor (FCGRT).

From such point, we focused on continuing with the works previously performed within the NAD project. We characterized the STAB-Mab using a number of techniques, from ELISA to TEM and mapped its epitope by MALDI and NMR. We further compared the performance of the chimeric Minibodies with the STAB-Mab by ELISA and Western Blot (WB). In addition, two *in vivo* studies were completed in 2016 [468] (part of this thesis) and 2017 [470] confirming the capability of different STAB-Mab-functionalized liposomes and nanoparticles to reverse biochemical effects and restore the deleterious effect of AD in mice memory.

3.1.1. Sub cloning and selection of best clones

Initially, the hybridoma was cultured in monolayers in standard vented and non-treated flasks using DMEM media. Purification was performed by protein precipitation and posterior G-protein affinity chromatography, manually operated. In order to improve antibody production yields and hybridoma growth in our new media and conditions, we decided to subclone the original hybridoma clone, named 9E8 1A3 1H8. Traditional limiting dilution method was used for isolating and test individual clones of the original cell line. After two subclonings, a first one where we did not obtain any good producing clone, we isolated a clone (9E8 1A3 1H8 2F9) with slightly better performance.

The media was also reformulated to increase the production yield, optimise the operation time, increase supernatant volumes and to accommodate to automated purification by protein G chromatography with GE HiTrap Protein G 1 mL columns operated by an AKTA Prime system. The use of Glutamax DMEM from Gibco was decided to reduce risks on glutamine degradation when culturing cells in bioreactors where medium is changed only once a week or so. The addition of 2-mercaptoethanol was intended to reduce the oxidation risk of the antibodies produced and secreted to medium (Table 6.1).

Binding buffers for protein G chromatography were also slightly modified from manufacturer´s instructions. The lower pH of the elution buffer (2.7 to 2.5) helped to recover more protein from the column, because we detected important losses in such step. Binding and elution buffers were freshly prepared and filtered through 0.45 µm filters each purification, and so the equilibration buffer pH was optimized each day for neutralizing the lower pH of the eluted fractions and keep it around physiological levels.

3.1.2.In-lab production tests

As previously indicated, due to poor antibody production yields, the old hybridoma was subcloned and tested for better antibody production. Results represented below confirmed small but noticeable yields in the 4 producing platforms used, traditional Corning T150 flasks, Corning Hyperflask, Wheaton CELLine Biorreactor and Sarstedt Miniperm Biorreactor, although none of the clones performed well in terms of antibody production when growing in high density suspension cultures (Figure 3.1).

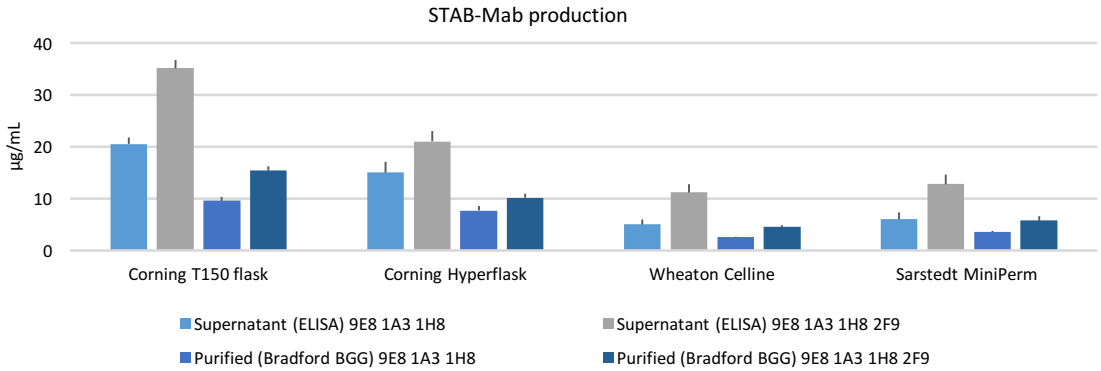

Figure 3.1. STAB-MAb production in µg/mL. It is represented the concentration of antibody in the crude supernatant and the final purified antibody respect to the total volume of fresh supernatant. It was observed that the new subclone (9E8 1A3 1H8 2F9) produce about double amount of Mab than the old clone (9E8 1A3 1H8) when using almost any of the producing platforms.

Monoclonal antibodies stability is something important to be assessed due to its common analytical use can be extended for months or even years. Also the production of large batches sometimes is technically difficult and implies the storage of the antibodies for medium-large term. The generally recommended storage temperature is -20ºC, but if the storage time will be long, maybe -80ºC would be a more secure location. On the other hand, if the antibody is repeatedly used, thaw-freeze cycles must be avoided due to the known negative effect in the stability and aggregation of most proteins, so the most adequate option is to store the antibody aliquots at 4ºC.

For this reason, we believed important to assess the STAB-Mab stability under these three temperatures during 6 months checking the hypothetical monthly variations in the ELISA´s intensity signal of each batch each month, using synthetic Aβ(1-42) peptide. The conditions of the ELISA are the standard ones described in Material and Methods section, using a concentration of 0.05 µg/mL for both STAB-Mab and the synthetic Aβ(1-42) peptide for the plate coating (Figure 3.2).

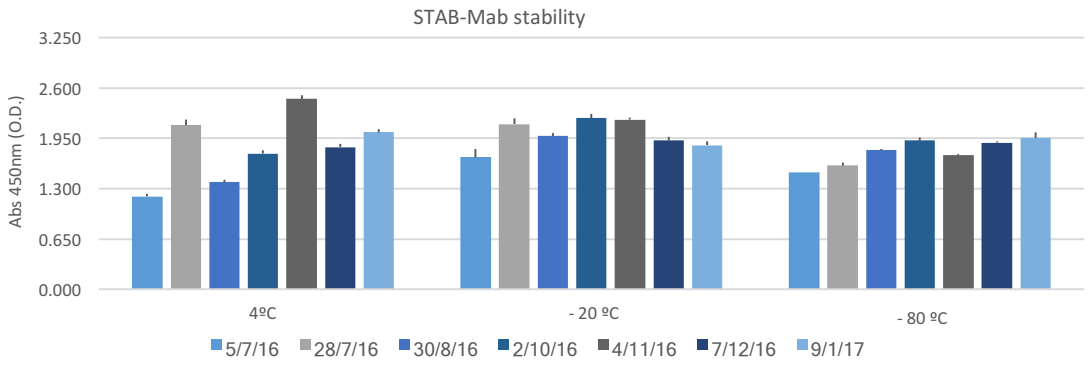

Figure 3.2. Bars graphic representing the ELISA results of the monthly assay for testing the functionality of the antibody. Concentrations for the synthetic Aβ(1-42) peptide coating and STAB-Mab: 0.05 µg/mL.

The cell culture doubling time is defined as the time it takes a population to double the number of cells. Although cells can grow at different rates at each of the different phases of the growth cycle,

the calculation of doubling time may integrate data of growth during more than one of these phases. Moreover, it is also known that growth during exponential log phase is fairly constant, so it can be taken as a reference. The calculation for our new clone was one of the aspects we wanted to check, so the new clone was tested in the different flasks and bioreactors and the cell doubling time was calculated.

It was observed that cell doubling times were reduced for the new subclone in comparison with the clone of origin when growing in almost all the culturing platforms but, as expected, the differences were not dramatic and the way we handled the cells was not affected (Figure 3.3).

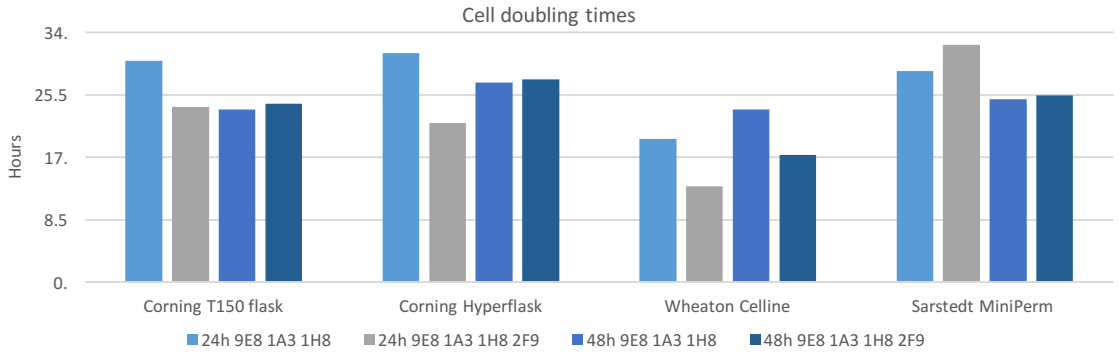

Figure 3.3. Cell doubling times: for the starting clone (9E8 1A3 1H8) and for the new subclone (9E8 1A3 1H8 2F9), considering time points 24 and 48 hours after starting cultures for four culture platforms: Corning T150 flasks, Corning Hyperflask solution, Wheaton CELLine bioreactor and Sarstedt Miniperm bioreactor. The new subclone showed slightly lower doubling times for almost all the platforms tested.

3.2. Characterization of anti-Aβ antibodies

3.2.1. Anti-Aβ STAB-Mab characterization

3.2.1.1. Western Blot

WB analysis showed that STAB-Mab and 6E10 (a gold-standard murine antibody that binds the N-terminal region of the Aβ peptide) can detect Aβ in monomeric as well as in oligomeric forms. Indeed, both antibodies exhibited similar band profiles for human Aβ monomers and oligomers. Moreover, we tested the ability of anti-Aβ antibody and 6E10 to detect APP as well as Aβ monomers and oligomers on mouse brain extract (Figure 3.4).

None of the antibodies recognized any peptides sufficiently well from the brain of WT mice, whereas from transgenic mouse brain extracts both antibodies showed similar bands pattern. However, the signal strength was higher in older mice (16 months-old) and when using anti-Aβ antibody (Figure 3.4).

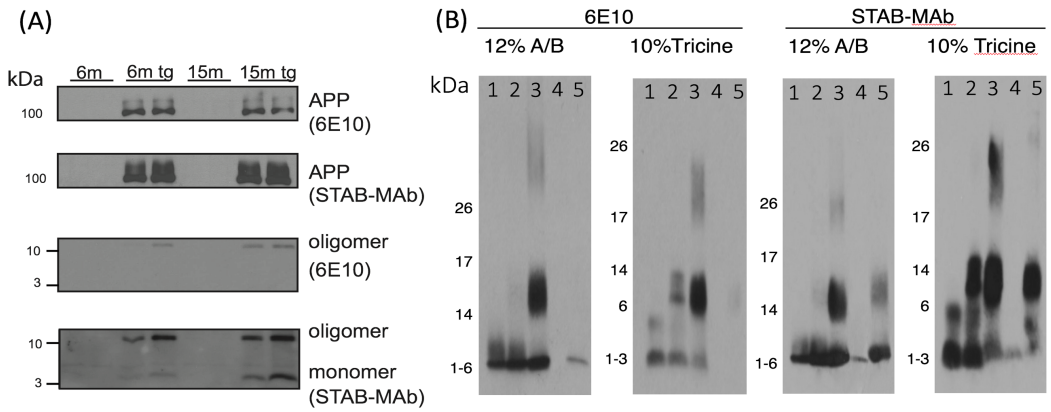

Figure 3.4. WB analysis confirmed that both STAB-Mab and 6E10 antibodies interact with human Aβ monomer and oligomers. (A) However, STAB-Mab antibody further showed affinity towards mouse Aβ(1-42) monomer and oligomers, and to a lesser extent for Aβ(1-40) monomer. In addition, STAB-Mab antibody further detected a ~100 kDa Mw band protein in brain extracts of transgenic mice (6 and 15 month-old) which presumably correspond to full-length APP. WB of

antibody reactivity with brain extracts from 6 to 15 month-old transgenic (TG) APP/PS1 and wild-type (WT) mice. (B) WB of STAB-Mab antibody and 6E10 binding to human and mouse Aβ synthetic peptides confirmed that, meanwhile STAB-Mab is capable to bind both human and rodent sequences, specially in the case of Aβ(1-42), 6E10 is more specific for the human peptide. We also confirmed that both antibodies can bind different sizes of oligomeric species. A/B: acrylamide/bisacrylamide gel; Lanes: 1: human Aβ(1-40); 2: human Aβ(1-42); 3: human Aβ(1-43); 4: mouse Aβ(1-40); 5: mouse Aβ(1-42).

For confirming if the anti-Aβ STAB-Mab antibody was specific for Aβ or, on the other hand, and due to its flexibility for recognizing different Aβ lengths and species, was also capable of binding APP. In this regard, STAB-Mab antibody was compared with 4G8 and Y188 in a WB of two lysates of N2A cell cultures, one WT (endogenous APP) and another transfected with a plasmid encoding an APP human allele (overexpressed APP). 4G8 is a gold standard antibody commonly used in post mortem diagnosis of AD that targets the C-terminal region of Aβ, meanwhile Y188 is one of the most used antibodies for specifically targeting APP.

N2A (Neuro-2a, ATCC® CCL-131™) is a murine cell line used for studying the mechanisms of vinblastine precipitation of microtubular protein, the kinetics of GTP binding to isolated protein, turnover of microtubules *in vivo*, or microtubular protein synthesis and assembly. Here, we transfected the cell line for overexpressing human APP gene. As expected, STAB-Mab antibody recognized APP mainly in the overexpressed APP lane, while the signal from 4G8 was much weaker and Y188 exhibited the highest sensitivity and cleaner bands than the other two (Figure 3.5).

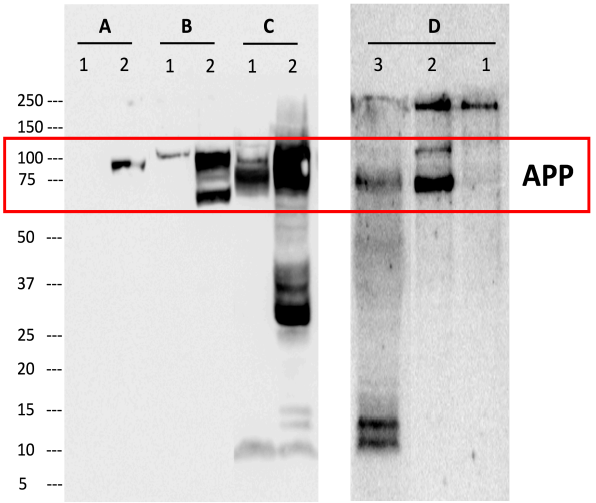

Figure 3.5. WB comparing STAB-Mab with other commercial antibodies: (A) 4G8, (B, D) STAB-Mab and (C) Y188. Samples from two N2A cell cultures and from mouse brain lysates were separated by SDS-PAGE and analyzed by WB. Lane 1 contains N2A lysate with endogenous APP; lane 2, N2A lysate over-expressing APP; and lane 3, 3-months old APP/PS1 mouse brain lysate. STAB-Mab seems to recognize both endogenous N2A APP and overexpressed APP, but in a lesser extent than the APP-specific Y188. 4G8 antibody delivered poor performance in this case due to its specificity for Aβ(1-42).

3.2.1.2. Immunostainings

Several immunostainings in different tissues and preparations were performed in order to prove the functionality of the STAB-Mab antibody and moreover, to compare with other recognized gold-standard antibodies used in research and diagnostic.

In collaboration with Wandosell´s Group at CBMSO (Madrid), we managed to test the performance of the STAB-Mab as marker for different cerebral Aβ depositions in APP/PS1 and WT mice. Immunostainings of 11 months-old APP/PS1 mouse comparing anti-Aβ antibody with several antibodies were performed. As expected, STAB-Mab antibody showed similar staining pattern than 6E10 and the polyclonal anti-Aβ from Cell Signaling #2454, revealing both dense and diffuse plaques along the hippocampus and somatosensory cortex. As expected again, in the WT mouse brain, neither anti-Aβ antibody nor 6E10 showed any staining due to the low amyloid accumulation in this genotype. The other antibodies tested targeting APP (Sigma A8717 and Millipore MAB348) did not reported any detectable signal (Figure 3.6).

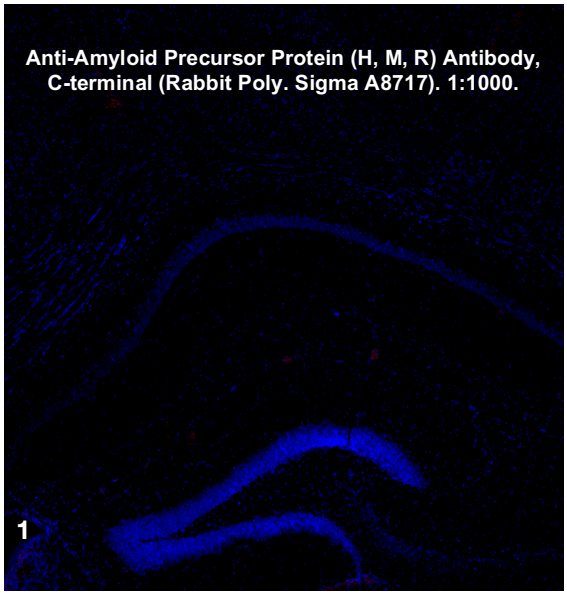
Anti-Amyloid Precursor Protein (H, M, R) Antibody, C-terminal (Rabbit Poly. Sigma A8717). 1:1000.
1

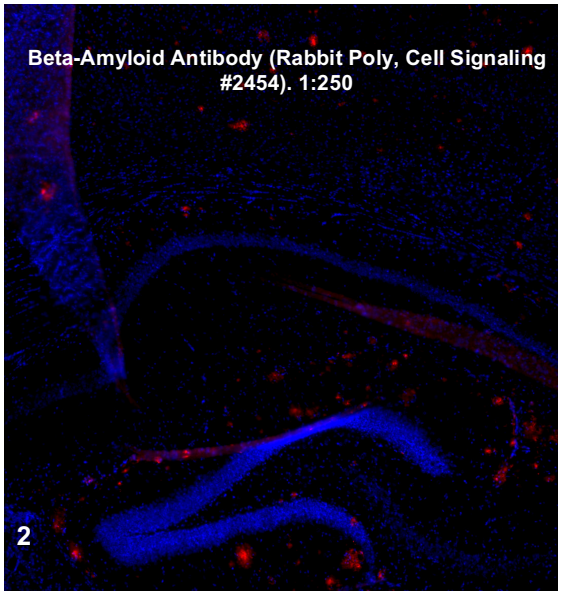
Beta-Amyloid Antibody (Rabbit Poly, Cell Signaling #2454). 1:250
2

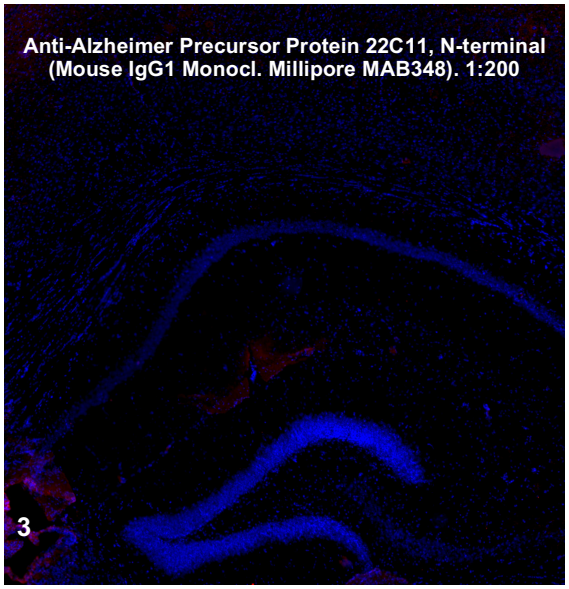
Anti-Alzheimer Precursor Protein 22C11, N-terminal (Mouse IgG1 Monocl. Millipore MAB348). 1:200
3


6E10, Human Beta amyloid (Mouse IgG1 Monocl. Covance SIG-39320). 1:1000
4

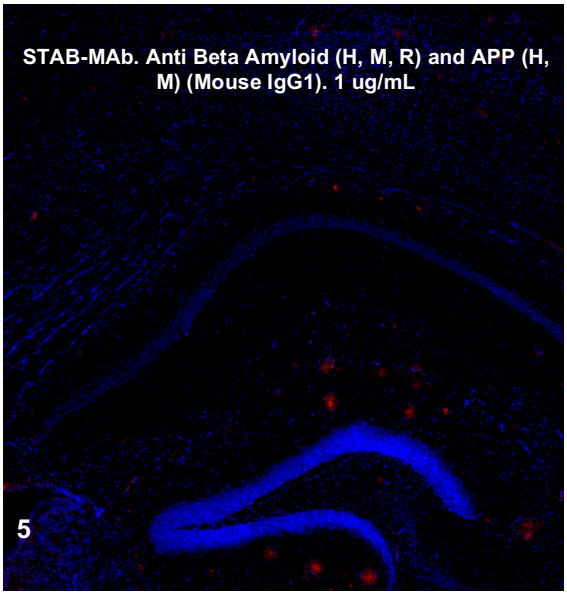
STAB-MAb. Anti Beta Amyloid (H, M, R) and APP (H, M) (Mouse IgG1). 1 ug/mL
5

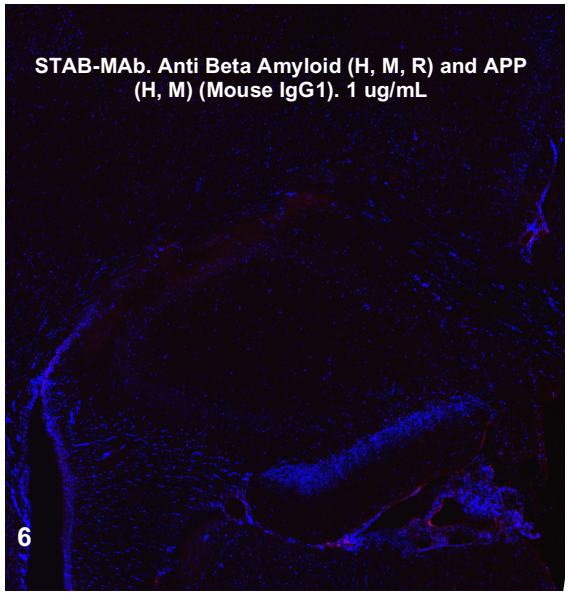
STAB-MAb. Anti Beta Amyloid (H, M, R) and APP (H, M) (Mouse IgG1). 1 ug/mL
6

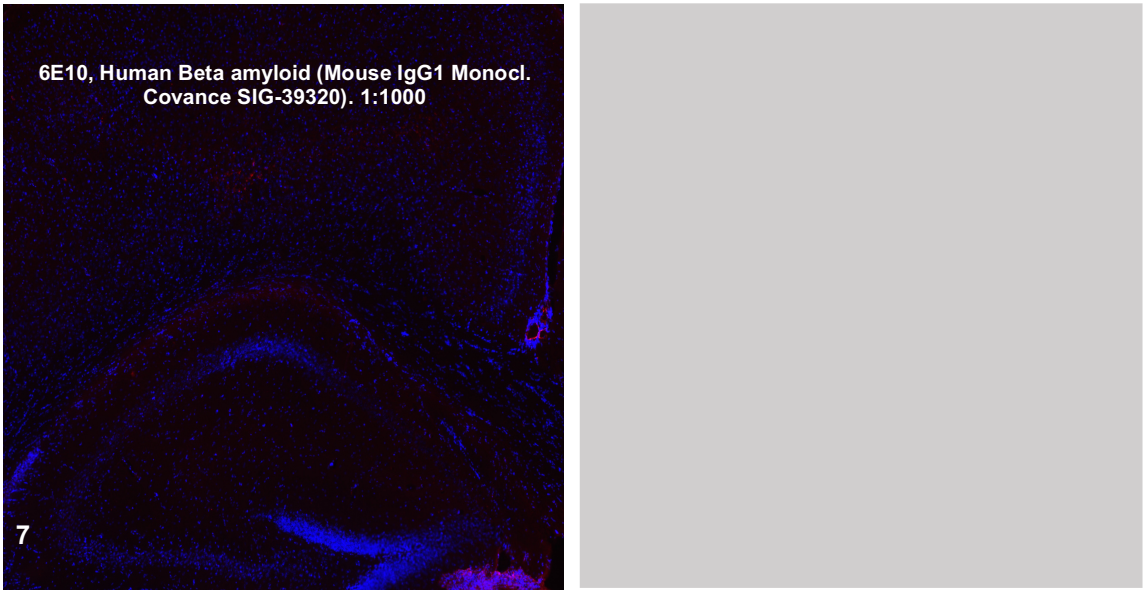

Figure 3.6. Staining of cryoslices of 11 months-old APP/PS1 mouse hippocampus. Blue color corresponds with nuclear DAPI staining while red color determines senile (amyloid) plaques. Dilutions used for each antibody were the recommended by the manufacturer and are indicated in each image. Polyclonal anti-mouse IgG ab conjugated with Alexa 594 was used as secondary antibody

In collaboration with Herms´ group at DZNE (Munich) we had access to several PFA-fixed brain samples from WT, APP KO and APP/PS1 mice lines and formalin-fixed human AD brains. Moreover, we had access to several microscopy techniques such as fluorescence and confocal microscopy. STAB-Mab was compared with 4G8, one of the gold-standards used for AD diagnostic due to its high sensitivity or versatility labelling both diffuse and dense human and mouse Aβ deposits. We also compared STAB-Mab with other standard, the antibody anti-APP Y188, highly specific for APP.

Confocal microscopy imaging confirmed that both STAB-Mab and 4G8 antibodies showed similar plaque staining in PFA/paraffin-fixed slices of APP/PS1 mice somatosensory cortex, while in WT and APP KO mice slices none of them gave any signal, as expected. On the other hand, the Y188 antibody labelled some neuronal bodies containing APP, clearly visible in the APP/PS1 mice, but also slightly visible in the sample from WT mice. Importantly, in APP KO samples, no signal was detected (Figure 3.7).

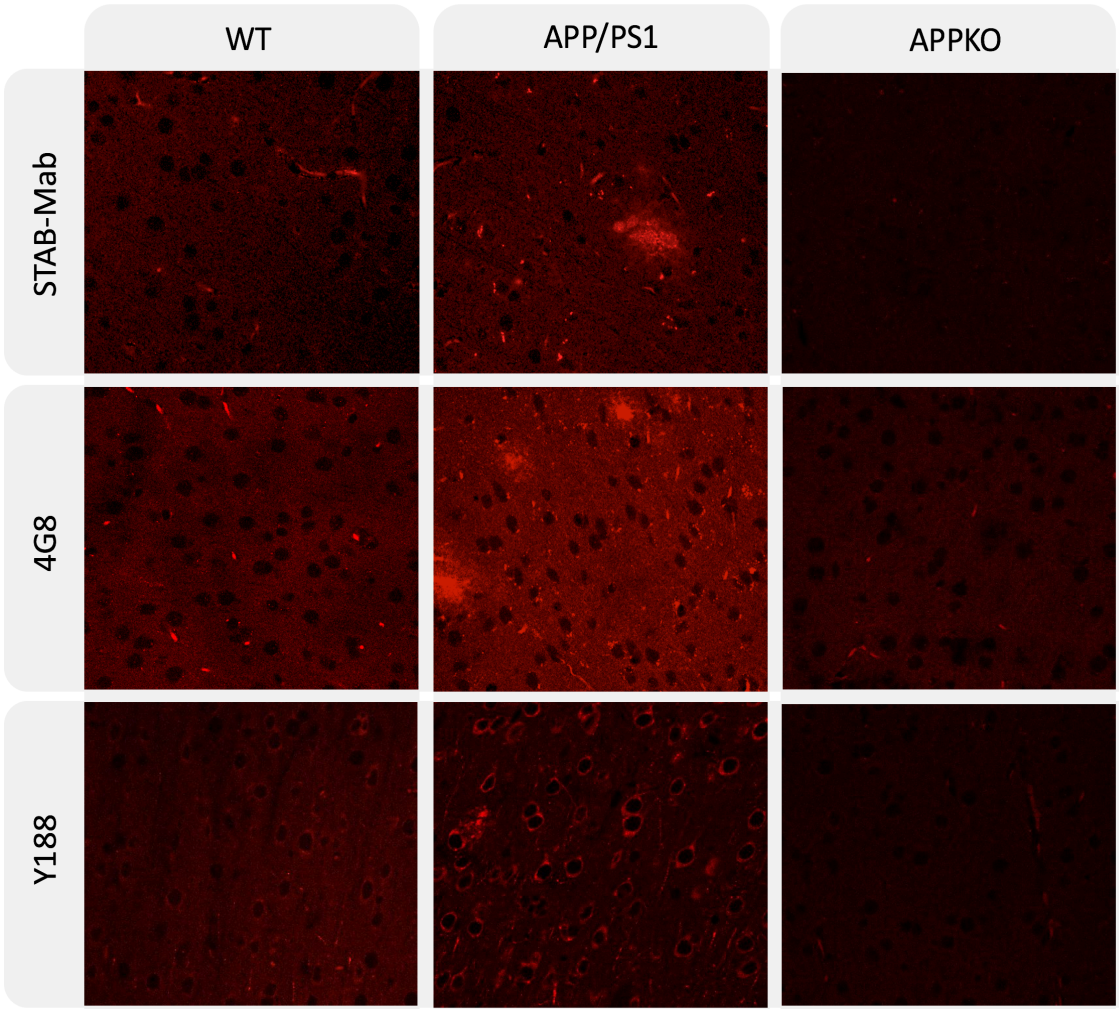

Figure 3.7. Confocal images of PFA-fixed WT, APP KO and APP/PS1 mice slices labelled with STAB-Mab, Y188 and 4G8 antibodies. All antibodies were used at the same concentration (1µg/mL). Polyclonal anti-mouse IgG ab conjugated with Alexa 594 was used as secondary antibody.

In addition to the confocal images taken to mice and human samples, we had de opportunity to use a fluorescence microscope with Apotome module, which allowed us to visualize some entire mouse brain slices. The overall pattern of deposited Aβ plaques obtained with STAB-Mab not only was as clear as with the gold-standard 4G8 at the same concentrations and conditions, but the number of deposits visualized was higher, helping to allocate easier the areas with different Aβ plaque load. The principal areas with higher density of plaques were in both cases, as expected, the hippocampus and different layers of the somatosensory cortex (Figure 3.8).

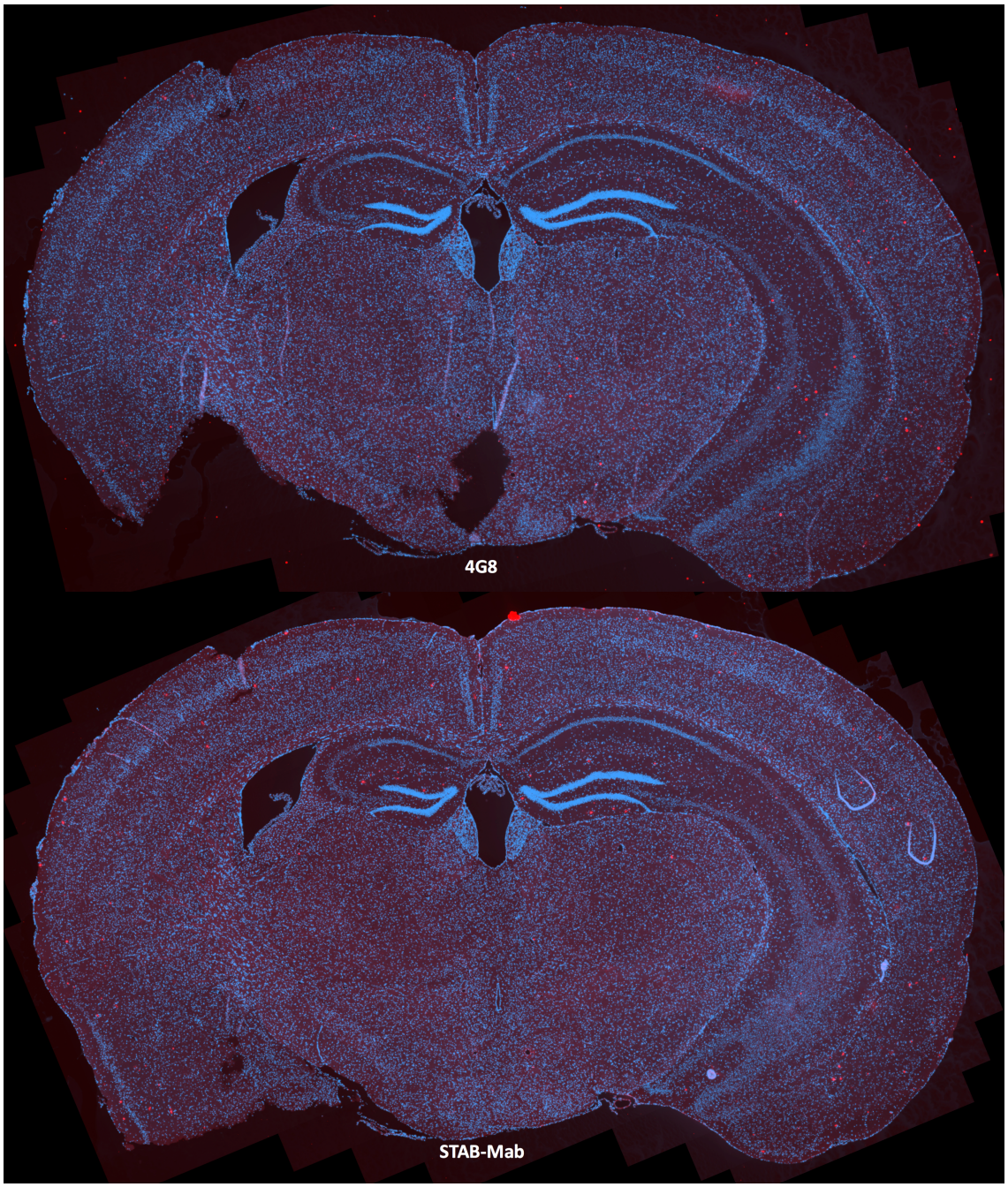

Figure 3.8. 4G8 and STAB-Mab stainings of entire slices of paraffin fixed mouse brains. In red, amyloid deposits labelled by the antibodies. In blue, DAPI-stained cell nuclei. Both antibodies, as previously showed, labelled insoluble amyloid deposits (plaques), which were mainly located in the hippocampus and somatosensory cortex, as expected in this mouse genotype.

Another type of samples we had access in Munich were human paraffin-fixed AD patient´s brains. As with mice samples, several cortical brain slices were stained with DAPI and two antibodies, 4G8 and STAB-Mab. 4G8 is one of the gold-standard antibodies used for post-mortem diagnosis of AD patients by examining amyloid brain deposits. The objective was to confirm the performance of STAB-Mab in entirely human samples and, as expected, both antibodies performed similarly, staining both diffuse and dense amyloid plaques (Figure 3.9).

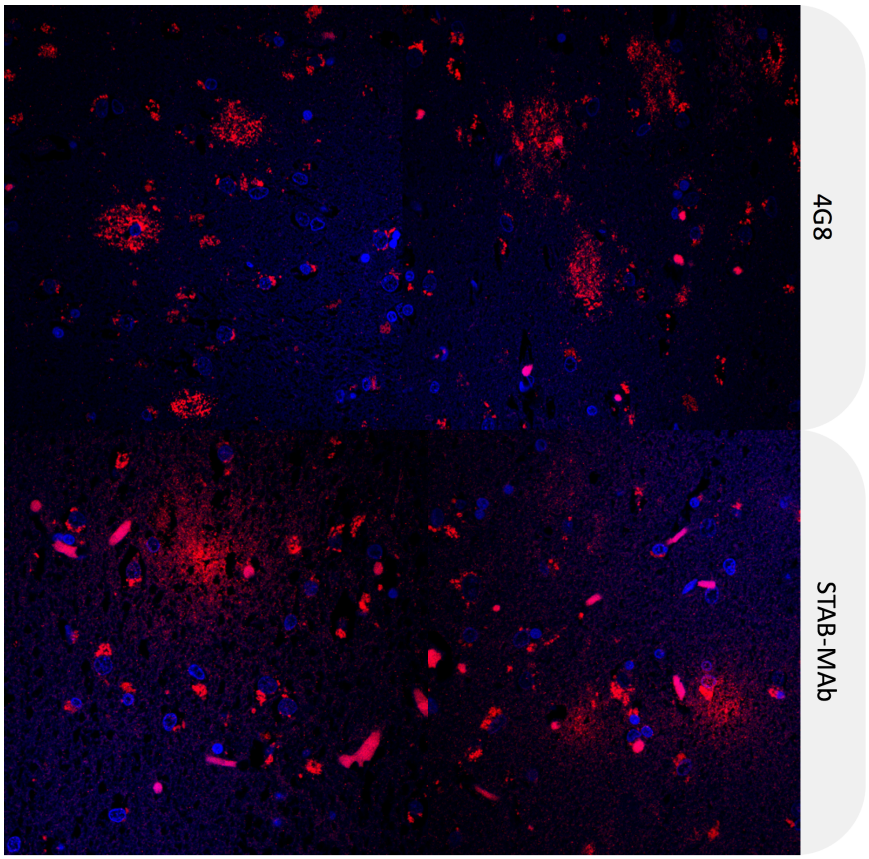

Figure 3.9. Cortical paraffin-fixed brain slices from AD patients stained with both 4G8 and STAB-Mab antibodies. It can be observed several Aβ plaques with different density. In red, Aβ deposits. In blue, DAPI stained cell nuclei.

3.2.1.3. Thioflavin T-monitored aggregation kinetics

The assays consisted in monitoring by ThT the aggregation of a supposedly monomeric solution of Aβ(1-42) through 120 minutes in conditions that should facilitate the aggregation, 37ºC and agitation (25" before each measurement), and compare the controls with the presence of inhibitors and the antibody. Those inhibitors used were phenol red and morin.

In the first assay, Aβ(1-42) was resuspended in cold buffer at 4ºC and plated immediately before fluorescence reading. We used the same concentrations recommended by manufacturer´s kit, 46 μM for Aβ(1-42) and 100 μM for the aggregation inhibitor compounds morin and phenol red, while for our antibody, due to technical limitations, the molar concentration was 11.2 μM. Results showed a significant reduction in Aβ(1-42) aggregation lead by the presence of phenol red, a slightly aggregation inhibition in the case of morin, but there was no significant reduction observed in the reaction wells with our antibody (Figure 3.10A).

In a second assay, a new Aβ(1-42) aliquot was resuspended in cold buffer at 4ºC and plated immediately before fluorescence reading. In this case, we used with lower concentration of Aβ(1-42) (30 μM), the same kit concentration for phenol red (100μM) and higher concentration of our antibody (30 μM), for achieving a 1:1 molar ratio STAB-Mab: Aβ(1-42), results variated remarkably. ThT fluorescence curves indicated a complete and immediate inhibition of Aβ(1-42) aggregation both in the presence of phenol red and STAB-MAb, being more intense in the last case, in which fluorescence decreased from the t=0 about 2000 RFU until t=60 (Figure 3.10 B).

In a third assay, a new Aβ(1-42) aliquot was resuspended in cold buffer at 4ºC and after that, incubated for 24 hours at 37ºC for aggregation. Then, there was carried out a similar test to the previous one, but comparing only the absence with the presence of our antibody in solution in a 1:1 molar ratio with the Aβ(1-42) peptide and avoiding the phenol red due to assay limitations. The in this case, ThT fluorescence remarkable decreased from a maximum value at t=0 to around a 30% of the initial value at t=120. Both control and antibody´s curves shaped similar, with no further influence of the presence of the antibody further than slightly lower fluorescence values in such case (Figure 3.10 C).

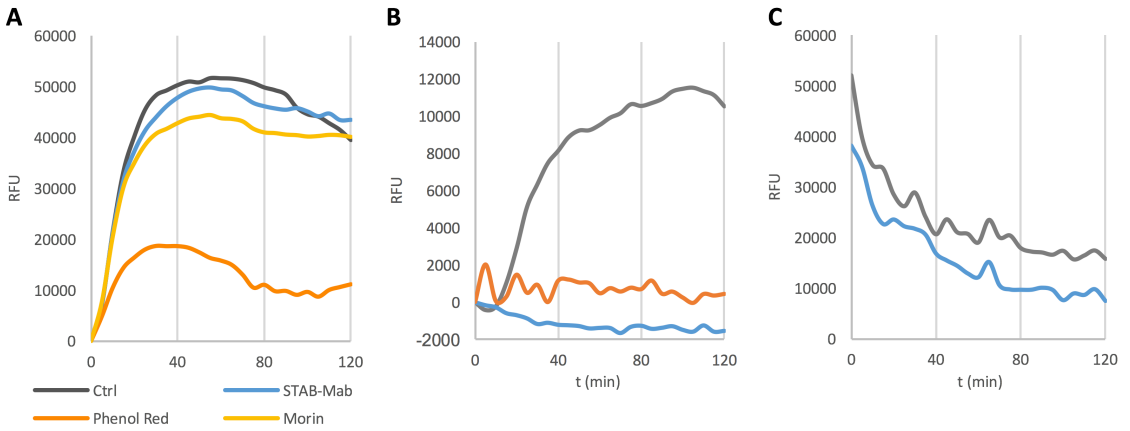

Figure 3.10. ThT fluorescence emission 2-hour curves in the presence of Aβ(1-42). (A) RFU curves representing a 46 μM Aβ(1-42) solution aggregation alone and in the presence of phenol red, morin and STAB-Mab. (B) RFU curves representing a 30 μM Aβ(1-42) solution aggregation alone and in the presence of Phenol Red and STAB-Mab at equal molar ratio. (C) RFU curves of a solution of pre-aggregated Aβ(1-42) at 30 μM concentration alone and in presence of STAB-Mab. Data represented is the result of the average of duplicated experiments. RFU: Relative Fluoresce Units.

3.2.1.4. TEM analysis of Aβ aggregation

EM experiments seem to confirm STAB-Mab ability to inhibit, *in vitro*, the formation of amyloid organized aggregates and to disrupt preformed fibrils. As exemplified in Figure 3.11, it was not possible to find any organized Aβ(1-42) aggregate when STAB-Mab was present during or added after the incubation of Aβ(1-42) solutions. However, when the antibody was not present, the Aβ was able to aggregate in organized structures like fibrils (Figure 3.11 B)

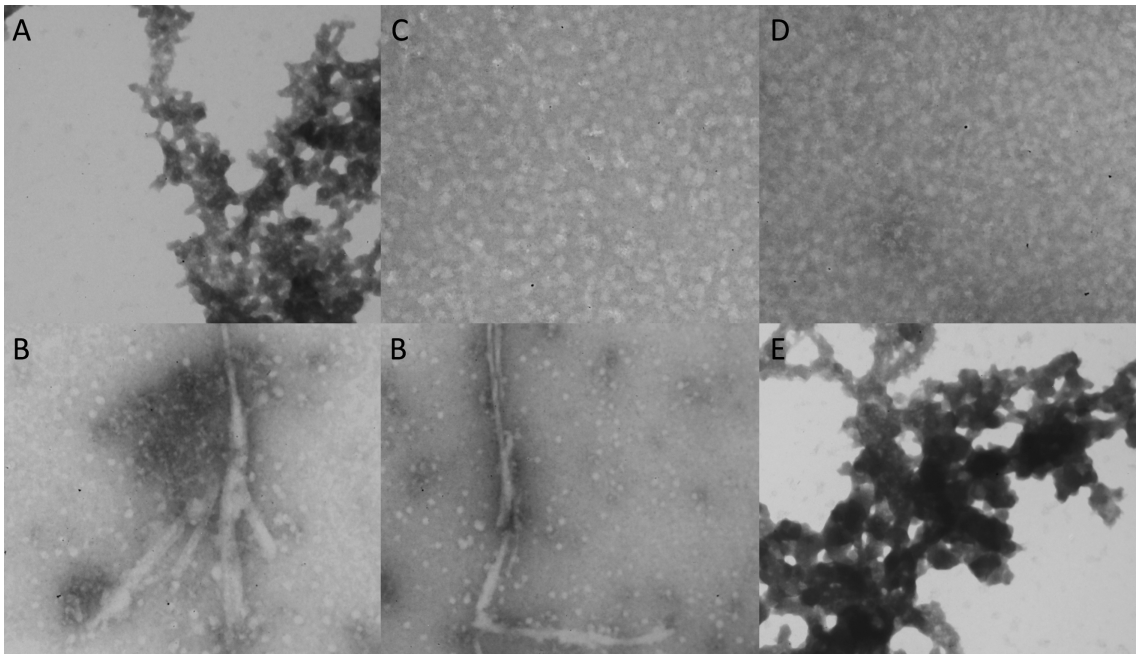

Figure 3.11. EM analysis of the effect of STAB-Mab in the formation and disaggregate Aβ(1-42) assemblies *in vitro*. (A) Electron micrograph of a 50 μM Aβ(1-42) freshly-resuspended sample in PBS 10 mM. (B) Fibrillary assemblies in a 50 μM Aβ(1-42) solution after 4 day-incubation at 37°C. (C) Electron micrograph of 50 μM Aβ(1-42) after 4 day-incubation with 25 μM STAB-Mab at 37°C. (D) Electron micrograph of 50 μM Aβ(1-42) after 4 day-incubation with 50 μM STAB-Mab at 37°C (E) Electron micrograph of 25 μM Aβ(1-42) after 4 day-incubation before a 24-h short incubation with 25 μM STAB-Mab at 37°C.

3.2.1.5. STAB-Mab epitope mapping

3.2.1.5.1. ELISAs

In order to determine the STAB-Mab affinity for the different Aβ peptides, compare with other popular commercial antibodies and determine the antibodies´ preferred region within the Aβ peptide sequence, we performed several ELISAs

We first assessed the binding affinity of STAB-MAb for Aβ peptides and subsequently, we tried to locate the epitope sequence [511, 539]. Accordingly, we used three different synthetic human and rat/mouse Aβ peptides (Aβ(1-40), Aβ(1-42) and Aβ(1-43)) as well as different peptide fragments from the human sequence of Aβ(1-42). We further performed a comparison study between STAB-Mab, 4G8 and 6E10 antibodies, some well-known commercially available anti-Aβ monoclonal antibodies.

The ELISA results with complete Aβ peptides showed higher affinity of STAB-Mab for all tested human and rat/mouse Aβ peptides compared with 6E10 and 4G8 antibodies (Figure 3.12A). 6E10, as expected, made evident its specificity for human sequences, exhibiting a good performance for all Aβ(1-40), Aβ(1-42) and Aβ(1-43) human-sequence peptides. On the other hand, 4G8 antibody, as a strongly C-terminal-directed antibody only was capable to react against peptides (both human and rat/mouse) incorporating the two-three last residues.

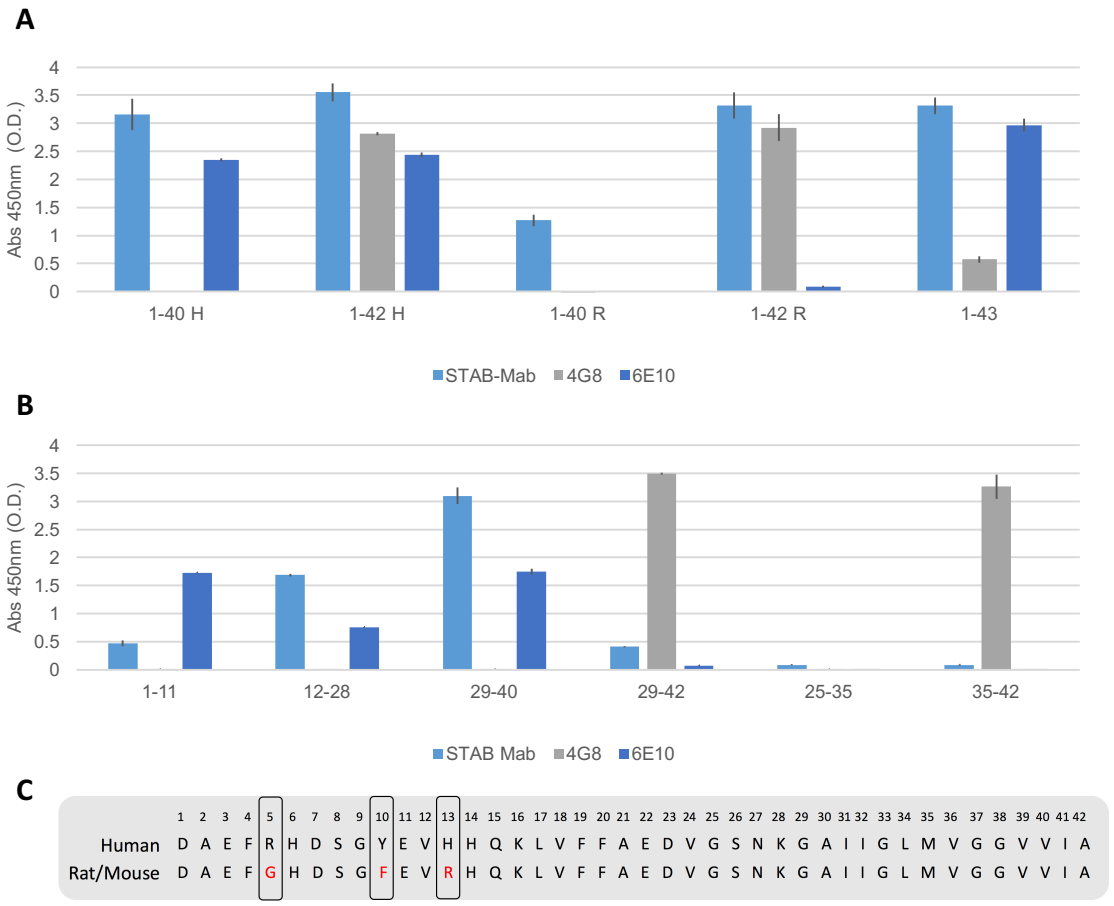

Figure 3.12. ELISA results on Aβ recognition by STAB-Mab, 4G8 and 6E10 MAb. (A) ELISA determination of antibody binding to human and rat/mouse Aβ peptides (Aβ(1-40), Aβ(1-42) and Aβ(1-43)). Antibody concentration = 0.0625 μg/mL; peptide concentration = 0.25 μg/mL. (B) ELISA determination of antibody binding to Aβ peptide fragments Aβ(1-11), Aβ(12-28), Aβ(29-40), Aβ(29-42), Aβ(35-42) and Aβ(25-35). Antibodies concentration = 0.25 μg/mL; Aβ fragment concentration = 50 μg/mL. (C) Aligned Aβ sequences from human and rat/mouse. Differential residues are: Arg5-to-Gln, Tyr10-to-Phe and His13-to-Arg.

When locating the epitope of these antibodies, we found that the STAB-Mab strongly recognized linear sequences Aβ(29-40) and Aβ(12-28) (Figure 3.12B), but also exhibiting weaker affinity for sequences Aβ(1-11) and Aβ(29-42). The preferred binding region for 6E10, as expected for an antibody directed towards the N-terminal region, was spread out the Aβ N-terminal region (fragment Aβ(1-11)), but surprisingly also showing some affinity for the Aβ(29-40) and Aβ(12-28) fragments. With no surprises, 4G8-interacting residues were exclusively the ones wearing the two last residues: Aβ(29-42) and Aβ(35-42) (Figure. 3.12B).

3.2.1.5.2. MALDI-TOF spectrometry

For completing the epitope mapping data extracted from the previous ELISA results, we decided to use proteolytic extraction and MALDI-TOF spectrometry techniques. The experimental approach consisted in the functionalization of some structure with the STAB-Mab to allow us to put it in contact with the Aβ peptides and fragments and recover it afterwards, permitting us to isolate the interacting and not interacting molecules [384, 385, 540]. See Material and Methods section for a better explanation and a scheme of the experiment performed.

The first choice for antibody functionalization was to synthetize custom magnetic nanoparticles covered by a silica shell for allowing the easy antibody conjugation (Si@MNPs). Two batches of Si@MNPs were synthesized and characterized in collaboration with BIOSCOPE Group.

The first batch was composed by regular rounded multi-core Si@MNPs, with a thick silica shell and certain tendency for aggregation with a diameter of 75 nm (Figure 3.13). For the second batch produced, we increased the time to let the magnetic cores growth more and shorted the silica shell synthesis protocol steps for achieving biggest magnetic cores and single-core particles with a thinnest silica shell (Figure 3.13B).

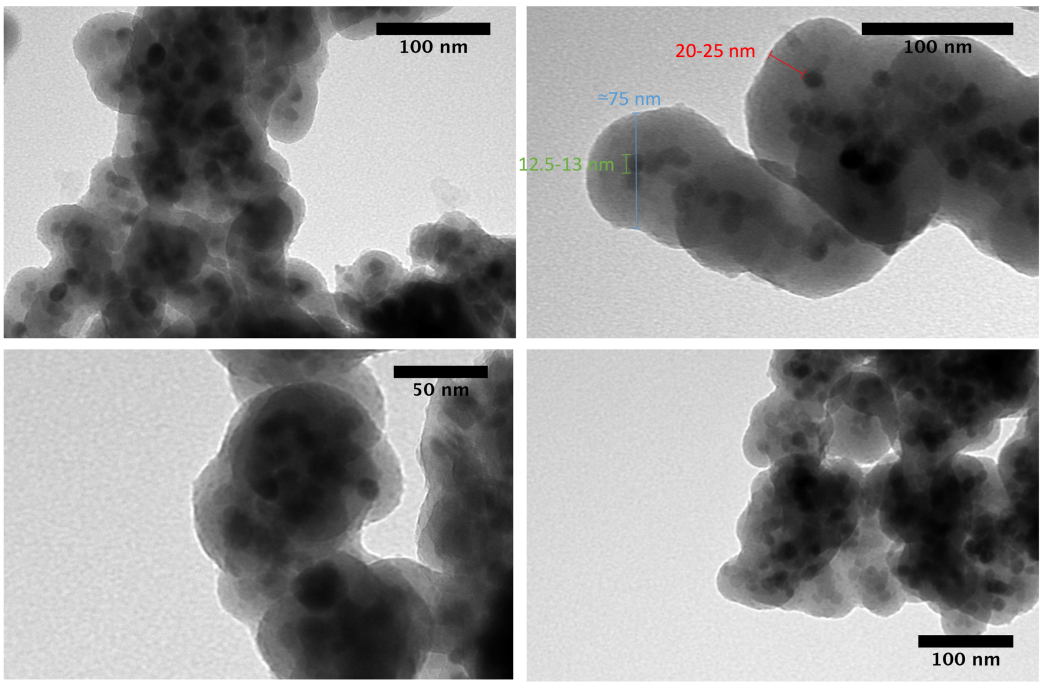

	Batch 1	Batch 2
Form	Rounded	Rounded
Size	75 nm	75 nm
Number of cores	2-4	1
Size of nuclei	12.5-13 nm	20-25 nm
Thickness of the Si shell	20-25 nm	10-15 nm

Figure 3.13. TEM imaging of the MNPs synthesized for the MALDI-TOF epitope mapping of STAB-Mab. (A)TEM images of the Batch 1 of Si@MNPs. Rounded particles, about 75 nm diameter, composed by several rounded magnetic cores (12.5-13 nm each) in the center surrounded a 20-25 nm silica shell. (B) General characteristics of both batches 1 and 2 of synthetized Si@MNPs. Images kindly taken by Dr. Javier Lodeiro (BIOSCOPE Group).

Then, the second batch of Si@MNPs of 75 nm with single magnetic cores and a 10-15 nm silica shell was functionalized and used in the experiment. The STAB-Mab was conjugated at a molar ratio of 1:10 so as to maximize the number of antibody molecules associated with each MNP. As previously reported, a 100 nm particle has the capacity to bind around 103 protein molecules with an average diameter of 6 nm; thus, each MNP would have a sufficient amount of SATB-Mab to bind Aβ peptides at this ratio. Successful conjugation of the antibody with the Si-MNPs was confirmed by Nanodrop (Figure 3.14).

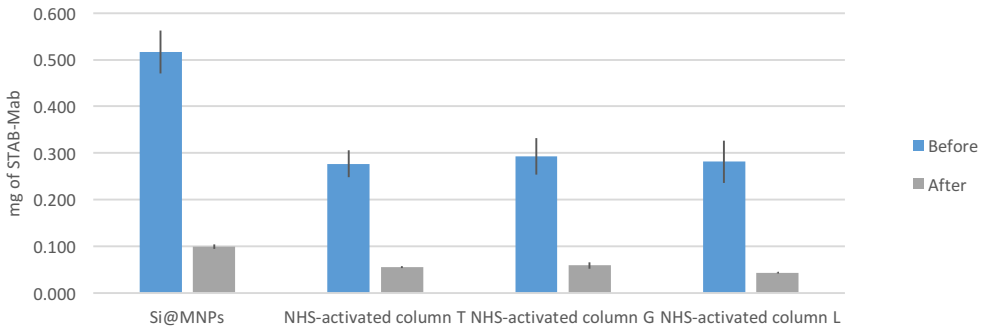

Figure 3.14. Si@MNPs and NHS-activated columns functionalization rate (in mg) before and after functionalization with each platform).

The capacity of the STAB-Mab-MNPs for binding Aβ was also confirmed by ELISA as shown in Figure 3.15. Although we detected certain rate of possible unspecific adsorption of Aβ, relying in the MALDI-TOF technique sensibility, we moved ahead with the Aβ digestions, incubations and spectrometric analysis.

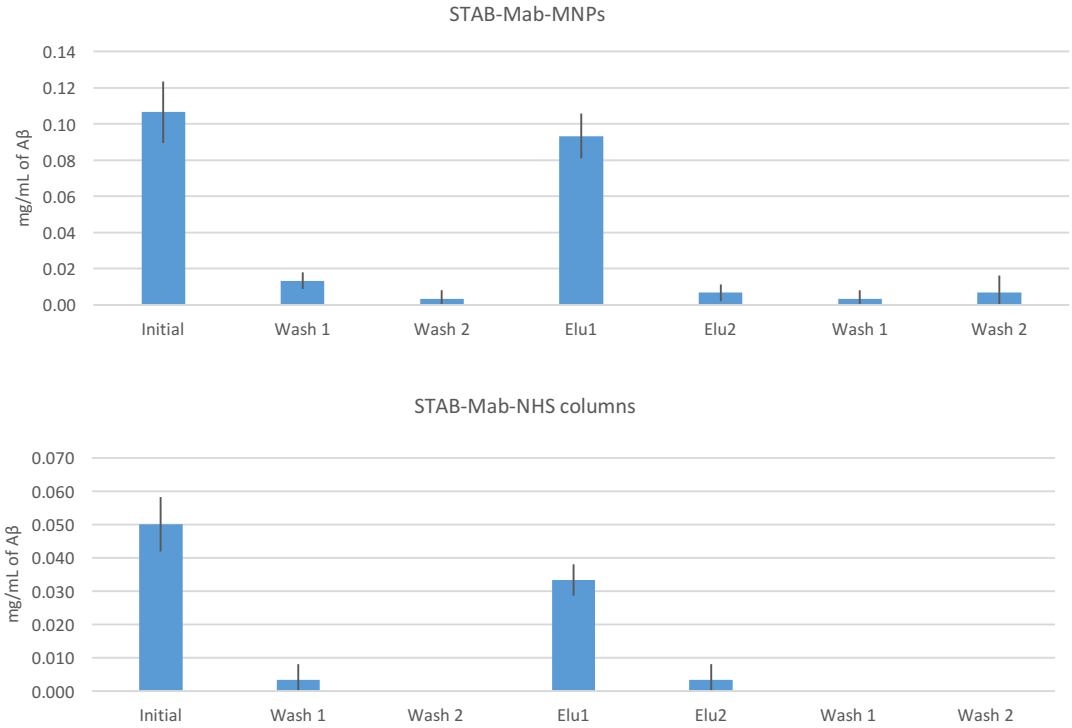

Figure 3.15. Confirmation of functionalized SATB-Mab-MNPs and STAB-Mab-NHS-activated columns Aβ binding and releasing capacity. Calculated by Nanodrop, measuring the concentration of the peptide in the pre-MNPs/columns solution with the concentration remaining after washings and elutions.

The Aβ fragments resulting of the enzymatic reactions and MNPs/columns incubations are summarized below (Figure 3.16). As it can be observed, it was only some of the digested products corresponded to the theoretical counterparts (orange color). Regarding the antibody interacting peptides (eluted peptides, blue color), we found that mainly N-terminal fragments such as Aβ(1-11), Aβ(1-16), Aβ(1-28) seemed to interact with the STAB-Mab when using the NHS columns and Aβ(1-5), Aβ(1-7) and Aβ(1-16) in the case of the STAB-Mab-MNPs (Figure 3.16).

Figure 3.16. Summarized results of the two approaches for mapping the epitope through MALD-TOF using MNPs and NHS-activated columns. The proteolytic enzymatic digestion of the Aβ peptides with the three enzymes (Trypsin, GluC and LysC) produced a pool of fragments (orange squares), which were incubated with the MPs and columns. Unbound fragments found in the flow-through fractions are represented in yellow. Proteolytic peptide fragments found in the eluted fractions, the ones supposedly interacting with the antibody are colored in blue.

3.2.1.5.3. NMR epitope mapping

NMR is a commonly used and sensitive method for detection of macromolecular interactions. The 2D 1H/15N HSQC spectra of isotopically labelled Aβ(1-40) and Aβ(1-42) are well resolved and have been already assigned [527]. To confirm the ELISA and MALDI-TOF experimental results obtained with synthetic peptides and proteolytic fragments of Aβ, we carried out solution NMR analysis on Aβ(1-40) and Aβ(1-42) in the presence and absence of STAB-Mab.

The 15N labelled peptides were solubilized into the monomeric state as described in Methods section. The 15N HSQC spectra in Figures 3.19 and 3.20 shows sharp peaks representing the main chain amides, confirming the sample was free from aggregation at before starting serial titrations with STAB-Mab. Upon addition of antibody at molar ratios 1:0.11, 1:0.33, 1:0.66, 1:1.5 and to 1:3 (Aβ:antibody), we began to observe shift perturbations and gradual line broadening (disappearance of peaks) in a certain subsets of peaks, indicating the residues interacting with the antibody and/or located in close proximity of the interaction area.

The significant shift perturbations detected within the Aβ(1-40) peptide when adding the antibody allowed us to observe that the first peaks suffering shift perturbations were mainly located in the first half of the peptide, while in the last titrations, these significant perturbations were detected in the second half after to most of the N-terminal residues consequently suffered extreme line broadening (Figure 3.17A).

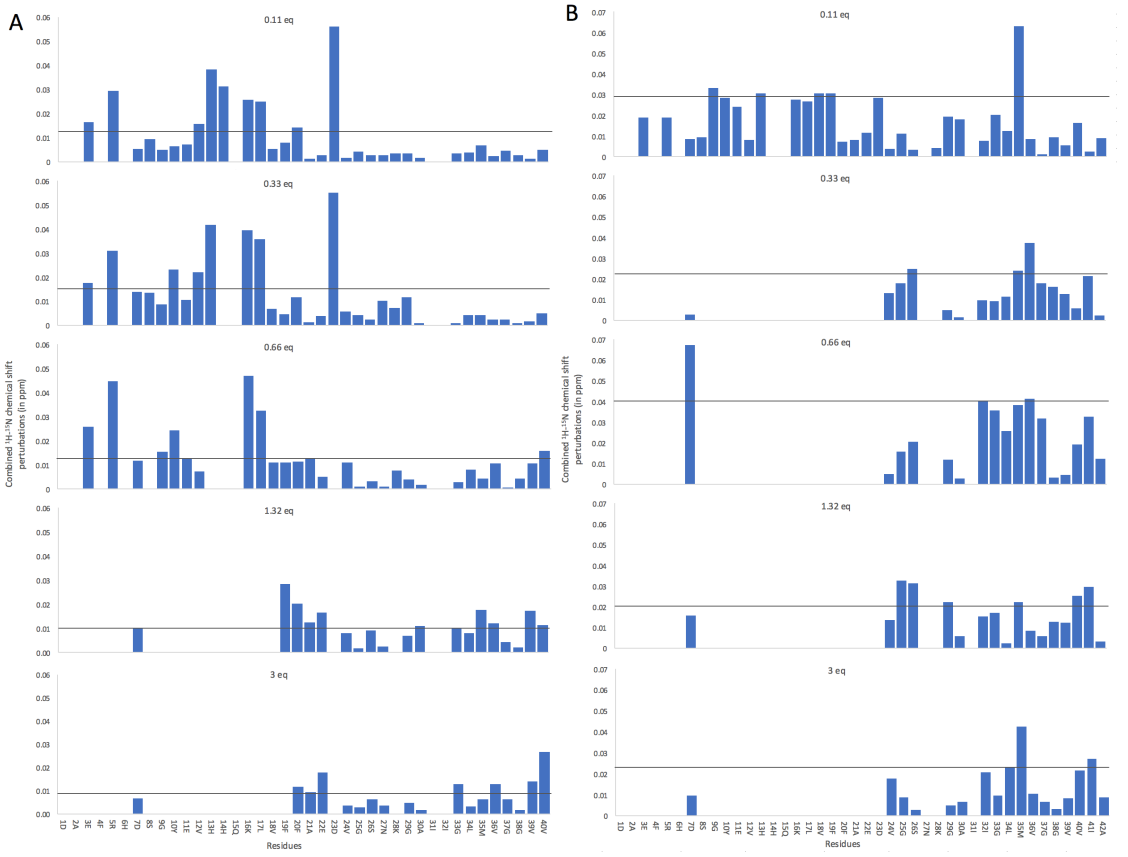

Figure 3.17. Combined 1H/15N chemical shift perturbations of Aβ(1-40) and Aβ(1-42) following titration with the STAB-Mab. Histograms represent residue-specific chemical shift changes (in ppm) of 15N isotopically labelled Aβ(1-40) (A) and Aβ(1-42) (B) in the presence of 1:0.11, 1:0.33, 1:066, 1:1.32 and 1:3 rations of labelled peptide to unlabelled STAB-Mab, respectively. The horizontal grey line corresponds to the chemical shift cut-off value, above which residues are classed as interacting with the STAB-Mab.

The same phenomenon was observed with the Aβ(1-42) peptide, confirming that the antibody must have preference for the N-terminal region, but is also capable to interact with some of the residues closer to the C-terminal (Figure 3.17B).

On the other hand, residues directly interacting with the antibody or very close by the epitope region suffered significant line broadening, allowing us to map the epitope. There is a special observable behavior, where, for both peptides (especially for the Aβ(1–42)) the intensity (peak height) diminishes, as expected when increasing antibody concentrations, but suddenly, at the last or two last titrations, peaks height increase. These phenomena is clearly observable in most of the residues that are not suffering extreme line broadening at titrations 1.5 and 3 eq, mainly placed at the C-terminal region of the peptide. This could be a symptom of a subjacent mechanism through which the antibody stabilizes some kind of structure in such part of the peptide after the first interaction with the N-terminal region (Figure 3.18).

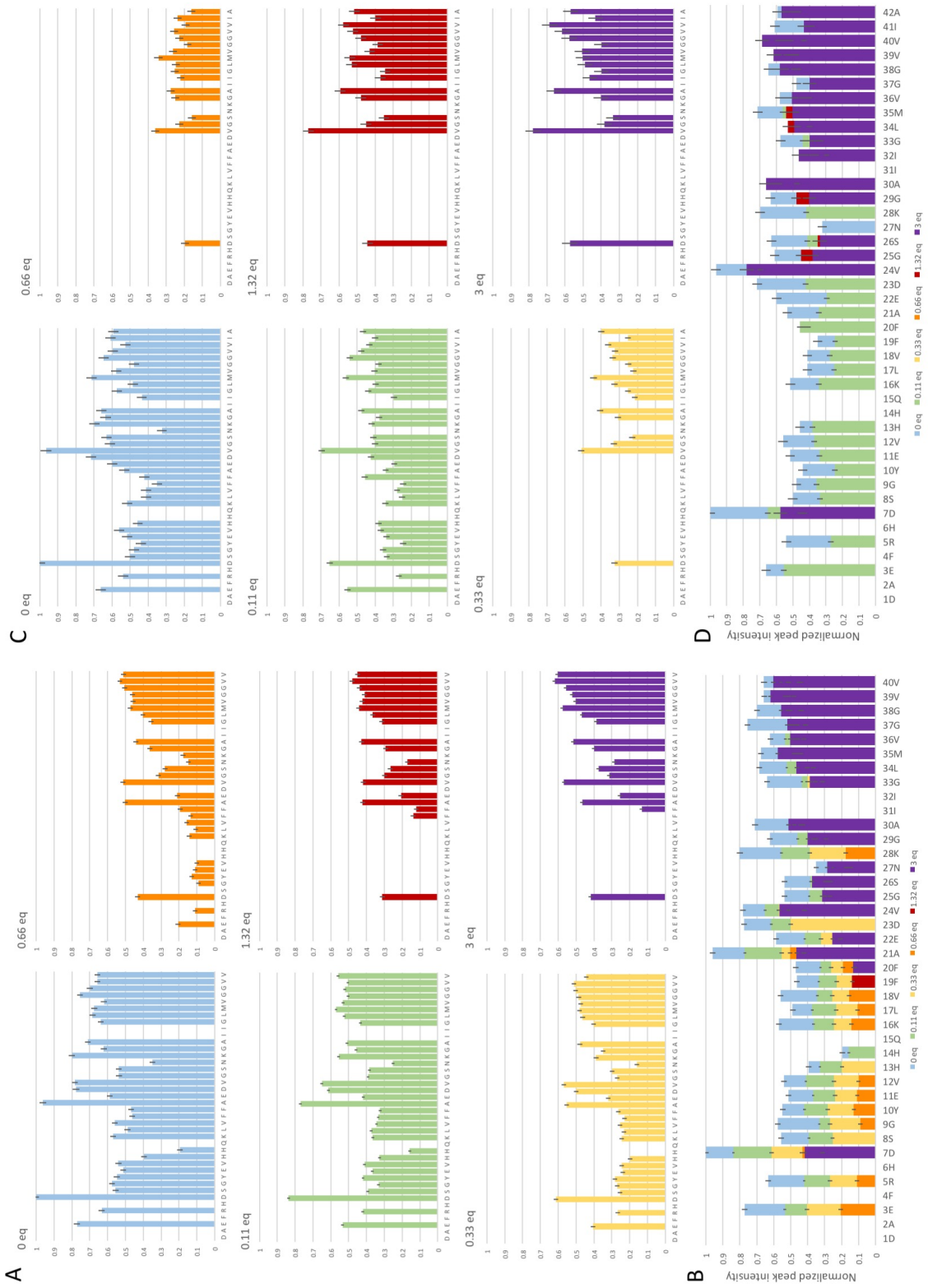

Figure 3.18. Combined 1H/15N peak intensity of Aβ(1-40) and Aβ(1-42) following titration with the STAB-Mab. Histograms represent residue-specific normalized intensity (in arbitrary units) of 15N isotopically labelled Aβ(1-40) (A & B) and Aβ(1-42) (B & C) in the absence and presence of 1:0.11, 1:0.33, 1:066, 1:1.32 and 1:3 ratios of labelled peptide to unlabeled STAB-Mab, respectively.

At maximum titrations of the antibody, at the Aβ(1-40) peptide´s spectra, we observed that the main region interacting with the antibody was located between the residues S8 and V18. However, some more N-terminal residues such as G3 and R5 or other central like N23 and K28 also suffered significant line broadening. As regards to Aβ(1-42) peptide, similar regions seemed to be affected by the antibody presence. Two large regions, from S to H and K16 to D23 suffered significant line broadening, among other isolated peaks corresponding to residues N27 (the first peak to vanish), E3 and K28 (Figure 3.18, 3.19, 3.20).

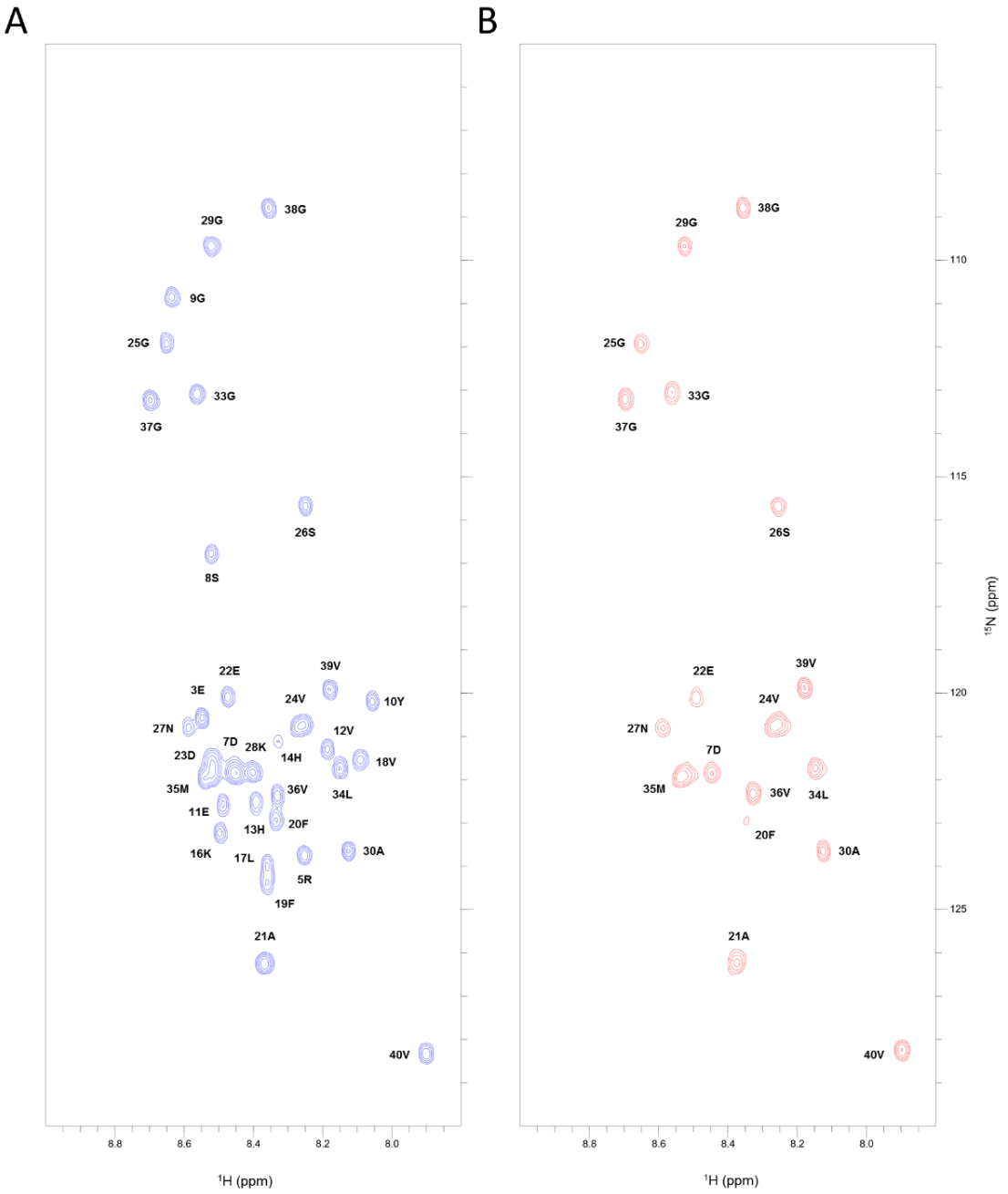

Figure 3.19. NMR HMQC spectrum of Aβ(1-40) and STAB-Mab mapped the epitope. Comparison of the 1H/15N correlated NMR spectra of 15N isotopically labelled Aβ(1-40) in the absence (A) and presence (B) of STAB-Mab. The figures show the region of the resonances corresponding to the backbone amide groups. (A) 1H-15N SOFAST-HMQC spectrum of 20 μM Aβ(1-40) in solution. Peaks were labelled according to published assignments. (B) The same spectrum of Aβ(1-40) in the presence of a 1:3 ratio of labelled Aβ(1-40) to unlabeled STAB-Mab.

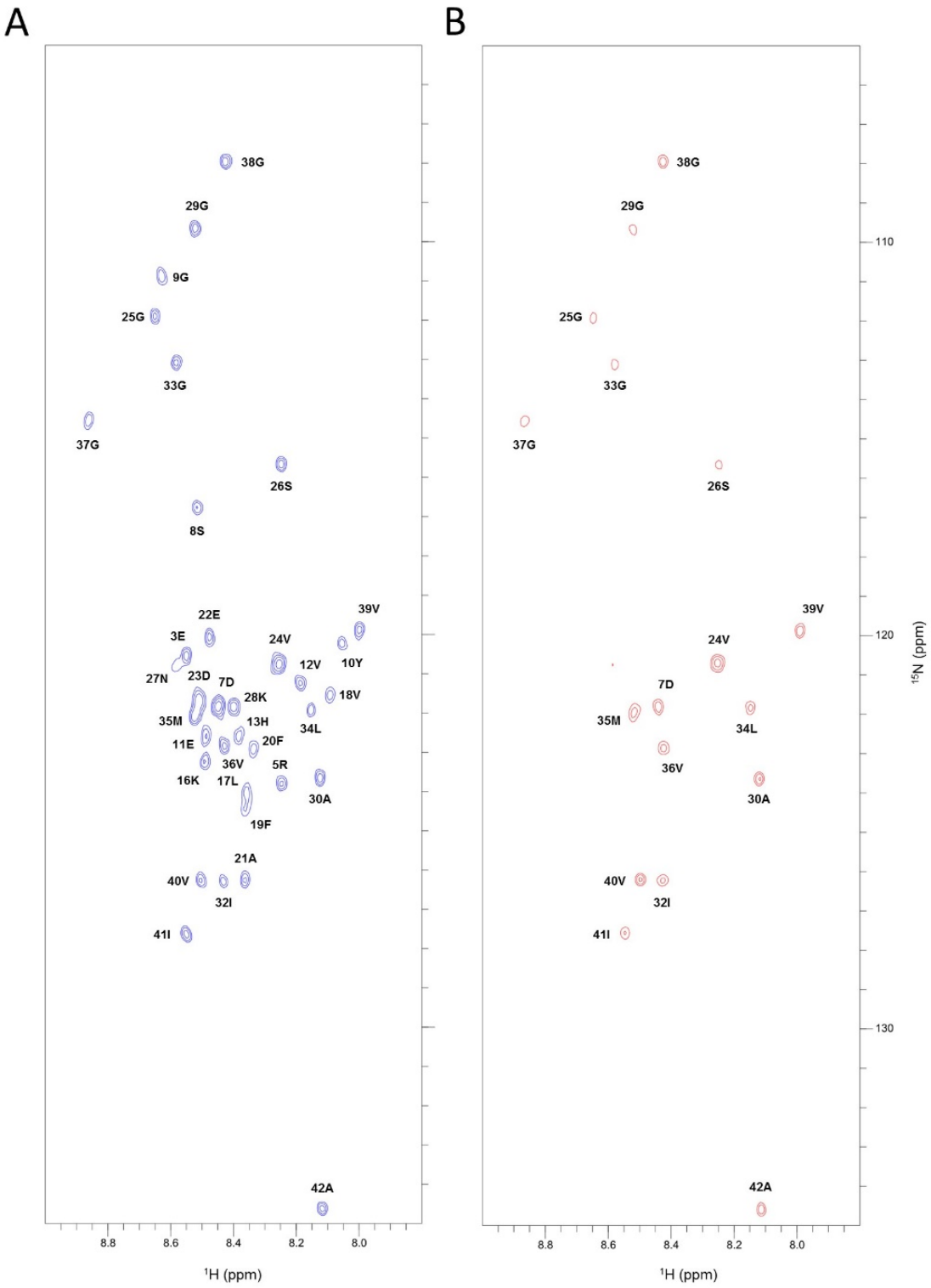

Figure 3.20. NMR HMQC spectrum of Aβ(1-42) and STAB-Mab mapped the epitope. Comparison of the 1H/15N correlated NMR spectra of 15N isotopically labelled Aβ(1-42) in the absence (A) and presence (B) of STAB-Mab. The figures show the region of the resonances corresponding to the backbone amide groups. (A) 1H-15N SOFAST-HMQC spectrum of 20 μM Aβ(1-42) in solution. Peaks were labelled according to published assignments. (B) The same spectrum of Aβ(1-42) in the presence of a 1:3 ratio of labelled Aβ(1-42) to unlabeled STAB-Mab.

3.2.2.Anti-Aβ Minibodies 1 and 2 characterization

The Minibodies 1 and 2 are two chimeric antibodies derived from STAB-Mab, oriented to two purposes: lighter molecular weight and bifunctionalization, both modifications aiming to increase the therapeutic efficacy of the antibodies and their BBB crossing. As chimeric antibodies, Minibodies have a scFv-Fc structure, they are formed by part mouse and part human sequence. In this case, it is conserved one of the scFv of the STAB-Mab, while incorporating a hinge region and constant heavy chains (CH) from a human IgG1. In the case of the Minibody 2, it is added a second scFv from a human anti-insulin IgG1 (Figure 3.21).

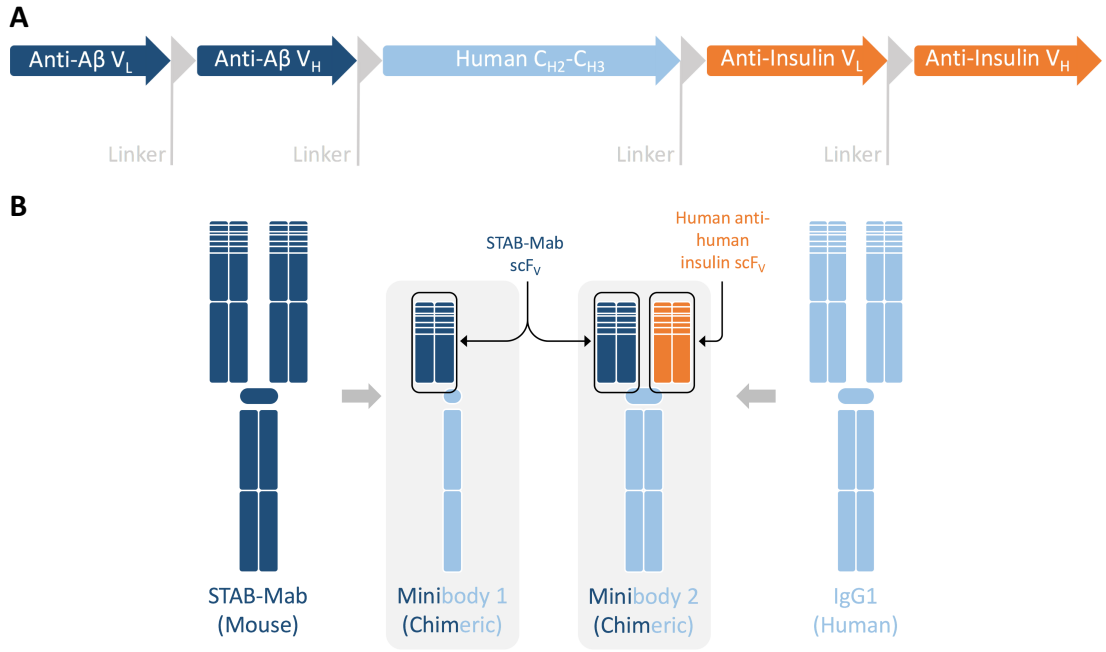

Figure 3.21. STAB-Mab-derived Minibodies 1 and 2. (A) Schematic representation of the coding sequence inserted in the expression vector for the Minibody 2 (2491 bp length). (B) Schematic representation of both Minibodies 1 and 2, STAB-Mab and a human IgG1.

3.2.2.1. Western Blot

In order to characterize and, at the same time, compare Minibodies with the original STAB-Mab, we tested them with the same samples by WB. N2A cell culture lysates served us for comparing, running them in acrylamide/bisacrylamide gels and performing a WB for trying to detect the overexpressed or endogenous APP with the three antibodies.

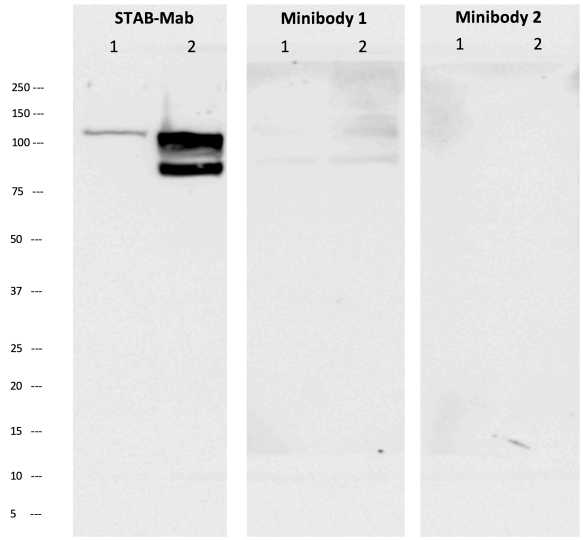

We observed, as previously confirmed, that STAB-Mab is capable to bind both endogenous and overexpressed APP, but it impossible to detect any bands when blotting with Minibody 2. Regarding Minibody 1, we barely managed to detect bands corresponding to APP (Figure 3.21).

Figure 3.22. WB comparing STAB-Mab, Minibody 1 and Minibody 2. Samples from two N2A cell cultures by SDS-PAGE and analyzed by WB. Lane 1 contains N2A lysate expressing endogenous APP. Lane 2, N2A lysate over-expressing human APP.

3.2.2.2. ELISA

ELISA results confirmed that the ability of the Minibodies to bind Aβ is significantly reduced respect to the STAB-Mab. Meanwhile STAB-Mab displays an outstanding affinity for Aβ, Minibodies behaved strangely, generating more signal when the plate was not coated than when using Aβ for coating the wells. However, it is observable that Minibody 1 is slightly capable to detect Aβ, but Minibody 2 does not (Figure 3.23). Surprisingly, both Minibodies generated more signal when there was no Aβ(1-42) coating in the wells, even using 3% BSA blocking.

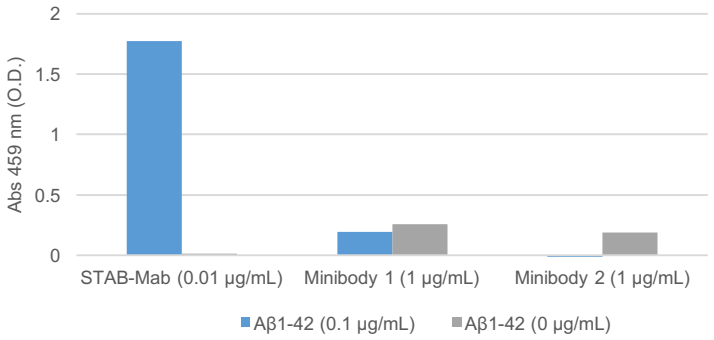

Figure 3.23. Histogram representing the ELISA results comparing the reactivity of STAB-Mab, Minibody 1 and Minibody 2 with Aβ(1-42) synthetic peptide. To obtain a detectable signal from Minibodies, we had to increase the concentration of the antibody from 0.01 µg/mL used with STAB-Mab to 1 µg/mL in the case of the Minibodies, and we only managed to detect a weak signal from Minibody 1.

3.3. Anti-Aβ antibodies *in vivo* pre-clinical assays

3.3.1.STAB-Mab *in vivo* pre-clinical trial

For testing the therapeutic potential of the STAB-Mab, a collaboration between Moghimi´s Group (University of Copenhagen), Wandosell´s Group (CBMSO, Madrid) and STAB-VIDA decided to develop a multi-platform pre-clinical assay in WT and APP/PS1 mice models.

We addressed a novel therapeutic approach using multivalent structures involving the conjugation of STAB-Mab [511, 539, 470] to PEGylated liposomes. The engineered immunoPEGliposomes, with IgG antibodies attached to the distal end of the reactive PEG chains, were first optimized for Aβ targeting and modulation of Aβ uptake by human brain capillary endothelial cells (suppressing uptake) and macrophage cell lines (stimulating uptake) in the presence of serum/plasma proteins (data not shown) [468]. The beneficial effect of immunoPEGliposomes therapy was then confirmed in the double APP/PS1 transgenic mouse model that resembles the amyloid pathology in the brain of AD patients, with different outcomes from when directly administrating the STAB-Mab antibodies to the mice.

Note: This pre-clinical assay was performed in collaboration with 3 institutions. The STAB-Mab antibodies were produced and characterized at STAB VIDA, the immunoPEGliposomes were synthetized and characterized at Moghimi´s Group, and the the administration of the treated mice and the biomarkers analysis and imaging were performed at Wandosell´s Group. Regarding my contribution to the pre-clinical assay, my works encompassed from the ELISA characterization of STAB-Mab to the analysis of several biomarkers of the treated mice by WB and fluorescence imaging, and the discussion of the results among the writting of the paper that was later published at Biomaterials journal [468].

3.3.1.1. ImmunoPEGliposomes characterization

Details of liposome composition, hydrodynamic size distribution and surface antibody density are shown in Table 3.1. The uniformity in the size and molecules/liposome between the control liposomes and the ones functionalized with the two different ligands was confirmed [468].

Table 3.1. Composition and characteristics of immunoPEGliposomes		
Liposome type	Size (nm) ± S.E.M. (n=3)	Nº of antibody molecules/liposome
Control (Lip)	146±6	None
Lip-IgG	158±4	52±3
Lip-Mab	169±6	51±6

3.3.1.2. ImmunoPEGliposome treatment in "adult" mice

Previously, the ability of immunoPEGliposomes to bind Aβ in human plasma was assessed, confirming that Lip-Mab were capable of capturing both Aβ monomers and oligomers from plasma to a considerable extent and in a yield dependent on the number of STAB-Mab molecules in the surface [468]

As a general model of amyloidosis of AD, we used APP/PS1 transgenic mice [484,485,515], which has been amplified and characterized over the past 6 years in our laboratory. During this period, it was confirmed the presence of Aβ(1-40) and Aβ(1-42) peptides in blood and the brain as well as the presence of amyloid plaques in the brain of both "adult" (10 month-old) and "aged" (16 month-old) mice [485]. The efficacy of the therapeutic protocol was first tested on the "adult" mice, since the brain amyloid burden at this age is considerably lower than "aged" animals [485].

3.3.1.3. Aβ levels

The results showed no significant differences in plasma levels of Aβ(1-40) and Aβ(1-42) on repeated STAB-MAb and Lip- MAb treatments over the four-month period and, indeed, comparable with control liposome and non-specific antibody (IgG)-treated groups (Figure 3.24). Furthermore, the levels of both Aβ(1-40) and Aβ(1-42) in cortex and hippocampus remained unaffected by STAB-MAb and Lip-MAb treatment and again comparable with control groups (Figure 3.24).

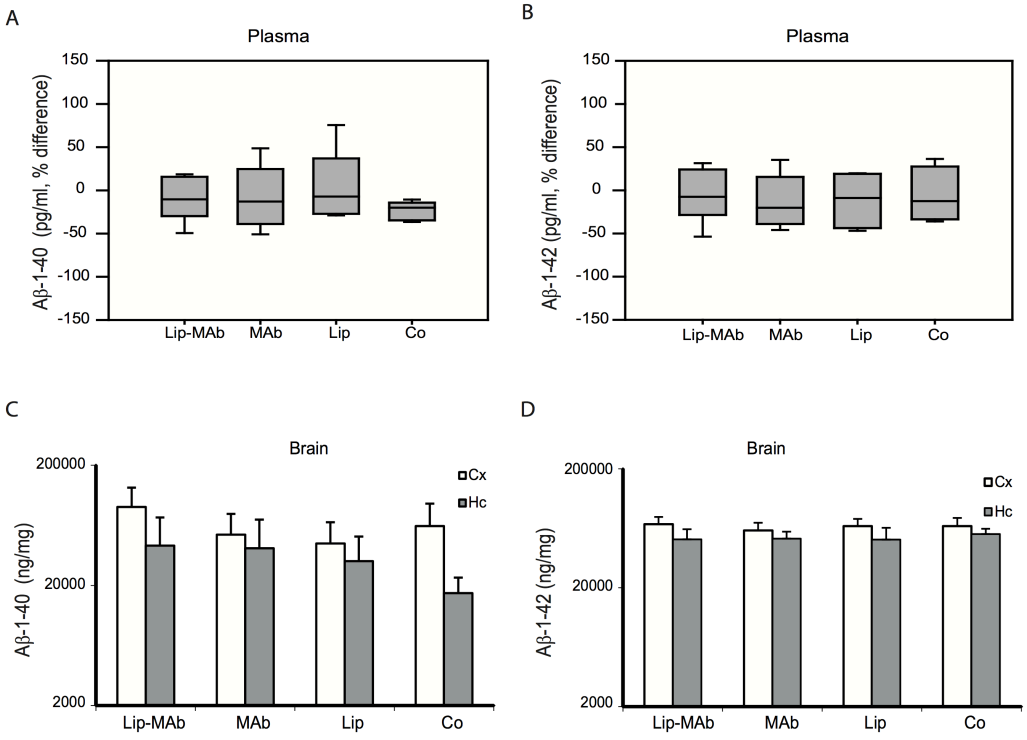

Figure 3.24. Plasma and brain Aβ levels in "aged" mice. (A&B): plasma Aβ(1-40) and Aβ(1-42) levels. Levels expressed as percentage of modification with respect to the initial levels at the start of therapy. (C&D): brain Aβ(1-40) and Aβ(1-42) levels. The results are mean ± S.E.M (n=6, 3 male and 3 female mice). Lip-MAb=STAB-MAb conjugated to PEGylated liposomes; STAB-MAb=free STAB-MAb; Co=Control animals (animals received free non-specific murine IgG).

3.3.1.4. ImmunoPEGliposome treatment in "aged" mice

Next, we implemented the same therapeutic protocol on 16 month-old mice, but extending the dosing to 6 months.

3.3.1.5. Aβ levels

Here, Lip- MAb treatment reduced the levels of both Aβ(1-40) and Aβ(1-42) in plasma compared with STAB-MAb and control IgG groups (Figure 3.25 A-B). In addition, Lip-MAb treatment reduced brain Aβ(1-40) compared with IgG or non-treated mice (p 0.05), and particularly Aβ(1-42) levels, which were significantly lower than both IgG (p= 0.01), STAB-MAb-treated (p= 0.05) or non-treated (p= 0.001) animals (Figure 3.25 C-D).

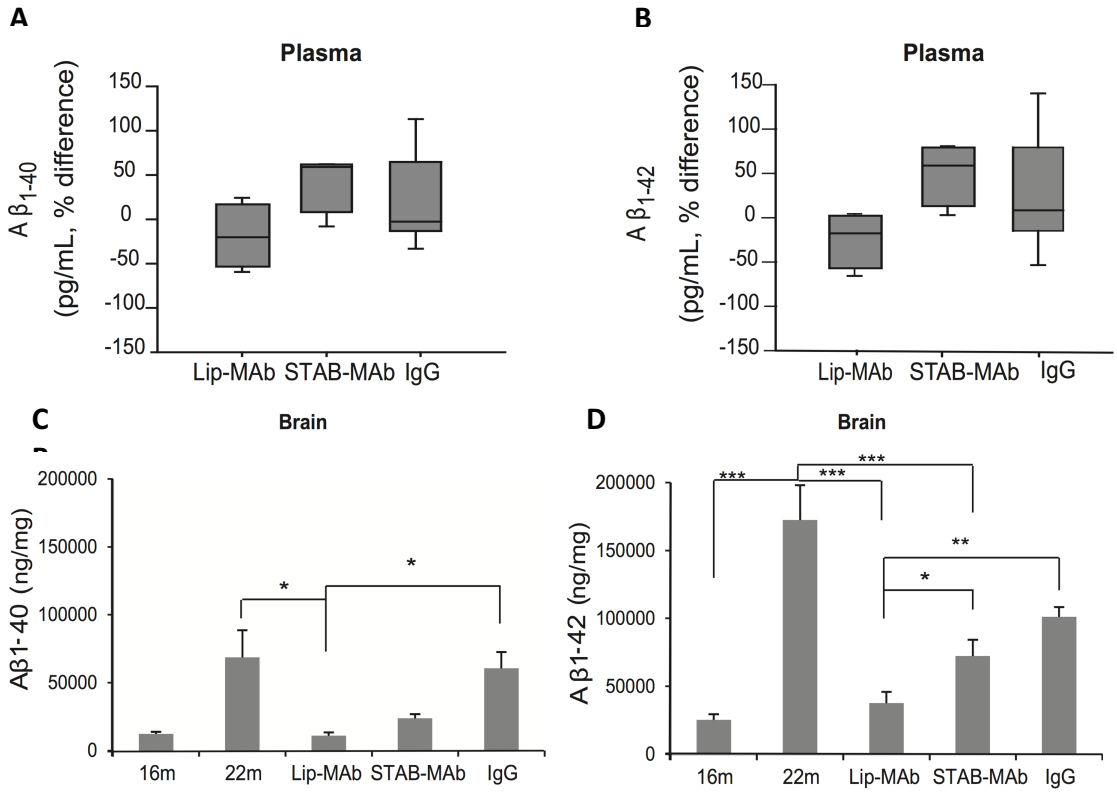

Figure 3.25. Plasma and brain Aβ levels in "aged" mice. (A&B): plasma Aβ(1-40) and Aβ(1-42) levels. Levels expressed as percentage of modification with respect to the initial levels at the start of therapy. (C&D): brain Aβ(1-40) and Aβ(1-42) levels. The results are mean ± S.E.M (n=6, 3 male and 3 female mice). *p 0.05, **p 0.01, ***p 0.001. 16 m=16 months-old animals (with no treatment); 22 m=22 months-old animals (with no treatment); Lip-MAb=STAB-MAb conjugated to PEGylated liposomes; STAB-MAb=free STAB-MAb; IgG=Control animals (animals received free non-specific murine IgG).

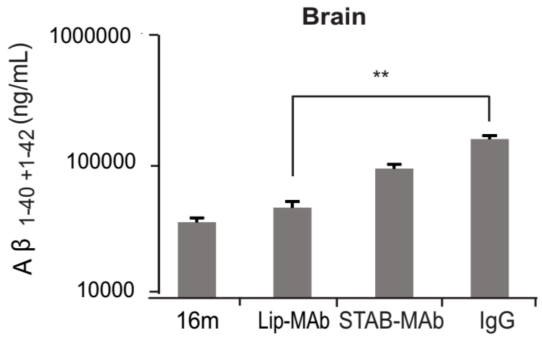

Interestingly, with Lip-MAb treatment, total brain Aβ levels at the end of dosing schedule (end of month 22) were found to be similar to the starting level (the levels in 16 month-old mice, prior to Lip-MAb treatment) (Figure 3.25C-D and Figure 3.26).

Figure 3.26. Total Aβ levels in brain in the different treated groups respect to the levels in 16-month old mice (equivalent to the starting point of the experiment). **p 0.01. 16 m=16 months-old animals (with no treatment); Lip-MAb=STAB-MAb conjugated to PEGylated liposomes; STAB-MAb=free STAB-MAb; IgG=Control animals (animals received free non-specific murine IgG).

3.3.1.6. Other biomarkers

In parallel, we studied and quantified the amount of reactive astrocytes in the affected brain regions with an antibody against glial fibrillary acidic protein (GFAP). The “GFAP-occupied area”, representing the level of GFAP-positive cells, was significantly lower ($p<0.05$) in Lip-MAb-treated mice, and particularly in the hippocampus region, compared with IgG treatment (Figure 3.27). These observations strongly correlate with the reduction of amyloid burden in these areas (Figure 3.27).

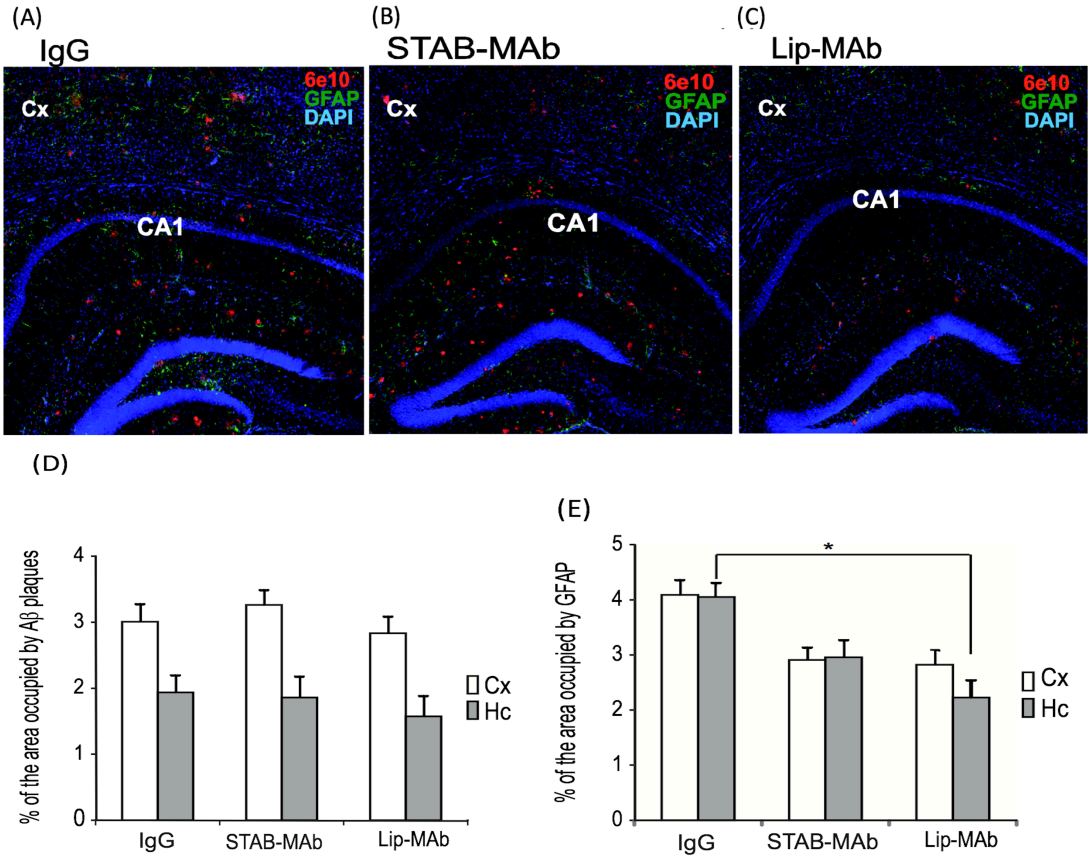

Figure 3.27. Immunofluorescence analysis of mouse brain sections. Brain coronal fixed section from mice treated with non-specific IgG1 (A), STAB-MAb (B) and Lip-MAb (C) were stained with 6E10 antibody (red) and an anti-GFAP antibody (green). CA1 refers to the region 1 of hippocampus. In addition, the amyloid plaques were counted in two cerebral regions, cortex (Cx) and hippocampus (Hc) (D). The area occupied by Aβ and GFAP-positive cells was determined in cortex and hippocampus (E) (blue are nuclei stained with DAPI). *p 0.05.

We also tested whether reduction in Aβ burden correlates with the levels of key neuronal and/or glial biochemical markers. We found no effect of STAB-MAb and Lip-MAb dosing on modifications of activity-regulated cytoskeleton-associated protein (Arc), PSD95 (a scaffolding protein in the excitatory postsynaptic density and a potent regulator of synaptic strength), neuronal phosphoprotein (synapsin), BACE1 and APP (Figure 3.28). It is plausible that reduced plasticity in aged mice may have masked the effect of reduced Aβ burden on the synaptic activity. In AD, the neuronal cytoskeleton in the brain is progressively disrupted and replaced by tangles of PHF and straight filaments, predominantly composed of hyperphosphorylated forms of tau. Hyperphosphorylation impairs the microtubule binding function of Tau, resulting in destabilization of microtubules in AD brains [486]. Accordingly, we further assessed the total amounts of Tau (Tau 5 antibody) and its phosphorylated form (PHF-1 antibody). The Lip-MAb treated group showed a lower level of PHF1 immunoreactivity and a less complex band pattern in Tau 5 compared with 16 month-old (pre-treatment) and 22 month-old mice, indicating differences in some phosphorylation sites. In addition, Lip-MAb treatment reduced PHF-1 to total Tau ratio ($p=0.024$) as well as the GFAP level ($p=0.015$) compared with control (Figure 3.28B). The latter observation indicates decrease in reactive “astrogliosis”.

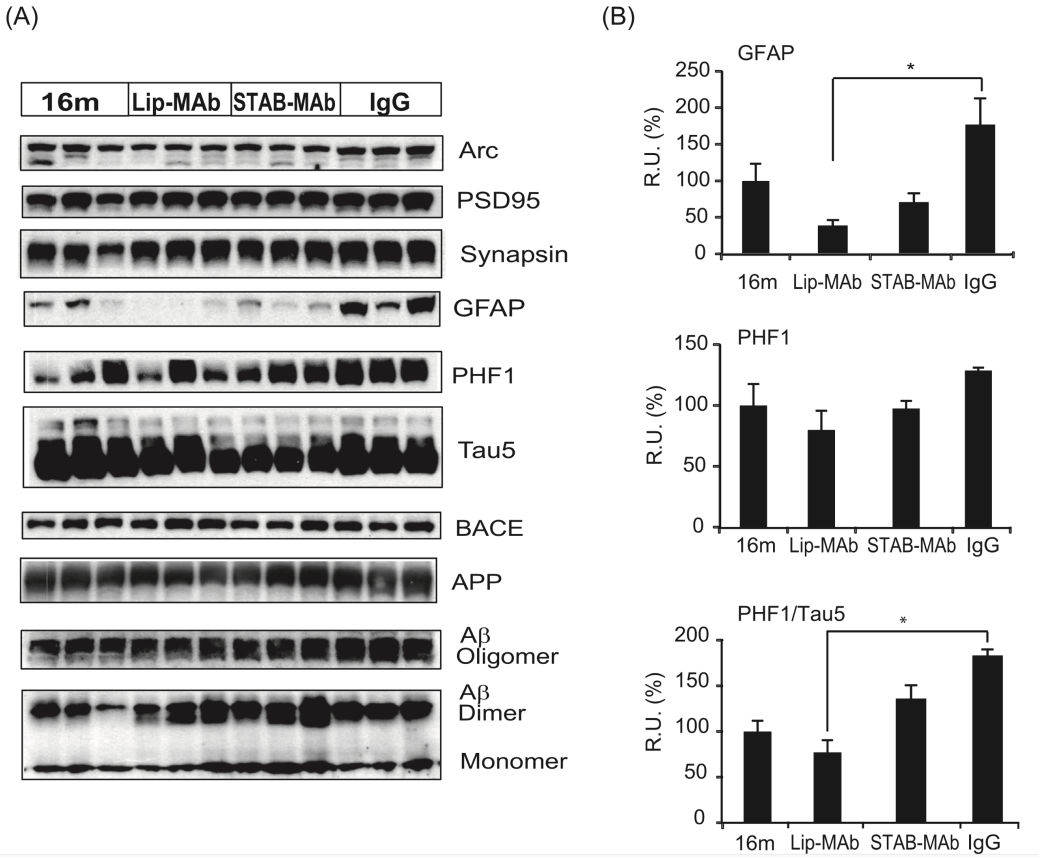

Figure 3.28. WB of Aβ production and synaptic markers after the treatment. (A) Western blots of full length APP, Ab monomers and oligomers, BACE, Synapsin, Arc or PSD95. 16m=16 month-old animals (no treatment); Lip-MAb=STAB-MAb immunoPEGliposomes. (B) quantitative analysis of GFAP, PHF-1 and PHF-1/Tau-5. The data was normalized with respect to actin and represented as relative units to 16-month old mice (16m) as control (referred to as 100%). *p 0.05. We strongly stress that in APP/PS1 transgenic model there are large differences between animals and even among littermates for levels of some kinases and phosphorylated Tau proteins [484,485], which may account for large variations seen in the regions 16m/GFAP, 16M/PHF1, 16m/PHF1, Lip-MAb/PHF1 and Lip-MAb/tau5.

3.3.2.Minibody 2 *in vivo* pre-clinical trial

In this case we have addressed another therapeutic approach using multivalent antibodies with the aim to test a hypothetical improvement in the ability to cross the BBB. The engineered antibody used in this study is the Minibody 2, result of the reengineering of the STAB-Mab. This antibody, as already presented, wears an anti-Aβ scFv from STAB-Mab and a second anti-insulin scFv from a human IgG(Figure 3.21). The rest of the constant region, lacking light constant regions for reducing molecular weight is also human-sequenced. The effect of Minibody 2 therapy was tested in the double APP/PS1 transgenic mouse model that resembles the amyloid pathology in the brain of AD patients.

Due to Mini2 is a chimeric antibody, it has a constant section with human origin that would be recognized and targeted by the immune system of the mice. In order to avoid as far as possible immunologic reactions, mice were immunodepressed using Fortecortin drug by oral administration (2 mg/L in drinking water).

Total amyloid levels in blood were assessed before starting the experiment for all mice. At the end of the treatment it was performed a behavioral test for novel object recognition and a blood sample extraction before sacrificing the animals. After that, brains were extracted and divided in two hemibrains, one for lysis and posterior analysis by ELISA and WB, and the other for eventual future immunostaining.

3.3.2.1. Aβ levels

Aβ plasma levels in treated group remained unaltered from values obtained before starting the experiment while in the vehicle group were elevated, but differences are not enough to be

significant. In brain samples, it was not possible to detect any differences between control and treated groups at the end of the treatment protocol (Figure 3.29).

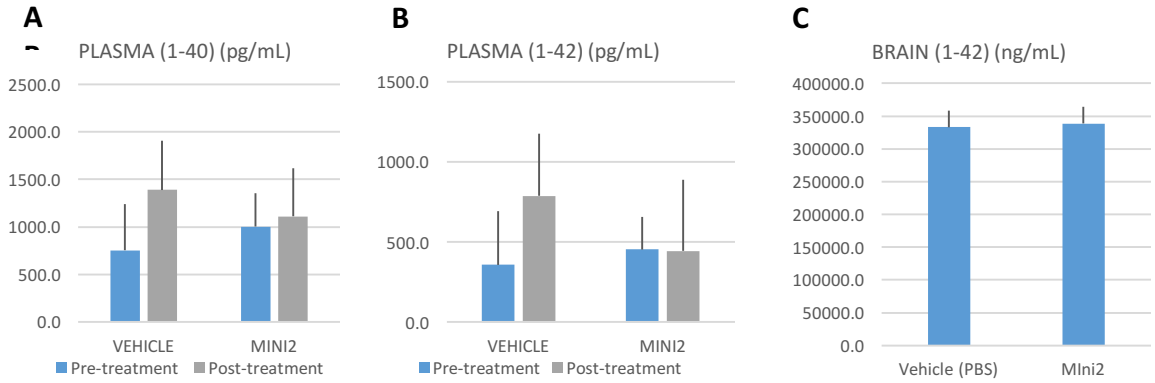

Figure 3.29. Plasma and brain Aβ levels of the mice in the Minibody 2 treatment. (A&B) Plasma Aβ(1-40) (A) and Aβ(1-42) (B) levels before (blue bars) and after (grey bars) the treatment. (C) Brain Aβ(1-42) levels of both treated and untreated groups after the treatment. The results are mean ± S.E.M (n=10 mice).

3.3.2.2. Other biomarkers

According to analyzed biomarkers, APP and GFPA seems significantly elevated in the treated group, which would indicate an increase in glial activation, maybe lead by the abnormal production or accumulation of APP. However, other synaptic markers such BACE-1, PSD-95, P120 or p-Synapsin remained mostly unaltered (Figure 3.30).

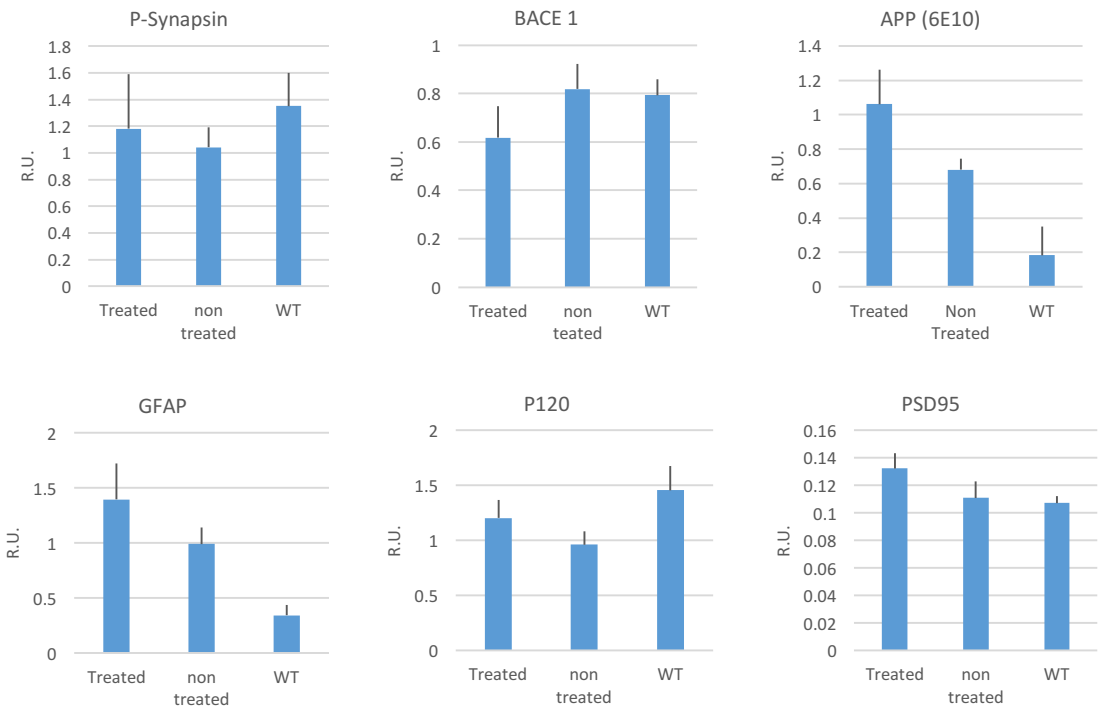

Figure 3.30. WB of APP production and synaptic markers biomarkers of the two experimental groups plus another group with WT animals with the same age. BACE-1, P-Synapsin, GFAP, P120, Synaptophysin, APP and PSD-95 expression were analyzed by WB. Quantification of BACE-1, P-Synapsin, GFAP, P120, APP and PSD-95 WB was normalized with respect to actin. R.U. Relative Units.

3.3.2.3. Behavioral tests

To evaluate the effect of Minibody 2 treatment on memory recovery, mice were evaluated by a NOR (Novel Object Recognition) test. NOR is a memory test that relies on spontaneous animal behavior and has become a widely used model for investigating memory alterations [482]. Figure 3.32 shows that APP/PS1 animals receiving both PBS and Minibody 2 spent more time in the novel object than exploring the familiar one, as it was with the WT group (Figure 3.31 A).

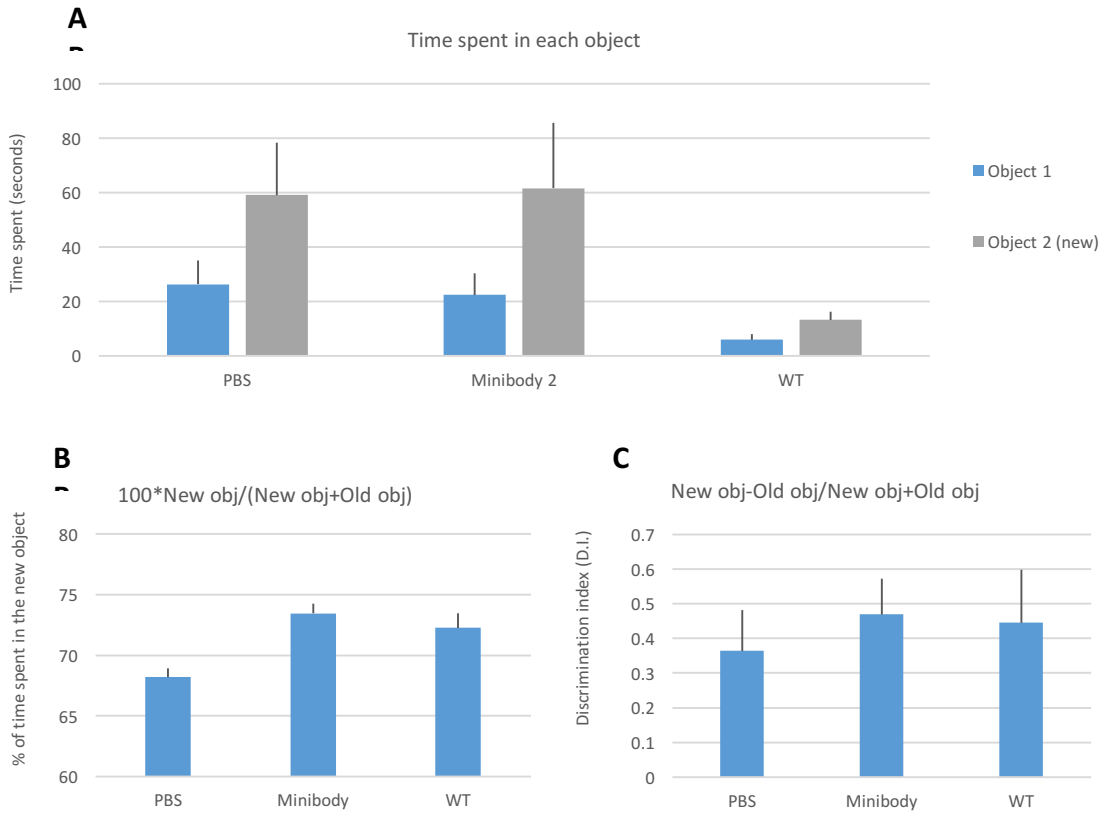

Figure 3.31. Impact of Minibody 2 treatment on APP/PS1 mice memory (n=6). Memory evaluation after PBS or Minibody 2 administration: (A) Total time spent (s) in both objects by the three groups. (B) time % investigation on the novel vs. the familiar object at the end of treatment. (C) quantification of DI. Histograms represent mean ± S.E.M.

However, the total activity period of the WT group around the objects was significantly lower than in the TG groups (12 seconds versus 85 and 84 seconds for the PBS and Minibody 2 groups respectively). In terms of percentage, Figure 3.31 B shows that Minibody 2-treated mice spent the highest percentage of the time invested in exploring the objects in the novel object, 73.4±5.2 %, much closer to the WT group (72.3±7.6 %) than the PBS-administrated group (68.2±5.9 %). However, when considering the discrimination index (D.I.= (seconds spent on novel–seconds spent on familiar)/(total time spent on objects), although Minibody 2-treated group is closer to the WT group values than the PBS-treated group, differences are negligible (Figure 3.31 C).

3.4. Chapter 3 discussion

3.4.1.Anti-Aβ STAB-Mab production

The objective of this works was to optimize the antibody production from the pre-existing hybridoma. For this purpose, different media and culture platforms were tested and the original hybridoma cell line was subcloned using limiting dilution techniques. Hybridomas are not such stable producing antibodies as other mammalian or bacterial cell lines and, as any other cell line under intensive culturing, cell cycles and handling, protein and antibodies production can be even more affected. This is a common problem when using hybridoma lines for producing monoclonal

antibodies, and each some time, it could be necessary to subclone the line in order to "reset" the cell population and isolate the better production cells. As our original hybridoma clone 9E8 1A3 1H8 producing STAB-Mab never was subcloned since it was isolated 5 years ago and after several media and culture platforms used, it was necessary to make an update.

The production yield of the original clone (named as 9E8 1A3 1H8) was around 20 µg/mL of antibody in fresh supernatant measured by ELISA and the cell doubling time was around 30h. After the subcloning, one of the subclones was selected for scaling and antibody production. This new clone (9E8 1A3 1H8 2F9) showed slightly shorter cell doubling times and between 30 and 100% higher antibody production yields depending on the cell culture conditions (suspension or monolayer) and the culture platform used (bioreactor, stacked flasks or standard flasks).

Production protocols were also simplified and reagents optimized for the acceleration and optimization of the production and purification of antibodies in the laboratory, avoiding serum IgG depletion, supernatant concentration and protein precipitation steps, which also permitted to increase significantly the antibodies production.

Therefore, we can conclude that, first, this hybridoma cell line, independently on the effect of the subcloning, is not able to grow properly and produce antibodies when being cultured in suspension and high cell densities, and second, the new clone performs significantly better than the old one, allowing to increase stable production rates in laboratory.

As exposed previously, unlike polyclonal antibodies, which are produced in live animals, monoclonal antibodies are produced *in vitro* using cell-culture techniques. Production of monoclonal antibodies is a very expensive and time-consuming process that may take weeks of culturing to provide enough antibodies for an experiment or to treat a single patient. Even though, monoclonal antibodies clinical use has been extensively used in the last years, positioning as the main therapeutic approach in neurodegenerative diseases and cancer treatment. Although there exist several unknown or poorly known mechanisms underlying some of the processes unchained by these immunotherapeutic approaches and certain handicaps to surpass, there is an undoubtable potential in these kind of approaches.

When addressing AD, two main targets rapidly come out: Aβ and tau protein. As also showed, there exist several pre-clinical and clinical phase trials currently running targeting these two molecules. The road to the clinical phase or even to the market is long and hard, requiring a depth biophysical characterization and strong and stable pre-clinical output. Although the new “autoantibodies” or “fully human antibodies” are reporting interesting results and gaining tons of interest, at the same time, antibody recombination and humanization techniques are evolving rapidly, allowing reliable and easy ways to create interesting variants and new approaches, such as Fc-fusion proteins. Here, we presented some new characters in this scenario, STAB-Mab, and the Minibodies 1 and 2. The objective behind the STAB-Mab creation was to develop a new monoclonal antibody to be, not only an alternative to the other contemporary clinical antibodies such as Bapineuzumab, Solanezumab or Crenezumab, but also to be used in diagnosis and in new nanoplatforms with theranostic purposes. However, as the antibody did not pass to clinical phases yet, humanization nor large-scale production were required, so hybridoma production was continued and optimized for antibody production, stocking, and selling.

3.4.2. Anti-Aβ STAB-Mab characterization

STAB-Mab is an in-house developed IgG1 isotype murine monoclonal antibody raised against Aβ. The original clone producing STAB-Mab was obtained by mice immunization with an Aβ(1-42) solution followed by hybridoma fusion. In previously published studies, SPR data confirmed picomolar affinities of STAB-MAb for both monomers and fibrils of synthetic Aβ(1-42) (KD= 80 and 130 pM, respectively), which were even better than the affinities measured in parallel with the commercial anti-Ab antibody 6E10 (KD= 300 pM). When biotinylated, the antibody´s affinity was lower although still in the low nanomolar range (KD= 2.1±0.6 and 1.6±0.4 nM, for monomers and fibrils, respectively) [511]. Such effects due to biotinylation have been previously observed for other antibodies as well [512], and it was suggested that the reactive free amino groups of the antibody that interact with N-hydroxysuccinimidobiotin (for biotinylation) are essential for binding and bioreactivity of the molecule.

The antibody has also been used for functionalization of different platforms and nanostructures such as PEGylated liposomes [468, 511] or poly (alkyl cyanoacrylate) (PACA) nanoparticles [470]

designed with theranostic purposes. STAB-Mab-functionalized liposomes showed to bind Aβ with a two-fold lower affinity for monomers than fibrils (KD= 2.8±0.5 and 1.6±0.2 nM, respectively) and specifically stain amyloid plaques both in paraffin and frozen sections of AD patient brains [511].

When tested *in vitro* and *in vivo* pre-clinical tests, the presence of these structures and even the antibody alone reported interesting and promising data showing memory recovering and AD-related biomarkers improvements [468, 470, 511, 513].

The aim to relate the characteristics of the antibody with its therapeutic effect and compare with other therapy-oriented antibodies required a finest characterization of the mechanism of action and the epitope of the STAB-Mab, leading to this group of experiments. Through a variety of techniques available at STAB VIDA company and several other collaborating groups from FCT (NOVA Lisbon University), CEDOC (NMS Lisbon Unversity), CBMSO (Madrid) or DZNE (Munich), we managed to identify the range of molecules the antibody is capable to bind, comparing it to other commercial options, to determine the effect of the antibody in the amyloid beta kinetics and to map its epitope with a single-residue detail.

3.4.2.1. Western Blot

WB analysis done at Claudia Almeida´s Group (CEDOC) showed that STAB-Mab owns a wide variety of Aβ species and aggregates, even from synthetic origin (human and mouse) or from mouse brain lysates. In Figure 3.4 it is shown a comparison between a gold-standard murine monoclonal 6E10 and STAB-Mab. Although 6E10 has an N-terminal restricted epitope and STAB-Mab has a spatial and more central epitope, the blotting patterns between both antibodies. However, some differences can be noted. Meanwhile, STAB-Mab is able to recognise both mouse and human Aβ with almost the same facility, 6E10 demonstrated to be more prone to bind the human sequence of Aβ. It is also noticeable that STAB-Mab seems to show more affinity than 6E10 at the same concentrations used, something remarkable even though we were expecting better affinity observed in previous SPR data [511], due to the 6E10 is one of the first choices in research and diagnosis of amyloidopathies thanks to its great sensitivity [468].

Based on ELISA results we intuited that STAB-Mab may have a broad binding capability, so we wanted to confirm if this antibody was able to recognise APP as well. WB of several lysates from N2A cell cultures producing both endogenous and overexpressed APP and brains of WT and APP/PS1 transgenic mice were used for proving this. In our case, the N2A cell line was overexpressing transiently the human version of APP [516, 517]. APP/PS1 mice (B6-Tg(Thy1-APPswe; Thy1-PS1 L166P) contain human transgenes for both APP bearing the Swedish mutation and PSEN1 containing an L166P mutation, both under the control of the Thy1 promoter. In these mice, expression of the human APP transgene is approximately 3-fold higher than endogenous murine APP, and Aβ plaque deposition starts at approximately six weeks of age in the neocortex. Deposits appear in the hippocampus at about three to four months, and in the striatum, thalamus, and brainstem at four to five months (Figure 3.4) [514, 515].

WB results confirmed STAB-Mab recognizes APP from human and mouse origin, but we also wanted to compare with other gold standard antibodies such as 4G8 (another monoclonal murine anti-Aβ antibody widely used in post-mortem diagnosis of AD in human brain slices) and Y188 (a well-known rabbit APP-specific antibody). While with 4G8 was only possible to visualize a single band at 100 Da in N2A cell culture overexpressing APP lysate, with Y188 was possible to identify several bands around 100 Da (APP) in both N2A lanes and several unidentified thick bands around 30 Da (Figure 3.14).

STAB-Mab showed a performance between 4G8 and Y188 antibodies when using the same 1µg/mL concentration. STAB-Mab marked the same two bands than with Y188 around 100 kDa (presumably corresponding to endogenous/mature and overexpressed/immature APP) in the lanes loaded with lysates from transfected N2A cell cultures (lanes 2) and with APP/PS1 mouse brain lysate (lane 3). It was also possible to see 2 more bands between 10 and 15 kDa, possibly corresponding to small-sized Aβ oligomers.

With these experiments we confirmed that STAB-Mab is capable to recognize APP as good as a gold-standard as it is Y188 antibody under the same conditions, at least using this particular technique.

3.4.2.2. Stainings

Four sets of stainings were performed and analyzed in collaboration with two groups (Wandosell´s Group at CBMSO, Madrid, and Herms´ Group, at DZNE, Munich) for the need of samples and microscopy equipment that was not available at STAB VIDA nor FCT.

At Wandosell´s Group, hemi-brain cryoslices from 11 months-old APP/PS1 and wt were stained with a pool of commercially available antibodies for comparing the STAB-Mab. Fluorescence microscopy images showed in Figure 3.6 display the hippocampal region and part of the somatosensory cortex where blue color labels cell nuclei and red, Aβ deposits. As previously noted, hippocampus and somatosensory cortex are two of the main affected areas by the AD-related Aβ pathology, and so it is in the animal model examined here, APP/PS1.

As described in the results section and as expected in the APP/PS1 mice slices, STAB-Mab labelled different size Aβ plaques in a similar way to 6E10 or the rabbit polyclonal anti-Aβ antibody #2454 from Cell Signaling, which showed the strongest Aβ plaques labelling. On the other hand, the antibodies targeting APP did not allow us to identify any visible signal. And so was regarding the WT mice slices incubated with STAB-Mab and 6E10.

During one of the secondments performed within the EXTRABRAIN Project at Herms´ Group (DZNE), we had de opportunity to compare the STAB-Mab with the already known Y188 and 4G8 antibodies in new samples and with other microscopy techniques. 6-month old female mice from three mice genotypes (WT, APP/PS1, and APPKO) were perfused with PFA and 10 µm thickness sections were obtained with a microtome prior to the immunostainings with the selected antibodies (Figure 3.7).

In APPKO animals (B6.129S7-Apptm1Dbo/J), the endogenous APP gene was disrupted by replacing a 3.8 kb sequence encoding the promoter and exon 1 with a neomycin resistance cassette by homologous recombination. At birth, mice homozygous for the targeted allele are viable and do not display any gross physical or behavioral abnormalities. No APP gene product (mRNA or protein) is detected. By 14 weeks, the mice exhibit elevated reactive gliosis in the hippocampus and neocortex compared to levels observed in wild-type animals. Neurological evaluation showed reduced forelimb grip strength and decreased locomotor activity [518]. Also, spasm-like movements have occasionally been observed when anesthetizing animals.

Confocal images confirmed what we were expecting regarding the 4G8 and Y188 antibodies. 4G8 successfully labelled the Aβ plaques in the sections from APP/PS1 mice, but nothing was distinguishable from noise in the other two genotypes (WT and APPKO). On the other hand, Y188 clearly directed against APP, allowed us to observe the typical APP disposition around the neuronal body, much more visible in the APP/PS1 model than in the WT, while nothing was detectable in the APP KO mice slices. STAB-Mab showed similar staining pattern than the 4G8, labelling different diffuse and dense Aβ plaques, but with a little bit more background noise.

In addition to the detailed pictures from the confocal microscopy, we also had the opportunity to use the fluorescence microscope and, with the help of the Apotome module, we took photos all over the coronal mice brain sections. This allowed us to test the antibodies STAB-Mab and 4G8 and have an “overall” view of the whole brain and the disposition of the Aβ plaques. The stainings showed similar Aβ patterns with both antibodies, although when using STAB-Mab, more number of plaques were visible (Figure 3.8).

The collaboration at DZNE made possible as well to access to the Faculty of Medicine of the LMU and analyze some AD human samples. Paraffin-included slices from AD patient´s brains were treated with the same protocol as the ones from mice and stained with both 4G8 and STAB-Mab antibodies. Again, the pattern displayed by both antibodies was very similar, labelling Aβ plaques with different density.

These results strongly supported previous observations, confirming that STAB-Mab high affinity, broad binding capabilities, and versatility under different techniques make it a good antibody for research and diagnosis purposes and even for therapy [324, 334, 336].

3.4.2.3. ThT-monitored aggregation inhibition test / Influence of anti-Aβ STAB VIDA MAb in a solution of Aβ(1-42)

As showed, the antibody not only interacts in some manner with several monomeric and aggregated species, but also impedes the formation on organized aggregates as ThT assays

results reportedly showed, which denote a flexibility and a broad binding profile (Figure 3.10). This broadly in antigen recognition in a monoclonal antibody is not common but highly interesting in Aβ-targeted immunotherapy considering the variety of AD-related species [324, 334, 336].

Aggregation tests confirmed that the antibody is capable to completely inhibit the formation of the β-sheet motif required for the arrangement of highly organized aggregates [361, 362] in the Aβ(1-42) monomeric solution in physiological-like conditions (37ºC and aqueous polar solution). However, to inhibit aggregation, the antibody needed to be present in a similar molar ratio than Aβ(1-42). This fact, in conjunction with the already published affinity measurements by Canovi *et al.* [511], could imply that the first residues the antibody recognize would not be the ones necessarily related to the β-sheet arrangement.

On the other hand, starting from an already aggregated solution, the antibody showed no capacity for disaggregating the Aβ(1-42) complexes, at least, not enough for being detectable by the ThT assay, which could suggest that it is not capable to access the residues responsible for the formation and maintenance of the β-sheet that, indeed, were exposed in the pre-aggregated solution.

3.4.2.4. Transmission Electron Microscopy (TEM) analysis

Although it is not a quantitative experiment, we believe that visualization of the effect of the STAB-Mab in the formation of Aβ aggregates in solution would be interesting and informative. As shown in Figure 3.11, we observed hints pointing to that STAB-Mab could have the ability to inhibit, *in vitro*, the formation of amyloid organized aggregates (at 1 and 0.5 molar equivalents) and more interestingly, eventually disrupt preformed fibrils (Figure 3.11 E).

We have confirmed that STAB-Mab has a broad capacity for binding a number of Aβ species, among monomers, oligomers, and fibrils. Now, we noticed that it also may be capable to influence and structurally alter big and organized aggregates such Aβ fibrils, as it has already observed with other types of molecules [469]. The mechanisms underlying this ability may lie in the residues interacting with the antibody (epitope) and in the way the antibody forces Aβ molecules to acquire some defined molecular structure.

Nevertheless, we must be cautious in this since the technique used is not the most adequate to confirm such phenomenon.

Therefore, in order to determine the residues interacting with the CDRs and uncover the mechanisms of action of the antibody that allow that broad recognition of different Aβ species, a battery of experiments for epitope mapping was designed using Aβ(1-40) and Aβ(1-42) synthetic peptides.

3.4.2.5. STAB-Mab epitope mapping

Following the results observed in the WB and the different stainings, we needed to unveil the mechanisms by which STAB-Mab was recognizing and binding the Aβ peptide. What residues were interacting? In which order? Does it have a linear or a discontinuous epitope?

3.4.2.5.1. ELISA-based epitope mapping

ELISA results comparing affinities for the whole Aβ peptides of STAB-Mab, 6E10 and 4G8 commercial antibodies using the same concentrations and conditions confirmed the better performance of the STAB-Mab over the other two, especially when referring to versatility detecting any of the peptides, even from human or mouse/rat. 4G8 is a strongly C-terminal-oriented antibody, requiring the presence of the Aβ residues in positions 41 and 42 for binding the peptide (both human and mouse/rat). Regarding 6E10 antibody, as an anti-human N-terminal Aβ-directed antibody, it was able to bind all human Aβ peptides but none of the mouse/rat peptides (Figure 3.12 A).

On the other hand, as our principal goal, we wanted to locate the STAB-Mab epitope within the Aβ peptide. For this purpose, we coated an ELISA plate with different synthetic fragments of the Aβ(1-42) sequence: 1-11, 12-28, 29-40, 29-42, 25-35 and 35-42. Results confirmed the specificity of 4G8 for the C-terminal region of Aβ exclusively binding fragments carrying the two last residues of Aβ, the 29-42, and the 35-42. The N-terminal preference of the 6E10 was also confirmed,

although we observed interaction with fragments 12-28 and 29-40 meanwhile its reported epitope is located within the 3rd and the 8th amino acids of the Aβ peptide [519]. Maybe similar spatial conformation acquired by these 6 residues (EFRHDS) is also reproduced in some part of the 12-28 and 29-40 fragments. Moving to the STAB-Mab, we observed interesting data, justifying its "broad" character, now observable along the entire sequence of the Aβ peptide. We confirmed STAB-Mab is able to bind fragments from residues 1 to 42, but with important differences between the fragments used and some curious behaviors. The antibody showed increased preference for the 1-11 fragment, 12-28 and showing the highest affinity the 29-40 fragment. Until here, everything seems pretty straight-forward and confirm what we were expecting, but the interesting thing is that, when using the fragment 25-35 (sequence partially included in the 29-40 fragment), the signal obtained was almost indistinguishable from noise. In a similar way, the same happened with the 29-42 fragment, only differentiated from the 29-40 by the two last residues, something that seems to affect the binding capacity of the antibody to such peptide. And again, when using the 35-42 fragment, we obtained similar results than with the 25-35 fragment (Figure 3.12 B) [468].

Part of these data makes us infer that the presence of the last two highly apolar residues of the Aβ(1-42) molecule (IA) may influence the entire conformation of the 29-4X fragment, hindering the optimal binding structure to the antibody. Coincidentally, this is a hydrophobic region highly involved in the formation of ordered aggregates and which tends to forms β-sheet structures [523].

And when it comes to the 25-35 fragment, which is a very toxic derivative of the Aβ molecule and a key part of the aggregation and β-strand structure formation in Aβ dynamics [81, 82, 83, 522], we know it commonly acquire α-helical structures in a variety of media (PDB ID: 1QWP [520], PDB ID: 1QCM [521]). This fact of this peptide to spontaneously form organised and closed α-helical structures could be affecting the accessible areas STAB-Mab needs to bind the such fragment.

3.4.2.5.2. MALDI-TOF

Mass spectrometry is a commonly used technique for mapping antibodies paratopes and epitopes [384], and the opportunity to collaborate with a proteomics-specialized group at the FCT (Bioscope Group) for continue the STAB-Mab characterization arise. The methodology followed, based in some previously published works [384], consisted in the enzymatic digestion of the Aβ peptides by Trypsin, GluC and LysC and analysis of the spectra of the flow-through and eluted fractions after passing digested products through a STAB-Mab-functionalized platform. This would give us the picture of both the antibody-interacting and non-interacting digested peptide fragments.

Based in previously published works [385], to create a functionalized platform, we first tried to use custom Si@MNPs produced in collaboration with BIOSCOPE Group and use magnetism for separating antibody-interacting fragments from the rest of digested fragments pool. After two batches of Si@MNPs, we functionalized the second batch with the antibody via NHS due to an increased magnetism and less aggregation tendency. Results confirmed unspecific Aβ retention by non-functionalized Si@MNPs, which together with the difficulty to avoid particles aggregation and clean MALDI-TOF spectra, we rethought the protocol and decided to use inexpensive and more reliable commercial NHS-activated sepharose columns from GE.

NHS-activated sepharose columns are commonly used for purifications and sample enrichment and are easy and fast to operate, including automated pump systems. NHS-activated columns were satisfactorily functionalized with the STAB-Mab and no unspecific Aβ adsorption was observed. Moreover, MALDI-TOF spectra were much clearer, solving two problems of the Si@MNPs previously used.

Once we had our three functionalized columns we started to analyze and compare initial digested peptide pools, and column flow-through and eluted fractions. We noted that we did have a new problem, the mediocre initial representation of the whole theoretical digestion products we should obtain with the three enzymes previous to the columns passing. This would influence and mask the final results due to some of the fragments absence in the initial digestion pool may be part of the antibody epitope. However, in the best case, we managed to obtain 4 of 9 expected trypsin-digested fragments, 10 of 19 expected GluC digested fragments and 3 of 5 expected LysC fragments pool. We also knew some of the fragments would not be detectable in the MALDI-TOF spectra due to its poor representation or its proximity to other more intense peaks.

Although the lack of the robustness in the results, the final analysis revealed that only N-terminal fragments remained in the columns and was released with the elution buffer. If we consider the experiment using the Si@MNPs, the same pattern was observed, being N-terminal fragments the ones remaining attached to the nanoparticles after washings and posteriorly released by the elution buffer (Figure 3.32).

Figure 3.32. Schematic representation of Aβ molecule (the interacting region in green background) and all the fragments obtained after enzymatic digestion (both Si@MNPs and NHS-activated columns experiments). Blue bars correspond to the fragments identified in the eluted fractions (also identified in the flow-through but not in the sequential washings). Yellow bars correspond to the fragments identified in the flow-through fractions. Reddish bars represent fragments present in the initial digestion pool but that were impossible to identify in later fractions after the Si@MNPs or columns incubations.

These results point to a strong N-terminal preferred epitope, something that partially agrees with the previous ELISA results, where we observed that the antibody actually bind the synthetic fragments 1-11 and 12-28 (although the highest affinity observed was for the 29-40 fragment). However, the technical problems, the limitation of the techniques and the long and complex protocol made these results unreliable and us to consider other techniques for mapping STAB-Mab epitope with more precision and robustness

3.4.2.5.3. NMR epitope mapping

After the failed MALDI-TOF epitope mapping, we tried to use another of the most used techniques, Nuclear Magnetic Resonance (NMR). Solution NMR spectroscopy is especially adequate for characterizing intermolecular interactions, including the determination of antibody epitopes [430]. The NMR signal is extremely sensitive to the local chemical environment, therefore, when an intermolecular complex is formed, the chemical environment of the atomic interface of a molecule changes as they get close to the atoms of the interacting partner and so does the NMR signal. Through studying the NMR spectra form before and after the complex formation, interface atoms can be identified thanks to the changes in their NMR signal. This is very useful for determining the exact individual residues interacting, and the order they interact with each other in an epitope-paratope interaction.

Spectra plots obtained from the 15N-HSQC NMR experiment of each titration with Aβ(1-40) and Aβ(1-42) peptides from 0 to 3 molar equivalents of antibody over Aβ peptides confirmed several significant peak shifts and broadenings, indicating several residues interacting with the antibody in a concentration-dependent pattern. The starting 15N labelled Aβ(1-40) and Aβ(1-42) peptides' spectra showed sharp and well-defined peaks, which were labelled according to the assignments previously published (Figures 3.18, 3.19) [527].

The NMR data on Aβ(1-40) and Aβ(1-42) revealed a hypothetical 2-step mechanism by which the STAB-Mab interacts with the peptides. The antibody seems to recognize in a first place an N-terminal subset of residues, as depicted by the observed shift perturbations.

The first residues perturbed are roughly concentrated in the region from S8 to D23, followed by the central- to C-terminal residues S26, G33, M35, V36 and V40, in both Aβ(1-40) and Aβ(1-42) spectra. Lysine in position 28, suffered extreme line broadening in both cases, even at low concentrations of STAB-Mab indicating that this residue might be interacting strongly with the antibody or with a region within the Aβ peptide intensively influenced by the interaction with the STAB-Mab.

Subsequently, with increasing antibody concentration extreme line broadening appears and several central- to C-terminal residues also interact with the antibody. Although with slight differences between both Aβ peptides, the pattern is quite similar. Also, the increasing intensity of the C-terminal residues at higher concentrations indicate the stabilization of a defined structure in such area after the first interaction.

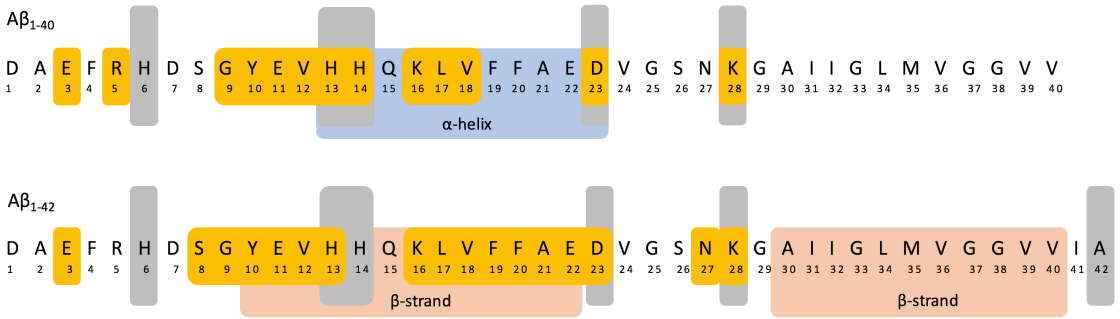

Figure 3.33. Schematic representation of disappearing peaks from NMR spectra over two solved and published structures for Aβ(1-40) and Aβ(1-42) in monomeric form (PDB ID Aβ(1-40): 2LFM, PDB ID Aβ(1-42): 1Z0Q) (A) and when being part of fibrils (Aβ(1-40): 2LMN, Aβ(1-42): 2MXU) In clear red, β-sheets-forming regions, in clear blue, α-helix-forming regions and in darker greys, residues involved in aggregation and β-sheets stabilization.

Considering our NMR data and the information already published from solved structures, in the case of Aβ(1-40), the N-terminal region affected by the presence of the antibody might be forming an α-helix occupying hydrophobic residues from H13 to D23 (PDB ID: 2LFM) [526]. On the other hand, in the case of the Aβ(1-42) peptide, according to Tomaselli *et al*. (2006), under our experimental conditions, the same region should tend to form β-strand structures (PDB ID: 1Z0Q) (Figure 3.33) [525].

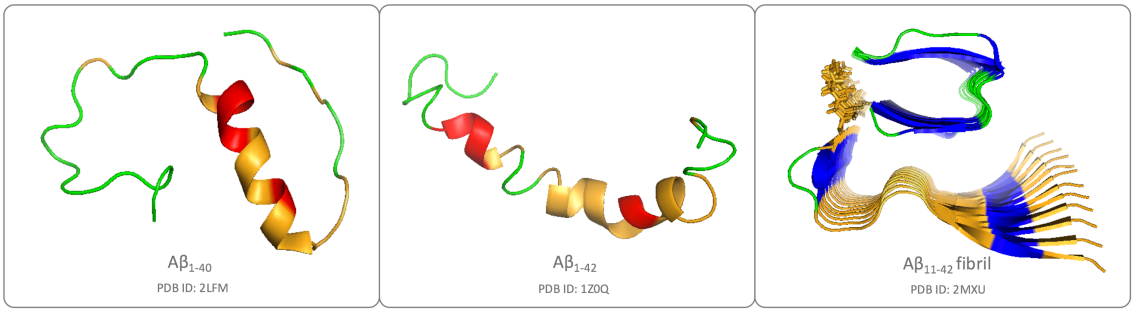

Figure 3.34. Aβ structures spatial representations labelled with the interacting residues. A. Aβ(1-40) structure in aqueous environment (PDB ID: 2LFM) submitted Vivekanandan *et al*. (2011) forming a more compact structure and a helix between residues H13-D23. B. Aβ(1-42) structure in apolar environment (PDB ID: 1IYT) published by Crescenzi *et al*. (2002) forming two α-helices in residues S8-G25 and K28-G38 linked by a β-turn. Regions interacting with the antibody (residues suffering extreme line broadening) from our NMR spectra in presence of the STAB-Mab) are colored in yellow.

Nonetheless, chemical shift perturbations are not very big in comparison with other published works, leading us to support in a bigger manner our epitope mapping hypothesis on the height and extreme line broadening peak data. Such observations, together with the variation of peak

intensity and shifting during the intermediate titrations may point to that the antibody does not radically alter the peptides´ structure, but stabilize one of the major structures already present in the solution meanwhile impeding its aggregation.

For both Aβ(1-40) and Aβ(1-42), according to studies published by Paravastu *et al.* (2008) (PDB ID: 2LMN) [120] and Xiao *et al.* (2015) (PDB ID: 2MXU) [538], the N-terminal and central regions where we observed significant influence of the presence of the STAB-Mab seem to play important roles in the formation of β-sheet structures and Aβ aggregates (Figure 3.33, 3.35).

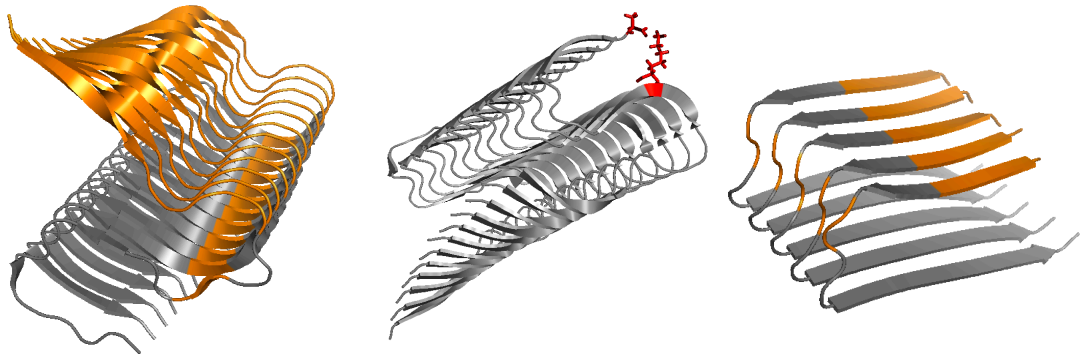

Figure 3.35. Aβ fibrillar structures representations labelled with the interacting residues. A. Fibril structure (PDB ID: 2MXU) solved by Xiao *et al.* (2015) by NMR in polar ambient formed from 1(1-42) Aβ peptide showing a triple β-sheet motif [538]. B. Fibril structure (PDB ID: 2BEG) solved by Luhrs *et al.* (2005) where residues 18-42 form a β-strand-turn-β-strand motif that contains two intermolecular, parallel, in-register β-sheets [118]. Orange-colored regions represent the residues disappearing in our NMR spectra in presence of the STAB-Mab. C. Solved structure of Aβ1(1-42) (PDB ID: 2MXU) highlighting the proximity and interaction of the residues K28 and A42 described by Xiao *et al* (2015) [538].

Regarding the C-terminal region, the only residue that suffered extreme line broadening, K28, has been reported to function as an important β-hairpin stabilizer in several solved structures by forming salt bridges with A42 [538] and N23 [562] residues. A preferential interaction with the STAB-Mab might preclude this β-hairpin stabilizing effect (Figure 3.35).

Characterization final conclusions

The data from NMR experiments are partially in agreement with what we observed in the ELISAs results, where the antibody showed to bind several Aβ fragments, from residues 1 to 40. However, STAB-Mab showed the highest affinity for the Aβ(29-40) fragment in the ELISAs, meanwhile, according to NMR data, there are no residues interacting with the antibody in such region. According to the NMR results, most of the residues interacting are within the first 23 amino acids of the peptide (Figure 3.32), with the exception of the K28. A feasible explanation for the disagreement between NMR and ELISA results would be in the different spatial structures that the complete Aβ peptide and the Aβ(29-40) fragment can acquire in the different conditions of each assay. Meanwhile, in the ELISA the fragments are absorbed in the plastic well through hydrogen bonds coated under a high pH (carbonate/bicarbonate buffer pH 9.4), in the solution NMR, residues are in suspension at a physiological pH. It exists the remote possibility that the Aβ(29-40) fragment could adopt some spatial conformation under determined conditions that mimics some antibody preferred structures.

The NMR data would also confirm some of the observations from in the ThT-monitored Aβ aggregation experiments. The ThT is an intercalant compound which intercalates inside the inner groove of the β-sheet and interacting mainly with the tyrosine residues [528]. Previous experiments confirmed that STAB-Mab is capable of binding not only monomers, oligomers and fibrils, but also is able to completely impede Aβ aggregation.

With the available techniques and collaborations, we tried to unveil some of the characteristics of STAB-Mab. We centered our efforts in trying to find the basis for the STAB-Mab behavior, to better understand its mechanism when used not only with analytic purposes; comparing it with several gold-standards in a number of techniques; but also, and more importantly, with

therapeutic aim. Data from these characterization experiments may confirm some interesting characteristics of STAB-Mab. Although with a slightly higher preference of STAB-Mab for Aβ(1-42) peptide than for the Aβ(1-40) it also maintains an outstanding affinity for the Aβ(1-40) and other peptide fragments and aggregated species [468]. This flexibility for binding different structures may make this antibody a interesting option for passive immunotherapy [324, 334, 336].

In comparison to other similar therapy-oriented antibodies, Bapineuzumab interacts with the N-terminal region (Figure 1.24), while Solanezumab interacts with a more central region (Figure 1.25), but both of them stabilize a sort of helical conformation in the Aβ peptide [324, 428], something feasible to happen with the STAB-Mab. On the other hand, Crenezumab (very similar epitope sequence to the STAB-Mab, Figure 1.26) and Ponezumab target central and C-terminal residues (Figure 1.27), respectively, and stabilize extended coil conformations [430, 328]. Regarding the new generation of fully-human antibodies, Gantenerumab is capable to bind both monomers and fibrils, in a similar way to STAB-Mab, and X-ray diffraction solved structures showed that the monomeric Aβ peptide acquires an extended-coil conformation (Figure 1.28) [118]. Aducanumab, the most recent and promising new generation antibody recognizes a very compact N-terminal epitope in an extended-coil conformation [331]. STAB-Mab observed epitope has important similarities to some of these therapeutic antibodies, such as Solanezumab or Crenezumab, although its binding profile also holds similarities with other antibodies such as Gantenerumab (Table 1.10).

STAB-Mab high affinity, its broad neutralization spectrum, together with its widespread epitope are quite special characteristics that may deserve better understanding. The antibody-antigen interface should be studied through techniques such as X-ray crystallography. Data from such experiment would enlighten several doubts regarding the antibody´s preference for one or another structure, from monomers to fibrils and its influence in such structures.

3.4.3.STAB-Mab *in vivo* pre-clinical trial discussion

Numerous active and passive immunotherapeutic approaches to AD are currently under investigation at both experimental and clinical stages (check Alzforum database) [320, 323, 324, 329]. Some of these studies have suggested that elicited as well as therapeutic monoclonal antibodies may cross the BBB. Considering that only a small fraction of antibodies may reach the brain parenchyma [546], the peripheral-sink hypothesis for Aβ-related neuropathologies [471, 472] might be a very plausible mechanism responsible for some the observed therapeutic effects of immunotherapy protocols.

Accordingly, we tested such sink hypothesis by attaching STAB-Mab to PEGylated liposomes to increase multivalency and improve vesicular avidity for Aβ in serum/plasma. We initially assessed whether immunoPEGliposome can suppress Aβ uptake by brain capillary endothelial cells while mediating Aβ (monomers and oligomers) clearance by macrophages *in vitro* [468]. On the other hand, liposomal presence dramatically accelerated Aβ uptake by macrophages through both Fc- and complement-receptor mediated processes, presumably as a result of avid and stable liposome-Aβ complex/aggregate formation [468].

The biophysical characteristics of the engineered immunoPEGliposomes were in line with guidelines necessary for achieving prolonged circulation times [540, 541], and therefore suitable for parenteral administration. We chose an intraperitoneal route of injection for gradual delivery of Lip-MAb to the blood circulation via stomata in diaphragm, and associated regional draining lymphatic channels. The extent of vesicular PEGylation described here is known to minimize immunoliposome capture by peritoneal and regional lymph node macrophages, while improving their drainage into the lymphatic system [541]. The dosing schedule was every three weeks, and far less frequent compared with other recently described Aβ-specific nanoparticle dosing [469,468], as to minimize possible immunogenicity and improve safety [542].

The *in vivo* results demonstrated that Lip-MAb was capable of improving AD pathology in “aged” mice on repeated intraperitoneal injection compared with an equivalent dose of free antibody. Here, Lip-MAb treatment dropped circulating levels of Aβ considerably. This presumably resulted from improved liposomal avidity for circulating Aβ resulting in the formation of stable immune complexes susceptible for rapid clearance by macrophages of the reticuloendothelial system, as Lip-MAb structures are unlikely to reach the brain parenchyma in the absence of targeting ligands [543]. This suggestion is further supported by evidence of their poor uptake when bound to Aβ by

hCMEC/D3 cells *in vitro* [468]. Again, the observed reduction of brain Aβ levels with Lip-MAb dosing is consistent with vesicular impact on circulating Aβ levels and the peripheral-sink hypothesis. The effect of Lip-MAb treatment on Aβ brain burden not only correlated with the reduction of the ratio of hyperphosphorylated tau to total tau, but was further associated with a strong reduction in GFAP-positive cells (particularly in the hippocampus) [451, 453, 455]. These observations may reflect some capacity for damaged neurons to recover. We, therefore, propose that immunoPEGliposome therapy may diminish neuronal stress induced by the Aβ burden, and reduce gliosis. It is also possible that the peripheral immunoPEGliposome therapy may have triggered some proteolytic degradation of Aβ in the brain. It has also been suggested that circulating Aβ may cause abnormal vascular reactivity in the absence of vascular deposition or vessel wall dysfunction [544]. Accordingly, Lip-MAb-mediated reduction of Aβ and particularly Aβ(1-42), in the blood could represent a promising therapeutic strategy over recently described AD-specific nanomedicines [469, 485] (due to higher affinity for Aβ and less frequent dosing) to prevent frequent strokes due to the amyloid deposition in small arteries and capillaries in vessels affected by amyloidosis [48, 544]. Indeed, it has already been demonstrated that Aβ(1-42) is essential in parenchymal and vascular amyloid deposition [48, 49, 50, 145].

Our results also showed some beneficial therapeutic effects of free STAB-MAb administration in "aged" animals. Particularly by considering the changes in the level of GFAP protein and in the fact that Aβ levels in blood were increased respect to the control group meanwhile in brain were maintained at levels of the start of the treatment. This may have been due to the antibody translocation into the brain, as it has been observed that around 0.1%of the circulating immunoglobulins can cross through and enter the brain parenchyma [546]. Indeed, it has been recently observed [548] that when antibodies bind Aβ while living free certain N-terminal residues, passage across the BBB through RAGE is significantly improved. Moreover, a number of studies have suggested altered functionality of the BBB in "aged" transgenic APP/PS1 mice [545] may permit macromolecular (e.g., IgG) extravasation from the blood into the brain parenchyma. Within these notions, the quantitative contribution of the peripheral-sink effect to the final observed therapeutic effect of STAB-MAb, however, is difficult to measure, since depletion of circulating Aβ was not substantial. The results of *in vitro* studies with THP-1 phagocytes also confirmed that free STAB-MAb could marginally increase the uptake of labelled-Aβ compared with Lip-MAb. However, we cannot discard the possibility that administration of higher doses of STAB-MAb and/or shorter injection intervals would have improved its therapeutic efficacy, but in parallel, this could have induced immune reactions. Nevertheless, on the basis of our findings, we further suggest that a combination therapy involving free STAB-MAb (targeting brain Aβ and/or anti-tau antibodies (targeting hyperphosphorylated, aggregated, and insoluble tau in the brain), and immunoPEGliposomes (targeting peripheral Aβ may be even more effective in improving AD pathology.

Finally, in contrast to "aged" animals, complete lack of AD improvement in "adult" mice is quite perplexing. These may have been due to insufficient antibody translocation into the brain parenchyma (as the BBB integrity is not yet compromised) and/or inadequate antibody or Lip-MAb dosing. In line with the peripheral-sink hypothesis, another plausible explanation is differential reactivity of STAB-MAb with circulating forms of Aβ in "adult" animals. For instance, alterations of plasma protein composition and concentration (e.g., some apolipoprotein isoforms) may induce some conformational transformation of circulating Aβ [547], thereby masking Aβ binding epitopes. These possibilities may require further investigation.

3.4.4.Minibody 2 *in vivo* pre-clinical trial discussion

Addressing a different focus on AD immunotherapy, in this *in vivo* study with Minibody 2 we tried to confirm if the modifications on STAB-Mab actually improved the brain entry and the therapeutic effect in mice.

As previously showed, Minibody 2 is a chimeric antibody wearing a scFv from STAB-Mab combined with an anti-insulin human scFv and a lower molecular weight that, together, would virtually improve the BBB crossing and brain entry. To prove this, we administrated 12 month-old mice with Minibody 2 (150 μg/3 weeks) and PBS, analyze several biomarkers among Aβ and other synaptic markers and finally performed a NOR test for analyzing any memory improvement derived from the treatment.

Regarding Aβ, Minibody 2 treatment was able to maintain blood Aβ(1-40) and Aβ(1-42) levels unaltered compared to the beginning of the trial, not as the control treatment, where levels were increased around 100%. It seems that Minibody 2 is capable to bind plasma Aβ and somehow trigger its clearance from blood. However, the differences between animals from the same group are too big for considering results significant. In brain, only Aβ(1-42) was measured, and no differences were found, suggesting that Minibody was not capable to cross the BBB or, at least, not in the sufficient amount to exert a significant effect in Aβ(1-42) burden.

Concerning other stress, vascular and synaptic biomarkers, the biggest differences are observed in APP and GFAP levels, biomarkers similarly affected by the treatments. Minibody 2 administration provoked a 500% increase of APP and GFAP production (or accumulation) respect to the WT group and around 50% increase respect to the control group administrated with PBS, denoting some sort induced neuronal stress by the Minibody 2. The approximately 300% increase of these biomarkers in the control Tg mice respect to the WT group may also point to genotype differences or maybe the administration of the immunosuppressant Fortecortin. On the other hand, BACE-1 expression seems to be slightly reduced in the Minibody 2 group, which could have contributed to elevate even more APP levels. Interestingly, P120 (p120 catenin, a component of the cadherin-catenin complex involved in synaptic maintenance and APP gamma-cleavage [549, 550]) and PSD95, two synaptic markers, appear elevated in Minibody 2-treated group respect to the control, pointing to a hypothetically neuroprotective effect of the treatment.

Performance in terms of memory improvement, NOR test results did not show significant improvements owing to Minibody 2 treatment. However, if we represent data in terms of percentage of the total time exploring both objects in the novel object, we can observe that Minibody 2 treated mice spent almost 6% more in the novel object (73.4%) than the control group (68.2%), and even a 2% more than the WT mice (72.3%). Nevertheless, these results are not sufficient to ensure that Minibody 2 administration improves nor worsens memory output in mice.

Altogether, these results do not represent a very promising scene for the Minibody 2 as it is configured. The reduced binding affinity for Aβ *in vitro* and the strange behavior in the ELISAs may have hobbled its purpose. It seems, as shown in the previous chapter that, in order to maintain the Aβ binding capacity of STAB-Mab, it may need both antigenic terminals. There are other unexplored ways to re-engineer the STAB-Mab for increasing BBB crossing, such as FC fusion proteins [551, 552]. However, until date, none of these initiatives have reached clinical phases.

Finally, the lack of an experiment for confirming the Minibody 2 BBB crossing into brain parenchyma due to several technical limitations during the process leaves us with a serious doubt: Is it actually working the anti-insulin scFv for helping the antibody to enter the brain through the insulin receptor? A simple way to ascertain this question could be to isotopically label a batch of Minibody 2 and administrate it to some animals. This could allow monitoring antibody efflux-influx from brain or any other organ ratios and times.

4. Anti-tau antibodies

Within the pursuit of new effective early diagnostic tools to achieve effective therapies for AD, a unique consortium combining neuroscientists, nanotechnologists, molecular imaging experts, clinicians, and enterprises was formed. This European H2020 funded initiative is the PANA project and is focusing its effort to develop nanostructures, in GMP-like form, that specifically recognize very-early molecular markers of AD for *in vivo* theranostic purposes. Nanostructures will be detectable by means of non-invasive imaging methodologies (MRI/PET) and will have the potential to include treatments for the disease to provide a complete theranostic action (https://www.panaproject.eu).

Although the precise cause of synaptic dysfunction and neurodegeneration at early-stages in AD is still not clear, in recent years the importance of tau oligomers, tau protein, and its post-translational modifications in the early pathophysiological processes of AD has become increasingly clear. In this regard, determination of different forms of tau protein in brain, CSF and also in blood has been postulated as a powerful tool for detection and monitoring of the disease in different stages and there is clear evidence of a profile of tau and other biomarkers modifications during AD progression [508]. However, there is no robust marker of tau oligomers for clinical diagnosis purposes available. In this direction, this project is focused on the development of multifunctional nanostructures for non-invasive assessment of tau oligomers in the brain for early diagnosis of AD. Moreover, due to the current absence of highly effective therapies for AD, the need to evaluate therapies targeting on post-translational changes of tau protein or tau oligomers has become a very attractive option.

In the diagnostic area, multimodal PET/MRI imaging has gained attention due to the complementary advantages of those technologies: It provides a combination of the exquisite structural characterization of tissue provided by MRI with the extremely high sensitivity of PET imaging [508]. The aim of the new generation of hybrid imaging scanners is to precisely and simultaneously co-register PET and MRI dynamic data (for example flow and metabolism or flow and delivery), and so the introduction of this multimodal imaging technology to clinical practice has generated the urgent need for bimodal imaging agents. Moreover, the use of dual PET/MRI nanoparticle contrast agents is expected to improve the spatial resolution (the smallest object which can be detected) and sensitivity (smallest intensity change which can be found) of each modality [508]. Therefore, PANA project aims to develop nanostructures that specifically recognize very-early molecular markers of AD for *in vivo* diagnostic purposes. These nanostructures would be detectable by means of non-invasive imaging methodologies (MRI/PET) for *in vivo* AD diagnosis purposes.

As part of the PANA Project, our main objective was to generate the new anti-tau antibodies that later on will be used in high affinity nanostructures focused on tau oligomers, which can be used as a theranostic agent for diagnosis of AD at early stages of the disease as well as a new therapeutic approach for this neurodegenerative disease.

Based on recently high-impact published works [219, 571], it was decided to develop a new monoclonal antibody for targeting acetylated tau. The almost complete absence of antibodies targeting acetylated tau, together with the increasing evidences of the importance of such posttranscriptional modifications in tau aggregation and loss of function pushes the consortium towards it. However, for increasing the success chances of the project, it was decided to develop a second antibody raised against phosphor-tau, one of the main suspects related to pathological tau during the last decades [181, 182, 391, 398]. The focus in this case was to find a similar or better antibody to the gold-standard AT8 [300] with analytical purposes but also with potential for diagnosis and therapy.

4.1. Immunogen selection and preparation

Two sequences of tau protein were chosen as immunogens for the new antibodies development. Each one with different post-transcriptional modifications based on their relation with different disease states and pathologic mechanisms.

One fragment, including residues belonging to the Proline-rich domine of tau, was chosen according to some recent findings supporting a relevant role of some acetylated residues in

microtubule assembly, tau degradation and aggregation. Particularly, some sites associated to the early pathology in both the brain of human AD patients as well as tau mice models relevant for the project were selected [218,219]. One of such acetylations has also been recently linked to microtubule destabilization and tau degradation inhibition [216]

The other fragment encompasses a sequence of residues close to repeated domain that seem to be an important target of several phosphorylations, very well-known post-transcriptional modifications related to microtubule reduced affinity and aggregation of tau. The election of this immunogen was given to the need of having a “backup” more reliable for aggregated tau targeting in the case of failing in the objective of finding a specific antibody for the acetylated tau [181,182,183,184].

Note: Due to confidential issues, it is not possible to disclose the selected sequences and post-transcriptional modifications of the immunogens.

4.2. Immunization and mice screenings

10 BALB-C mice (5 mice with each immunogen) were inoculated with the immunogens fused with KLH immunogenic protein 3 times including during the last 3 weeks and with a last intravenous boost 3 days before sacrificing and spleen harvesting (Figure 4.1).

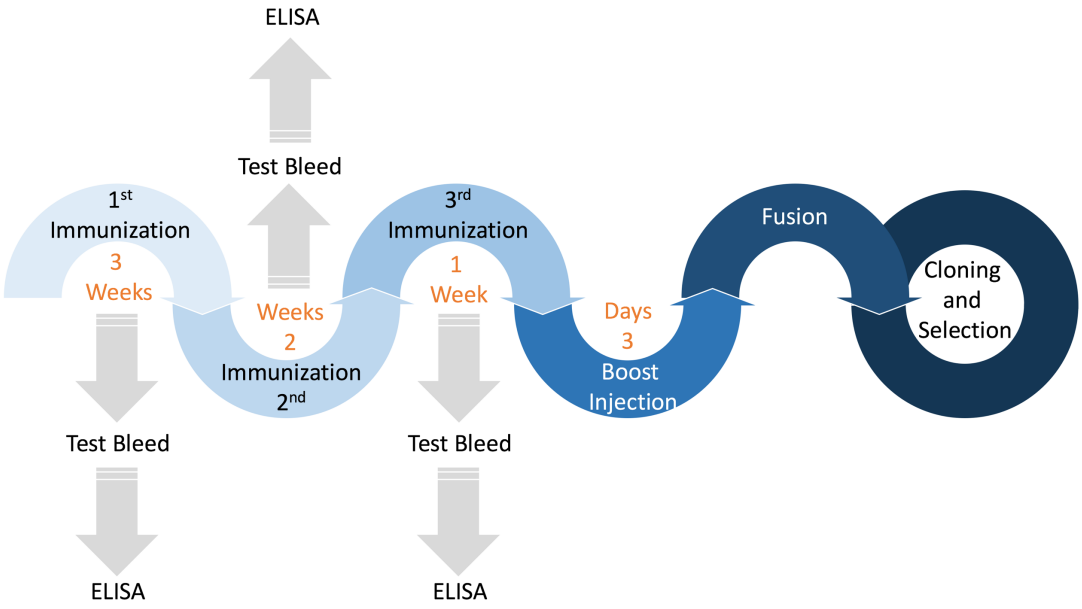

Figure 4.1. Immunization scheme. Mice were intraperitoneally injected 3 times with the immunogen plus adjuvant and a final intravenous boost without adjuvant just 3 days before harvesting spleens and performing the fusions.

Before the last boost, 2 out of 5 mice inoculated with the phosphorylated fragment had developed a good immunologic response while all the mice inoculated with the acetylated fragment showed high antibody production. All mice were used for fusion for increasing the chance of finding a specific antibody, especially difficult in the case of the acetylated immunogen (Figure 4.2).

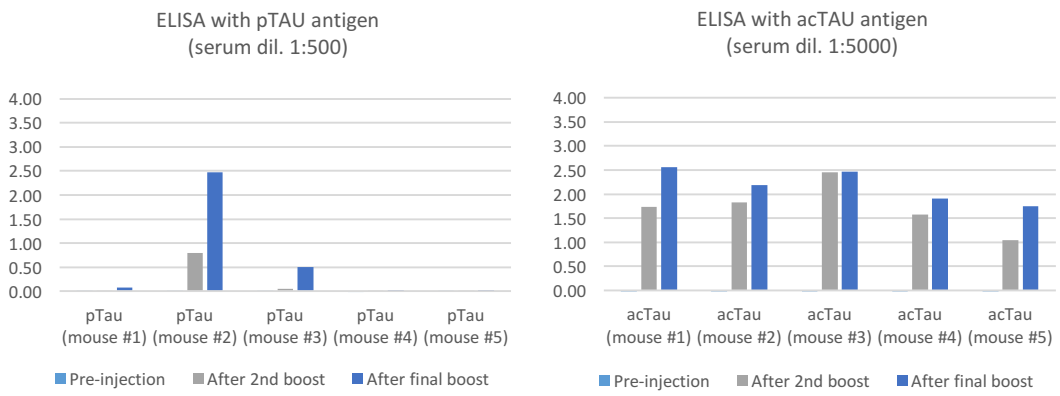

Figure 4.2. Immunization graphics for both acTAU and pTAU immunogens for the 10 mice bleedings before the start of the treatment and after every inoculation. It was strongly noticeable that the immunogenicity of the acTAU peptide (all mice reacted) (A) it was remarkably higher than with the pTAU immunogen (B), against which only two mice showed to produce the wanted antibodies.

4.3. Selection and production of best clones

4.3.1.Semi-solid medium-based selection

Mouse 3 immunized with the phosphorylated peptide and the mouse 2 immunized with the acetylated one were selected for fusion and screening via semi-solid method using the ClonaCell HY kit. The fusion mixes were plated in T75 culture flasks and grown for 24 hours for reducing the fibroblasts contamination in the semisolid medium. After that, fused cells were plated in 6-well culture plates using the semi-solid selection medium following the instructions of the manufacturer.

A total of 14 plates (7 for each mouse) were filled with the fusion product and incubated for 15 days. After that, the isolated colonies were picked and plated in 96-well plates with liquid medium. When most wells were about 75% confluent, the plates were screened for reactivity against the immunogens (Figure 4.2). A total of 68 positive colonies for pTAU immunogen and 33 positive colonies for acTAU immunogen were isolated in 96-well plates and submitted to a second negative screening.

Figure 4.3. Scheme and results of the first screening of the picked colonies from semi-solid medium. 68 positive colonies for pTAU immunogen and 33 positive colonies for acTAU immunogen were isolated in 96-well plates.

After positive clones were identified, we selected them for a second negative screening for the peptides without post-transcriptional modifications. Unfortunately, we did not manage to isolate a single specific clone for the immunogens wearing the post-transcriptional phosphorylations nor acetylations. Only 2 clones for the phosphorylated immunogen (K1D1 and K2D5), and 3 clones (K1A1, K1C3 and K1D5) for the acetylated peptide showed antibody production above cut-off levels (Figure 4.4). These clones were expanded and stored in LN2.

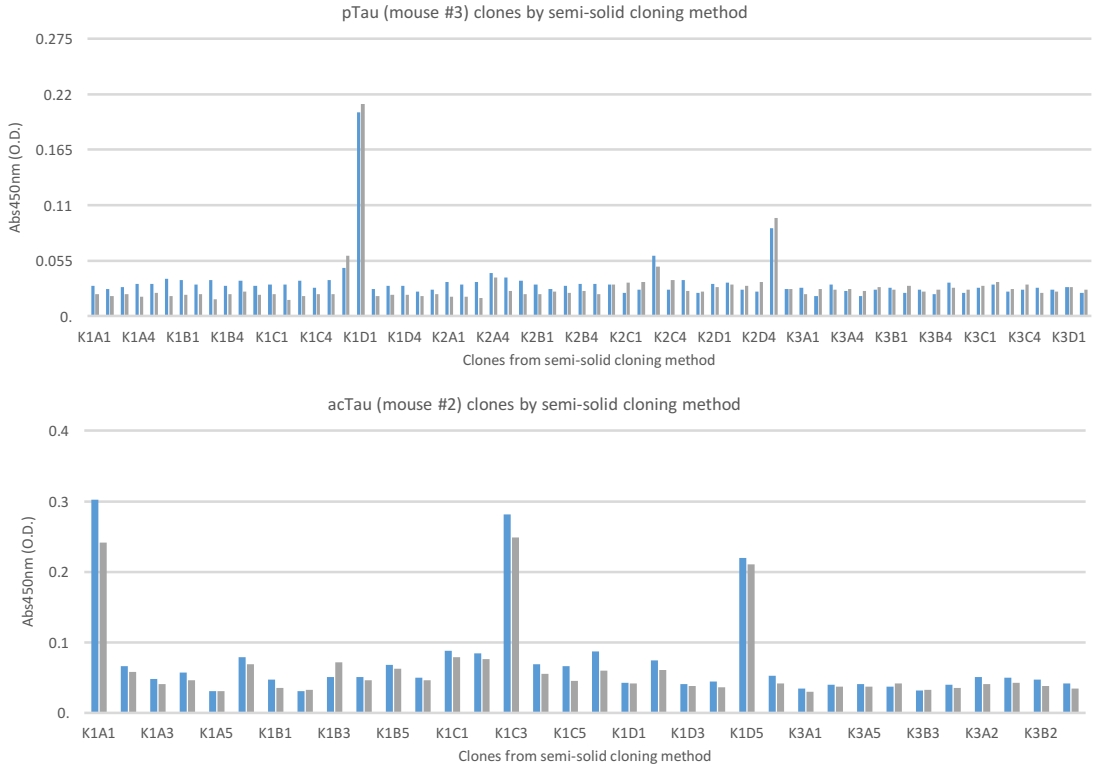

Figure 4.4. Results of the second screening of the anti-pTAU (A) and anti-acTAU (B) clones obtained by the semi-solid medium technique. There was not possible to identify any clone expressing only specific antibodies against any of the peptides wearing the post-transcriptional modifications (blue bars) instead the peptides without post-transcriptional modifications (grey bars). Coating: 1 µg/mL of peptide. Secondary ab used: mice IgG1anti-gamma chain.

4.3.2.Traditional limiting dilutions-based selection method

On the other hand, results of the traditional method using fusion and limiting dilution for isolating clones, were different. The fusions were performed in liquid medium and two 96-well plates were seeded for each mouse, 16 96-well “Master Plates” in total. After 15 days of feeding with HAT-supplemented medium, most of the wells were about 75% confluent and was time for the first screening prior to limiting dilution. Results are schematized below, including the graphic representation of the limiting dilution results from some of the selected wells from the Master Plates” (Figures 4.5 and 4.6).

pTau (mouse #1)

Selection and Cloning

Master Plate #1A

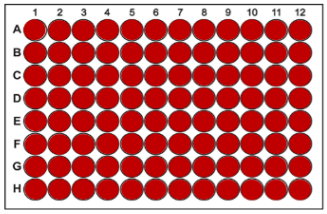

Master Plate #1B

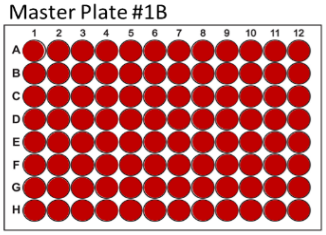

Limited dilution cloning - Screening

Did not proceed to limited dilution cloning (no positive polyclonal where found)

LEGEND:

- Monoclonal reactive only with pTau
- Monoclonal reactive with pTau and normal Tau
- Poly/monoclonal non-reactive with pTau nor normal Tau
- Clonality not achieved
- Polyclonal reactive with pTau (not proceeded to limited dilution cloning)
- Polyclonal reactive with pTau (proceeded to limited dilution cloning)

pTau (mouse #4)

Selection and Cloning

Master Plate #1A

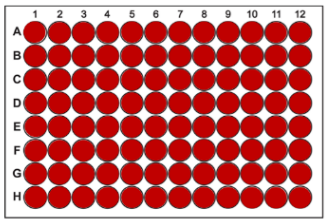

Master Plate #1B

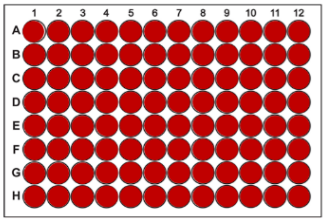

Limited dilution cloning - Screening

Did not proceed to limited dilution cloning (no positive polyclonal where found)

LEGEND:

- Monoclonal reactive only with pTau
- Monoclonal reactive with pTau and normal Tau
- Poly/monoclonal non-reactive with pTau nor normal Tau
- Clonality not achieved
- Polyclonal reactive with pTau (not proceeded to limited dilution cloning)
- Polyclonal reactive with pTau (proceeded to limited dilution cloning)

pTau (mouse #5)

Selection and Cloning

Master Plate #1A

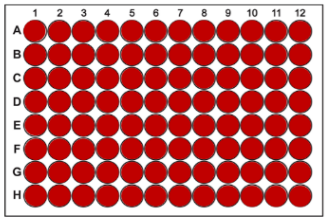

Master Plate #1B

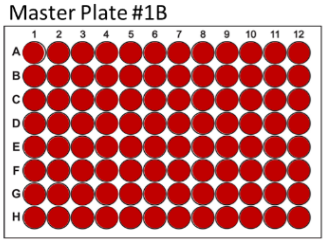

Limited dilution cloning - Screening

Did not proceed to limited dilution cloning (no positive polyclonal where found)

LEGEND:

- Monoclonal reactive only with pTau
- Monoclonal reactive with pTau and normal Tau
- Poly/monoclonal non-reactive with pTau nor normal Tau
- Clonality not achieved
- Polyclonal reactive with pTau (not proceeded to limited dilution cloning)
- Polyclonal reactive with pTau (proceeded to limited dilution cloning)

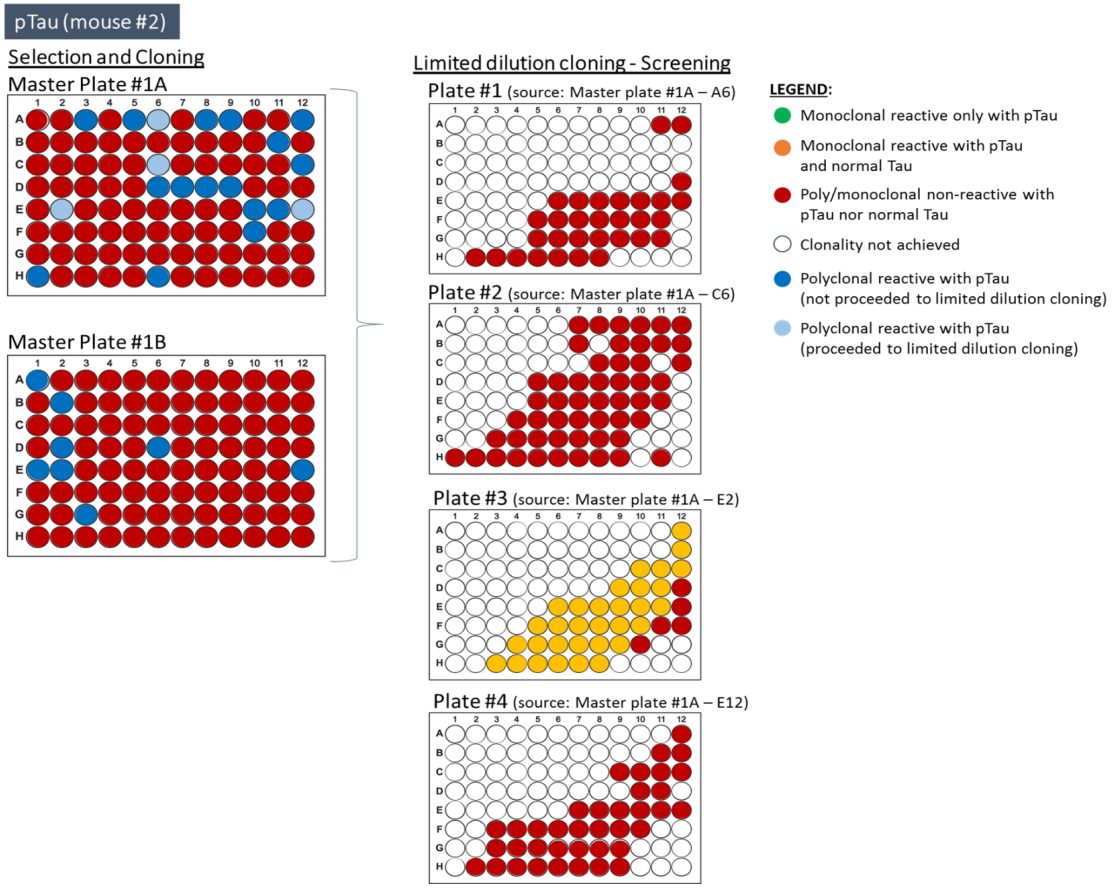

Figure 4.5. Schematic results from the pTau-immunized mice. There are shown "Master Plates" first screening and the subsequent screening for specificity of some clones isolated from "Master Plates" selected wells. Two specific clones isolated from from Plate#3, well C2 - namely, clones D4 and B6. Screening results are showed below.

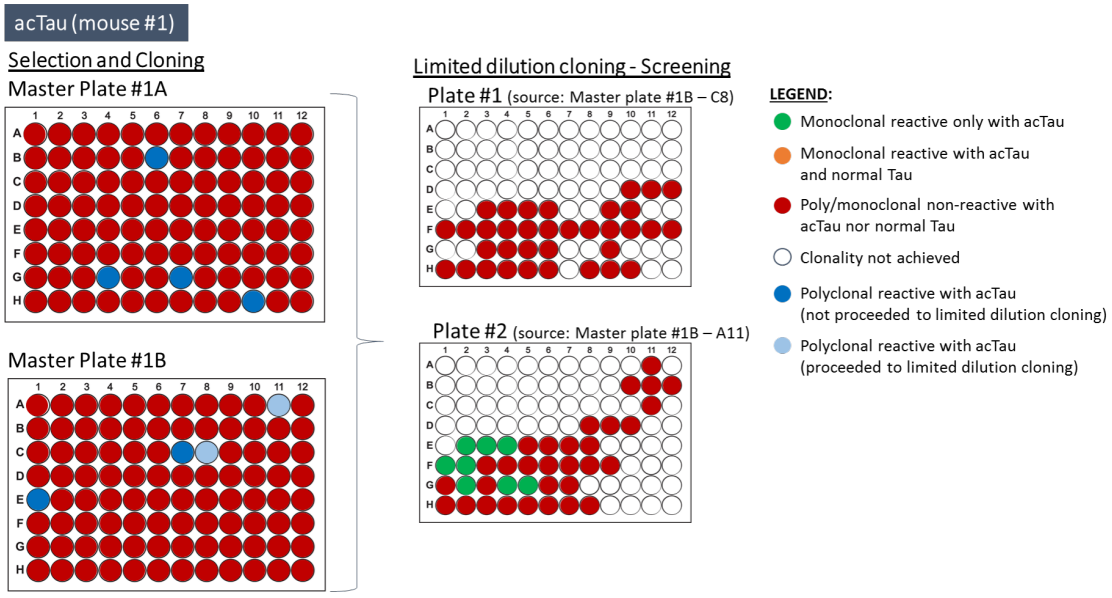

acTau (mouse #3)

Selection and Cloning

Master Plate #1A

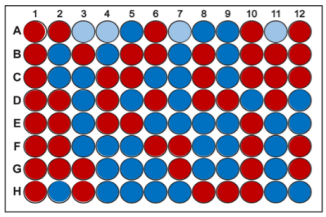

Master Plate #1B

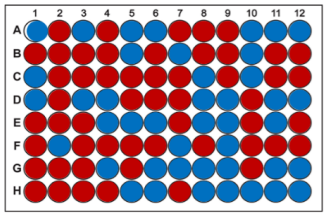

Limited dilution cloning - Screening

Plate #1 (source: Master plate #1A – A3)

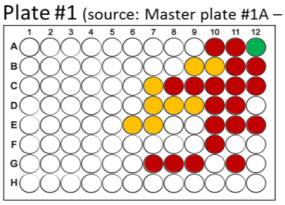

Plate #2 (source: Master plate #1A – A4)

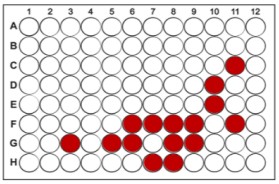

Plate #3 (source: Master plate #1A – A7)

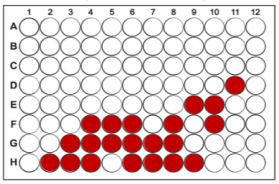

Plate #4 (source: Master plate #1A – A11)

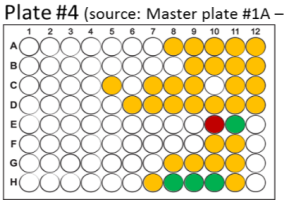

LEGEND:

- Monoclonal reactive only with acTau
- Monoclonal reactive with acTau and normal Tau
- Poly/monoclonal non-reactive with acTau nor normal Tau
- Clonality not achieved
- Polyclonal reactive with acTau (not proceeded to limited dilution cloning)
- Polyclonal reactive with acTau (proceeded to limited dilution cloning)

acTau (mouse #4)

Selection and Cloning

Master Plate #1A

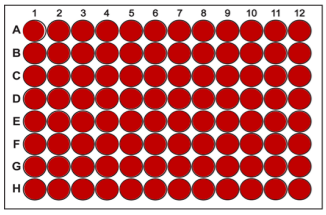

Master Plate #1B

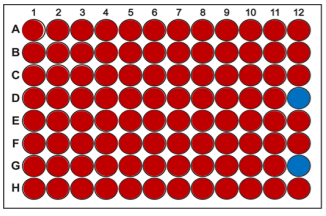

Limited dilution cloning - Screening

Did not proceed to limited dilution cloning

LEGEND:

- Monoclonal reactive only with acTau
- Monoclonal reactive with acTau and normal Tau
- Poly/monoclonal non-reactive with acTau nor normal Tau
- Clonality not achieved
- Polyclonal reactive with acTau (not proceeded to limited dilution cloning)
- Polyclonal reactive with acTau (proceeded to limited dilution cloning)

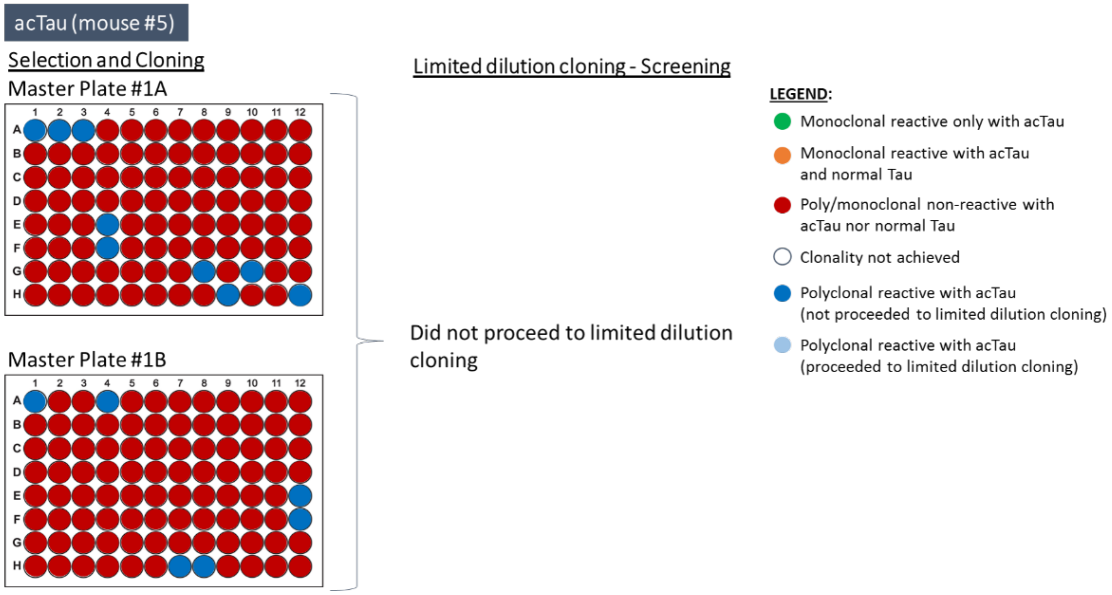

Figure 4.6. Schematic results from the acTau-immunized mice. There are shown "Master Plates" first screening and the subsequent screening for specificity of some clones isolated from "Master Plates" selected wells.

Cells from 119 wells on the master plates were positive for the acetylated peptide and 28 were positive for the phosphorylated peptide. Those cells were expanded in cell culture 24 and 6-wells prior to seed T75 flasks and stored in LN2 or cloned by limiting dilution for obtaining single clone cell lines producing specific antibodies for the immunogens. The clones resulting were tested for assessing antibody production yields and selected for subcloning or expansion and antibody production (Figure 4.7).

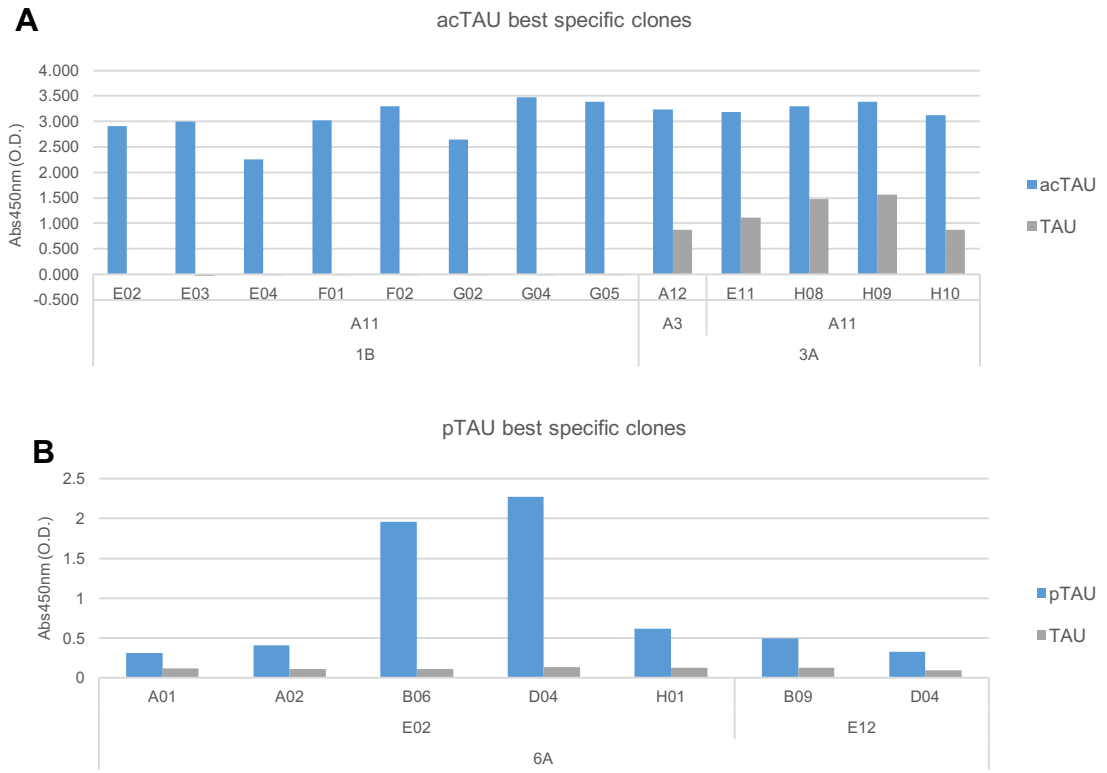

Figure 4.7. ELISA results of the screening of the best clones producing anti-acTAU (A) and anti-pTAU (B) antibodies. Coating: 1 µg/mL of peptide. Supernatant dilution 1:1000. Secondary ab used: anti-gamma chain of mice IgG1. (C) 1BA11F01 clone and derived subclones screening. Coating: 1 µg/mL of peptide. Primary ab dilution 1:1000. Secondary ab used: anti-gamma chain of mice IgG1

The 4 lines derived from of acTAU 1BA11F01 subcloning (Figure 4.8) were expanded and the purified product (1 mg each, produced following the protocol described previously for the STAB-Mab) was delivered among the purified product from anti-pTAU 6AE02B06 and 6AE02D04 to the partners of the PANA project (labelled in red in Figure 4.9) for further characterization.

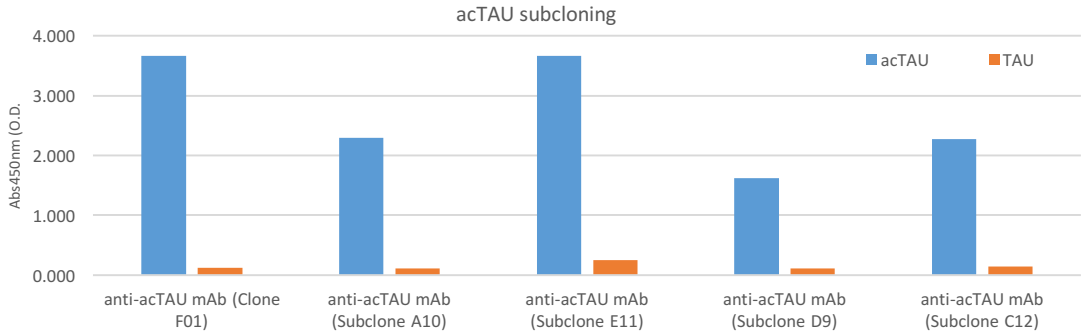

Figure 4.8. Histogram with ELISA results from the screening of the best subclones producing anti-acTAU derived from 1BA11F01 clone.

After 3 subclonings and subsequent screenings we reduced the pull of more that 140 wells to 12 clones and 5 subclones for the acetylated immunogen and 7 clones for the phosphorylated immunogen (Figure 4.9).

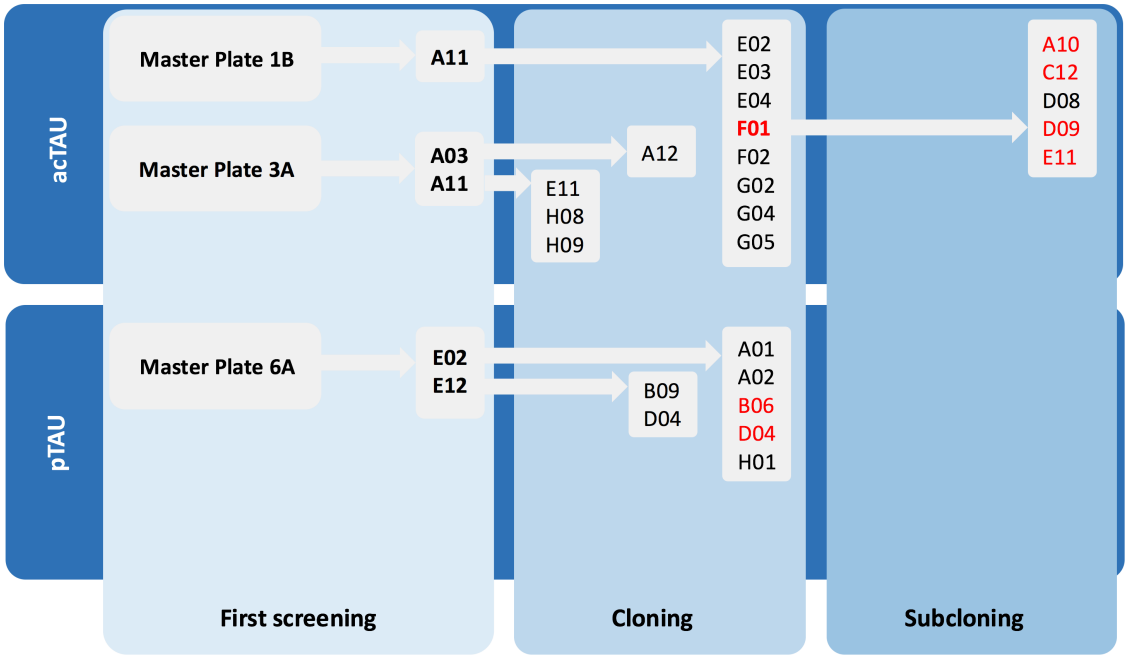

Figure 4.9. Scheme of all the subclones obtained by traditional fusion and selection method. Beginning with certain wells in the "Master Plates" and making several limiting dilutions we managed to isolate several clones (in bold) and subclones for each immunogen. Some of them were selected for expansion and antibody production for subsequent characterization (labelled in red).

4.4. Chapter 4 discussion

The acetylated peptide was chosen as the first immunogen based on previous partners´ experiences, considering the animal and cell models that will be used ahead in the PANA project and, obviously, based on the most recent publications assessing the tau acetylation´s role in AD pathology. As previously remarked, the selected acetylation sites have been associated to the

early human AD pathology stages [218, 219], and have also been recently linked in the same way to microtubule destabilization and tau degradation inhibition [216].

The second chosen fragment, including several phosphorylated residues is close to the repeated domain, seems to be an important target of several well-known post-transcriptional phosphorylations related to microtubule reduced affinity and aggregation of tau. This fragment harbors several phosphorylated residues that have been linked to microtubule reduced affinity of tau [181, 182, 183, 184, 510]. As previously pointed, the election of this immunogen was also given to the need of having a more solid option for aggregated tau targeting in the case of failing in the primary objective of finding a good antibody for the acetylated tau.

The first screenings performed in the immunized mice showed good immunoreaction to the acetylated immunogen in all mice, but only two mice (2 and 3) injected with the phosphorylated immunogen developed detectable antibodies against the peptide. Although the reason is unknown, due to both peptides were conjugated with the same KHL carrier protein, the same adjuvants, and the same protocols, it is possible that the phosphorylations are not as immunogenic as the acetylations in tau peptides.

After fusion and selection, only 2 positive clones for the phosphorylated peptide and 3 for the acetylated peptide were obtained from the semi-solid method using the kit from ClonaCell. Moreover, none of the isolated clones from the semi-solid method resulted to be specific for the peptides wearing the acetylations or phosphorylations. Once again, although this could be due to the mice selected for fusions and clonings using the semi-solid method were not the ones showing the highest immunoreactivity in the screenings, the reason is unclear.

Using the limiting dilution traditional method, we obtained 119 positive wells from the acTAU master plates and 28 more from the pTAU master plates which were expanded and added to the LN2 biobank. Afterwards, we started to clone and re-screen these samples for isolating single clones producing antibodies specifically recognizing phosphorylated or acetylated tau peptides and we managed to isolate and expand 5 subclones with good performance and specificity for acTAU immunogen and 2 more for pTAU immunogen (Table 4.1)

Table 4.1. The final selected subclones were sent to the PANA project partners for further characterization, final selection, and nanostructures functionalization.

Anti-acTAU	Anti-pTAU
1B A11 F01 A10	6A E02 B06
1B A11 F01 C12	6A E02 D04
1B A11 F01 D08	
1B A11 F01 D09	
1B A11 F01 E11	

These subclones were cultured and the supernatants purified according to the protocol described using G-protein affinity columns. 1 mg of each purified product was sent to the PANA Project partners for further characterization.

As previously exposed, the importance of finding a reliable and potent tool for targeting these specific pathological forms of tau is remarkable, allowing in the future the use of them (or fragments of them) in the nanostructures designed for diagnosis, for passive immunotherapy or even for delivering other drugs to specific areas in the brain.

Another remarkable aspect is that until date, there is not a unique commercially available monoclonal antibody against any acetylated form of tau [219, 509]. This may be due to the difficulty to elicit a sufficient immunoreaction in the animals against this specific post-transcriptional modification, but in our case, at least, the response to the immunization was more than satisfactory. We will have to wait for the biochemical characterization of our anti-acTAU antibodies to confirm the success of the experiment.

Regarding the pTAU antibody, as we used a similar immunogen, we may expect to observe similar characteristics to the gold-standard AT8, an antibody widely used in research and AD diagnosis for identifying hyperphosphorylated tau and paired helical filaments (PHF) in immunostainings, WB, ELISAs, etc. [181, 182, 183, 184, 391, 398, 510]. The first paper describing a research performed by the PANA consortium using this antibody, “Intranasal insulin activates

Akt2 signaling pathway in the hippocampus of wild-type but not in APP/PS1 Alzheimer model mice", was recently published [572]. In such work, the developed anti-pTAU (clone 6A E02 B06) performed exceptionally, so the researchers opted for using it, instead the gold-standard AT8, for the immunoblottings.

Nowadays, accordingly to NHIS database, only four passive immunotherapy-based drugs reached clinical phases and only 3 are still active [406, 407, 554]. All of them specifically binds extracellular forms of tau, except for the GR7345, that was discontinued in phase I. No one targets intracellular nor acetylated forms of tau, and considering the recently observed importance of these post-transcriptional modifications have in tau-associated pathologies [216, 217, 219, 571], to have the opportunity to develop a monoclonal antibody targeting acetylated tau is a very exciting and encouraging perspective. Now, future actions are conditioned by the characterization results of the isolated clones, what will determine if we must go back for seeking for new clones or, on the other hand, move ahead with the development of the different GMP-like forms of the antibodies and to large-scale production.

5. Conclusions

5.1. Overall discussion

Our data on STAB-Mab characterization, from immunostainings to TEM, allow us to confirm the good performance of the antibody in a variety of conditions, techniques and samples, at the same level to the most used antibodies in clinic and research. Data also encourage us to propose a quite attractive hypothesis for explaining the therapeutic mechanisms of action of the antibody and its potential. It may be possible that the antibody is somehow capable to stabilize the helical structures formed by the Aβ in polar aqueous environments and impede the formation of β-strand structures. By binding most of the residues located in the region His13-Asp23 and the Lys28, directly involved in the formation of such secondary and more complex β-sheet tertiary and quaternary structures, could difficult the aggregation of Aβ and/or even destabilize those pre-formed aggregates. The therapeutic potential behind those mechanisms is remarkable, as it was also confirmed in the *in vivo* assays.

In fact, the multivalent PEGylated immunoliposome-based therapeutic approach tested, that may boost the therapeutic effect through the peripheral depletion of Aβ and/or peripheral-sink effect proved to be highly effective [468]. Something confirmed with another kind of synthetic PEGylated nanoparticles of poly[hexadecyl cyanoacrylate-co-methoxypoly(ethylene glycol) cyanoacrylate] (P(HDCA-co-MePEGCA) in a recently published study using the STAB-Mab [470], where the treatment of AD-like transgenic mice with such nanoparticles led to complete correction of the memory defect; significant reduction of the Aβ soluble peptide and its oligomer level in the brain and significant increase of the Aβ levels in plasma. This study represents the first example of Aβ(1-42) monoclonal antibody-decorated nanoparticle-based therapy against AD leading to complete correction of the memory defect in an experimental model of AD. These pegylated nanoparticle-based approaches seem to be advantageous over other recently described attempts with related AD-specific nanosystems (e.g., sphingomyelin/phosphatidic acid based Aβ-binding liposomes decorated with BBB-specific targeting ligands) [469]. First, NPs-MAb showed improved target binding due to their high avidity, and required less frequent dosing) compared with other contemporary attempts [469, 485], which could minimize possible risks of immunogenic responses. Second, non-PEGylated AD-specific nanoparticles do not circulate for prolonged periods in the blood [469]. This reduces their chance of capturing circulating Aβ prior to their interception by macrophages of the reticuloendothelial system.

In this regard, there is a need of further investigation for better understanding of the mechanisms of action behind the effect of the antibodies we are working with. The crystal structure of the STAB-Mab complexed with the Aβ peptide is mandatory for unveiling the interaction and the mechanism behind the behaviors we have observed in the present work. Moreover, it is still critical to further understand the mechanisms by which those nanotechnology approaches exert their therapeutic efficacy, and within the context of integrated disease progression, and the role of immune system in both AD and nanoparticles processing. Improved understanding of these events may aid the development of multifunctional and personalized AD-specific nanomedicines either alone or more importantly in combination with free antibody therapeutics (e.g., anti-Aβ and/or anti-tau antibodies), and/or interventions that specifically modulate the functionality of the cerebral capillary-endothelial cell interface, nowadays one of the main handicaps in AD therapy [553].

Disappointingly, the chimeric minibodies did not perform as expected. Too many variables could be influencing the results we have observed, from the excessive storage time between the production and the characterization, to their controversial structure, which could be the reason for the lack of affinity of the Minibody 1 and the strange behavior of Minibody 2. It would be also necessary to confirm if the presence of the scFv against human insulin and its human FC increases its chances for crossing the BBB.

Regarding the novel anti-pTAU antibodies developed within this work, promising data from WB using samples from brain animal models and CSF and brain patient´s samples are confirming an exceptional performance, above well-stabilized alternatives such as the gold-standard AT8, of the clone 6A E02 B06. However, controversial results are coming from the analysis of similar samples with the antibodies against acTAU (data not shown). There could be due many reasons: (i) to the mechanism of action of the antibody; (ii) to the actual exposition of the residues that specifically

binds within the full length tau protein; (iii) because of the difficulty to find solid positive and negative controls. This last is a mandatory requisite for a reliable evaluation of the antibodies' performance. After that, further characterization, as it has been performed for the STAB-Mab, including an analysis of its crystal structure complexed with the antigen, should be completed. The remarkable potential of these antibodies must be explored.

5.2. Results summary

The work carried out during the last 4 years have fulfilled all the objectives proposed in this thesis, and left open a great potential for future developments not only within the STAB-VIDA company but also in AD immunotherapy.

The successfully developed anti-acTAU and pTAU antibodies are nowadays under characterization, opening a good start for the design of new diagnostic procedures, optimization of the existing ones and to explore new AD immunotherapeutic approaches targeting new pathologic forms of tau.

The setting up of a whole new facility for production and purification of monoclonal antibodies was a success. STAB-Mab antibody is nowadays ready to be produced in different platforms, purified, stored and sold to the clients.

The characterization of STAB-Mab confirmed some expected features and unveil several new characteristics that make it a very interesting antibody, both for research and therapy. Further analysis should be carried out in order to fully understand the mechanisms of action and the real potential of such antibody.

New therapeutic approaches were addressed in this thesis, using the STAB-Mab as the "core" of the assays. The promising *in vivo* data published in the paper that is part of this thesis and in others open another window to continue exploring the nanoparticle approach for AD immunotherapy.

Although the original antibody from it was derived reported such promising results, Minibody 2 did not seem to perform as well as STAB-Mab. The poor affinity for the Aβ peptide and the unspecific binding to other surfaces made almost impossible to analyse in depth its behavior, and the lack of significant improvements in mice treatment make obvious the need of a re-engineering.

5.3. Final remarks

The time of the rigid model of the "amyloid hypothesis" for addressing such a complex disease as AD and for developing treatments against it has ended. We already have enough evidences for believing that amyloid is not the only player in AD development. Amyloid deposition begins decades before the apparition of the first dementia symptoms and some individuals with substantial amyloid burdens never develop dementia. Furthermore, amyloid measures are not always correlated with dementia and variates with a number of conditions. Beyond this, most of the recent "traditional" clinical approaches exclusively based on targeting Aβ have shown no substantial impact on the disease progression. The possibility of that amyloid pathology could be a down-stream or a side-stream process part of a bigger degenerative mechanism that implies various pathologic changes is something we must consider. This is also supported by recent works demonstrating the implication of other factors such as tau metabolism, infections, or other metabolic disorders that may lead to amyloid deposition.

These observations should push us, the researchers, the universities and the governments to invest resources, to develop more effective diagnostic techniques, to test new therapeutic approaches and, of course, to re-think from the origin(s) this complex and serious disease over the tons of data we are acquiring every day. The worldwide social importance and the still hidden origin(s) and pathways of this disease make AD an incredibly exciting field from the research point of view, and as it is, I wish to get another chance as the one I had 4 years ago for continuing exploring its riddles and mysteries.

6. Materials and Methods

6.1. Material

6.1.1. Plastics and consumables

Cell culture plates and flasks were provided by Corning (96-well plates ref. #3595, 24-well plates ref. #3738, 6-well plates ref. #351146, T25 flasks ref. #431463, T75 flasks ref. #353133, T150 flasks ref. #431465). Vacuum filters (ref. 514-0300, ref. 514-0297), 50 mL conical tubes (ref. 525-0447), syringes (ref. 613-2044, 613-2047) and serological pipets (ref. 612-3703, ref. 612-3700, ref. 612-1270) were supplied by VWR. Cryotubes for LN2 biobank were from NUNC (ref. 368632). HiTrap protein G columns (ref. 17-0404-03, ref. 17-0405-01) were supplied by GE Healthcare. High binding Greiner Microlon Flat Bottom Black 96-well ELISA plates were supplied by PVL.

6.1.2. Media and reagents

DMEM Glutamax™ medium (ref. 61965240), Fetal Bovine Serum (FBS) (ref. 10270106), HAT supplement (ref. 21060017), HT supplement (ref. 11067030), MEM supplement (ref. 11140035), Penicillin/Streptomycin antibiotic (ref. 10378016), 2-mercaptoethanol (ref. 21985-023), recovery cell culture medium (ref. 12648010), Recovery™ Cell Culture Freezing Medium (12648010) and PEG-4000 (ref. A16151) were provided by ThermoFisher. HEPES (ref. L0180-100), sodium pyruvate (ref. L0642-100), PBS tabs (ref. E404-200TABS), DMSO (ref. 0231-500ML), bath antifungal solution (ref. 462-7000), Incuwater clean solution (ref. A5219), Tween 20 (ref. 28829.183), HCl (ref. E447), glycine (ref. 15527-013) were supplied by VWR. Sodium phosphate (ref. S-0876), Ammonium chloride (A9434-500G), SP2/0 Ag14 myeloma cell line and gentamicin solution (ref. G1272) were supplied by Sigma. FBS with ultra-low IgG content was bought from Pan Biotech (ref. P30-2801). HyClone endotoxin free water (ref. SH30529.02) and HyClone PBS (ref. H30256.01) were from GE Healthcare. ClonaCell HY kit was supplied by StemCell. HCFS (11363735001) was supplied by Roche. Fortecortin (Sigma), Freund adjuvant (Thermo). 1,2-Dipalmitoyl-sn-glycero-3-phosphocholine (DPPC), cholesterol, L-cysteine, anhydrous dimethyl sulfoxide and 1,1,1,3,3,3- hexafluoro-2-propanol (HFIP) were obtained from Sigma-Aldrich (Copenhagen, Denmark). 1,2-Distearoyl-sn-glycero-3- phosphoethanolamine-N-[methoxy(polyethylene glycol)2000] ammonium salt (mPEG2000-DSPE), 1,2-distearoyl-sn-glycero-3- phosphoethanolamine-N-[maleimide(polyethylene glycol)2000] ammonium salt (MPB-PEG2000-DSPE), 1,2-dipalmitoyl-sn-glycero-3-phosphoethanolamine-N-(lissamine rhodamine B sulfonyl) ammonium salt (Liss-Rhod-PE) and polycarbonate filters were from Avanti Polar Lipids, Inc. (AL, USA). Phosphocholine assay kit was obtained from MTI diagnostics GmbHP (Idstein, Germany). Novex SilverXpress Silver Staining Kit, Novex 4-12% Bis-Tris Gel 1.0 mm 12 well, Novex SDS Sample Buffer, NuPAGE Reducing Agent, Novex Tricine SDS Running Buffer, CBQCA Protein Quantitation Kit, Qubit Protein Assay Kit, Novex® ECL, chemiluminescent substrate and Hoechst 33342 nuclear dye were purchased from Life Technologies (CA, USA). Boric acid and Amicon Ultra Centrifugal Filters 3 kD and 50 kD were obtained from MERCK KGaA (Darmstadt, Germany). Sepharose CL-4B gel was obtained from GE-Healthcare (Brøndby, Denmark). Lepirudin (Refludan®) was from Hoechst (Frankfurt-am- Main, Germany). Compstatin and the control peptide were a kind gift from Prof. Tom Eirik Mollnes (Oslo University Hospital, Norway).

6.1.3. Antibodies

Antibodies 6E10 anti-Aβ monoclonal antibody from Biolegend (SIG-39320-200), Y188 anti-APP monoclonal antibody from abcam (ab32136) and 4G8 anti-Aβ monoclonal antibody from Acris Antibodies (AM00003 PU-N) were used for comparing with Anti-Aβ STAB-MAb. For slices staining characterization and comparison of Anti-Aβ STAB-MAb, anti-APP (H, M, R) Antibody, C-Terminal (Rabbit Poly. Sigma A8717), Aβ Antibody (Rabbit Poly, Cell Signaling #2454), Anti-APP 22C11, N-Terminal (Mouse IgG1 Monocl. Millipore MAB348), 6E10, Human Beta amyloid (Mouse IgG1 Monocl. Covance SIG-39320). Anti-mouse IgG1 HRP-conjugated antibody from SIGMA was used as secondary antibody for the ELISA and WB. Antibodies for different biomarkers used were obtained from several sources: anti-Arc and anti-Tau5 antibodies were from Abcam (Cambridge, UK); anti-synapsin, anti-PSD95, anti-BACE (D10E5), and anti-GAPDH were from

Cell Signalling Technology (MA, USA); anti- Aβ (1-16, 6E10) was from Covance (CA, USA); anti-GFAP was from Dako (Glostrup, Denmark); anti-PHF1 was kindly provided by Dr. P. Davies (Albert Einstein College of Medicine, New York, USA).

6.1.3.1. Synthetic peptides

The Aβ peptides and peptide fragments used in the ELISAs, WBs and MALDI experiment were provided by different sources: Aβ (1-40) (SP-BA40-1), Aβ (1-42) (SP-BA42- 1), Aβ (1-43) (SP-BA43-5), Aβ (29-40) (SP-BA2940-1), Aβ (29-42) (SP-BA2942- 1) and Aβ 25-35 (SP-BA2535-1) were supplied by Innovagen (Lund, Sweden), whereas fragments Aβ (1-11) (ab120834) and Aβ (12-28) (ab120838) were supplied by abcam (Cambridge, UK), and fragment Aβ (35-42) (RP20145) was obtained from BioNova Cientifica SL (Madrid, Spain). Aβ peptides and peptide fragments were diluted to 0.5 mg/mL in 10 mM NH4OH and incubated at room temperature for 10 min. Samples were sonicated for 10 min in a sonicator bath. The final preparation was desiccated (SpeedVac) and stored at -80 ºC. Prior to use, samples were re-suspended in 60 mM NaOH. For NMR epitope mapping 15N Aβ (1-40) (supplied as a lyophilized powder by Alexa Biotech) and 15N Aβ (1-42) (supplied as a lyophilized powder by Jena Biotek) were resuspended in DMSO at a concentration of 2 mM and used immediately or frozen at -20ºC. p-TAU and acTAU peptides conjugated with KHL carrier protein were chosen as immunogens and versions without KLH carrier protein and negative controls without post-transcriptional modifications, were all synthetized by Genecust.

6.1.3.2. Proteases

Trypsin from porcine (ref. T6567), LysC endoproteinase (ref., P3428) and GluC endoproteinase (ENDOGLUS-RO) were bought from Sigma).

6.2. Methods

6.2.1.STAB-Mab and anti-tau antibodies production and purification

6.2.1.1. Used media

Old recipe: Complete DMEM media were supplemented with sodium pyruvate (0.1 mM), HEPES (10 mM) and gentamycin (10 mg/L). 10% of standard filtered (0.45 µm) heat-inactivated FBS (DMEM +) was also added for expansion. For production, the same FBS were IgG-depleted using protein G affinity columns (GE Healthcare) and the same protocol used for antibody purification prior adding to the media.

New recipe: Complete DMEM media were supplemented with sodium pyruvate (0.1 mM), HEPES (10 mM), 2-mercaptoethanol (0.05 mM) and penicillin-streptomycin or gentamycin (10 mg/L) when necessary. 10% of standard filtered (0.45 µm) FBS (DMEM +) or ultra-low IgG FBS (DMEM -) was also added depending on the needs.

All media was filtered through 0.22 µm PES vacuum filters and stored aliquoted at 4ºC until use.

Storage medium: 0.45-filtered heat-inactivated FBS was supplemented with 10% of DMSO and filtered through 0.22 PES syringe filters and stored aliquoted at -20ºC until use.

Table 6.1. Comparison of the two recipes used for antibody production

Old recipe	New recipe
DMEM	DMEM Glutamax (Gibco)
10%FBS IgG depleted in lab	Commercial Ultra-Low IgG 10%FBS
10 mM HEPES	10 mM HEPES
0.1 mM Sodium Pyruvate	0.1 mM Sodium Pyruvate
10 mg/L Gentamicin	10 mg/L Gentamicin
	0.05M 2-mercaptoethanol

6.2.1.2. Antibody production

Different clones were cultured in T150 cell culture flasks refreshed each 48 hours with DMEM 10- or in disposable bioreactors. CELLine and MiniPerm bioreactors were inoculated with the recommended number of cells and refreshed following manufacturer indications. Samples for cell doubling times quantification and production yield evaluation were taken each 12 hours.

6.2.1.3. Antibody purification

Supernatant from hybridomas cultures were collected, centrifuged in 50 mL sterile conical tubes (VWR) at 1000 g to separate cell rests and bigger aggregates and filtered by 0.45 µm before passing through Protein G columns (GE Healthcare) with an AKTA Prime System (GE Healthcare). Depending on the supernatant volume columns with 1 or 5 mL were used maintaining a flow rate between 1 and 1.5 ml/min. 0.22 µm filtered sodium phosphate 20 mM pH 7, 100 mM glycine-HCl pH 2.5 and 1M Tris-HCl pH 9.0 solutions were used as binding/equilibration, elution and neutralization buffers respectively. Columns were washed with miliQ water and kept in ethanol 20% at 4ºC when not used as recommended. 1-2 mL fractions (plus 40-80 µL of neutralization buffer) were collected and dialysed for 24 h with 3 buffer exchanges at 4ºC in sterile 0.1 M PBS (AMRESCO) using Float-A-Lyzer cassettes (ThermoScientific). Dialyzed product was finally concentration-assessed by Bradford assay (BGG from ThermoScientific was used as standard), aliquoted and used immediately or stored at -20ºC and 1 mg/mL. For higher concentrations, Vivaspin 4 concentrators (Sartorius) were used.

6.2.1.4. Quality control

Bradford using bovine gamma globulin (BGG) standard was used for total protein quantification. ELISA with Aβ(1-42) or pTAU/acTAU peptides coating were used for assessing supernatant antibody content and functionality of purified monoclonal anti-Aβ STAB-Mab and for anti-pTAU and anti-acTAU antibodies, respectively. The protocol is described in Table 6.2:

Table 6.2. ELISA parameters for quality control of antibodies production.

Stage	Reagent	Concentration	Diluent	Incubation
Coating	Tau/pTau/acTau/Aβ	0.1 µg/mL (Tau/Aβ)	Carbonate/Bicarbonate buffer pH 9.2	O/N at 4ºC
Washing	Washing Buffer	0.1M PBS 0.05% T20	PBS-Tween20 pH 7.4	
Blocking	Blocking Buffer	3% BSA	0.1M PBS 0.05% T20 pH 7.4	1h at 37ºC
Washing	Washing Buffer	0.1M PBS 0.05% T20	PBS-Tween20 pH 7.4	
Samples	Filtered Supernatant	1:1000-20,000	0.1M PBS pH 7.4	1h at 37ºC
Washing	Washing Buffer	0.1M PBS 0.05% T20	PBS-Tween20 pH 7.4	
Secondary Ab	Rabbit anti mouse IgG1-HRP	1:2000	0.1M PBS 0.05% T20 1% BSA	1h at 37ºC
Washing	Washing Buffer	0.1M PBS 0.05% T20	PBS-Tween20 pH 7.4	
Substrate	One-Step Ultra TMB	1x	N/D	3 min at RT
Stop reaction	H_2SO_4	1M	MiliQ H_2O	

6.2.2.Production of anti-tau monoclonal antibodies

6.2.2.1. Used media

Complete DMEM media was supplemented with sodium pyruvate (0.1 mM), HEPES (10 mM), 2-mercaptoethanol (0.05 mM) and penicillin-streptomycin or gentamycin (10 mg/L) when necessary. 10% (DMEM 10) or 20% (DMEM 20) of standard filtered FBS (DMEM +) or ultra-low IgG FBS (DMEM -) was also added depending on the needs. HAT and HT supplements were used for hybridomas selection in recommended concentrations. All these media were stored at

4ºC until use and warmed in a warm bath immediately before use. Cell storage medium were composed by heat-inactivated filtered FBS plus a 10% of DMSO and kept at -20ºC.

6.2.2.2. Mice immunization

For anti-TAU monoclonal antibodies generation, acetylated, phosphorylated and negative control TAU peptides for the ELISAs were delivered lyophilized and resuspended in PBS at 2 mg/mL. TAU peptides used as immunogens fused with KLH were resuspended in water with 10% DMSO at 0.7 mg/mL due to the lower solubility. Before administration, peptides were brought to 0.3 mg/mL and a final PBS concentration of 10 mM and mixed with equal volume of CFA(complete Freund´s adjuvant)/IFA (incomplete Freund´s adjuvant) for creating the emulsion using Luer lock glass syringes.

Five 3 months-old BALB/C mice were immunized per immunogen according to the following scheduled pattern: Day 1, first intraperitoneal (IP) administration of 50 µg of immunogen among CFA. Days 12 and 20, second and third IP administration of 50 µg of immunogen among IFA. Day 44, final intravenous (IV) (tail) boost with 100 µg using PBS as vehicle. Animals were also bleed on days 1, 30 and 44 for testing sera immunoreactivity against the immunogens by ELISA. Tail bleeds were taken from each mice per immunogen and centrifuged at 6000 rpm for 10 min at RT. The serum was collected and stored at -20°C until screening. ELISAs were performed following the protocol in Table 6.3 using concentrations of 5 µg/mL for coating plates and the absorbance values were read in a Biotek Microplate reader at 450 nm.

Table 6.3. ELISA parameters for antibodies screening.

Stage	Reagent	Concentration	Diluent	Incubation
Coating	pTau/acTau	1-5 µg/mL	Carbonate/Bicarbonate buffer pH 9.2	O/N at 4ºC
Washing	Washing Buffer	0.1M PBS 0.05% T20	PBS-Tween20 pH 7.4	
Blocking	Blocking Buffer	3% BSA	0.1M PBS 0.05% T20 pH 7.4	1h at 37ºC
Washing	Washing Buffer	0.1M PBS 0.05% T20	PBS-Tween20 pH 7.4	
Samples	Filtered Supernatant	1:500/1:1000-20,000	0.1M PBS pH 7.4	1h at 37ºC
Washing	Washing Buffer	0.1M PBS 0.05% T20	PBS-Tween20 pH 7.4	
Secondary Ab	Rabbit anti mouse IgG1-HRP	1:2000	0.1M PBS 0.05% T20 1% BSA	1h at 37ºC
Washing	Washing Buffer	0.1M PBS 0.05% T20	PBS-Tween20 pH 7.4	
Substrate	One-Step Ultra TMB	1x	N/D	3 min at RT
Stop reaction	H_2SO_4	1M	MiliQ H_2O	

Three days after final IV boost all mice were sacrificed with CO_2 and spleens harvested. Cells were separated from debris and passed through a mesh for creating a cell suspension. Cells were centrifuged in a swinging-out rotor at 400 g and washed once with ammonium chloride solution for red cells lysis and 3 times with PRE-warmed serum free DMEM before fusion.

6.2.2.3. Cell fusion (liquid medium)

Ag14 sp2/0 myeloma cell line was used as partner for spleen cells fusion, cultured in Complete DMEM 10+ and expanded in the previous 10 days before fusion for achieving the necessary cell number for al fusions. Cell suspensions from mice 1, 3, 4, 5, 6, 8, 9 and 10 spleens were fused in Complete DMEM serum free with previously expanded Ag14 sp2/0 myeloma cell line in a 1:1 ratio adding drop-by-drop a pre-warmed 50% PEG4000 solution and plated in 96-well cell culture plates with Complete DMEM 20+. Two 96 well plates (master plates) were plated for each mouse, incubated in the CO_2 incubator and fed on days 1, 2, 3, 4, 5, 7, 9 and 11 with DMEM 20+ HAT supplemented. On day 14 HAT supplemented media was substituted by HT supplemented media and on day 15 both supplements were retired. In 3 days confluency was about 50% and cells ready for the first screening.

6.2.2.4. Cell fusion (semi-solid medium)

Cell fusions from mice 2 (immunized with acTAU) and 7 (immunized with pTAU) were performed according to manufacturer´s instructions (ClonaCell-HY kit from StemCell) using the same myeloma cell line than in the previous method.

6.2.2.5. Screening

Screenings were performed by ELISA following the procedures described in Table 6.3. Positive wells were expanded to 24 well plates and to T25 cell culture flasks for freezing and storing in liquid nitrogen and brought to a second negative screening using TAU peptides without posttranscriptional modifications. Double-positive wells were then cloned by limiting dilution.

6.2.2.6. Cloning and selection

Serial 1:2 limiting dilutions were performed in 96 well plates (Falcon) following the scheme represented below from a starting dilution of 2x104 cells/mL from selected master plate wells for obtaining single colonies using DMEM 20+ medium supplemented with HFCS and grown for 7 days in the CO_2 incubator.

Three days after plating wells, when confluence in marked wells was 50%-75%, hybridomas were screened for their ability to secrete Mabs specific for the peptides wearing the post transcriptional acetylations and phosphorylations and non-modified peptides (for negative control).

Selected wells were sequentially expanded in 24-well plates, T25 and T75 vented culture flasks (Corning) for 2 weeks at 37°C under 5% CO_2, the supernatant from each culture was again tested for the presence of antibodies against the peptide antigen and cells added to the biobank in LN2. Hybridomas secreting antibody at the highest titer were further subjected to another round of limiting dilution cloning. Finally, 5 final clones for each peptide were expanded for production in large T150 flasks (Corning).

The protocol followed was the one described in Table 6.3 using pTAU and acTAU peptides without conjugated KLH for coating the Greiner Microlon High Binding 96-well ELISA microplates at a concentration of 1 µg/mL. Assays for the screening of the clones were performed in triplicate. Data are reported as the average of the results from all experiments and replicates ± standard deviation (SD).

6.2.2.7. Animal ethic agreements

Immunized mice were property of Luís Graça´s Group (IMM) and every ethic aspect was fulfilled with IMM (Instituto de Medicina Molecular).

6.2.3.Anti-Aβ antibodies characterization

6.2.3.1. Western Blot characterization

The protocol followed for testing STAB VIDA MAb and 6E10 antibodies with synthetic Aβ peptides was based in the described by Hermann Schägger for tricine-SDS-PAGE using three different gel types: 12% acrylamide-bisacrylalmide (a/b) (30% 29:1, Thermo), tricine-SDS-PAGE gel composed by a 6% band and a larger section with a 10% of A/B and another tricine-SDS-PAGE gel composed by a 10% band and a final and larger section with a 16% of A/B. For brain and cell culture lysates were used 12,5% a/b gels. For the development of the membranes we used ECL (Thermo) and BioRad Chemidoc equipment.

Protein extracts of the cell cultures homogenates were obtained by physical disruption and using a 50 mM Tris-HCl pH 7.5, 100 mM NaCl, 1 mM DTT and 5% glycerol lysis buffer and resolved on SDS-PAGE before transfering to a nitrocellulose membrane (Whatman). The membrane was incubated in a 10% (w/v) solution of nonfat milk for 1 h at room temperature. After overnight incubation at 4 ºC with the primary antibody, the blots were washed in 0.1% w/v Tween-PBS and incubated with the horseradish peroxidase conjugated secondary antibody, which was detected by Western Lightning™ Chemiluminescence (Perkin Elmer, MA, USA).

6.2.3.2. ThT aggregation assays

SensoLyte® Thioflavin T Beta-Amyloid ((1-42)) Aggregation Kit (Anaspec) was used for monitoring Aβ(1-42) aggregation kinetics and spectra were recorded on a Tecan Infinite M200 equipment using a Greiner Microlon Flat Bottom Black 96-well plate (100 µL reaction per well). Excitation (9 nm bandwidth) and emission (20 nm bandwidth) wavelengths were 440 nm and 484 nm respectively, while the gain was manually set in 100 and the number of flashes per read was 20. The assays were conducted under 37ºC and orbital agitation (3 mm amplitude, for 25 seconds before each measurement), taking measurements each 5 minutes for 2 hours. The protocol followed and buffers used were the indicated in manufacturer´s kit instructions, but using different reagent concentrations depending on the assay. For the assay with pre-aggregated Aβ(1-42), the resuspended peptides were incubated at 37ºC for 24 hours.

6.2.3.3. Electronic microscopy

Prior to any incubation, the Aβ(1-42) peptides were dissolved in DMSO at a final concentration of 1 mM and then added to the PBS solutions with or without presence of the STAB-Mab antibody, depending on the condition to a final concentration of 50 µM. To obtain oligomers, the peptide was dissolved in PBS 10 mM pH 7.4 and incubated at 4ºC for 5 days. To obtain fibrils, the peptide was resuspended in PBS 10 mM pH 7.4 and incubated at 37ºC for 5 days. After incubation, samples were diluted to 5 µM in PBS and put into the grids. 300 mesh formvar and carbon grids were placed above a 30 µL drop of each sample, incubated for 5 minutes, then rinsed for 3 minutes into a MiliQ water drop, and finally 3 minutes into each of two drops of a uranyl acetate 1.5% solution for negative staining. Finally, any liquid remaining on the grids was blotted away and conserved in dried conditions until TEM examination. Photos were taken in JEOL 1200EX equipment at 10, 25, 50, 75 and 100 K and RAW data was treated with GIMP open-source tool.

6.2.3.4. Obtaining and immunostaining of mouse and human brain slices

For mice brain cryoslices immunostaining: Fixed hemi-brains from WT and APP/PS1 mice were cut to 30 µm thickness coronal sections in a cryostat (Leica) and pre-treated with 70% v/v formic acid prior to blocking in serum for 1 h. The sections were then incubated for 1 h with the STAB-Mab (1:1000 dilution), washed and then incubated with anti-mouse Alexa 555 conjugated secondary antibodies (Invitrogen, Paisley, UK). After washing, DAPI was used to label the cell nuclei and sections were mounted with Fluoromount G (Southern Biotech, AL, USA). Finally, sections were visualized by fluorescence microscopy (Axiovert200, Carl Zeiss Microscope, Göttingen, Germany) and images were captured using a SPOT RT Slider camera (Diagnostic, MI, USA). Analyses were performed using ImageJTM software and the area occupied by amyloid plaques represented as a percentage of the total area analysed.

For paraffin-fixed mice brain slices: 6 months-old mice (WT, APP KO and APP/PS1 genotypes) were anesthetised with isofluorane prior to a peritoneal injection of ketamine/xylazine (0.14 mg / g body weight; WDT / Bayer Health Care) and transcardially perfused with phosphate buffered saline (PBS) followed by 4% paraformaldehyde in 0.12 M PBS, pH: 7.4. The brain was removed and post-fixed for 24 h at 4°C in the same fixative. The brains were washed in 1% PBS and coronal sections of 50 µm were obtained at room temperature by the vibratome Leica VT 1000S (Leica Mikrosysteme Vertrieb GmbH, Wetzlar, Germany). Immunofluorescence was performed on free-floating sections. Sections were permeabilized (2% TritonX –PBS, Life Science, Darmstadt, De), gently shacked, overnight at 4°C. Blocking solution (10% normal goat or donkey serum - 1% PBS, Thermo Fisher Scientific Messtechnik GmbH, Munich, DE) was applied for 2 hours at room temperature (RT). Sections were incubated with primary antibodies diluted in 3% normal goat/donkey serum, 0,03% Triton-X, 0,05% sodium azide-PBS overnight at 4°C. Secondary antibodies (conjugated with Alexa 594 or Alexa 488 fluorophores) were all applied in a dilution of 1:500 in 3% normal goat/donkey serum, 0,03% Triton-X, 0,05% sodium azide-PBS for a minimum of 2 hours at room temperature. Brain sections were mounted on polysine slides with Dako Fluorescent Mounting Medium (#S3023, Thermo Fisher Scientific Messtechnik GmbH, Munich, DE).

6.2.3.5. Confocal and fluorescence microscopy

Confocal images were acquired using a Zeiss LSM 780 with a Plan Apochromat 40x/ NA 1.4 Oil DIC M27 with a Pinhole set to 1 airy unit. Brains were extracted and embedded in paraffin. Paraffin-fixed brains were cut to 10 µm thickness coronal sections in a microtome and deparaffinised using diminishing xylene and ethanol gradients, finishing with water. Antigen retrieval was performed by boiling samples in the microwave for 15 minutes in a sodium citrate solution (10mM sodium citrate, 0.05% Tween 20, pH 6.0). The sections were then incubated for 1 h with the primary antibodies (1:1000 dilution in PBS 10 mM) and washed prior to blocking in BSA 1% (in PBS-Tween20) for 1 h, washed again and then incubated with anti-mouse Alexa 555 conjugated secondary antibodies (Invitrogen, Paisley, UK) at 1:2000 dilution in blocking solution. After washing, DAPI was used to label the cell nuclei and sections were mounted with Fluoromount G (Southern Biotech, AL, USA). Finally, sections were visualized by fluorescence microscopy (Zeiss D4) and images were captured using a SPOT RT Slider camera (Diagnostic, MI, USA). Analyses were performed using ImageJTM software and the area occupied by amyloid plaques represented as a percentage of the total area analyzed.

Human paraffin fixed brain sections: AD patient´s paraffin-fixed slices from the biobank were deparaffinized using diminishing xylene and ethanol gradients, finishing with water. Antigen retrieval was performed by boiling samples in the microwave for 15 minutes in a sodium citrate solution (10mM sodium citrate, 0.05% Tween 20, pH 6.0). The sections were then incubated for 1 h with the primary antibodies (1:1000 dilution in PBS 10 mM) and washed prior to blocking in BSA 1% (in PBS-Tween20) for 1 h, washed again and then incubated with anti-mouse Alexa 555 conjugated secondary antibodies (Invitrogen, Paisley, UK) at 1:2000 dilution in blocking solution. After washing, DAPI was used to label the cell nuclei and sections were mounted with Fluoromount G (Southern Biotech, AL, USA). Finally, sections were visualized by fluorescence microscopy (Zeiss D4 Göttingen, Germany) and images were captured using a SPOT RT Slider camera (Diagnostic, MI, USA). Analyses were performed using ImageJTM software and the area occupied by amyloid plaques represented as a percentage of the total area analyzed.

The antibodies used for comparing with STAB-Mab were: Anti-Amyloid Precursor Protein (H, M, R) Antibody, C-Terminal (Rabbit Poly. Sigma A8717), Beta-AmyloidAntibody (Rabbit Poly, Cell Signaling #2454), Anti-Alzheimer Precursor Protein 22C11, N-Terminal (Mouse IgG1 Monocl. Millipore MAB348), 6E10, Human Beta amyloid (Mouse IgG1 Monocl. Covance SIG-39320).

6.2.3.6. ELISA epitope mapping

96-well ELISA plates (Greiner Bio-One GmbH, Frickenhausen, Germany) were coated with 100 mL of Aβ or Aβ peptide fragments in a carbonate buffer, pH 9.6, at 37ºC for 2 h. For blocking,100 mL of 3% w/v BSA (in PBS pH 7.4, containing 0.05% v/v Tween 20) was added and incubated for 1 h at 37ºC. Primary antibodies (100 mL) were diluted at the desired concentrations in 1% w/v BSA and 0.05% Tween 20 in PBS and incubated for 1 h at 37ºC. Secondary HRP conjugated antibodies were added (100 mL) in a 1:2000 dilution in the same buffer as for primary antibodies and incubated again at 37ºC for 1 h. Finally, 100 mL of HRP substrate was added (Thermo Fisher Scientific, MA, USA). Following 10 min incubation at room temperature, the reaction was stopped by the addition of 100 mL HCl (1 N). The plates were read in a BIOTEK Spectrophotometer MQX200 (VT, USA) at 450 nm. The washings steps (except after TMB addition) were performed 3 times with PBS-0.1% v/v Tween 20 (300 mL) in a DAS Plate Washer D1.

6.2.3.7. MALDI-MS/MS epitope mapping

Si@MNPs synthesis and functionalization: Treatment of the MNP with (3-aminopropyl)triethoxysilane (APTES) produced a self-assembled monolayer containing surface amino groups that were converted to carboxyl groups by reaction with glutaric anhydride. The carboxyl groups were activated by sequential reactions with 1-ethyl-3-(3-dimethylaminopropyl)carbodiimide (EDC) and N-hydroxysuccinimide (NHS). The resulting NHS groups were used for chemical conjugation of STAB-Mab to generate STAB-Mab-MNPs [385].

NHS-activated columns functionalization: The “standard coupling buffer” (0.2 M NaHCO3, 0.5 M NaCl, pH 8.3), “buffer A” (0.5 M Ethanolamine, 0.5 M NaCl, pH 8.3), “buffer B” (0.1 M Sodium acetate, 0.5 M NaCl, pH 4), “binding buffer” for the samples (Ammonium bicarbonate 12.5 mM, pH 8), “elution buffer” for the epitope fragments (0.1% TFA, pH 2) and the “columns storage

solution" (0.05 M Na_2HP_4, 0.1% NaN_3, pH7) solutions were prepared, filtered through 0.22 µm syringe filters (VWR) and stored at room temperature. (i) For columns coupling, the protocol of the manufacturer was followed, applying first 3 column volumes of an ice-cold 1 mM HCl solution for removing the isopropanol. Immediately, 1 ml of the ligand solution (500 µg the STAB-Mab dissolved in the coupling buffer at a 0,5 mg/mL) was added into the columns. Then, the columns were sealed and incubated for 60 minutes at 25°C. (ii) To evaluate the coupling, the coupling solution was washed out from the column with 3 column volumes of the coupling buffer, 1 ml of that solution is mixed with 1 ml 2 M glycine-HCl, pH 2.0 and the absorbance was measured at 280 nm. (iii) The deactivation of the excess active groups that have not coupled to the ligand, and wash out the non-specifically bound ligands, was performed by sequentially passing several volumes of buffers A and B. (iv)

Enzymatic digestion of Aβ: 25µg of lyophilized peptides were resuspended in 39 µL of binding buffer and incubated with 1µg of the corresponding enzyme (Trypsin, LysC or GluC) for 2 h at 37ºC. The reaction was stopped with 5µL of TFA 0.1%. (v) Sample application: Columns were sequentially washed with binding buffer and elution buffer and equilibrated before addition of the samples. Resuspended peptides or digestion products were dissolved in binding buffer until 1mL and added into the columns. (vi) Samples were incubated into the columns and/or MNPs for 2 h at 20ºC and gentle shaking. (vii) Flow-through fractions were obtained washing out unbound peptides with binding buffer and kept for MALDI analysis. (viii) Epitope-related fragments were released incubating columns with elution buffer for 15 min. (ix) Columns were washed and equilibrated again with binding buffer and stored with storage solution at 4ºC until next use. (x) The different flow-troughs and eluted fractions from the NHS-STAB-Mab columns were analyzed by MALDI: 5 µL of each sample was mixed with 10 µL of matrix solution (10 mg of α-cyano-4-hydroxy cinnamic acid in 1 mL of 50% acetonitrile and 2.5% aqueous trifluoroacetic acid). Then 1 µL of the sample-matrix solution was deposited onto a stainless steel plate and allowed to dry at room temperature. Mass spectra were obtained using a Bruker Daltonics Ultraflex MALDI TOF/TOF Mass Spectrometer operating in linear mode with positive ion extracting at 25,000 V and a delay time of 350 ns. The grid voltage and guide wire were adjusted to 95% and 0.05%, respectively. Each final spectrum was the accumulated result of at least 500 laser shots that were obtained from 10 different manually selected regions of the same sample, over a range of 650–4,500 Da. Two duplicates were made of each sample. The spectra were externally calibrated using a mixture of 2 pmol/µL oxidized B chain of insulin and 2 pmol/µL bovine insulin (Sigma-Aldrich). Baselines of spectra were corrected and noise was filtered out. Lists of m/z values with relative signal intensities higher than 2% were extracted from the mass spectral data.

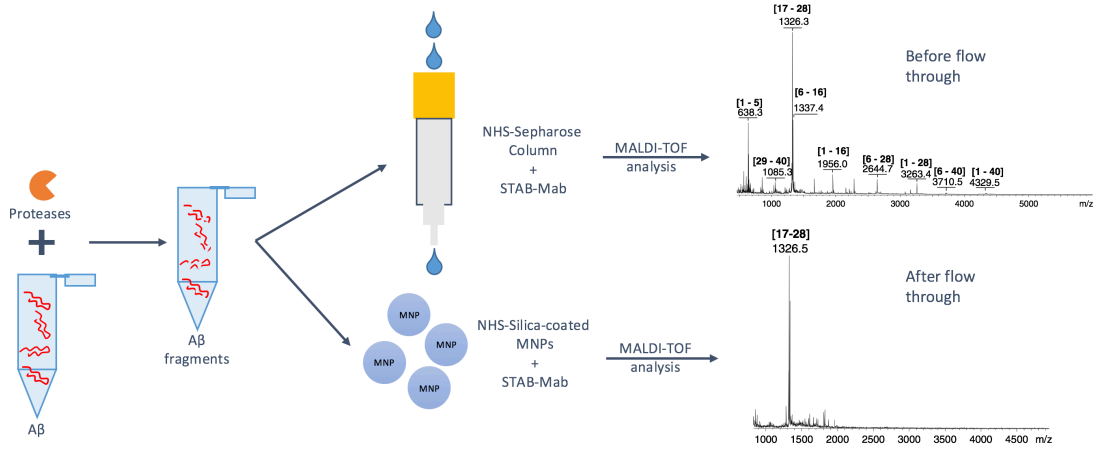

Figure 6.1. Scheme of the MALDI-TOF experiment for mapping the STAB-Mab epitope through proteolytic digestion and spectrometry analysis of the bound and unbound Aβ fragments through the functionalized columns and MNPs.

6.2.3.8. Epitope mapping by NMR (1H/15N HSQC experiment)

All NMR 1H/15N HSQC spectra were acquired with a Bruker Avance III 600 MHz spectrometer using a TCI cryo-probe. 15N-labeled Aβ(1-40) and Aβ(1-42) (Alexotech, Sweden) were initially dissolved as concentrated 2 mM stock solutions in DMSO-d6 (Sigma-Aldrich). Samples were then

diluted 100-fold in 10 mM PBS (Amresco) pH 7.4 containing 5% DMSO-d6, 50 μM TSP and the STAB-Mab antibody at 1:0.1, 1:0.3, 1:0.6, 1:1.5 and 1:3 ratios at a final pH of 7.30. NMR spectra were recorded in 5 mm tubes (Norell, North Carolina) at a temperature of 278 K. 2D 1H/15N SOFAST-HMQC spectra were recorded with 2048 data points in the proton dimension and 128 data points in the 15N dimension with a total of 128 scans. Spectra were processed with TopSpin (Bruker, Karlsruhe) with 2048 data points in the proton and 1024 data points in the 15N dimension. Spectra of the Aβ(1-40) and Aβ(1-42) peptides alone and in 1:0.1, 1:0.3, 1:0.6, 1:1.5 and 1:3 complexes with the STAB-Mab were recorded. The 1H/15N correlated spectra were assigned using the BMRB data base values (BMRB-ID 11435 and BMRB ID-25218). The 15N chemical shift was referenced indirectly to the TSP-derived 1H signal based on the relative gyromagnetic ratios of these nuclei. Data visualization and analysis was performed using CCPN (http://www.ccpn.ac.uk/about). Residues belonging to the binding epitopes of Aβ(1-40) and Aβ(1-42) were identified by signal intensity attenuation and combined 1H/15N chemical shift perturbations (Δδcomb). Residues with intensities below the noise or above the cut-off value, calculated in an iterative procedure as the corrected standard deviation to zero, were mapped to the epitope.

6.2.4.Anti-Aβ antibodies *in vivo* pre-clinical trials

6.2.4.1. STAB-Mab

6.2.4.1.1. ImmunoPEGliposome preparation and characterization

Mouse IgG and STAB-MAb were thiolated with Traut's reagent (10:1 M ratio of Traut's reagent to antibodies in degassed borate buffer, pH 8.3) [535]. After 1h of incubation at room temperature, unreacted Traut's reagent was removed by Amicon Ultra 15 mL centrifugal filter device (molecular weight cut-off, MWCO, 30 kDa) and the buffer was exchanged with degassed phosphate buffer (pH 7.4). The thiolated antibodies were added to the liposome (DPPC:Cholestrol:mPEG2000-DSPE:MPB-PEG2000-DSPE; mole ratio; 70:25:4:1) and incubated at room temperature for 12 h under nitrogen. Unreacted maleimide groups were inactivated by incubation with 0.5 mM cysteine for 15 min at room temperature. Unbound antibodies were separated from the immunoPEGliposomes by gel-permeation chromatography using Sepharose CL-4B with degassed PBS as buffer. In some studies, liposomes were labelled with Liss-Rhod-PE. A commercially available phosphocholine assay kit was used for determination of liposomal phospholipid content. The amount of unbound antibody was quantified with Qubits Protein Assay Kit.

Nanoparticle Tracking Analysis (NTA) was also used for vesicular size and concentration evaluation. Briefly, samples were diluted 106 times with purified water (18.2 MU cm) and monitored with an LM20 NanoSight mounted with a blue (405 nm) laser (Malvern Instruments, Malvern, UK) using the Nanosight 2.3 software for analysis [536]. The number of bound antibody molecules per liposome was calculated by considering an average occupied area of 75 Å per phospholipid polar head group and cholesterol and the mean vesicular size of 150 nm (from NTA). SDS-PAGE (12%) under reducing and non-reducing conditions with silver staining was used to determine whether antibodies were covalently bound to the distal end of PEG chains in liposomes and to confirm the integrity of bound antibodies.

6.2.4.1.2. Validation of double transgenic mice

The double transgenic mice of both female and male genders used in the present study incorporate a human APP construct bearing the Swedish double mutation and the exon-9-deleted PSEN1 mutation B6.Cg-Tg [(APPSwe, PSEN1dE9)85Dbo/J] (Jackson Laboratory, Bar Harbor, ME, USA; stock no. 005864). We confirmed mouse genotype by PCR of DNA isolated from tail biopsies [484, 485, 537]. All animal care and handling was in accord with current Spanish legislation and guidelines as well as those by the European Commission (directive 2010/63/EU).

6.2.4.1.3. Animal treatment protocols

Two therapeutic protocols were designed. For the first protocol we used 10 month-old mice (designated as ‘adult’ mice). Here, mice were divided in to four treatment groups (n= 6, 3 males and 3 females) receiving liposomes decorated with STAB VIDA MAb (Lip-MAb), free STAB VIDA

MAb, control liposomes without antibody decoration (Lip) and a non-specific mouse IgG1 preparation over a 4-month period. All preparations were injected intraperitoneally once every 3 weeks. The liposome dose corresponded to a total of 4 mg phospholipid, whereas the antibody dose was 150 mg (both in free form and in immunoPEGliposome preparation). For the second protocol, we used 16 month-old mice (designated as 'aged' mice). These animals were treated for 6 months with the abovementioned preparations, but with the exception of Lip treatment. The dosing schedule was kept once every 3 weeks. The Lip group was eliminated due to lack of any adverse (and therapeutic) effect in the first protocol. This decision was adopted following the advice of the ethical committee to reduce the number of animals used for the *in vivo* experiments.

6.2.4.1.4. Blood and tissue sampling

Blood samples were taken before and after the full-round treatment by the submandibular vein puncture. After mixing with 10 mM EDTA in PBS (1:1), the blood was centrifuged for 5 min at 10,000 g at room temperature to obtain the plasma fraction, which was stored at -80 ºC.

Mice were sacrificed by CO_2 asphyxiation. The brain was removed and cut into two hemi-brains. One hemi-brain was snap frozen on dry ice for subsequent homogenization and stored at -80 ºC until use. The second hemi-brain was fixed for 24 h in 4% v/v paraformaldehyde (PFA) in phosphate buffered saline (PBS, pH 7.4) and cryoprotected in graded concentrations of sucrose (15-30%) in PBS. The fixed tissue was finally set in O.C.T.TM com- pound (Tissue-Tek®Sakura, Sakura Finetek B.V. KvK, Leiden, NL) and frozen at -80 ºC.

6.2.4.1.5. Tissue processing

Previously frozen brain tissue was homogenized in 3 vol of ice-cold lysis buffer (20 mM Hepes, 100 mM NaCl, 100 mM NaF, 1 mM NaVO4, 5 mM EDTA, 1% v/v Triton-X100) containing protease inhibitor cocktail (Roche Diagnostic) and 1 mM okadaic acid (Calbiochem, CA, USA) as phosphatase inhibitor. The homogenate was then centrifuged at 4 ºC for 20 min at 16,000 g and the supernatant stored at -80 ºC. The protein concentration was measured using the BioRad DC Protein Assay (BioRad, Hertfordshire, UK) following the manufacturer's protocol. Prior to resolving the proteins by SDS/PAGE (PolyAcrylamide Gel Electrophoresis), loading buffer (10% SDS, 0.5 mM DTT, 325 mM TrisHCl [pH 6.8], 87% v/v glycerol, and bromophenol blue) was added to the supernatants. Tissue samples used for ELISA tests were homogenized in 8 vol of ice-cold guanidine buffer (5 M guanidine HCl/50 mM Tris HCl, pH 8). The homogenates were mixed for 3 h at room temperature and stored at -20ºC.

6.2.4.1.6. Plasma and brain Aβ(1-40) and (1-42) quantification by ELISA

Brain homogenates were diluted 1:50 in albumin-PBS-Tween buffer (5% w/w bovine serum albumin, 0.03% w/v Tween-20 in PBS) prior to centrifugation at 16,000 g for 20 min at 4 ºC. The amyloid levels were measured in plasma samples and diluted brain supernatants with an Aβ(1-40) or Aβ(1-42) Human ELISA kit (Invitrogen, Paisley, UK) according to the manufacturer's instructions. The absorbance in the plates was read at 450 nm on an Opsys MR Microplate reader (Dynex Technologies, VA, USA).

6.2.4.1.7. Western blots of brain protein extracts

Protein extracts of the brain homogenates were resolved on SDS-PAGE and transferred to a nitrocellulose membrane (Whatman). The membrane was incubated in a 10% (w/v) solution of non-fat milk for 1 h at room temperature. After overnight incubation at 4 ºC with the primary antibody, the blots were washed in 0.1% w/v Tween-PBS and incubated with the horseradish peroxidase conjugated secondary antibody (Santa Cruz Biotechnology, TX, USA), which was detected by Western LightningTM Chemiluminescence (Perkin Elmer, MA, USA) [22]. β-actin served as the internal control. The intensity of each band was determined with ImageJTM software (National Institute of Health, MD, USA).

6.2.4.1.8. Immunofluorescence studies of the brain sections

Fixed hemi-brains were cut to 30 mm thickness coronal cryostat (Leica) sections and pre-treated with 70% v/v formic acid prior to blocking in serum for 1 h. The sections were then incubated for 1 h with the 6E10 anti-Aβ antibody (1:1000 dilution) or anti-GFAP (1:1000 dilution), and after washing they were incubated with anti-rabbit or anti-mouse biotinylated secondary antibody for 30 min [485]. Antibody staining was visualized with the Vectastain Elite ABC kit (Vector Laboratories, CA, USA) using diaminobenzidine (DAB) as the chromogen (Sigma Aldrich, Poole, UK). Finally, the slices were mounted on slides and covered with Entellan New Medium (Electron Microscopy Sciences, PA, USA). For immunofluorescence staining, sections were treated with primary antibodies, washed and then incubated with anti-rabbit Alexa 488 and anti-mouse Alexa 555 conjugated secondary antibodies (Invitrogen, Paisley, UK). After washing, DAPI was used to label the cell nuclei and sections were mounted with Fluoromount G (Southern Biotech, AL, USA). Finally, sections were visualized by light or fluorescence microscopy (Axiovert200, Carl Zeiss Microscope, Göttingen, Germany) and images were captured using a SPOT RT Slider camera (Diagnostic, MI, USA). Analyses were performed using ImageJTM software and the area occupied by amyloid plaques represented as a percentage of the total area analyzed.

6.2.4.1.9. Statistical analysis

Sigma Plot software was used for all statistical analyses by t-test, one-way or two-way ANOVA, where appropriate. In all cases, differences were considered statistically significant when $p \leq 0.05$ (*), $p \leq 0.01$ (**) or $p \leq 0.001$ (***).

6.2.4.2. Minibody 2

6.2.4.2.1. Therapeutic approach

One group formed by 7 12-months old transgenic female mice was administrated with 150 µg of Minibody 2 IP each 3 weeks during 4 months for minimizing the risk of immunogenic responses. Another 7 transgenic mice were administrated with PBS (non-treated) and 6 wild type mice group without any treatment was used as controls.

Minibody 2 wears a human Fc that would be recognized and targeted by the immune system of the mice. In order to avoid as far as possible immunologic reactions, mice were immune-depressed using Fortecortin drug by oral administration (2 mg/L in drinking water).

6.2.4.2.2. Validation of double transgenic mice

14 mice bearing the Swedish double mutation and the exon-9-deleted PSEN 1 mutation B6.Tg-Tg (APPSwe, PSEN1dE9) 85Dbo/J (Jackson Laboratory, Bar Harbor) were used to perform this experiment. The genotype of the mice was confirmed by PCR of DNA isolated from tail biopsies [484, 485, 537]. All animal care and handling was in accord with current Spanish legislation and guidelines as well as those by the European Commission (directive 2010/63/EU).

6.2.4.2.3. Blood and tissue sampling

Blood samples were taken before and after the full-round treatment by the submandibular vein puncture. After mixing with 10 mM EDTA in PBS (1:1), the blood was centrifuged for 5 min at 10,000 g at room temperature to obtain the plasma fraction, which was stored at -80 ºC.

Mice were sacrificed by CO_2 asphyxiation. The brain was removed and cut into two hemi-brains. One hemi-brain was snap frozen on dry ice for subsequent homogenization and stored at -80 ºC until use. The second hemi-brain was fixed for 24 h in 4% v/v paraformaldehyde (PFA) in phosphate buffered saline (PBS, pH 7.4) and cryoprotected in graded concentrations of sucrose (15-30%) in PBS pH 7.4. The fixed tissue was finally set in O.C.T.TM com- pound (Tissue-Tek®Sakura, Sakura Finetek B.V. KvK, Leiden, NL) and frozen at -80 ºC.

6.2.4.2.4. Western blots of brain protein extracts

Protein extracts of the brain homogenates were resolved on SDS-PAGE and transferred to a nitrocellulose membrane (Whatman). The membrane was incubated in a 10% (w/v) solution of non-fat milk for 1 h at room temperature. After overnight incubation at 4 ºC with the primary antibody, the blots were washed in 0.1% w/v Tween-PBS and incubated with the horseradish peroxidase conjugated secondary antibody (Santa Cruz Biotechnology, TX, USA), which was detected by Western LightningTM Chemiluminescence (Perkin Elmer, MA, USA) [22]. β-actin served as the internal control. The intensity of each band was determined with ImageJTM software v1.5 (National Institute of Health, MD, USA).

6.2.4.2.5. Plasma and brain Aβ ((1-40) and (1-42)) quantification by ELISA

Brain homogenates were diluted 1:50 in albumin-PBS-Tween buffer (5% w/w bovine serum albumin, 0.03% w/v Tween-20 in PBS) prior to centrifugation at 16,000 g for 20 min at 4 ºC. The amyloid levels were measured in plasma samples and diluted brain supernatants with an Aβ(1-40) or Aβ(1-42) Human ELISA kit (Invitrogen, Paisley, UK) according to the manufacturer's instructions. The absorbance in the plates was read at 450 nm on an Opsys MR Microplate reader (Dynex Technologies, VA, USA).

6.2.4.2.6. Behavioral tests

At the end of the treatment, for the NOR test, mice were first introduced into an empty open-square grey arena (40 x 40 cm), 30 cm high and separated from the operator’s room for habituating to the area and for open-area behavior quantification. The next day, mice were again introduced into the arena containing two identical objects that they can explore freely. Twenty-four hours later mice are reintroduced into the arena, containing two different objects one of which previously presented (familiar) and a new completely different one (novel). The objects used were a black chess figure (2 x 5 cm), and a metal cube (3 x 5 cm). The task started with a habituation trial during which the animals were placed in the empty arena for 10 minutes and their movements recorded to provide an indication of both WT and APP/PS1 mice motor activity. The next day, mice were again placed in the same arena containing two identical objects (familiarization phase, chess figure). Exploration was recorded in a 10-minute trial by an investigator blinded to the genotype and treatment. Sniffing, touching and stretching the head close to the object at a distance of smaller than 2 cm were considered as object investigation. Twenty-four hours later (test phase) mice were again placed in the arena containing one of the objects presented during the familiarization phase (old object), and a new, different one (new object), and the time spent exploring the two objects was again recorded for 10 min. Results were expressed as amount of time spend in each object by the 3 mice groups, the difference of the average amount of time spent by each group in each object, % time of investigation on objects/10 min and as discrimination index (DI), that is: (seconds spent on novel – seconds spent on familiar)/(total time spent on objects).

7. Bibliography

1. Alzheimer, A. Über eine eigenartige Erkrankung der Hirnrinde. *Allgemeine Zeitschrift für Psychiatrie und psychisch-gerichtliche Medizin*. **64.** Band, Verlag von Georg Reimer. (1907).
2. World Alzheimer Report 2015: The Global Impact of Dementia. *London: Alzheimer Disease International*. (2015).
3. Kumar. A. & Dogra, S. Neuropathology and therapeutic management of Alzheimer's disease – an update. *Drugs Future.* **33**(5), 433–46. (2008).
4. Kurz, A. & Perneczky, R. Novel insights for the treatment of Alzheimer's disease. *Prog Neuropsychopharmacol Biol Psychiatry*; **35**(2), 373–9. (2011).
5. Salomone, S., Caraci, F., Leggio, G.M., Fedotova, J. & Drago, F. New pharmacological strategies for treatment of Alzheimer's disease: focus on disease modifying drugs. *Br J Clin Pharmacol.* **73**(4), 504–17. (2012).
6. Hardy, J. The amyloid hypothesis for Alzheimer's disease: a critical reappraisal. *J Neurochem*. **110**(4), 1129–34. (2009).
7. Rosenmann, H. Immunotherapy for targeting tau pathology in Alzheimer´s disease and tauopathies. *Curr Alzheimer Res.* **10**(3), 217–28. (2013).
8. Dal Pra, I. *et al*. Do astrocytes collaborate with neurons in spreading the "infectious" Ab and tau drivers of Alzheimer's disease? *Neuroscientist*. **21**(1), 9-29. (2014).
9. Antanitus, D.S. A theory of cortical neuron–astrocyte interaction. *Neuroscientist*. **4**(3), 154–9. (1998).
10. Müller, U.C., Deller, T. & Korte, M. Not just amyloid: physiological functions of the amyloid precursor protein family. *Nature Reviews Neuroscience*. **18**, 281–298. (2017).
11. McKhann, G. *et al*. Clinical diagnosis of Alzheimer's disease: Report of the NINCDS-ADRDA Work Group under the auspices of Department of Health and Human Services Task Force on Alzheimer's Disease. *Neurology*. **34**, 939 – 944. (1984).
12. McKhann, G.M. *et al*. The diagnosis of dementia due to Alzheimer's disease: Recommendations from the National Institute on Aging-Alzheimer's Association workgroups on diagnostic guidelines for Alzheimer's disease. *Alzheimer's Dement.* **7**: 263–269. (2011).
13. Rastas, S. *et al.* Vascular risk factors and dementia in the general population aged >85 years: Prospective population-based study. *Neurobiol Aging.* **31**(1), 1-7. (2010).
14. Elias, P.K., Elias, M.F., Robbins, M.A. & Budge, M.M. Blood pressure-related cognitive decline: Does age make a difference? *Hypertension.* **44**, 631–636. (2004).
15. Goble, A.J. Obesity in middle age and future risk of dementia: Problem is probably greater for women. *BMJ.* **331**, 454. (2005).
16. Luchsinger, J.A., Tang, M.X., Stern, Y., Shea, S. & Mayeux, R. Diabetes mellitus and risk of Alzheimer's disease and dementia with stroke in a multiethnic cohort. *Am J Epidemio.l* **154,** 635–641. (2001).
17. Doll, R., Peto, R., Boreham, J. & Sutherland, I. Smoking and dementia in male British doctors: Prospective study. *BMJ.* **320**, 1097. (2000).
18. Rajendran, L., & Annaert, W. Membrane trafficking pathways in Alzheimer's disease. *Traffic.* **13**, 759-770. (2012).
19. Takami, M., *et al.* Gamma-Secretase: successive tripeptide and tetrapeptide release from the transmembrane domain of beta-carboxyl terminal fragment. *J Neurosci.* **29**, 13042-13052. (2009).
20. De Strooper, B., and Karran, E. The Cellular Phase of Alzheimer's Disease. *Cell.* **164**, 603-615. (2016).
21. Jarosz-Griffiths, H. H., Noble, E., Rushworth, J. V., & Hooper, N. M. Amyloid-β Receptors: The Good, the Bad, and the Prion Protein. *J Biol Chem.* **291**, 3174-3183. (2016).
22. Zhang, Z. *et al*. Delta-secretase cleaves amyloid precursor protein and regulates the pathogenesis in Alzheimer's disease. *Nat Commun.* **6**, 8762. (2015).
23. Baranger, K. *et al.* MT5-MMP is a new pro-amyloidogenic proteinase that promotes amyloid pathology and cognitive decline in a transgenic mouse model of Alzheimer's disease. *Cell Mol Sci.* **73**, 217-236. (2016).
24. Willem, M., *et al.* Beta- Secretase processing of APP inhibits neuronal activity in the hippocampus. *Nature.* **526**, 443-447. (2015).

25. Bien, J., *et al.* The metalloprotease meprin beta generates amino terminal-truncated amyloid beta peptide species. *J Biol Chem.* **287**, 33304-13. (2012).
26. Schönherr, C., *et al.* Generation of aggregation prone N-terminally truncated amyloid β peptides by meprin β depends on the sequence specificity at the cleavage site. *Mol. Neurodegener.* **11**, 19. (2016).
27. Hook, G., Yu, J., Toneff, T., Kindy, M., & Hook, V. Brain pyroglutamate amyloid-beta is produced by cathepsin B and is reduced by the cysteine protease inhibitor E64d, representing a potential Alzheimer's disease therapeutic. *J. Alzheimer's Dis*. **41**, 129-149. (2014).
28. Portelius, E., *et al.* Brain amyloid-beta fragment signatures in pathological ageing and Alzheimer's disease by hybrid immunoprecipitation mass spectrometry. *Neurodegener Dis.* **15**, 50-57. (2015).
29. Jin, M. *et al.* Soluble amyloid beta-protein dimers isolated from Alzheimer cortex directly induce Tau hyperphosphorylation and neuritic degeneration. *Proc. Natl Acad. Sci. USA*. **108**, 5819-24. (2011).
30. Zempel, H., Thies, E., Mandelkow, E. & Mandelkow, E.M. Abeta oligomers cause localized Ca^{2+} elevation, missorting of endogenous Tau into dendrites, Tau phosphorylation, and destruction of microtubules and spines. *J Neurosci.* **30**, 11938-50. (2010).
31. De Felice, F.G. *et al.* Alzheimer's disease-type neuronal tau hyperphosphorylation induced by Abeta oligomers. *Neurobiol Aging.* **29**, 1334-47. (2008).
32. Cohen, S. I. A. *et al*. Proliferation of amyloid-β42 aggregates occurs through a secondary nucleation mechanism. *Proc. Natl Acad. Sci. USA.* **110**(24), 9758-63. (2013).
33. Schnabel, J. Amyloid: Little proteins, big clues. *Nature.* **475**(7355), S12-S14. (2011).
34. Ferri, C.P. *et al*. Global prevalence of dementia: A Delphi consensus study. *Lancet* **366,** 2112-17. (2005).
35. Xu, Y. *et al*. Neurotransmitter receptors and cognitive dysfunction in Alzheimer's disease and Parkinson's disease. *Prog Neurobiol.* **97**(1), 1-13. (2012).
36. Armato, U., Chakravarthy, B., Pacchiana, R. & Whitfield, J.F. Alzheimer's disease: an update of the roles of receptors, astrocytes and primary cilia. *Int J Mol Med*. **31**(1), 3-10. (2013).
37. Angevaren, M., Aufdemkampe, G., Verhaar, H., Aleman, A. & Vanhees, L. Physical activity and enhanced fitness to improve cognitive function in older people without known cognitive impairment. *Cochrane Database of Systematic Reviews* (Online). CD005381. (2008).
38. Cotman, C.W. & Berchtold, N.C. Exercise: A behavioral intervention to enhance brain health and plasticity. *Trends Neurosci* **25,** 295-301. (2002).
39. Chen, G.F. *et al*. Amyloid beta: structure, biology and structure-based therapeutic development. *Acta Pharmacol Sin*. **38**, 1205–1235. (2017).
40. Reuben, D.B., Judd-Hamilton, L., Harris, T.B. & Seeman, T.E. The associations between physical activity and inflammatory markers in high-functioning older persons: MacArthur Studies of Successful Aging. *J Am Geriatr Soc*. **51,** 1125-30. (2003).
41. Morris, M.C. *et al*. Dietary fats and the risk of incident Alzheimer disease. *Arch Neurol*. **60**, 194-200. (2003).
42. Schaefer, E.J. *et al*. Plasma phosphatidylcholine docosahexaenoic acid con- tent and risk of dementia and Alzheimer disease: The Framingham Heart Study. *Arch Neurol.* **63,** 1545-50. (2006).
43. van Gelder, B.M., Tijhuis, M., Kalmijn, S. & Kromhout, D. Fish consumption, n-3 fatty acids, and subsequent 5-y cognitive decline in elderly men: The Zutphen Elderly Study. *Am J Clin Nutr*. 85: 1142-47. (2007).
44. Wilson, R.S. *et al*. Participation in cognitively stimulating activities and risk of incident Alzheimer disease. *JAMA. **287***, 742-748. (2002).
45. Wilson, R.S., Scherr, P.A., Schneider, J.A., Tang, Y. & Bennett, D.A. Relation of cognitive activity to risk of developing Alzheimer disease. *Neurology* **69,** 1911-20. (2007).
46. Murphy, M.P. & LeVine III, H. Alzheimer's Disease and the β-Amyloid Peptide. *J Alzheimers Dis*. **19**(1), 311. (2010).
47. Akbaraly, T.N. *et al*. Leisure activities and the risk of dementia in the elderly: results from the Three-City Study. *Neurology.* **73,** 854-861. (2009).
48. Schneider, J.A. & Bennett, D.A. Where vascular meets neurodegenerative disease. *Stroke.* **41,** S144–S146. (2010).
49. Fein, G. *et al*. Hippocampal and cortical atrophy predict demen- tia in subcortical ischemic vascular disease. *Neurology.* **55**, 1626-35. (2000).

50. Jellinger, K.A. The pathology of ischemic-vascular dementia: An update. *J Neurol Sci.* **203-204**, 153-157. (2002).
51. Wen, Y, *et al*. Cdk5 is involved in NFT-like tauopathy induced by transient cerebral ischemia in female rats. *Biochim Biophys Acta* **1772**, 473-483. (2007).
52. Wen, Y. *et al*. Transcriptional regulation of b-secretase by p25/cdk5 leads to enhanced amyloidogenic processing. *Neuron.* **57**, 680-690. (2008).
53. Launer, L. *et al*. Midlife blood pressure and demen- tia: The Honolulu – Asia aging study. *Neurobiol Aging.* **21**, 49-55. (2000).
54. Wu, C. *et al*. Relationship between blood pressure and Alzheimer's disease in Linxian County, China. *Life Sci.* **72**, 1125-33. (2003).
55. Waldstein, S.R., Giggey, P.P., Thayer, J.F. & Zonderman, A.B. Nonlinear relations of blood pressure to cognitive function: The Baltimore Longitudinal Study of Aging. *Hypertension* **45**, 374-379. (2005).
56. Lithell, H. *et al*. The Study on Cognition and Prognosis in the Elderly (SCOPE): Principal results of a randomized double-blind intervention trial. *J Hypertens.* **21**, 875-886. (2003).
57. Tzourio, C. *et al*. Effects of blood pressure lowering with perindopril and indapamide therapy on dementia and cognitive decline in patients with cerebrovascular disease. *Arch Intern Med.* **163**, 1069-75. (2003).
58. Farris, W. *et al.* Insulin-degrading enzyme regulates the levels of insulin, amyloid b-protein, and the b-amyloid precursor protein intracellular domain *in vivo*. *Proc. Natl Acad. Sci. USA*. **100**, 4162-67. (2003).
59. Luchsinger, J.A., Tang, M.X., Shea, S. & Mayeux, R. Hyperinsulinemia and risk of Alzheimer disease. *Neurology*. **63**, 1187-92. (2004).
60. Selkoe, D.J. The origins of Alzheimer disease: A is for amyloid. *JAMA.* **283**, 1615-17. (2000).
61. Trujillo, M.E. & Scherer, P.E. Adiponectin-journey from an adipocyte secretory protein to biomarker of the metabolic syndrome. *J Intern Med*. **257**, 167-175. (2005).
62. Yu, Y.H. & Ginsberg, H.N. Adipocyte signaling and lipid homeostasis: Sequelae of insulin-resistant adipose tissue. *Circul Res.* **96**, 1042-52. (2005).
63. Reger, M.A. *et al.* Intranasal insulin improves cognition and modulates b-amyloid in early AD. *Neurology.* **70**, 440-448. (2008).
64. Goate, A. *et al.* Segregation of a missense mutation in the amyloid precursor protein gene with familial Alzheimer's disease. *Nature. 349*, 704-706. (1991).
65. Levy-Lahad, E. *et al.* Candidate gene for the chromosome 1 familial Alzheimer's disease locus. *Science*. **269**, 973-977. (1995).
66. Rogaev, E.I. *et al.* Familial Alzheimer's disease in kindreds with missense mutations in a gene on chromosome 1 related to the Alzheimer's disease type 3 gene. *Nature*. **376,** 775-778. (1995).
67. Sherrington, R. *et al.* Alzheimer's disease associated with mutations in presenilin 2 is rare and variably penetrant. *Human Mol Genet* **5**, 985-988. (1996).
68. Tanzi, R.E. The genetics of Alzheimer disease. *Cold Spring Harb Perspect Med.* **2**(10), a006296. (2012).
69. Corder, E.H. *et al*. Gene dose of apolipoprotein E type 4 allele and the risk of Alzheimer's disease in late onset families. *Science.* **261**, 921-923. (1993).
70. Slooter, A.J. *et al*. Risk estimates of dementia by apolipoprotein E genotypes from a population-based incidence study: The Rotterdam Study. *Arch Neurol.* **55,** 964-968. (1998).
71. Harold, D. *et al*. Genome-wide association study identifies variants at CLU and PICALM associated with Alzheimer's disease. *Nat Genet.* **41,** 1088-93. (2009).
72. Lambert, J.C. *et al*. Genome-wide association study identifies variants at CLU and CR1 associated with Alzheimer's disease. *Nat Genet.* **41,** 1094-99. (2009).
73. Seshadri, S. *et al*. Genome-wide analysis of genetic loci associated with Alzheimer disease. *JAMA.* **303**, 1832-40. (2010).
74. Carrasquillo, M.M. *et al*. Replication of CLU, CR1, and PICALM associations with Alzheimer disease. *Arch Neurol.* **67**, 961-964. (2010).
75. Jun, G. *et al*. Meta-analysis confirms CR1, CLU, and PIC- ALM as Alzheimer disease risk loci and reveals interactions with APOE genotypes. *Arch Neurol*. **67**, 1473-84. (2010).
76. Lee, J.H. *et al*. Identification of novel loci for Alzheimer disease and replication of CLU, PICALM, and BIN1 in Caribbean Hispanic individuals. *Arch Neurol.* **68**, 320-328. (2010).
77. Fowler, D.M. *et al*. Functional amyloid formation within mammalian tissue. *PLoS Biol.* **4**(1), e6. (2005).

78. Maji, S.K. *et al*. Functional amyloids as natural storage of peptide hormones in pituitary secretory granules. *Science.* **325**, 328-32. (2009).
79. Li, J. *et al*. The RIP1/RIP3 necrosome forms a functional amyloid signaling complex required for programmed necrosis. *Cell.* **150,** 339-50. (2012).
80. Ban, T. & Y. Goto. Direct observation of amyloid growth monitored by total internal reflection fluorescence microscopy. *Methods Enzymol*. **413,** 91-102. (2006).
81. Blackley, H. K. L. *et al*. In-situ atomic force microscopy study of beta-amyloid fibrillization. *J Mol Biol.* **298**, 833-840. (2000).
82. Chen, X. G., S. K. Brining, V. Q. Nguyen, & A. L. Yergey. Simultaneous assessment of conformation and aggregation of beta- amyloid peptide using electrospray ionization mass spectrometry. *FASEB J.* **11**, 817-823. (1997).
83. Goldsbury, C., P. Frey, V. Olivieri, U. Aebi, & S.A. Muller. Multiple assembly pathways underlie amyloid-beta fibril polymorphisms. *J Mol Biol.* **352,** 282-298. (2005).
84. Harper, J.D., S.S. Wong, C.M. Lieber, & P.T. Lansbury. Assembly of Abeta amyloid protofibrils: an *in vitro* model for a possible early event in Alzheimer's disease. *Biochemistry*. **38**, 8972-80. (1999).
85. Pallitto, M.M., & R.M. Murphy. A mathematical model of the kinetics of beta-amyloid fibril growth from the denatured state. *Biophys J.* **81**:1805-22. (2001).
86. Lomakin, A., D. B. Teplow, D. A. Kirschner & G.B. Benedek. Kinetic theory of fibrillogenesis of amyloid beta-protein. *Proc. Natl Acad. Sci. USA*. **94**, 7942-47. (1997).
87. Kayed, R. *et al*. Common structure of soluble amyloid oligomers implies common mechanism of pathogenesis. *Science*. **300,** 486-489. (2003).
88. Bucciantini, M. *et al*. Inherent toxicity of aggregates implies a common mechanism for protein misfolding diseases. *Nature*. **416**, 507-511. (2002).
89. Lambert, M.P. *et al*. Diffusible, nonfibrillar ligands derived from Abeta ((1-42)) are potent central nervous system neurotoxins. *Proc. Natl Acad. Sci. USA*. **95,** 6448-53. (1998).
90. Lee, S., E. J. Fernandez, & T. A. Good. Role of aggregation conditions in structure, stability, and toxicity of intermediates in the A beta fibril formation pathway. *Protein Sci*. **16,** 723-732. (2007).
91. Kimberly, W.T. *et al*. γ-secretase is a membrane protein complex comprised of presenilin, nicastrin, Aph-1, and Pen-2. *Proc. Natl Acad. Sci. USA.* **100**, 6382-87. (2003).
92. Bitan G. *et al*. Amyloid β-protein (Aβ) assembly: Aβ40 and Aβ42 oligomerize through distinct pathways. *Proc. Natl Acad. Sci. USA.* **100**, 330-35. (2003).
93. Modler, A.J., Gast, K., Lutsch, G. & Damaschun, G. Assembly of amyloid protofibrils via critical oligomers - a novel pathway of amyloid formation. *J Mol Biol.* **325**, 135-148. (2003).
94. Monzo, P. *et al*. CD2AP, Rabip4, and Rabip4′: Analysis of Interaction with Rab4a and Regulation of Endosomes Morphology. *Meth Enzymol. Academic Press*. 107–118. (2005).
95. Lesné, S. *et al*. A specific amyloid-β protein assembly in the brain impairs memory. *Nature.* **440**, 352-357. (2006)
96. Lambert, M.P. *et al*. Diffusible, nonfibrillar ligands derived from Aβ1–42 are potent central nervous system neurotoxins. *Proc. Natl Acad. Sci. USA.* **95,** 6448-53. (1998).
97. Kayed, R. *et al.* Fibril specific, conformation dependent antibodies recognize a generic epitope common to amyloid fibrils and fibrillar oligomers that is absent in prefibrillar oligomers. *Mol. Neurodegener*. **2**, 18. (2007).
98. Kayed, R. *et al*. Annular protofibrils are a structurally and functionally distinct type of amyloid oligomer. *J Biol Chem.* **284**, 4230–37. (2009).
99. Barghorn, S. *et al*. Globular amyloid β-peptide (1-42) oligomer - a homogenous and stable neuropathological protein in Alzheimer's disease. *J Neurochem.* **95,** 834-47. (2005).
100. Hoshi, M. *et al*. Spherical aggregates of β-amyloid (amylospheroid) show high neurotoxicity and activate tau protein kinase I/glycogen synthase kinase-3β. *Proc. Natl Acad. Sci. USA.* **100,** 6370-75. (2003)
101. Chimon, S. *et al*. Evidence of fibril-like β-sheet structures in a neurotoxic amyloid intermediate of Alzheimer's β-amyloid. *Nat Struct Mol Biol.* **14,** 1157-64. (2007).
102. Ahmed, M. *et al.* Structural conversion of neurotoxic amyloid-beta (1-42) oligomers to fibrils. *Nat Struct Mol.* Biol. **17,** 561-67. (2010).
103. Podlisny, M.B. *et al*. Aggregation of secreted amyloid β-protein into sodium dodecyl sulfate-stable oligomers in cell culture. *J Biol Chem*. **270,** 9564-70. (1995).
104. Harper, J.D., Wong, S., Lieber, C.M. & Lansbury, P.T. Observation of metastable Aβ amyloid protofibrils by atomic force microscopy. *Chem Biol*. **4**, 119–25 (1997).

105. Stroud, J.C., Liu, C., Teng, P.K. & Eisenberg, D. Toxic fibrillar oligomers of amyloid-β have cross-β structure. *Proc. Natl Acad. Sci. USA* **109,** 7717-22. (2012).
106. Parthasarathy, S. *et al*. Structural insight into an Alzheimer's brain-derived spherical assembly of amyloid β by solid-state NMR. *J Am Chem Soc.* **137,** 6480-83. (2015)
107. O'Nuallain, B. *et al*. Amyloid β-protein dimers rapidly form stable synaptotoxic protofibrils. *J Neurosci*. **30,** 14411-19. (2010).
108. Matsumura, S. *et al*. Two distinct amyloid β-protein (Aβ) assembly pathways leading to oligomers and fibrils identified by combined fluorescence correlation spectroscopy, morphology, and toxicity analyses. *J Biol Chem*. **286**, 11555-62. (2011).
109. Fu, Z., Aucoin, D., Davis, J., Van Nostrand, WE. & Smith SO. Mechanism of nucleated conformational conversion of Aβ42. *Biochemistry.* **54**, 197-207. (2015).
110. Lasagna-Reeves, C.A., Glabe, C.G. & Kayed, R. Amyloid-β annular protofibrils evade fibrillar fate in Alzheimer disease brain. *J Biol Chem.* **286**, 22122-30. (2011).
111. Vassar, R. et al. Beta-secretase cleavage of Alzheimer's amyloid precursor protein by the transmembrane aspartic protease BACE. Science. 286, 735–741. (1999).
112. Saunders, A.J. et al. BACE maps to chromosome 11 and a BACE homolog, BACE2, reside in the obligate Down syndrome region of chromosome 21. Science. 286, 1255. (1999).
113. Bennett, B.D. et al. Expression analysis of BACE2 in brain and peripheral tissues. J Biol Chem. 275, 20647-51. (2000).
114. Paravastu, A.K., Leapman, R.D., Yau, W.M. & Tycko, R. Molecular structural basis for polymorphism in Alzheimer's β-amyloid fibrils. *Proc. Natl Acad. Sci. USA.* **105**,18349-54. (2008).
115. Petkova, A.T., Yau, W.M. & Tycko, R. Experimental constraints on quaternary structure in Alzheimer's β-amyloid fibrils. *Biochemistry.* **45**, 498-512. (2006).
116. Bertini I, Gonnelli L, Luchinat C, Mao J & Nesi A. A new structural model of Aβ40 fibrils. *J Am Chem Soc.* **133,** 16013-22. (2011).
117. Colvin, M.T. *et al.* Atomic resolution structure of monomorphic Aβ42 amyloid fibrils. *J Am Chem Soc.* **138**, 9663-74. (2016).
118. Luhrs, T. *et al.* 3D structure of Alzheimer's amyloid-β(1–42) fibrils. *Proc. Natl Acad. Sci. USA.* **102**, 17342-47. (2005).
119. Benilova, I., Karran, E. & De Strooper, B. The toxic Aβ oligomer and Alzheimer's disease: an emperor in need of clothes. *Nat Neurosci*. **15,** 349-57. (2012).
120. Paravastu AK, Leapman RD, Yau WM & Tycko R. Molecular structural basis for polymorphism in Alzheimer's β-amyloid fibrils. *Proc. Natl Acad. Sci. USA.* **105,** 18349-54. (2008).
121. Petkova, A.T., Yau, W.M. & Tycko, R. Experimental constraints on quaternary structure in Alzheimer's β-amyloid fibrils. *Biochemistry.* **45,** 498-512. (2006).
122. Bertini I, Gonnelli L, Luchinat C, Mao J, Nesi A. A new structural model of Aβ40 fibrils. *J Am Chem Soc.* **133,** 16013-22. (2011).
123. Lu, J.X. *et al*. Molecular structure of β-amyloid fibrils in Alzheimer's disease brain tissue. *Cell.* **154**, 1257-68. (2013).
124. Guimas Almeida, C., Sadat Mirfakhar, F., Perdigão, C. & Burrinha, T. Impact of late-onset Alzheimer's genetic risk factors on beta-amyloid endocytic production. *Cell. Mol. Life Sci*. **75**(14): 2577. (2018).
125. Török, M. *et al*. Structural and dynamic features of Alzheimer's Aβ peptide in amyloid fibrils studied by site-directed spin labeling. *J Biol Chem.* **277,** 40810-15. (2002).
126. Luhrs, T. *et al.* 3D structure of Alzheimer's amyloid-β(1–42) fibrils. *Proc. Natl Acad. Sci. USA.* **102**, 17342-47. (2005).
127. Serio, T.R. *et al*. Nucleated conformational conversion and the replication of conformational information by a prion determinant. *Science*. **289,** 1317-21. (2000).
128. Morris, A.M., Watzky, M.A. & Finke, R.G. Protein aggregation kinetics, mechanism, and curve-fitting: a review of the literature. *Biochim Biophys Acta.* **1794,** 375–97. (2009).
129. Chen, S., Ferrone, F.A. & Wetzel, R. Huntington's disease age-of-onset linked to polyglutamine aggregation nucleation. *Proc. Natl Acad. Sci. USA.* **99,** 11884-89. (2002).
130. Ferrone, F.A. Assembly of Aβ proceeds via monomeric nuclei. *J Mol Biol.* **427,** 287-90. (2015).
131. Cohen, S.I. *et al*. Proliferation of amyloid-β42 aggregates occurs through a secondary nucleation mechanism. *Proc. Natl Acad. Sci. USA.* **110,** 9758-63. (2013).
132. Meisl, G. *et al*. Differences in nucleation behavior underlie the contrasting aggregation kinetics of the Aβ40 and Aβ42 peptides. *Proc. Natl Acad. Sci. USA.* **111,** 9384–89. (2014).

133. Wang, X., Perry, G., Smith, M.A. & Zhu, X. Amyloid-beta-derived diffusible ligands cause impaired axonal transport of mitochondria in neurons. *Neurodegener Dis.* **7**, 56-59. (2010).
134. Reed, M.N. *et al.* Cognitive effects of cell-derived and synthetically derived Abeta oligomers. *Neurobiol Aging.* **32**, 1784-94. (2011).
135. Dominguez, D. et al. Phenotypic and biochemical analyses of BACE1- and BACE2-deficient mice. J Biol Chem. 280, 30797-806. (2005).
136. Deshpande, A., Mina, E., Glabe, C. & Busciglio, J. Different conformations of amyloid beta induce neurotoxicity by distinct mechanisms in human cortical neurons. *J Neurosci.* **26**, 6011-18. (2006).
137. Kuperstein, I. *et al.* Neurotoxicity of Alzheimer's disease Abeta peptides is induced by small changes in the Abeta42 to Abeta40 ratio. *EMBO*. **29**, 3408-3420. (2010).
138. Hartley, D.M. *et al.* Transglutaminase induces protofibril-like amyloid beta-protein assemblies that are protease-resistant and inhibit long-term potentiation. *J Biol Chem.* **283**, 16790–16800. (2008).
139. Sandberg, A. *et al.* Stabilization of neurotoxic Alzheimer amyloid-beta oligomers by protein engineering. *Proc. Natl Acad. Sci. USA*. **107**, 15595-15600. (2010).
140. Walsh, D.M. *et al.* Naturally secreted oligomers of amyloid beta protein potently inhibit hippocampal long-term potentiation *in vivo*. *Nature* 416, 535–539 (2002).
141. Cleary, J.P. *et al.* Natural oligomers of the amyloid-beta protein specifically disrupt cognitive function. *Nat. Neurosci.* 8, 79–84 (2005).
142. Li, S. *et al.* Soluble oligomers of amyloid Beta protein facilitate hippocampal long-term depression by disrupting neuronal glutamate uptake. *Neuron.* **62**, 788–801 (2009).
143. Cummings, K. et al. Alzheimer's disease drug development pipeline: 2018. Alzheimer's & Dementia: Translational Research & Clinical Interventions. 4, 195-214. (2018).
144. Shankar, G.M. *et al.* Amyloid- protein dimers isolated directly from Alzheimer's brains impair synaptic plasticity and memory. *Nat Med.* **14**, 837–842 (2008).
145. Roher, A.E. *et al.* Morphology and toxicity of Abeta-((1-42)) dimer derived from neuritic and vascular amyloid deposits of Alzheimer's disease. *J Biol Chem*. **271**, 20631–20635. (1996).
146. Noguchi, A. *et al.* Isolation and characterization of patient-derived, toxic, high mass amyloid beta-protein (Abeta) assembly from Alzheimer disease brains. *J Biol Chem.* **284**, 32895–32905. (2009).
147. Braak, H., Del Tredici, K. Evolutional aspects of Alzheimer's disease pathogenesis. *J Alzheimer's Dis* **33**(1), S155–61. (2013).
148. Crimins, J.L., Pooler, A., Polydoro, M., Luebke, J.I. & Spires-Jones, T.L. The intersection of amyloid beta and Tau in glutamatergic synaptic dysfunction and collapse in Alzheimer's disease. *Ageing Res Revs.* **12,** 757–63. (2013).
149. Kayed, R., Lasagna-Reeves, C.A. Molecular mechanisms of amyloid oligomers toxicity. *J Alzheimers Dis*. **33**(1), S67–78. (2013)
150. Selkoe, D.J. Biochemistry and molecular biology of amyloid beta-protein and the mechanism of Alzheimer's disease. *Handb Clin Neurol.* **89,** 245–60. (2008).
151. Selkoe, D.J. Soluble oligomers of the amyloid beta-protein impair synaptic plasticity and behavior. *Behav Brain Res.* **192,** 106–13. (2008).
152. Klein, W.L. Synaptotoxic amyloid-β oligomers: a molecular basis for the cause, diagnosis, and treatment of Alzheimer's disease? *J Alzheimers Dis.* **33**(1), S49–65. (2013).
153. Abramov, E., Dolev, I., Fogel, H., Ciccotosto, G.D., Ruff, E. & Slutsky, I. Amyloid-beta as a positive endogenous regulator of release probability at hippocampal synapses. *Nat Neurosci.* **12**, 1567–76. (2009).
154. Garcia-Osta, A. & Alberini, C.M. Amyloid beta mediates memory formation. *Learn Mem*. **16,** 267–72. (2009).
155. Kumar, S. & Walter, J. Phosphorylation of amyloid beta (Aβ) peptides—a trigger for formation of toxic aggregates in Alzheimer's disease. *Aging*. **3**, 803–12. (2011).
156. Kumar, S. *et al*. Phosphorylation of amyloid-β peptide at serine 8 attenuates its clearance via insulin-degrading and angiotensin-converting enzymes. *J Biol Chem.* **287,** 8641–51. (2012).
157. Kawahara, M. Neurotoxicity of β-amyloid protein: oligo- merization, channel formation, and calcium dyshomeostasis. *Curr Pharm Des.* **16,** 2779–89. (2010).
158. Zhao, L.N., Long, H., Mu, Y. & Chew, L.Y. The toxicity of amy- loid β oligomers. *Int J Mol Sci*. **13,** 7303–27. (2012).
159. Koo, E.H. & Squazzo, S.L. Evidence that production and release of amyloid beta-protein involves the endocytic pathway. *J Biol Chem.* **269,** 17386-89. (1994).

160. Rajendran, L. *et al*. Alzheimer's disease beta-amyloid peptides are released in association with exosomes. *Proc. Natl Acad. Sci. USA.* **103,** 11172-77. (2006).
161. Sannerud, R. & Annaert, W. Trafficking, a key player in regulated intramembrane proteolysis. *Semin Cell Dev Biol*. **20**, 183–190. (2009).
162. Zheng H, Koo EH. The amyloid precursor protein: beyond amyloid. *Mol Neurodegener.* **1**, 5. (2006).
163. Soba, P. *et al*. Homo- and heterodimerization of APP family members promotes intercellular adhesion. *EMBO J*. **24**, 3624–3634. (2005).
164. Kogel, D., Deller, T. & Behl, C. Roles of amyloid precursor protein family members in neuroprotection, stress signaling and aging. *Exp Brain Res*. **217**(3-4), 471-9. (2012).
165. Nikolaev, A., McLaughlin, T., O'Leary, D.D. & Tessier-Lavigne, M. APP binds DR6 to trigger axon pruning and neuron death via distinct caspases. *Nature*. **457,** 981-989. (2009).
166. Konietzko, U. AICD nuclear signaling and its possible contribution to Alzheimer's disease. *Curr Alzheimer Res.* **9**(2). (2012).
167. Moghekar, A. *et al*. Large quantities of Abeta peptide are constitutively released during amyloid precursor protein metabolism *in vivo* and *in vitro*. *J Biol Chem.* **286**, 15989-97. (2011).
168. Gouras, G.K. *et al*. Intraneuronal Abeta42 accumulation in human brain. *Am J Pathol*. **156,** 15-20. (2000).
169. Takahashi, R.H. *et al*. Intraneuronal Alzheimer abeta42 accumulates in multivesicular bodies and is associated with synaptic pathology. *Am J Pathol.***161**, 1869-79. (2002).
170. Knobloch, M., Farinelli, M., Konietzko, U., Nitsch, R.M. & Mansuy, I.M. Abeta oligomer-mediated long-term potentiation impairment involves protein phosphatase 1-dependent mechanisms. *J Neurosci*. **27,** 7648-53. (2007).
171. Wirths, O. *et al*. Intraneuronal APP/A beta trafficking and plaque formation in beta-amyloid precursor protein and presenilin-1 transgenic mice. *Brain Pathol*. **12,** 275-286. (2002).
172. Oddo, S., Caccamo, A., Kitazawa, M., Tseng, B.P. & LaFerla, F.M. Amyloid deposition precedes tangle formation in a triple transgenic model of Alzheimer's disease. *Neurobiol Aging.* **24**, 1063-70. (2003).
173. Ginsberg, S.D. *et al.* Microarray analysis of hippocampal CA1 neurons implicates early endosomal dysfunction during Alzheimer's disease progression. *Biol Psychiatry*. **68,** 885-893. (2010).
174. Boland, B., Kumar, A., Lee, S., Platt, F.M., Wegiel, J., Yu, W.H. & Nixon, R.A. Autophagy induction and autophagosome clearance in neurons: relationship to autophagic pathology in Alzheimer's disease. *J Neurosci.* **28,** 6926-37. (2008).
175. Yu, W.H. *et al*. Macroautophagy – a novel beta-amyloid peptide-generating pathway activated in Alzheimer's disease. *J Cell Biol*. **171,** 87-98. (2005).
176. Rajendranm L. *et al.* Alzheimer's disease beta-amyloid peptides are released in association with exosomes. *Proc. Natl Acad. Sci. USA*. **103**, 11172-77. (2006).
177. Aguzzi, A. & Rajendran, L. The transcellular spread of cytosolic amyloids, prions, and prionoids. *Neuron*. **64**, 783-790. (2009).
178. Cirrito, J.R. *et al.* Synaptic activity regulates interstitial fluid amyloid-beta levels *in vivo*. *Neuron*, **48**, 913-922. (2005).
179. Wang, Y. & Mandelkow, E. Tau in physiology and pathology. *Nature* Reviews *Neuroscience*. **17**, 22–35. (2016)
180. Hasegawa, M. *et al.* Protein sequence and mass spectrometric analyses of tau in the Alzheimer's disease brain. *J Biol Chem*. **267**, 17047-54. (1992).
181. Alonso, A. C., Grundke-Iqbal, I. & Iqbal, K. Alzheimer's disease hyperphosphorylated tau sequesters normal tau into tangles of filaments and disassembles microtubules. *Nat Med.* **2**, 783-787. (1996).
182. Wang, J. Z., Grundke-Iqbal, I. & Iqbal, K. Restoration of biological activity of Alzheimer abnormally phosphorylated tau by dephosphorylation with protein phosphatase-2A, -2B and -1. *Brain Res Mol Brain Res.* **38**, 200–208. (1996).
183. Alonso, A. D. *et al.* Interaction of tau isoforms with Alzheimer's disease abnormally hyperphosphorylated tau and *in vitro* phosphorylation into the disease-like protein. *J Biol Chem.* **276**, 37967-73. (2001).
184. Wang, J. Z., Grundke-Iqbal, I. & Iqbal, K. Kinases and phosphatases and tau sites involved in Alzheimer neurofibrillary degeneration. *Eur J Neurosci.* **25**, 59–68. (2007)
185. Andreadis, A. Misregulation of tau alternative splicing in neurodegeneration and dementia. *Prog Mol Subcell Biol.* **44**, 89-107 (2006).

186. LoPresti, P., Szuchet, S., Papasozomenos, S. C., Zinkowski, R. P. & Binder, L. I. Functional implications for the microtubule-associated protein tau: localization in oligodendrocytes. *Proc Natl Acad Sci USA.* **92**, 10369-73. (1995).
187. Lee, G., Cowan, N. & Kirschner, M. The primary structure and heterogeneity of tau protein from mouse brain. *Science.* **239**, 285–288. (1988).
188. Dickson, D. W., Kouri, N., Murray, M. E. & Josephs, K. A. Neuropathology of frontotemporal lobar degeneration-tau (FTLD-tau). *J Mol Neurosci.* **45**, 384-389. (2011).
189. Goedert, M. & Jakes, R. Expression of separate isoforms of human tau protein: correlation with the tau pattern in brain and effects on tubulin polymerization. *EMBO J.* **9**, 4225-30. (1990).
190. Chen, J., Kanai, Y., Cowan, N. J. & Hirokawa, N. Projection domains of MAP2 and tau determine spacings between microtubules in dendrites and axons. *Nature.* **360**, 674–677. (1992).
191. Frappier, T. F., Georgieff, I. S., Brown, K. & Shelanski, M. L. τ regulation of microtubule-microtubule spacing and bundling. *J. Neurochem.* **63**, 2288-94. (1994).
192. Liu, C. & Gotz, J. Profiling murine tau with 0N, 1N and 2N isoform-specific antibodies in brain and peripheral organs reveals distinct subcellular localization, with the 1N isoform being enriched in the nucleus. *PLoS One.* **8**, e84849. (2013).
193. Zhong, Q., Congdon, E. E., Nagaraja, H. N. & Kuret, J. Tau isoform composition influences rate and extent of filament formation. *J Biol Chem*. **287**, 20711-19. (2012).
194. Lee, V. M., Goedert, M. & Trojanowski, J. Q. Neurodegenerative tauopathies. *Annu Rev Neurosci.* **24**, 1121-59. (2001).
195. Feinstein, S. C. & Wilson, L. Inability of tau to properly regulate neuronal microtubule dynamics: a loss-of-function mechanism by which tau might mediate neuronal cell death. Biochim Biophys Acta. **1739**, 268-279. (2005).
196. Mandelkow, E. M. & Mandelkow, E. Biochemistry and cell biology of tau protein in neurofibrillary degeneration. *Cold Spring Harb Perspect Med.* **2**, a006247. (2012).
197. Kadavath, H. *et al.* Tau stabilizes microtubules by binding at the interface between tubulin heterodimers. *Proc. Natl Acad. Sci. USA.* **112**, 7501-06. (2015).
198. Stamer, K., Vogel, R., Thies, E., Mandelkow, E. & Mandelkow, E. M. Tau blocks traffic of organelles, neurofilaments, and APP vesicles in neurons and enhances oxidative stress. *J Cell Biol.* **156**, 1051–1063. (2002).
199. Caceres, A. & Kosik, K. S. Inhibition of neurite polarity by tau antisense oligonucleotides in primary cerebellar neurons. *Nature*. **343**, 461–463. (1990).
200. Knops, J. *et al.* Overexpression of tau in a nonneuronal cell induces long cellular processes. *J Cell Biol.* **114**, 725-733. (1991).
201. Frandemiche, M. L. *et al*. Activity-dependent tau protein translocation to excitatory synapse is disrupted by exposure to amyloid-β oligomers. *J Neurosci.* **34**, 6084-97. (2014).
202. Violet, M. *et al*. A major role for Tau in neuronal DNA and RNA protection *in vivo* under physiological and hyperthermic conditions. *Front Cell Neurosci*. **8**, 84. (2014).
203. Sultan, A. *et al*. Nuclear tau, a key player in neuronal DNA protection. *J Biol Chem.* **286**, 4566-75. (2011).
204. Roberson, E. D. *et al*. Reducing endogenous tau ameliorates amyloid β-induced deficits in an Alzheimer's disease mouse model. *Science.* **316**, 750-754. (2007).
205. Ittner, L. M. *et al*. Dendritic function of tau mediates amyloid-β toxicity in Alzheimer's disease mouse models. *Cell*. **142**, 387-397. (2010).
206. Gheyara, A. L. *et al*. Tau reduction prevents disease in a mouse model of Dravet syndrome. *Ann. Neurol.* **76**, 443–456. (2014).
207. Holth, J. K. *et al*. Tau loss attenuates neuronal network hyperexcitability in mouse and Drosophila genetic models of epilepsy. *J Neurosci.* **33**, 1651-59. (2013).
208. Leroy, K. *et al*. Lack of tau proteins rescues neuronal cell death and decreases amyloidogenic processing of APP in APP/PS1 mice. *Am J Pathol.* **181**, 1928-40. (2012).
209. Kanemaru, K., Takio, K., Miura, R., Titani, K. & Ihara, Y. Fetal-type phosphorylation of the tau in paired helical filaments. *J Neurochem.* **58**, 1667-75. (1992).
210. Köpke, E. *et al*. Microtubule-associated protein tau. Abnormal phosphorylation of a non-paired helical filament pool in Alzheimer disease. *J Biol Chem.* **268**, 24374-84. (1993).
211. Hanger, D. P., Anderton, B. H. & Noble, W. Tau phosphorylation: the therapeutic challenge for neurodegenerative disease. *Trends Mol Med.* **15**, 112–119. (2009).

212. Lu, P. J., Wulf, G., Zhou, X. Z., Davies, P. & Lu, K. P. The prolyl isomerase Pin1 restores the function of Alzheimer-associated phosphorylated tau protein. *Natur.e* 399, 784–788. (1999).
213. Gong, C. X., Singh, T. J., Grundke-Iqbal, I. & Iqbal, K. Phosphoprotein phosphatase activities in Alzheimer disease brain. *J Neurochem.* **61**, 921–927. (1993).
214. Chen, S., Li, B., Grundke-Iqbal, I. & Iqbal, K. IPP2A1 affects tau phosphorylation via association with the catalytic subunit of protein phosphatase 2A. *J Biol Chem.* **283**, 10513-21. (2008).
215. Sontag, E. *et al.* Downregulation of protein phosphatase 2A carboxyl methylation and methyltransferase may contribute to Alzheimer disease pathogenesis. *J Neuropathol Exp Neurol.* **63**, 1080-91. (2004).
216. Min, S. W. *et al*. Acetylation of tau inhibits its degradation and contributes to tauopathy. *Neuron* **67**, 953–966. (2010).
217. Cook, C. *et al*. Acetylation of the KXGS motifs in tau is a critical determinant in modulation of tau aggregation and clearance. *Hum. Mol. Genet.* **23**, 104–116. (2014).
218. Irwin, D. J. *et al*. Acetylated tau neuropathology in sporadic and hereditary tauopathies. *Am. J. Pathol.* **183**, 344–351. (2013).
219. Min, S. W. *et al*. Critical role of acetylation in tau- mediated neurodegeneration and cognitive deficits. *Nat. Med.* **21**, 1154-62. (2015).
220. Martin, L., Latypova, X. & Terro, F. Post-translational modifications of tau protein: implications for Alzheimer's disease. *Neurochem. Int.* **58**, 458–471. (2011).
221. Tracy, T. E. and Gan, L. Acetylated tau in Alzheimer's disease: An instigator of synaptic dysfunction underlying memory loss. *Bioessays.* 39: n/a. (2017).
222. Wischik, C. M. *et al*. Isolation of a fragment of tau derived from the core of the paired helical filament of Alzheimer disease. *Proc Natl Acad Sci U S A*. **85**, 4506-10. (1988).
223. Braak, E., Braak, H. & Mandelkow, E. M. A sequence of cytoskeleton changes related to the formation of neurofibrillary tangles and neuropil threads. *Acta Neuropathol*. **87**, 554–567. (1994)
224. Lasagna-Reeves, C.A. *et al*. Identification of oligomers at early stages of tau aggregation in Alzheimer's disease. *FASEB journal: official publication of the Federation of American Societies for Experimental Biology*. **26**:1946–1959. (2012).
225. Ren, Y. & Sahara, N. Characteristics of tau oligomers. *Frontiers in neurology.* **4**:102. (2013).
226. Barghorn, S. & Mandelkow, E. Toward a unified scheme for the aggre- gation of tau into Alzheimer paired helical filaments. *Biochem.* **41**:14885–96. (2002).
227. Makrides, V. *et al*. Microtubule-dependent oligomerization of tau. Impli- cations for physiological tau function and tauopathies. *J Biol Chem.* **278**:33298–304. (2003).
228. Gao, Y. & Pimplikar, S.W. The gamma -secretase-cleaved C-terminal fragment of amyloid precursor protein mediates signaling to the nucleus. *Proc Natl Acad Sci U S A*. **98**(26), 14979-84. (2001).
229. Kuret, J. *et al*. Pathways of tau fibrilliza- tion. *Biochim Biophys Acta.* **1739**:167–78. (2005).
230. Maeda, S. *et al*. Granular tau oligomers as intermediates of tau filaments. *Bio- chemistry.* **46**:3856–61. (2007).
231. Sahara, N. *et al*. Assembly of two distinct dimers and higher-order oligomers from full-length tau. *Eur J Neurosci.* **25**:3020–9. (2007).
232. Zilka, N. *et al*. Truncated tau from sporadic Alzheimer's disease suffices to drive neurofibrillary degeneration *in vivo*. *FEBS Lett*. **580**, 3582-88. (2006).
233. Gamblin, T. C. *et al*. Caspase cleavage of tau: linking amyloid and neurofibrillary tangles in Alzheimer's disease. *Proc Natl Acad Sci U S A.* **100**, 10032-37. (2003).
234. Pérez, M., Valpuesta, J. M., Medina, M., Montejo de Garcini, E. & Avila, J. Polymerization of tau into filaments in the presence of heparin: the minimal sequence required for tau–tau interaction. *J Neurochem*. **67**, 1183-90. (1996).
235. Kontsekova, E., Zilka, N., Kovacech, B., Novak, P. & Novak, M. First-in-man tau vaccine targeting structural determinants essential for pathological tau–tau interaction reduces tau oligomerisation and neurofibrillary degeneration in an Alzheimer's disease model. *Alzheimers Res Ther*. **6**, 44. (2014).
236. Yuzwa, S. A. *et al.* Mapping *O*-GlcNAc modification sites on tau and generation of a site-specific *O*-GlcNAc tau antibody. *Amino Acids.* **40**, 857–868. (2011).
237. Liu, F. *et al.* Reduced *O*-GlcNAcylation links lower brain glucose metabolism and tau pathology in Alzheimer's disease. *Brain* **132**, 1820-32. (2009).

238. Gong, C. X., Liu, F., Grundke-Iqbal, I. & Iqbal, K. Impaired brain glucose metabolism leads to Alzheimer neurofibrillary degeneration through a decrease in tau *O*-GlcNAcylation. *J. Alzheimers Dis.* **9**, 1-12 (2006).
239. Hara, T., Nakamura, K., Matsui, M., Yamamoto, A., Nakahara, Y., Suzuki-Migishima, R., Yokoyama, M., Mishima, K., Saito, I., Okano, H. and Mizushima, N. Suppression of basal autophagy in neural cells causes neurodegenerative disease in mice. *Nature* **441**, 885–889. (2006).
240. Komatsu, M., Waguri, S., Chiba, T., Murata, S., Iwata, J., Tanida, I., Ueno, T., Koike, M., Uchiyama, Y., Kominami, E. and Tanaka, K. Loss of autophagy in the central nervous system causes neurodegeneration in mice. *Nature* **441**, 880–884. (2006).
241. Mori, H., Kondo, J. & Ihara, Y. Ubiquitin is a component of paired helical filaments in Alzheimer's disease. *Science* **235**, 1641–1644. (1987).
242. Cohen, T.J., Guo, J.L., Hurtado, D.E., Kwong, L.K., Mills, I.P., Trojanowski, J.Q. and Lee, V.M. The acetylation of tau inhibits its function and promotes pathological tau aggregation. *Nat Commun.* **2**, 252. (2011).
243. Babu, J.R., Geetha, T. & Wooten, M.W. Sequestosome 1/p62 shuttles polyubiquitinated tau for proteasomal degradation. *J. Neurochem*. **94**, 192–203. (2005).
244. Tan, J.M., Wong, E.S., Kirkpatrick, D.S., Pletnikova, O., Ko, H.S., Tay, S.P., Ho, Troncoso, M.W. *et al*. Lysine 63-linked ubiquitination promotes the formation and autophagic clearance of protein inclusions associated with neurodegenerative diseases. *Hum Mol Genet*. **17**, 431–439. (2008).
245. Petrucelli, L. *et al*. CHIP and Hsp70 regulate tau ubiquitination, degradation and aggregation. *Hum Mol Genet*. **13**, 703–714. (2004).
246. Shimura, H., Schwartz, D., Gygi, S.P. & Kosik, K.S. CHIP–Hsc70 complex ubiquitinates phosphorylated tau and enhances cell survival. *J Biol Chem.* **279**, 4869–AT6. (2004).
247. Dickey, C.A. *et al*. Deletion of the ubiquitin ligase CHIP leads to the accumulation, but not the aggregation, of both endogenous phospho- and caspase-3-cleaved tau species. *J Neurosci.* **26**, 6985–6996. (2006).
248. Sahara, N. *et al.* In vivo evidence of CHIP up-regulation attenuating tau aggregation. *J Neurochem*. **94**, 1254-63. (2005).
249. Wang, Y., Garg, S., Mandelkow, E.M. & Mandelkow, E. Proteolytic processing of tau. *Biochem Soc Trans*. **38**, 955–961. (2010)
250. Garg, S., Timm, T., Mandelkow, E.M., Mandelkow, E. & Wang, Y. Cleavage of Tau by calpain in Alzheimer's disease: the quest for the toxic 17 kD fragment. *Neurobiol Aging* **32**, 1–14. (2011).
251. Karsten, S.L. *et al*. A genomic screen for modifiers of tauopathy identifies puromycin-sensitive aminopeptidase as an inhibitor of tau-induced neurodegeneration. *Neuro.n* **51**, 549–560. (2006).
252. Sengupta, S. *et al*. Degradation of tau protein by puromycin-sensitive aminopeptidase *in vitro*. *Biochemistry* **45**, 15111-19. (2006).
253. Chow, K.M., Guan, H. & Hersh, L.B. Aminopeptidases do not directly degrade tau protein. *Mol Neurodegener*. **5**, 48. (2010).
254. Kudo, L.C. *et al*. Puromycin-sensitive aminopeptidase (PSA/NPEPPS) impedes development of neuropathology in hPSA/TAU(P301L) double-transgenic mice. *Hum Mol Genet*. **20**, 1820-33. (2011).
255. Wong, E. & Cuervo, A.M. Integration of clearance mechanisms: the proteasome and autophagy. *Cold Spring Harbor Perspect Biol*. **2**, a006734. (2010).
256. Shang, F. & Taylor, A. Ubiquitin–proteasome pathway and cellular responses to oxidative stress. *Free Radical Biol Med*. **51**, 5–16 (2011).
257. Wang, Y., *et al.* Tau fragmentation, aggregation and clearance: the dual role of lysosomal processing. *Hum Mol Genet.* **18**, 4153-70. (2009).
258. Massey, A., Kiffin, R. & Cuervo, A.M. Pathophysiology of chaperone-mediated autophagy. *Int J Biochem Cell Biol.* **36**, 2420-34. (2004).
259. Cohen, T. J. *et al*. "The acetylation of tau inhibits its function and promotes pathological tau aggregation," *Nat Commun*. **2**(1), 252. (2011).
260. B. L. Goode and S. C. Feinstein, "Identification of a novel microtubule binding and assembly domain in the developmentally regulated inter-repeat region of tau," *J Cell Biol*. **124**(5), 769–781. (1994).
261. Trzeciakiewicz, H. *et al.* A Dual Pathogenic Mechanism Links Tau Acetylation to Sporadic Tauopathy. *Sci rep.* **7**: 44102. (2017).

262. Wang, Y. & Mandelkow, E. Degradation of tau protein by autophagy and proteasomal pathways. *Biochem Soc Trans*. **40**, 644-652. (2012).
263. Santacruz, K. *et al*. Tau suppression in a neurodegenerative mouse model improves memory function. *Science.* **309**, 476–481. (2005).
264. Van der Jeugd, A. *et al*. Cognitive defects are reversible in inducible mice expressing pro-aggregant full-length human Tau. *Acta Neuropathol*. **123**, 787–805. (2012).
265. Sydow, A. *et al*. Tau-induced defects in synaptic plasticity, learning, and memory are reversible in transgenic mice after switching off the toxic Tau mutant. *J Neurosci.* **31**, 2511-25. (2011).
266. Iqbal, K. *et al*. Defective brain microtubule assembly in Alzheimer's disease. *Lancet* **2**, 421–426. (1986).
267. Kopke, E. *et al*. Microtubule-associated protein tau. Abnormal phosphorylation of a non-paired helical filament pool in Alzheimer disease. *J. Biol. Chem*. **268**, 24374-84. (1993).
268. Alonso, A., Zaidi, T., Novak, M., Grundke-Iqbal, I. & Iqbal, K. Hyperphosphorylation induces self-assembly of tau into tangles of paired helical filaments/straight filaments. *Proc Natl Acad Sci U S A.* **98**, 6923-28. (2001).
269. Alonso, A. D., Grundke-Iqbal, I., Barra, H. S. & Iqbal, K. Abnormal phosphorylation of tau and the mechanism of Alzheimer neurofibrillary degeneration: sequestration of microtubule-associated proteins 1 and 2 and the disassembly of microtubules by the abnormal tau. *Proc Natl Acad Sci U S A.* **94**, 298–303. (1997).
270. Iqbal, K., Zaidi, T., Bancher, C. & Grundke-Iqbal, I. Alzheimer paired helical filaments. Restoration of the biological activity by dephosphorylation. *FEBS Lett*. **349**, 104–108. (1994).
271. Lemere, CA. Immunotherapy for Alzheimer's disease: hoops and hurdles. *Molecular Neurodegener.* 2013, **8**:36. (2013).
272. Shepard, J. F., Secor, G. A., & Purcifull, D. E. Immunochemical cross-reactivity between the dissociated capsid proteins of PVY group plant viruses. *Virology.* 58, 464–475. (1974).
273. Dougherty, W., Willis, L., & Johnston, R. E. Topographic analysis of tobacco etch virus capsid protein epitopes. *Virology* **144**, 66–72. (1985).
274. Reineke, U. & Schutkowski, M. Epitope Mapping Protocols. (*Springer Protocols,* 2009).
275. Zolla-Pazner, S. Identifying epitopes of HIV-1 that induce protective antibodies. *Nat Rev Immunol*. **4**, 199–210. (2004).
276. Folgori, A. *et al.* A general strategy to identify mimotopes of pathological antigens using only random peptide libraries and human sera. *EMBO J.* **13**, 2236-43. (1994).
277. Delmastro, P., Meola, A., Monaci, P., Cortese, R., & Galfrè, G. Immunogenicity of filamentous phage displaying peptide mimotopes after oral administration. *Vaccine* **15**, 1276-85. (1997).
278. Lipman, N.S., Jackson, L.R., Trudel, L.J. & Weis-Garcia, F. Monoclonal Versus Polyclonal Antibodies: Distinguishing Characteristics, Applications, and Information Resources. *ILAR Journal*. **46**(3), 258–268. (2005).
279. Shirazi, S.K. & Wood, J.G. The protein tyrosine kinase, fyn, in Alzheimer's disease pathology. *Neuroreport*. **4**(4), 435–437. (1993).
280. Cochran, J. N., Hall A. M., & Roberson, E. D. The dendritic hypothesis for Alzheimer's disease pathophysiology. *Brain Res Bull.* **103**, 18–28. (2014).
281. H. B. Nygaard, C. H. van Dyck, and S. M. Strittmatter. Fyn kinase inhibition as a novel therapy for Alzheimer's disease. *Alzheimer Res Ther*. **6**(1): 8. (2014).
282. Yang, K., Belrose, J., Trepanier, C.H., Lei, G., Jackson, M.F. & MacDonald, J.F. Fyn, a potential target for Alzheimer's disease. *J Alzheimers Dis*. **27**(2), 243-52. (2011).
283. Hardy, J. & Selkoe, D.J. The amyloid hypothesis of Alzheimer's disease: progress and problems on the road to therapeutics. *Science*. **297(**5580), 353-356. (2002).
284. Castello, M.A. & Soriano, S. On the origin of Alzheimer's disease. Trials and tribulations of the amyloid hypothesis. *Ageing Res Rev*. **13**(1), 10-12. (2014).
285. Drachman, D.A. The amyloid hypothesis, time to move on: amyloid is the downstream result, not cause, of Alzheimer's disease. *Alzheimers Dement.* **10**(3), 372-380. (2014).
286. Nalivaeva, N.N., Fisk L.R., Belyaev N.D. & Turner A.J. Amyloid-degrading enzymes as therapeutic targets in Alzheimer's disease. *Curr Alzheimers Res*. **5**(2), 212-224. (2008).
287. Wilkinson, D., Windfeld, K. & Colding-Jørgensen, E. Safety and efficacy of idalopirdine, a 5-HT6 receptor antagonist, in patients with moderate Alzheimer's disease (LADDER): a randomised, double-blind, placebo-controlled phase 2 trial. *Lancet Neurol*. **13(**11), 1092-99. (2014).

288. Woolley, M.L., Bentley, J.C., Sleight, A.J., Marsden, C.A. & Fone, K.C. A role for 5-ht 6 receptors in retention of spatial learning in the Morris water maze. *Neuropharmacology*. **41**(2), 210-219 (2001).
289. Ramirez, M. J. Lai, M. K. P., Tordera, R. M. & Francis, P.T. Serotonergic therapies for cognitive symptoms in alzheimer's disease: rationale and current status," *Drugs.* **74(**7), 729-736 (2014).
290. Weinreb, O., Amit, T., Bar-Am, O. & Youdim, M.B.H. Ladostigil: a novel multimodal neuroprotective drug with cholinesterase and brain-selective monoamine oxidase inhibitory activities for Alzheimer's disease treatment. *Curr Drug Targets*. **13(**4), 483–494. (2012).
291. Weinreb, O., Amit, T., Bar-Am, O. & Youdim, M.B.H. A novel anti-Alzheimer's disease drug, ladostigil: neuroprotective, multimodal brain-selective monoamine oxidase and cholinesterase inhibitor. *Int Rev Neurobiol*. **100**, 191–215. (2011).
292. Selkoe, D. J. & Wolfe, M. S. Presenilin: running with scissors in the membrane. Cell 131, 215–221. (2007).
293. Folch, J. *et al*. Masitinib for the treatment of mild to moderate Alzheimer's disease," *Expert Rev of Neurother*. **15**(6), 587–596. (2015).
294. Piette, F. *et al*. Masitinib as an adjunct therapy for mild-to-moderate Alzheimer's disease: a randomised, placebo-controlled phase 2 trial," *Alzheimers Res Ther*. **3**:16. (2011).
295. Konishi, K. *et al*. Hypothesis of endogenous anticholinergic activity in Alzheimer's disease. *Neurodegenerative Diseases*. **15**(3), 149–156. (2015).
296. Tata, A.M. Velluto, L., D'angelo, C. & Reale, M. Cholinergic system dysfunction and neurodegenerative diseases: cause or effect?" *CNS Neurol Disord Drug Targets*. **13**(7), 1294–1303. (2014).
297. Wallace, T.L. & Bertrand, D. Importance of the nicotinic acetylcholine receptor system in the prefrontal cortex. *Biochem Pharmacol*. **85**(12), 1713-20. (2013).
298. Mehta, D.C., Short, J.L., Hilmer, S.N. & Nicolazzo, J.A. Drug access to the central nervous system in Alzheimer's disease: preclinical and clinical insights. *Pharm Res*. **32**(3), 819–839 (2015).
299. Berk, C., Paul, G. & Sabbagh, M. Investigational drugs in Alzheimer's disease: current progress. *Expert Opin Investig Drugs*. **23(**6), 837–846. (2014).
300. Tanemura, K. *et al.* Formation of tau inclusions in knock-in mice with familial Alzheimer disease (FAD) mutation of presenilin 1 (PS1). *J Biol Chem.* **281**(8), 5037-41. (2006).
301. Grüninger, F. Invitedreview: drug development for tauopathies. *Neuropathol Appl Neurobiol.* **41(**1), 81–96. (2015).
302. Iqbal, K. Gong, C.X. & Liu, F. Microtubule-associated protein tau as a therapeutic target in Alzheimer's disease. *Expert Opin Ther Targets*. **18(**3), 307–318. (2014).
303. de la Torre, A.V. *et al*. GSK3β inhibition is involved in the neuroprotective effects of cyclin-dependent kinase inhibitors in neurons*. Pharmacol Res*. **65(**1), 66–73. (2012).
304. Jorda, E.G. *et al*. Neuroprotective action of avopiridol, a cyclin-dependent kinase inhibitor, in colchicine-induced apoptosis. *Neuropharmacology*. **45(**5), 672–683. (2003).
305. Lovestone, S. *et al*. A phase II trial of tideglusib in Alzheimer's disease," J Alz Dis. **45**, 75–88. (2015).
306. Corcoran, N.M. *et al*. Sodium selenate specifically activates PP2A phosphatase, dephosphorylates tau and reverses memory deficits in an Alzheimer's disease model. J Clinical Neuroscience. **17(**8), 1025-33. (2010).
307. De Strooper, B., Iwatsubo, T. & Wolfe, M. S. Presenilins and γ-secretase: structure, function, and role in Alzheimer disease. Cold Spring Harb. Persp. Medi. 2: a006304. (2012).
308. LaFerla, F.M., Green, K.N. & Oddo, S. Intracellular amyloid-beta in Alzheimer's disease. Nat Rev Neurosci. 8(7), 499-509. (2007).
309. Wischik, C. M. *et al*. Tau aggregation inhibitor therapy: an exploratory phase 2 study in mild or moderate Alzheimer's disease. *J Alzheimers Dis*. **44**(2), 705–720. (2015).
310. Shemesh, O.A. & Spira, M.E. Rescue of neurons from undergoing hallmark tau-induced Alzheimer's disease cell pathologies by the antimitotic drug paclitaxel. *Neurobiol Dis*. **43(**1), 163–175. (2011).
311. Zhang, B. *et al*. The microtubule-stabilizing agent, epothilone D, reduces axonal dysfunction, neurotoxicity, cognitive deficits, and alzheimer-like pathology in an interventional study with aged tau transgenic mice. *J Neuroscience*. **32**(11), 3601-11. (2012).

312. Wisniewski, T. & Goñi, F. Immunotherapeutic approaches for Alzheimer's disease. *Neuron*. **85**(6), 1162-76. (2015).
313. Solomon, B., Koppel, R., Hanan, E. & Katzav, T. Monoclonal antibodies inhibit *in vitro* fibrillar aggregation of the Alzheimer β-amyloid peptide. *Proc Natl Acad Sci U S A*, **93,** 452–455. (1996).
314. Solomon, B., Koppel, R., Frenkel, D. & Hanan-Aharon, E. Disaggregation of Alzheimer β-amyloid by site-directed mAb. *Proc Natl Acad Sci U S A.*, **94**, 4109-12. (1997).
315. Schenk, D. *et al.* Immunization with amyloid-β attenuates Alzheimer-disease-like pathology in the PDAPP mouse. *Nature.* **400,** 173-177. (1999).
316. Gilman, S. *et al.* Clinical effects of Aβ immunization (AN1792) in patients with AD in an interrupted trial. *Neurology.* **64**, 1553-62. (2005).
317. Bard, F. *et al.* Peripherally administered antibodies against amyloid β-peptide enter the central nervous system and reduce pathology in a mouse model of Alzheimer disease. *Nat Med*. **6**, 916–919. (2000).
318. Rinne, J.O. *et al.* 11C-PiB PET assessment of change in fibrillar amyloid-β load in patients with Alzheimer's disease treated with bapineuzumab: a phase 2, double-blind, placebo-controlled, ascending-dose study. *Lancet Neurol.* **9,** 363–372. (2010).
319. Crespi, G.A., Ascher, D.B., Parker, M.W. & Miles, L.A. Crystallization and preliminary X-ray diffraction analysis of the Fab portion of the Alzheimer's disease immunotherapy candidate bapineuzumab complexed with amyloid-β. *Acta Crystallogr F Struct Biol Commun*. **70**(3), 374-7. (2014).
320. Duvvuri, M del S. *et al.* First-In-Human safety and long-term exposure data for AAB-003 (PF-05236812) and biomarkers after intravenous infusions of escalating doses in patients with mild to moderate Alzheimer's disease. *Alzheimers Res Ther.* **8**: 12. (2016).
321. DeMattos, R.B. e*t al.* Peripheral anti-a beta antibody alters CNS and plasma a beta clearance and decreases brain a beta burden in a mouse model of Alzheimer's disease. *Proc Natl Acad Sci U S A.* **98,** 8850-55. (2001).
322. Donohue, M.C. *et al.* Australian Imaging, Biomarkers, and Lifestyle Flagship Study of Ageing, Alzheimer's Disease Neuroimaging Initiative, Alzheimer's Disease Cooperative Study. The preclinical Alzheimer cognitive composite: measuring amyloid-related decline. *JAMA Neurol*. **71**(8), 961-70. (2014).
323. Blaettler, T. Clinical trial design of CREAD: a randomized, double-blind, placebo-controlled, parallel-group Phase-3 study to evaluate crenezumab treatment in patients with prodromal-to-mild Alzheimer's disease. Alzheimer's & Dementia: *J Alzheimers Association.* **12**: 7. (2016).
324. Bohrmann, B. *et al*. Gantenerumab: A Novel Human Anti-Aβ Antibody Demonstrates Sustained Cerebral Amyloid-β Binding and Elicits Cell-Mediated Removal of Human Amyloid-β. *J Alzheimers Dis.* **28**(1), 49-69. (2012).
325. Nilsberth, C. *et al*. The 'Arctic' APP mutation (E693G) causes Alzheimer's disease by enhanced Abeta protofibril formation. *Nat Neurosci*. **4**(9), 887-93. (2001).
326. Andreasen, N. *et al*. First administration of the Fc-attenuated anti-β amyloid antibody GSK933776 to patients with mild Alzheimer's disease: a randomized, placebo-controlled study. *PLoS One*. **10**(3):e0098153. (2015).
327. Leyhe, T. *et al*. Modulation of β-amyloid by a single dose of GSK933776 in patients with mild Alzheimer's disease: a phase I study. *Alzheimers Res Ther.* **6**(2):19. (2014).
328. La Porte, S.L. *et al*. Structural Basis of C-terminal β-Amyloid Peptide Binding by the Antibody Ponezumab for the Treatment of Alzheimer's Disease. *J Mol Biol*. **421**, 525-536. (2012).
329. Sevigny, J. *et al*. The antibody aducanumab reduces Aβ plaques in Alzheimer's disease. *Nature.* **537**, 50-56. (2016).
330. Moreth, J., Mavoungou, C. & Schindowski, K. Passive anti-amyloid immunotherapy in Alzheimer's disease: What are the most promising targets? *Immun & Ageing*. **10**: 18. (2013).
331. Bussiere, T. *et al*. Biogen Idec International Neuroscience Gmbh, assignee. A Method Of Reducing Brain Amyloid Plaques Using Anti-Aβ Antibodies. United States patent application WO2014089500 A1. 2014 Jun 12.
332. Schenk, D. B. B. CA. Passive immunization treatment of Alzheimer's disease. United States patent (2004).
333. Leyhe, T. *et al*. Modulation of beta-amyloid by a single dose of GSK933776 in patients with mild Alzheimer's disease: a phase I study. Alzheimers Res. **6**, 19. (2014).

334. Holtzman, D. M. *et al*. Humanized Antibodies That Sequester Amyloid Beta Peptide. United States patent US 8338120. 2002 Dec 25.
335. Lannfelt, L. et al. Perspectives on future Alzheimer therapies: amyloid-β protofibrils - a new target for immunotherapy with BAN2401 in Alzheimer's disease. Alzheimers Res Ther. 6, 16. (2014).
336. Tucker, S. et al. The murine version of BAN2401 (mAb158) selectively reduces amyloid-β protofibrils in brain and cerebrospinal fluid of tg-ArcSwe mice. J Alzheimer's Dis. 43, 575–588. (2015).
337. Gabriela A. N. Crespi, Stefan J. Hermans, Michael W. Parker & Luke A. Miles. Molecular basis for mid-region amyloid-β capture by leading Alzheimer's disease immunotherapies. *Sci Rep.* 5: 9649
338. Zahnd, C., Sarkar, C.A. & Pluckthun, A. Computational analysis of off-rate selection experiments to optimize affinity maturation by directed evolution. *Protein Eng Des Sel*. **23,** 175–184. (2010).
339. Derda, R. *et al.* Diversity of phage-displayed libraries of peptides during panning and amplification. *Molecules*. **16**: 1776–1803. (2011).
340. Srebalus Barnes, C.A. & Lim, A. Applications of mass spectrometry for the structural characterization of recombinant protein pharmaceuticals. *Mass Spectrom Rev*. **26**, 370–388. (2007).
341. Jenkins, N., Murphy, L. & Tyther, R. Posttranslational modifications of recombinant proteins: significance for biopharmaceuticals. *Mol Biotechnol.* **39,** 113–118. (2008).
342. Singh, M.B. & Bhalla, P.L. Recombinant expression systems for allergen vaccines. *Inflamm Allergy Drug Targets.* **5,** 53–59. (2006).
343. Sanchez, Y. *et al.* Humoral and cellular immunity to hepatitis B virus-derived antigens: comparative activity of Freund complete adjuvant alum, and liposomes. *Infect Immun*. **30,** 728–733. (1980).
344. Billiau, A. & Matthys, P. Modes of action of Freund's adjuvants in experimental models of autoimmune diseases. *J Leukoc Biol*. **70,** 849–860. (2001).
345. Odunsi, K., *et al.* Vaccination with an NY-ESO-1 peptide of HLA class I/II specificities induces integrated humoral and T cell responses in ovarian cancer. *Proc Natl Acad Sci U S A.* **104,** 12837.42. (2007).
346. Kung, P. *et al*. Monoclonal antibodies defining distinctive human T cell surface antigens. *Science.* **206,** 347–349. (1979).
347. Zhang, C. *et al*. A cell surface receptor defined by a mAb mediates a unique type of cell death similar to oncosis. *Proc Natl Acad Sci U S A*. **95**, 6290-95. (1998).
348. Robinson, H.L. & Pertmer, T.M. Nucleic acid immunizations. *Curr Protoc Immunol Chapter.* **2**: 2.14. (2001).
349. Rivinoja, A. & Laakkonen, P. Identification of homing peptides using the *in vivo* phage display technology. *Methods Mol Biol.* **683,** 401–415. (2011).
350. Hanes, J. & Plückthun, A. In vitro selection and evolution of functional proteins by using ribosome display. *Proc Natl Acad Sci U S A.* **94**:4937–4942. (1997).
351. He, M. & Taussig, M.J. Antibody-ribosome- mRNA (ARM) complexes as efficient selection particles for *in vitro* display and evolution of antibody combining sites. *Nucleic Acids Res.* 25:5132–5134. (1997).
352. Roberts, R.W. & Szostak, J.W. RNA-peptide fusions for the *in vitro* selection of peptides and proteins. *Proc Natl Acad Sci U S A.* **94**, 12297-302. (1997)
353. Boder, E.T. & Wittrup, K.D. Yeast surface display for screening combinatorial polypeptide libraries. *Nat Biotechnol.* **15**, 553–557. (1997).
354. Köhler G, Milstein C: Continuous cultures of fused cells secreting antibody of prede ned speci city. *Nature.* **256**(5517), 495–497 (1975).
355. Masahiro Tomita & Kanta Tsumoto. Hybridoma technologies for antibody production. *Immunotherapy.* **3**(3), 371–380. (2011).
356. Lee, C.M.Y., Iorno, N., Sierro, F. & Christ, D. Selection of human antibody fragments by phage display. *Nature Protocols*. **2**: 11. (2007).
357. Smith, G.P. Filamentous fusion phage: novel expression vectors that display cloned antigens on the virion surface. *Science.* **228**, 1315-17. (1985).
358. McCafferty, J., Griffiths, A.D., Winter, G. & Chiswell, D.J. Phage antibodies: filamentous phage displaying antibody variable domains. *Nature.* **348**, 552–554. (1990).

359. Whaley, S.R., English, D.S., Hu, E.L., Barbara, P.F. & Belcher, A.M. Selection of peptides with semiconductor binding specificity for directed nanocrystal assembly. *Nature.* **405**, 665–668. (2000).
360. Lorenz, H.M. Technology evaluation: adalimumab, Abbott laboratories. *Curr. Opin. Mol. Ther.* **4**, 185–190. (2002).
361. Chiti, F. & Dobson, C.M. Protein Misfolding, Amyloid Formation, and Human Disease: A Summary of Progress Over the Last Decade. *Annu. Rev. Biochem*. 86:35.1–35.42. (2017).
362. Cerf, E. *et al*. Antiparallel β-sheet: a signature structure of the oligomeric amyloid β-peptide. *Biochemical Journal.* **421**(3), 415-423. (2009).
363. Hollingworth, P. *et al*. Common Variants in ABCA7, MS4A6A/MS4A4E, EPHA1, CD33 and CD2AP Are Associated with Alzheimer's Disease. *Nature genetics.* **43**(5), 429–435. (2011).
364. Gatz, M. *et al*. Role of genes and environments for explaining Alzheimer disease. *Arch Gen Psychiatry.* **63,** 168–74. (2006).
365. Biffi, A. *et al*. Genetic variation and neuroimaging measures in Alzheimer disease. *Arch Neurol*. 67, 677–85. (2010).
366. Naj, A.C. Common variants in MS4A4/MS4A6E, CD2AP, CD33 and EPHA1 are associated with late-onset Alzheimer's disease. *Nat Genet.* **43**(5), 436-41. (2011).
367. Chapman, J. *et al*. A Genome-Wide Study Shows a Limited Contribution of Rare Copy Number Variants to Alzheimer's Disease Risk. *Hum Mol Genet.* **22(**4), 816–824. (2013).
368. Lars Bertram, Rudolph E. Tanzi; Genome-wide association studies in Alzheimer's disease. *Hum Mol Genet*. **18**(2), 137–145. (2009).
369. Mayeux, R. & Stern, Y. Epidemiology of Alzheimer Disease. *Cold Spring Harb Perspect Med.* **2**:a006239. (2012).
370. Murakami, K. Conformation-specific antibodies to target amyloid β oligomers and their application to immunotherapy for Alzheimer's disease. *Biosci Biotechnol Biochem.* **78**(8), 1293-1305. (2014).
371. Marcus, G. *et al.* Neprilysin and Aβ clearance: impact of the APP intracellular domain in NEP regulation and implications in Alzheimer's disease. *Front Aging Neurosci.* **5:** 98. (2013).
372. Ubelmann, F. *et al*. Bin1 and CD2AP polarise the endocytic generation of beta-amyloid. *EMBO Reports*. **18**, 102–122. (2017).
373. Decker, J. M. *et al*. Pro-aggregant Tau impairs mossy fiber plasticity due to structural changes and Ca++ dysregulation. *Acta Neuropathol. Commun*. **3**, 23. (2015).
374. Hoover, B. R. *et al*. Tau mislocalization to dendritic spines mediates synaptic dysfunction independently of neurodegeneration. *Neuron.* **68**, 1067-81. (2010)
375. Thies, E. & Mandelkow, E. M. Missorting of tau in neurons causes degeneration of synapses that can be rescued by the kinase MARK2/Par-1. *J Neurosci.* **27**, 2896–2907. (2007)
376. Tai, H. C. *et al*. Frequent and symmetric deposition of misfolded tau oligomers within presynaptic and postsynaptic terminals in Alzheimer inverted question marks disease. *Acta Neuropathol. Commun*. **2**, 146. (2014)
377. Sultan, A. *et al*. Nuclear tau, a key player in neuronal DNA protection. *J. Biol. Chem.* **286**, 4566-75. (2011)
378. Green, L.L. *et al.* Antigen-specific human monoclonal antibodies from mice engineered with human Ig heavy and light chain YACs. *Nat Genet.* **7**, 13–21. (1994).
379. Mendez, M.J. *et al.* Functional transplant of megabase human immunoglobulin loci recapitulates human antibody response in mice. *Nat Genet.* **15,** 146–156. (1997).
380. Ishida, I. *et al.* Production of human monoclonal and polyclonal antibodies in TransChromo animals. *Cloning Stem Cells.* **4**, 91-102. (2002).
381. Moser, M., Dendritic cells, in Fundamental Immunology, 5th ed., Paul, W.E., Lippincott Williams & Wilkins. Philadelphia. (2003).
382. Gordon, S., Macrophages and the immune response, in Fundamental Immunology, 5th ed., Paul, W.E., Lippincott Williams & Wilkins. Philadelphia. (2003).
383. Hui, Chao. *et al.* Core-shell Fe3O4@SiO2 nanoparticles synthesized with well-dispersed hydrophilic Fe3O4 seeds. *Nanoscale*. **3**, 701-705. (2011).
384. Parker, C.E. & Tomer, K.B. MALDI/MS-Based Epitope Mapping of Antigens Bound to Immobilized Antibodies. *Mol Biotech.* **20**(1), 49-62. (2002)
385. Saem Mun & Suk-Jung Choi. Detection of Salmonella typhimurium by Antibody/ Enzyme-Conjugated Magnetic Nanoparticles. *BioChip J.* **9**(1), 10-15. (2015).

386. Cohen, T.J. *et al*. The acetylation of tau inhibits its function and promotes pathological tau aggregation. *Nature Comm.* **2**: 252. (2011).
387. Asuni, A.A., Boutajangout, A., Quartermain, D. & Sigurdsson, E.M. Immunotherapy targeting pathological tau conformers in a tangle mouse model reduces brain pathology with associated functional improvements. *J Neurosci.* **27**: 9115-29. (2007).
388. Bi, M., Ittner, A., Ke, Y.D., Götz, J. & Ittner, L.M. Tau-Targeted Immunization Impedes Progression of Neurofibrillary Histopathology in Aged P301L Tau Transgenic Mice. *PLoS One,* **6**(12): e26860. (2011).
389. Theunis, C. *et al.* Efficacy and safety of a liposome-based vaccine against protein Tau, assessed in tau.P301L mice that model tauopathy. *PLoS One.* **8:** e72301. (2013).
390. Boimel, M. *et al.* Efficacy and safety of immunization with phosphorylated tau against neurofibrillary tangles in mice. *Exp Neurol*. **224**, 472–85. (2010).
391. Troquier, L. *et al*. Targeting phospho-Ser422 by active Tau Immunotherapy in the THYTau22 mouse model: a suitable therapeutic approach. *Curr Alzheimer Res.* **9**, 397–405. (2012).
392. Boutajangout, A. & Wisniewski, T. Tau Based Therapeutic Approaches for Alzheimer's Disease. *Gerontology*. **60**(5), 381–385. (2014).
393. Ando, K. *et al.* Vaccination with Sarkosyl insoluble PHF-tau decrease neurofibrillary tangles formation in aged tau transgenic mouse model: a pilot study. *J Alzheimers Dis*. **40**, S135-145. (2014).
394. Wencheng, Liu. *et al*. Vectored Intracerebral Immunization with the Anti-Tau Monoclonal Antibody PHF1 Markedly Reduces Tau Pathology in Mutant Tau Transgenic Mice. *J Neurosci*. **37**(13): 3734. (2017).
395. d'Abramo, C., Acker, C.M., Jimenez, H.T. & Davies, P. Tau passive immunotherapy in mutant P301L mice: antibody affinity versus specificity. *PLoS One*. **8**: e62402. (2013).
396. Collin, L. *et al.* Neuronal uptake of tau/pS422 antibody and reduced progression of tau pathology in a mouse model of Alzheimer's disease. *Brain*. **137**(10), 2834-46. (2014).
397. Yanamandra, K. *et al*. Anti-tau antibodies that block tau aggregate seeding *in vitro* markedly decrease pathology and improve cognition *in vivo*. *Neuron.* **80**, 402-14. (2013).
398. Castillo-Carranza, D.L. *et al.* Passive immunization with Tau oligomer monoclonal antibody reverses tauopathy phenotypes without affecting hyperphosphorylated neurofibrillary tangles. *J Neurosci.* **34**, 4260-72. (2014).
399. Gröninger, F. Drug development for tauopathies. *Neuropathol Appl Neurobiol.* **41**(1), 81-96. (2014).
400. Congdon, E. E., Gu, J., Sait, H. B. & Sigurdsson, E. M. Antibody uptake into neurons occurs primarily via clathrin-dependent Fcγ receptor endocytosis and is a prerequisite for acute tau protein clearance. *J. Biol. Chem.* **288**, 35452–35465. (2013).
401. Collin, L. *et al*. Neuronal uptake of tau/pS422 antibody and reduced progression of tau pathology in a mouse model of Alzheimer's disease. Brain **137**, 2834–2846. (2014).
402. Kondo, A. *et al*. Antibody against early driver of neurodegeneration cis P-tau blocks brain injury and tauopathy. *Nature.* **523**, 431–436 (2015).
403. d'Abramo, C., Acker, C. M., Jimenez, H. T. & Davies, P. Tau passive immunotherapy in mutant P301L mice: antibody affinity versus specificity. *PLoS One.* **8**, e62402 (2013).
404. Castillo-Carranza, D. L. *et al*. Passive immunization with Tau oligomer monoclonal antibody reverses tauopathy phenotypes without affecting hyperphosphorylated neurofibrillary tangles. *J Neurosci.* **34**, 4260-72. (2014).
405. Yanamandra, K. *et al*. Anti-tau antibodies that block tau aggregate seeding *in vitro* markedly decrease pathology and improve cognition *in vivo*. *Neuron.* **80**, 402–414 (2013).
406. Yanamandra, K. *et al*. Anti-Tau Antibodies that Block Tau Aggregate Seeding In Vitro Markedly Decrease Pathology and Improve Cognition In vivo. *Neuron*. **80**(2), 402-14. (2013).
407. Yanamandra K, *et al*. Anti-tau antibody reduces insoluble tau and decreases brain atrophy. *Ann Clin Transl Neurol.* **2**(3), 278-88. (2015).
408. Buée, L., Bussière, T., Buée-Scherrer, V., Delacourte, A. & Hof, P.R. Tau protein isoforms, phosphorylation and role in neurodegenerative disorders. *Brain Res Brain Res Rev*. **33**(1), 95-130. (2000).
409. Kontsekova, E., Zilka, N., Kovacech, B., Novak, P. & Novak, M. First-in-man tau vaccine targeting structural determinants essential for pathological tau-tau interaction reduces tau oligomerisation and neurofibrillary degeneration in an Alzheimer's disease model. *Alzheimers Res Ther*. **6**(4): 44. (2014).

410. Theunis, C. *et al*. (2013) Efficacy and Safety of A Liposome-Based Vaccine against Protein Tau, Assessed in Tau.P301L Mice That Model Tauopathy. *PLoS One.* **8**(8): e72301.
411. Michael Steinitz (ed.), Human Monoclonal Antibodies: Methods and Protocols, Methods in Molecular Biology, vol. 1060
412. Schenk, D. *et al*. Immunization with amyloid-β attenuates Alzheimer-disease-like pathology in the PDAPP mouse. *Nature.* **400**:173–177. (1999).
413. Janus, C. *et al.* A beta peptide immunization reduces behavioural impairment and plaques in a model of Alzheimer's disease. *Nature.* **408**(6815), 979–982. (2000).
414. Morgan, D. *et al.* A beta peptide vaccination prevents memory loss in an animal model of Alzheimer's disease. *Nature.* **408**(6815), 982–985. (2000).
415. Fu, H.J., Liu, B., Frost, J.L., & Lemere, C.A. Amyloid-β Immunotherapy for Alzheimer's Disease. *CNS Neurol Disord Drug Targets*. **9**(2), 197–206. (2010).
416. Bard, F. *et al*. Peripherally administered antibodies against amyloid beta-peptide enter the central nervous system and reduce pathology in a mouse model of Alzheimer disease. *Nat Med.* **6**(8):916–919. (2000).
417. Chahboun, S. *et al.* Isolation of a nanomolar scFv inhib- iting the endopeptidase activity of botulinum toxin A, by single-round panning of an immune phage-displayed library of macaque origin. *BMC Biotechnol.* **11**:113. (2011).
418. Pelat, T, *et al.* High-affinity, human antibody-like antibody fragment (single-chain variable fragment) neutralizing the lethal factor (LF) of Bacillus anthracis by inhibiting protective antigen-LF complex formation. *Antimicrob Agents Chemother* **51**, 2758-64. (2007).
419. Pelat, T. *et al*. Isolation of a human-like antibody fragment (scFv) that neutralizes ricin biological activity. *BMC Biotechnol.* **9**:60. (2009).
420. Alonso-Ruiz, A. *et al.* Tumor necrosis factor alpha drugs in rheumatoid arthritis: systematic review and metaanalysis of efficacy and safety. *BMC Musculoskelet Disord* **9**:52. (2008).
421. Peeters, M., Price, T. & Van Laethem, J.-L. Anti-epidermal growth factor receptor mono-therapy in the treatment of metastatic colorectal cancer: where are we today? *Oncologist.* **14**, 29–39. (2009).
422. Chatenoud, L. & Bluestone, J.A. CD3- specific antibodies: a portal to the treatment of autoimmunity. *Nat Rev Immunol* **7:**622–632. (2007).
423. Adams, G.P. & Weiner, L.M. Monoclonal antibody therapy of cancer. *Nat Biotechnol* **23**, 1147-57. (2005).
424. Moss, M.L., Sklair-Tavron, L. &Nudelman, R. Drug insight: tumor necrosis factor-converting enzyme as a pharmaceutical target for rheumatoid arthritis. *Nat Clin Pract Rheumatol* .**4**, 300–309. (2008).
425. Dalle, S., Thieblemont, C., Thomas, L. & Dumontet, C. Monoclonal antibodies in clinical oncology. *Anticancer Agents Med Chem* **8**, 523–532. (2008).
426. Jones, S.E. Metastatic breast cancer: the treatment challenge. *Clin Breast Cancer.* **8**, 224–233. (2008).
427. Osbourn, J., Groves, M. & Vaughan, T. From rodent reagents to human therapeutics using antibody guided selection. *Methods.* **36**, 61–68. (2005).
428. Miles, L.A., Crespi, G.A.N., Doughty, L. & Parker, M.W. Bapineuzumab captures the N-terminus of the Alzheimer's disease amyloid-beta peptide in a helical conformation. *Sci Rep.* **3**: 1302. (2013).
429. Prins, N.D. & Scheltens, P. Treating Alzheimer's disease with monoclonal antibodies: current status and outlook for the future. *Alzheimer's Research & Therapy*, **5**(6): 56. (2013).
430. Ultsch, M. *et al.* Structure of Crenezumab Complex with Aβ Shows Loss of β-Hairpin. *Sci Rep*. **6**: 39374. (2016).
431. Blair, L.J., Sabbagh, J.J. & Dickey, C.A. Targeting Hsp90 and its co-chaperones to treat Alzheimer's disease. *Expert Opin. Ther. Targets.* **18**, 1219-32. (2014).
432. Wischik, C. M. *et al*. Tau aggregation inhibitor therapy: an exploratory phase 2 study in mild or moderate Alzheimer's disease. *J. Alzheimers Dis.* **44**, 705–720. (2015).
433. Lovestone, S. *et al*. A phase II trial of tideglusib in Alzheimer's disease. *J. Alzheimers Dis.* **45**, 75–88. (2015).
434. McCullough & Summerfield. Basic concepts of immune response and defense development. *ILAR J*. **46**(3), 230-40. (2005).
435. Reineke, U. & Schutkowski, M. Epitope Mapping Protocols. *Humana Press*. (2009).
436. Zhao, L.N., Lu, L., Chew, L.Y. & Mu, Y. A Panorama Glimpse. *Int. J. Mol. Sci.* **15**, 12631-50. (2014).

437. Aisen, P.S. *et al.* Clinical core of the Alzheimer's Disease Neuroimaging Initiative: progress and plans. *Alzheimers Dement.* **6**(3), 239–246. (2010).
438. Hooks, M.A., Wade, C.S. & Millikan, W.J. Jr. Muromonab CD-3: a review of its pharmacology, pharmacokinetics, and clinical use in transplantation. *Pharmacotherapy*. **11**(1), 26-37. (1991).
439. Folch, J. *et al.* Current Research Therapeutic Strategies for Alzheimer's Disease Treatment. *Neural Plast.* 2016, 8501693. (2016).
440. Lee, S. *et al*. The E2 Domains of APP and APLP1 Share a Conserved Mode of Dimerization. *Biochemistry*. **50**(24), 5453–5464. (2011).
441. Hoefgen, D., Dahms, S.O., Oertwig, K. & Than, M.E. The Amyloid Precursor Protein Shows a pH-Dependent Conformational Switch in Its E1 Domain. J Mol Biol. **427**(2), 433-442. (2015).
442. Dahms, S.O. *et al.* Structure and biochemical analysis of the heparin-induced E1 dimer of the amyloid precursor protein. *Proc Natl Acad Sci U S A.* **107**, 5381-86. (2010).
443. Barrett, P.J., Song, Y., Van Horn, W.D., Hustedt, E.J. & Schafer, J.M., Hadziselimovic, A., Beel, A.J., Sanders, C.R. The amyloid precursor protein has a flexible transmembrane domain and binds cholesterol. *Science.* **336**, 1168-71. (2012).
444. Li, H. *et al.*Structure of the C-terminal Phosphotyrosine Interaction Domain of Fe65L1 Complexed with the Cytoplasmic Tail of Amyloid Precursor Protein Reveals a Novel Peptide Binding Mode. *TJBC*. **283**(40), 27165-78. (2008).
445. Hsieh, C.L. *et al*. A role for TREM2 ligands in the phagocytosis of apoptotic neuronal cells by microglia. *J Neurochem*. **109**(4), 1144-56. (2009).
446. Lee, C.Y.D. & Landreth, G.E. The role of microglia in amyloid clearance from the AD brain. *J Neural Transm.* **117**, 949–60. (2010).
447. Spangenberg, E.E. & Green, K.N. Inflammation in Alzheimer's disease: Lessons learned from microglia-depletion models. *Brain Behav Immun.* **61,** 1–11. (2017).
448. Akiyama, H. *et al*. Inflammation and Alzheimer's disease. *Neurobiology of Aging*. **21**, 383–421. (2000).
449. Hoarau, J.J. *et al*. Activation and control of CNS innate immune responses in health and diseases: a balancing act finely tuned by neuroimmune regulators (NIReg). *CNS Neurol. Disord.* **10**, 25–43. (2011).
450. Polazzi, E., Monti, B., 2010. Microglia and neuroprotection: from *in vitro* studies to therapeutic applications. *Prog. Neurobiol*. **92**, 293–315.
451. Koenigsknecht-Talboo, J., Landreth, G.E., 2005. Microglial phagocytosis induced by fibrillar beta-amyloid and IgGs are differentially regulated by proinflammatory cytokines. *J Neurosci.* **25**, 8240–8249.
452. Hellwig, S., Masuch, A., Nestel, S., Katzmarski, N., Meyer-Luehmann, M., Biber, K., 2015. Forebrain microglia from wild-type but not adult 5xFAD mice prevent amyloid-beta plaque formation in organotypic hippocampal slice cultures. *Sci. Rep.* **5**, 14624.
453. Condello, C., Yuan, P., Schain, A., Grutzendler, J., 2015. Microglia constitute a barrier that prevents neurotoxic protofibrillar Ab42 hotspots around plaques. *Nat. Commun.* **6**, 6176.
454. Hamelin, L. *et al*. Early and protective microglial activation in Alzheimer's disease: a prospective study using 18F-DPA-714 PET imaging. *Brain.* **139**, 1252–1264. (2016).
455. Venegas, C. *et al.* Microglia-derived ASC specks cross- seed amyloid-β in Alzheimer's disease. *Nature*. **552**, 355–361. (2017)
456. Wyss-Coray, T. & Rogers, J. Inflammation in Alzheimer Disease-A Brief Review of the Basic Science and Clinical Literature. *Cold Spring Harb Perspect Med.* **2:** a006346. (2012).
457. G. Modi, V. Pillay, Y. E. Choonara, V.M.K. Ndesendo, L.C. Du Toit, D. Naidoo. Nanotechnological applications for the treatment of neurodegenerative disorders. *Prog Neurobiol*. **88**, 272. (2009).
458. H. Koo, M.S. *et al*. In vivo targeted delivery of nanoparticles for theranosis. *Acc Chem Res*. **44**, 1018. (2011).
459. S.G. Antimisiaris, S. Mourtas, E. Markoutsa, A. Skouras, and K. Papadia. Nanoparticles for Diagnosis and/or Treatment of Alzheimer's. *Adv Healthc Mater*. 87–180. (2014)
460. Liu, Y., Miyoshi, H. & Nakamura, M. Nanomedicine for drug delivery and imaging: a promising avenue for cancer therapy and diagnosis using targeted functional nanoparticles. *Int. J. Cancer*. **120**, 2527. (2007).
461. Allen, T. M. & Cullis, P. R. Drug Delivery Systems: Entering the Mainstream. *Science*. **201**, 1818-22. (2004).

462. Faraji, A.H. & Wipf, P. Nanoparticles in cellular drug delivery. *Bioorg Med Chem.* **17**, 2950-62. (2009).
463. Xie, J. Lee, S. & Chen, X. Nanoparticle-based theranostic agents. *Adv Drug Delivery Rev*. **62**, 1064-7. (2010).
464. Querfurth, H.W. & LaFerla, F.M. Alzheimer´s Disease. *N Engl J Med,* Vol. **362(4)**, 329-344. (2010).
465. Torchilin, V.P. Pasive and active drug targeting: drug delivery to tumors as an example. *Handb Exp Pharmacol*. **197**, 3-53. (2010).
466. Silva, G.A. Nanotechnology applications and approaches for neuroregeneration and drug delivery to the central nervous system. *Ann NY Acad Sci*. **1199**, 221-230 (2010).
467. Leinenga, G. & Götz, J. Scanning ultrasound removes amyloid-b and restores memory in an Alzheimer's disease mouse model. *Sci Trans Med.* **7**(278), 278-333. (2015).
468. Ordóñez-Gutiérrez, L. *et al.* ImmunoPEGliposome-mediated reduction of blood and brain amyloid levels in a mouse model of Alzheimer's disease is restricted to aged animals. *Biomaterials.* **112,** 141-152. (2017).
469. Balducci, C. *et al*. Multifunctional Liposomes Reduce Brain -Amyloid Burden and Ameliorate Memory Impairment in Alzheimer's Disease Mouse Models. *J Neurosci*. **34**(42), 14022-31. (2014).
470. Carradori, D. *et al*. Antibody-functionalized polymer nanoparticle leading to memory recovery in Alzheimer's disease-like transgenic mouse model. *Nanomedicine: NBM*. **14**(2), 609-618. (2017).
471. Sutcliffe, J.G., Hedlund, P.B., Thomas, E.A., Bloom, F.E. & Hilbush, B.S. Peripheral reduction of beta-amyloid is sufficient to reduce brain beta-amyloid: implications for Alzheimer's disease, *J Neurosci. Res.* **89,** 808-814. (2011).
472. Wisniewski, T. & Konietzko, U. Amyloid-b immunisation for Alzheimer's disease, *Lancet Neurol*. **7,** 805-811. (2008).
473. DeMattos, R.B. *et al.* Peripheral anti-Ab antibody alters CNS and plasma Ab clearance and de- creases brain Ab burden in a mouse model of Alzheimer's disease, *Proc Natl Acad Sci U S A.* **98,** 8850-55. (2001).
474. Lemere, C.A. *et al*. Evidence for peripheral clearance of cerebral Ab protein following chronic, active Ab immunization in PSAPP mice, *Neurobiol. Dis.* **14,** 10-18. (2003).
475. Menéndez-González, M. *et al.* Immunotherapy for Alzheimer's Disease: Rational Basis in Ongoing Clinical Trials. *Curr Pharm Des*. **17**, 508-520. (2011).
476. Bard, F. *et al*. Peripherally administered antibodies against amyloid beta-peptide enter the central nervous system and reduce pathology in a mouse model of Alzheimer disease. *Nat Med.* 6, 916-9. (2000).
477. Das, P. *et al.* Amyloid-beta immunization effectively reduces amyloid deposition in FcRgamma-/- knock-out mice. *J Neurosci.* **23**, 8532-38. (2003).
478. Klyubin, I. *et al*. Amyloid beta protein immunotherapy neutralizes Abeta oligomers that disrupt synaptic plasticity *in vivo*. *Nat Med.* **11**, 556-61. (2005).
479. Yamada, K. *et al*. Abeta immunotherapy: intracerebral sequestration of Abeta by an anti-Abeta monoclonal antibody 266 with high affinity to soluble Abeta*. J Neurosci*. **29,** 11393-98. (2009).
480. Liao, F. *et al.* Targeting of non-lipidated, aggregated apoE with antibodies inhibits amyloid accumulation. *Journal of Clinical Investigation*. (2018).
481. Mancini S, *et al.* The hunt for brain Aβ oligomers by peripherally circulating multi-functional nanoparticles: Potential therapeutic approach for Alzheimer disease. *Nanomedicine: NBM*. **12,** 43-52. (2016).
482. Antunes, M. & G. Biala. The novel object recognition memory: neurobiology, test procedure, and its modifications. *Cogn Process*. **13,** 93-110. (2012).
483. Radde, R. *et al.* Abeta42-driven cerebral amyloidosis in transgenic mice reveals early and robust pathology. *EMBO Rep*. **7**(9), 940-946. (2006).
484. Ordoñez-Gutierrez, L. Anton, M. & Wandosell, F. Peripheral amyloid levels present gender differences associated with aging in AbetaPP/PS1 mice, *J. Alzheimer. Dis*. **44,** 1063-68. (2015).
485. Ordoñez-Gutierrez, L. *et al*. Repeated intraperitoneal injections of liposomes containing phosphatidic acid and cardiolipin reduce amyloid-beta levels in APP/PS1 transgenic mice. *Nanomedicine.* **11**, 42(1-43)0. (2015).
486. C. Ballard, S. Gauthier, A. Corbett, C. Brayne, D. Aarsland, E. Jones, C, Alzheimer's disease, *Lancet*. **377,** 1019-31. (2011).

487. Clifford R., J. *et al*. NIA-AA Research Framework: Toward a biological definition of Alzheimer's disease. *Alzheimers Denent*. **14**(4), 535-562. (2018).
488. Bateman, R.J. *et al*. Clinical and biomarker changes in dominantly inherited Alzheimer's disease. *N Engl J Med*. **367**, 795–804. (2012).
489. Chabrier, M.A. *et al.* Soluble abeta promotes wild-type tau pathology *in vivo*. *J Neurosci*. **32**, 17345–50. (2012).
490. Braak, H. & Braak, E. Frequency of stages of Alzheimer-related lesions in different age categories. *Neurobiol Aging*. **18**, 351–357. (1997).
491. Kaufman, S.K. *et al*. Tau Prion Strains Dictate Patterns of Cell Pathology, Progression Rate, and Regional Vulnerability. In vivo. *Neuron.* **92**, 796–812. (2016).
492. Jack, C.R. Jr. *et al*. Tracking pathophysiological processes in Alzheimer's disease: an updated hypothetical model of dynamic biomarkers. *Lancet Neurol.* **12**, 207–16. (2013).
493. Jack, C.R. Jr & Holtzman, D.M. Biomarker modeling of Alzheimer's Disease. *Neuron*. **80**:1347–58. (2013).
494. Daneman, R. & Prat, A. The blood–brain barrier. *Cold Spring Harb Perspect Biol.* **7**: a020412. (2015).
495. Zlokovic, B.V., Begley, D.J. & Chain-Eliash, D.G. Blood–brain barrier permeability to leucine-enkephalin, d-alanine2-d- leucine5-enkephalin and their N-terminal amino acid (tyrosine). *Brain Res.* **336**, 125–132. (1985).
496. Yamada, K. *et al*. Neuronal activity regulates extracellular tau *in vivo*. *J Exp Med.* **211**, 387–393. (2014).
497. Deane, R. & Zlokovic, B.V. Role of the blood–brain barrier in the pathogenesis of Alzheimer's disease, *Curr Alzheimer Res*. **4**, 191–197. (2007).
498. Deane, R. *et al*. LRP/amyloid beta-peptide interaction mediates differential brain efflux of Abeta isoforms. *Neuron.* **43**, 333–344. (2004).
499. Shibata, M. *et al*. Clearance of Alzheimer's amyloid-ss((1-40)) peptide from brain by LDL receptor-related protein-1 at the blood–brain barrier. *J Clin Invest,* **106**, 1489-99. (2000).
500. Deane, R. *et al*. RAGE mediates amyloid-beta peptide transport across the blood–brain barrier and accumulation in brain. *Nat Med.* **9**, 907–913. (2003).
501. Alonso, R. *et al.* Fungal infection in patients with Alzheimer's disease. *J Alzheimers Dis*. **41**(1), 301-311. (2014).
502. Lehrer, S. & Rheinstein, P.H. Is alzheimer's disease autoimmune inflammation of the brain that can be treated with nasal nonsteroidal anti-inflammatory drugs? *Am J Alzheimers Dis Other Demen.* **30**(3), 225-227. (2015).
503. Latorre, E. *et al*. Small molecule modulation of splicing factor expression is associated with rescue from cellular senescence. *BMC Cell Biol.* **18**, 31. (2017).
504. Vemuri, P. *et al*. Evaluation of amyloid protective factors and Alzheimer disease neurodegeneration protective factors in elderly in- dividuals. *JAMA Neurol.* **74,** 718–726. (2017).
505. Craig-Schapiro, R. *et al*. YKL-40: a novel prognostic fluid biomarker for preclinical Alzheimer's disease. *Biol Psychiatry*. **68,** 903–912. (2010).
506. Seeley, W.W., Crawford, R.K., Zhou, J., Miller, B.L. & Greicius, M.D. Neurodegenerative diseases target large-scale human brain networks. *Neuron.* **62**, 42–52. (2009).
507. Brookmeyer, R., Abdalla, N., Kawas, C.H. & Corrada, M.M. Forecasting the prevalence of preclinical and clinical Alzheimer's disease in the United States. *Alzheimers Dement*. **14,** 121–129. (2018).
508. Guzmán-Martinez, L., Farías, G.A. & Maccioni, R.B. Tau Oligomers as Potential Targets for Alzheimer's Diagnosis and Novel Drugs. *Front Neurol*. **4**, 167. (2013).
509. Cohen, T.J., Constance, B.H., Hwang, A.W., James, M. & Yuan, C-X. Intrinsic Tau Acetylation Is Coupled to Auto-Proteolytic Tau Fragmentation. *PLoS One.* **11**(7): e0158470. (2016).
510. Wang, Y. *et al*. The tyrosine phosphatase PTPN13/FAP-1 links calpain-2, TBI and tau tyrosine phosphorylation. *Sci Rep.* **7**(1):11771. (2017).
511. Canovi, M. *et al.* The binding affinity of anti-Ab(1-42) MAb-decorated nanoliposomes to Ab(1-42) peptides *in vitro* and to amyloid deposits in post-mortem tissue. *Biomaterials.* **32,** 5489-97. (2011).
512. Michel, E. & Parsons, J.A. Characterization of a biotin-conjugated ovine prolactin ligand. *Mol Cell Endocrinol.* **56**, 71-79. (1988).

513. Markoutsa, E. e*t al.* Comparison of various types of ligand decorated nanoliposomes for their ability to inhibit amyloid aggregation and to reverse amyloid cytotoxicity. *Curr Top Med Chem*. **15**(22), 2267-76. (2015).
514. Radde, R. *et al.* Abeta42-driven cerebral amyloidosis in transgenic mice reveals early and robust pathology. *EMBO Rep*. **7**(9):940-6. (2006).
515. Lok, K. Characterization of the APP/PS1 mouse model of Alzheimer's disease in senescence accelerated background. *Neurosci Lett.* **557**, 84-89. (2013).
516. Olmsted, J.B. *et al*. Isolation of microtubule protein from cultured mouse neuroblastoma cells. *Proc Natl Acad Sci U S A*. **65**: 129-136. (1970).
517. Klebe, R.J. & Ruddle, F.H. Neuroblastoma: Cell culture analysis of a differentiating stem cell system. *J. Cell Biol*. **43**: 69A. (1969).
518. Zheng, H. *et al.* beta-Amyloid precursor protein-deficient mice show reactive gliosis and decreased locomotor activity. *Cell*. **81**(4):525-31. (1995).
519. Davis, A.A., Fritz, J.J., Wess, J., Lah, J.J. & Levey, A.I. Deletion of M1 muscarinic acetylcholine receptors increases amyloid pathology *in vitro* and *in vivo*. *J Neurosci*. **30**(12), 4190-96. (2010).
520. D'Ursi, A.M. *et al.* Solution structure of amyloid beta-peptide (25-35) in different media. *J.Med.Chem*. **47**: 423(1-42)38. (2004).
521. Kohno, T., Kobayashi, K., Maeda, T., Sato, K. & Takashima, A. Three-dimensional structures of the amyloid beta peptide (25-35) in membrane-mimicking environment. *Biochemistry.* **35**, 16094-104. (1996).
522. Serpell, L.C. Alzheimer's amyloid fibrils: structure and assembly. Biochimica et Biophysica Acta (BBA). *Molecular Basis of Disease.* **1502**(1), 16-30. (2000).
523. Woojin Kim and Michael H. Hecht. Generic hydrophobic residues are sufficient to promote aggregation of the Alzheimer's Aβ42 peptide. *Proc Natl Acad Sci U S A*. **103**(43), 15824-29. (2006).
524. Crescenzi, O. *et al*. Solution structure of the Alzheimer amyloid beta-peptide ((1-42)) in an apolar microenvironment. Similarity with a virus fusion domain. *Eur J Biochem*. **269**, 5642-48. (2002).
525. Tomaselli, S. *et al*. The alpha-to-beta Conformational Transition of Alzheimer's Abeta-((1-42)) Peptide in Aqueous Media is Reversible: A Step by Step Conformational Analysis Suggests the Location of beta Conformation Seeding. *Chembiochem* **7**, 257-267. (2006).
526. Vivekanandan, D., Brender, J.R. & Lee, S.Y., Ramamoorthy, A. A partially folded structure of amyloid-beta(1–40) in an aqueous environment. *Biochem Biophys Res Comm*. **411**(2), 312-316. (2011).
527. Fawzi, N. L., Ying, J., Ghirlando, R., Torchia, D. A. & Clore, G. M. Atomic-resolution dynamics on the surface of amyloid-beta protofibrils probed by solution NMR. *Nature* **480**, 268–272. (2011).
528. Wu, C., Biancalana, M., Koide, S. & Shea, J-E. Binding Modes of Thioflavin-T to the Single-Layer β-Sheet of the Peptide Self-Assembly Mimics. *J. Mol. Biol*. **394**, 627–633. (2009).
529. Arndt, J.W. *et al.* Structural and kinetic basis for the selectivity of aducanumab for aggregated forms of amyloid-β. *Sci Rep*. **8**, 6412. (2018).
530. Lemkul, J.A. & Bevan, D.R. Morin Inhibits the Early Stages of Amyloid β-Peptide Aggregation by Altering Tertiary and Quaternary Interactions to Produce "Off-Pathway" Structures, *Biochem.* **51**(30), 5990–6009. (2012).
531. Gilead, S. & Gazit, E. Inhibition of Amyloid Fibril Formation by Peptide Analogues Modified with α-Aminoisobutyric Acid. *Angew Chem*. **43**, 4041-44. (2004).
532. Stine, W.B., Jungbauer, L., Yu, C. & LaDu, M.J. Preparing Synthetic Aβ in Different Aggregation States. *Methods Mol Biol*. **670**, 13–32. (2011).
533. Necula, M., Kayed, R., Milton, S. & Glabe, C.G. Small Molecule Inhibitors of Aggregation Indicate That Amyloid β Oligomerization and Fibrillization Pathways Are Independent and Distinct. *J Biol Chem*. **282**(14), 10311-24. (2007).
534. Zhang, X. *et al*. 3D Structural Fluctuation of IgG1 Antibody Revealed by Individual Particle Electron Tomography. *Sci Rep.* **5**: 9803. (2015)
535. Jølck, R.I., Feldborg, L.N., Andersen, S., Moghimi, S.M. & Andresen, T.L. Engineering of liposomes and nanoparticles for biological targeting. *Adv. Biochem. Eng. Biotechnol*. **125,** 251-280. (2011).
536. Wu, L.-P., Wang, D., Parhamifar, L., Hall, A., Chen, G.-Q. & Moghimi, S.M. Poly(3-hydroxybutyrate-co-R-3-hydroxyhexanoate) nanoparticles with poly-ethylenimine coat as

simple, safe, and versatile vehicles for cell targeting: population characteristics, cell uptake, and intracellular trafficking. *Adv. Healthc. Mater* **3,** 817-824. (2014).
537. Ordóñez-Gutierrez, L. *et al*. Cellular prion protein modulates b-amyloid deposition in aged APP/PS1 transgenic mice. *Neurobiol Aging.* **34**, 2793-2804. (2013).
538. Xiao, Y. *et al*. A beta ((1-42)) fibril structure illuminates self-recognition and replication of amyloid in Alzheimer's disease. *Nat Struct Mol Biol.* **22,** 499-505. (2015).
539. Markoutsa, E., Papadia, K., Clemente, C., Flores, O. & Antimisiaris S.G. Anti-Ab- MAb and dually decorated nanoliposomes: effect of Ab(1-42) peptides on interaction with hCMEC/D3 cells. *Eur J Pharm Biopharm*. 81, 49-56. (2012).
540. Moghimi, M. & Moghimi, S.M. Lymphatic targeting of immuno-PEG-liposomes: evaluation of antibody coupling procedures on lymph node macrophage uptake, *J Drug Target.* 16, 586-590. (2008).
541. Moghimi, S.M. The effect of methoxy-PEG chain length and molecular archi- tecture on lymph node targeting of immuno-PEG liposomes. *Biomaterials.* **27,** 136-144. (2006).
542. Moghimi, S.M. & Gray, T. A single intravenous dose of poloxamine-based long- circulating nanospheres triggers macrophage clearance of subsequent doses in rats. *Clin Sci.* 93, 371-379. (1997).
543. Lajoie, J.M. & Shusta, E.V. Targeting receptor-mediated transport for delivery of biologics across the blood-brain barrier. *Annu Rev Pharmacol Toxicol*. **55,** 613-631. (2015).
544. Akinyemi, R.O., Mukaetova-Ladinska, E.B., Attems, J., Ihara M. & Kalaria, R.N. Vascular risk factors and neurodegeneration in ageing related dementias: Alzheimer's disease and vascular dementia. *Curr. Alzheimer Res*. **10,** 642-653. (2013).
545. A.M. Minogue, R.S. Jones, R.J. Kelly, C.L. McDonald, T.J. Connor, M.A. Lynch, Age-associated dysregulation of microglial activation is coupled with enhanced blood-brain barrier permeability and pathology in APP/PS1 mice, *Neurobiol. Aging* **35,** 1442-52. (2014).
546. Yu, Y.J. & Watts, R.J. Developing Therapeutic Antibodies for Neurodegenerative Disease. *Neurotherapeutics*. **10**(3): 459–472. (2013).
547. Wisniewski, T. & Konietzko, U. Amyloid-b immunisation for Alzheimer's disease, *Lancet Neurol*. **7,** 805-811. (2008).
548. Bachmeier, C. J., Beaulieu-Abdelahad, D., Mullan, M. J. & Paris, D. Epitope-dependent effects of beta-amyloid antibodies on beta-amyloid clearance in an *in vitro* model of the blood–brain barrier. *Microcirculation*. **18**, 373-379. (2011).
549. Uribe-Arias, A. *et al*. p120-catenin is necessary for neuroprotection induced by CDK5 silencing in models of Alzheimer's disease. *J Neurochem*. Aug; **138**(4), 624–639. (2016).
550. Kouchi, Z. *et al.* p120 catenin recruits cadherins to gamma-secretase and inhibits production of Abeta peptide. *J Biol Chem*. **284**(4),1954-61. (2009).
551. Boado, R.J., Lu, J.Z., Hui, E.K. & Pardridge, W.M. IgG-single chain Fv fusion protein therapeutic for Alzheimer's disease: Expression in CHO cells and pharmacokinetics and brain delivery in the rhesus monkey. *Biotechnol Bioeng*. **105**, 627-635. (2010).
552. Boado, R.J., Zhang, Y., Zhang, Y., Xi, C-F. & Pardridge, W.M. Fusion antibody for Alzheimer's disease with bi-directional transport across the blood-brain barrier and abeta fibril disaggregation. *Bioconjug Chem*. **18**(2), 447–455. (2007).
553. Moghimi, S.M. Bionanotechnologies for treatment and diagnosis of Alzheimer's disease, *Nanomedicine.* **7,** 515-518. (2011).
554. Lee, S.H. *et al.* Antibody-Mediated Targeting of Tau In vivo Does Not Require Effector Function and Microglial Engagement. *Cell Rep*. **16**(6),1690-1700. (2016).
555. Monoclonal Antibody Therapeutics Market by Application (Cancer, Autoimmune Diseases, Infection, Hematological Diseases, and Others), By Source and By End Users: Global Industry Perspective, Comprehensive Analysis and Forecast, 2017-2023.
556. World Alzheimer Report 2016: Improving healthcare for people living with dementia coverage, quality and costs now and in the future. London: Alzheimer Disease International. (2016).
557. World Alzheimer Report 2010: The Global Economic Impact of Dementia. London: Alzheimer's disease international. (2010).
558. Takeda, S. & Morishita, R. Diabetes and Alzheimer's Disease. In: Yamagishi S. (eds) Diabetes and Aging-related Complications. Springer, Singapore. (2018).
559. Readhead, B. *et al*., Multiscale Analysis of Independent Alzheimer's Cohorts Finds Disruption of Molecular, Genetic, and Clinical Networks by Human Herpesvirus, *Neuron.* **99**, 1-19. (2018)

560. Andrew, R.J., Kellett, K.A.B., Thinakaran, G. & Hooper, N.M. A Greek Tragedy: the Growing Complexity of Alzheimer Amyloid Precursor Protein Proteolysis. *J Biol Chem.* **291**(37), 19235-44. (2016).
561. Sticht, H. *et al*. Structure of amyloid A4-((1-40))-peptide of Alzheimer's disease. *Eur.J.Biochem*. **233**: 293-298. (1995).
562. Ahmed, M. *et al.* Structural conversion of neurotoxic amyloid-β1–42 oligomers to fibrils. *Nature Structural & Molecular Biology*. **17**, 561–567. (2010).
563. Qiu, W.Q. & Folstein, M.F. Insulin, insulin-degrading enzyme and amyloid-beta peptide in Alzheimer's disease: review and hypothesis. *Neurobiol Aging*. **27**, 190–198. (2006).
564. A.R. Nelson, A.P. Sagare, B.V. Zlokovic, Chapter 9 - Blood–Brain Barrier Transport of Alzheimer's Amyloid β-Peptide, Editor(s): Michael S. Wolfe, Developing Therapeutics for Alzheimer's Disease, Academic Press, 2016, Pages 251-270
565. Khalid Iqbal, Fei Liu and Cheng-Xin Gong. Tau and neurodegenerative disease: the story so far. *Nature Reviews Neurology* volume **12**, pages 15–27 (2016)
566. Galasko, D. *et al*. Clinical trial of an inhibitor of RAGE-Aβ interactions in Alzheimer disease. *Neurology*. **82**(17): 1536–1542. (2014).
567. Granic I, Nyakas C, Luiten PG, Eisel UL, Halmy LG, Gross G, Schoemaker H, Möller A, Nimmrich V. Calpain inhibition prevents amyloid-beta-induced neurodegeneration and associated behavioral dysfunction in rats. *Neuropharmacology*. 2010 Sep-Oct;**59**(4-5):334-42
568. Hori, Y. *et al.* A Food and Drug Administration-approved asthma therapeutic agent impacts amyloid β in the brain in a transgenic model of Alzheimer disease. *J Biol Chem*. **290**(4):1966-78. (2015).
569. Langbaum, J.B. *et al.* Establishing Composite Cognitive Endpoints for Use in Preclinical Alzheimer's Disease Trials. *J Prev Alzheimers Dis*. **2**(1), 2-3. (2015).
570. Lycke, J. Monoclonal antibody therapies for the treatment of relapsing-remitting multiple sclerosis: differentiating mechanisms and clinical outcomes. *Ther Adv Neurol Disord.* **8**(6), 274-93. (2015).
571. Tracy, T.E. *et al*. Acetylated Tau Obstructs KIBRA-Mediated Signaling in Synaptic Plasticity and Promotes Tauopathy-Related Memory Loss. *Neuron* **90**, 1–16. (2016).
572. Sami Gabbouj, Teemu Natunen, Hennariikka Koivisto, Kimmo Jokivarsi, Mari Takalo, Susanna Kemppainen, Reyhaneh Naderi, Adrián Posado-Fernández, Petra Mäkinen, Kaisa M. A. Paldanius, Gonçalo Doria, Pekka Poutiainen, Orfeu Flores, Annakaisa Haapasalo, Heikki Tanila, Mikko Hiltunen. Intranasal insulin activates Akt2 signaling pathway in the hippocampus of wild-type but not in APP/PS1 Alzheimer model mice. *Neurobiology of Aging*. **75**, 98-108. (2019).

8. Annexes

8.1. Thesis-related in press or submitted papers until date

8.1.1. Reference 468

Lara Ordóñez-Gutiérrez*, Adrián Posado-Fernández*, Davoud Ahmadvand*, Barbara Lettiero, Linping Wu, Marta Antón, Orfeu Flores, Seyed Moein Moghimi, Francisco Wandosell. ImmunoPEGliposome-mediated reduction of blood and brain amyloid levels in a mouse model of Alzheimer's disease is restricted to aged animals. *Biomaterials*. **112**, 141-152. (2017).

8.1.2. Reference 572

Sami Gabbouj, Teemu Natunen, Hennariikka Koivisto, Kimmo Jokivarsi, Mari Takalo, Susanna Kemppainen, Reyhaneh Naderi, Adrián Posado-Fernández, Petra Mäkinen, Kaisa M. A. Paldanius, Gonçalo Doria, Pekka Poutiainen, Orfeu Flores, Annakaisa Haapasalo, Heikki Tanila, Mikko Hiltunen. Intranasal insulin activates Akt2 signaling pathway in the hippocampus of wild-type but not in APP/PS1 Alzheimer model mice. *Neurobiology of Aging*. **75**, 98-108. (2019).

8.1.3. Submitted (October 2018)

Adrián Posado-Fernández, Cláudia Afonso, Gonçalo Dória, Orfeu Flores, Eurico J. Cabrita. Epitope Mapping by NMR of a Novel Anti-Aβ Antibody (STAB-Mab). *Scientific Reports*. (2018).

* These authors contributed equally to this work

8.2. STAB-Mab´s in press papers

8.2.1. Reference 511

Mara Canovi, Eleni Markoutsa, Adina N. Lazar, Georgios Pampalakis, Carla Clemente, Francesca Re, Silvia Sesana, Massimo Masserini, Mario Salmona, Charles Duyckaerts, Orfeu Flores, Marco Gobbi & Sophia G. Antimisiaris. The binding affinity of anti-Aβ(1-42) MAb-decorated nanoliposomes to Aβ(1-42) peptides in vitro and to amyloid deposits in post-mortem tissue. *Biomaterials*. **32**, 5489-97. (2011).

8.2.2. Reference 539

E. Markoutsa, K. Papadia, C. Clemente, O. Flores & S.G. Antimisiaris. Anti-Ab- MAb and dually decorated nanoliposomes: effect of Aβ(1-42) peptides on interaction with hCMEC/D3 cells. *European Journal of Pharmaceutics and Biopharmaceutics*. **81**, 49-56. (2012).

8.2.3. Reference 513

Eleni Markoutsa, Spyridon Mourtas, Erika Bereczki, Cristiano Zona, Barbara La Ferla, Fransesco Nicotra, Orfeu Flores, Jin-Jing Pei & Sophia G. Antimisiaris. Comparison of Various Types of Ligand Decorated Nanoliposomes for their Ability to Inhibit Amyloid Aggregation and to Reverse Amyloid Cytotoxicity. *Current Topics in Medicinal Chemistry*. **15**(22), 2267-76. (2015).

8.2.4. Reference 468

Lara Ordóñez-Gutiérrez*, Adrián Posado-Fernández*, Davoud Ahmadvand*, Barbara Lettiero, Linping Wu, Marta Antón, Orfeu Flores, Seyed Moein Moghimi, Francisco Wandosell. ImmunoPEGliposome-mediated reduction of blood and brain amyloid levels in a mouse model of Alzheimer's disease is restricted to aged animals. *Biomaterials*. **112**, 141-152. (2017).

8.2.5. Reference 470

Dario Carradori, Claudia Balducci, Francesca Re, Davide Brambilla, Benjamin Le Droumaguet, Orfeu Flores, Alice Gaudin, Simona Mura, Gianluigi Forloni, Lara Ordonñez-Gutierrez, Francisco Wandosell, Massimo Masserini, Patrick Couvreur, Julien Nicolas & Karine Andrieux. Antibody-Functionalized Polymer Nanoparticle Leading to Memory Recovery in Alzheimer's Disease-like Transgenic Mouse Model. *Nanomedicine: Nanotechnology, Biology, and Medicine*. **4**(2), 609-618. (2018).

* These authors contributed equally to this work

8.3. National and international congresses poster presentations related to the thesis´ works

8.3.1. Poster 1

Adrián Posado-Fernández, Orfeu Flores.. A Novel Anti-Beta Amyloid Monoclonal Antibody. Production and Characterization. Warsaw Special Symposium on Emotional Brain. (2015).

8.3.2. Poster 2

Lara Ordóñez-Gutiérrez, Adrián Posado-Fernández, Davoud Ahmadvand, Barbara Lettiero, Linping Wu, Marta Antón, Orfeu Flores, Seyed Moein Moghimi & Francisco Wandosell. Reduction in blood and brain amyloid levels in elder APP/PS1 transgenic mice after treatment with. CIBERNED Congress. (2016).

8.3.3. Poster 3

Lara Ordóñez-Gutiérrez, Adrián Posado-Fernández, Davoud Ahmadvand, Barbara Lettiero, Linping Wu, Marta Antón, Orfeu Flores, Seyed Moein Moghimi & Francisco Wandosell. Anti-Aβ ImmunoPEGliposomes for Alzheimer´s Disease Treatment. National Congress of the Portuguese Association of Biotechnology. (2016).

8.3.4. Poster 4

Gonçalo Doria, Adrián Posado-Fernández, Carlos Bernardes, Orfeu Flores, José Rivas, Manuel Bañobre-López, Uwe Himmelreich, Dick Terwell, Elga de Vries, Mikko Hiltunen, Carlos Manchado Perdiguero, Vladas Bumelis, Ángeles Almeida & Tomas Sobrino. PANA project - Promoting active ageing: functional nanostructures for Alzheimer's disease at ultra-early stages. *National Congress of the Portuguese Association of Biotechnology.* (2016).

8.3.5. Poster 5

Adrián Posado-Fernández, Cláudia Afonso, Eurico J. Cabrita & Orfeu Flores. STAB-Mab. A New Tool for Alzheimer´s Disease Passive Immunotherapy. *CiiEM International Congress.* (2018).

2018

In the Siege of Alzheimer´s Caste: Contribution to Immunotherapy

Adrián Posado-Fernández